Dissertation

submitted to the

Combined Faculty of Natural Sciences and Mathematics

of Heidelberg University, Germany

for the degree of

Doctor of Natural Sciences

Put forward by

Aleksandr N. Mikheev

born in: Kazan, Russia

Oral examination: February 17, 2023

Far-from-equilibrium universal scaling dynamics in ultracold atomic systems and heavy-ion collisions

Referees: Prof. Dr. Thomas Gasenzer

Prof. Dr. Carlo Ewerz

Zusammenfassung

Die Klassifizierung und das Verständnis von Skalierungslösungen in isolierten Quantensystemen, die weit vom thermischen Gleichgewicht entfernt sind und als nichtthermische Fixpunkte bezeichnet werden, sind eines der offenen Probleme in der Nichtgleichgewichts-Vielteilchenquantentheorie. Die übliche Methode beinhaltet die Suche nach möglichen selbstähnlichen Lösungen für eine (nicht-perturbative) Evolutionsgleichung, z. B. Boltzmann oder Kadanoff-Baym, ausgehend von einer gleichgewichtsfernen Anfangsbedingung. In dieser Arbeit entwickeln wir einen alternativen Ansatz, der auf der Übereinstimmungen zwischen Skalierung und Fixpunkten der Renormierungsgruppe basiert. Am Beispiel eines ultrakalten Bose Gases zeigen wir, wie mögliche gleichgewichtsferne Skalierungslösungen systematisch durch die Lösung von Fixpunkt-Renormierungsgruppen-Gleichungen erhalten werden können. Im zweiten Teil dieser Arbeit untersuchen wir die Dynamik, die einer voll entwickelten selbstähnlichen Evolution vorausgeht. Wir verwenden die Hamilton-Formulierung der kinetischen Theorie, um eine Stabilitätsanalyse von nicht-thermischen Fixpunkten in einem expandierenden nicht-Abelschen Plasma durchzuführen, das durch den Fokker-Planck-Kollisionsintegral charakterisiert ist. Unter Verwendung einer adiabatischen Entwicklung erstellen wir eine Störungstheorie, die es uns ermöglicht, Stabilitätsgleichungen für Skalierungsexponenten abzuleiten und die Ljapunow-Relaxationsraten zu erhalten, die mit einem nichtthermischen Fixpunkt verbunden sind.

Abstract

Classification and understanding of scaling solutions in closed quantum systems far from thermal equilibrium, known as nonthermal fixed points, are one of the open problems in nonequilibrium quantum many-body theory. The usual method involves searching for possible self-similar solutions to a (nonperturbative) evolution equation, e.g., Boltzmann or Kadanoff–Baym, starting from a far-from-equilibrium initial condition. In this work, we develop an alternative approach based on the correspondence between scaling and fixed points of the renormalization group. Using an ultracold Bose gas as an example we show how possible far-from-equilibrium scaling solutions can be systematically obtained by solving fixed-point renormalization-group equations. In the second part of this thesis, we investigate dynamics preceding a fully developed self-similar evolution. We use the Hamiltonian formulation of kinetic theory to perform a stability analysis of nonthermal fixed points in an expanding non-Abelian plasma characterized by the Fokker–Planck collision kernel. Employing an adiabatic expansion we develop a perturbation theory, which at next-to-leading order allows us to derive stability equations for scaling exponents and obtain the Lyapunov relaxation rates associated with a nonthermal fixed point.

Contents

Chapter 1

General introduction

Relaxation dynamics of closed quantum many-body systems quenched *far from equilibrium* has been studied intensively during recent years. Examples range from thermalization and hadronization of a quark-gluon plasma and evolution of the early universe after the inflation epoch to relaxation of ultracold atomic systems in extreme conditions studied in table-top experiments. Yet, despite a great effort, a complete systematization of potential evolution pathways is far from being achieved. A great variety of possible scenarios has been proposed and observed, such as prethermalization [1, 2], generalized Gibbs ensembles (GGE) [3–5], critical and prethermal dynamics [6–9], many-body localization [10], turbulence [11], decoherence and revivals [12], prescaling [13, 14], universal scaling dynamics and the approach of a nonthermal fixed point [15–17]. The broad spectrum of possible phenomena occurring during the evolution reflects a deep difference of quantum dynamics as compared to the relaxation of classical systems.

In this work, we focus on studying universal dynamics of two (seemingly) vastly different systems: a dilute Bose gas quenched far from equilibrium and a non-Abelian plasma forming in ultrarelativistic hadron-hadron collisions. Universality here means that the evolution after some time becomes independent of the initial condition and microscopic details, and such a universal intermediate state is determined only by symmetry properties and possibly a limited set of relevant quantities and/or functions that characterize the initial state. This allows categorizing systems into universality classes based on their symmetry properties and to which family of far-from-equilbrium states does the initial condition belong to. The situation highly resembles the ideas of the classical theory of critical phenomena. The concepts of universality and scaling were first introduced in the pioneering works of Widom, Kadanoff, and Wilson [18–21] and almost immediately generalized to the case of dynamics [22, 23]. This discussion was then extended to coarsening and phase-ordering kinetics [24], glassy dynamics and ageing [25], (wave-)turbulence [26–28], and its variants in the quantum realm of superfluids [29, 30]. Recently, various possible realizations of

prethermal and universal dynamics of far-from-equilibrium quantum many-body systems were studied [2, 31–51], of which many considered ultracold atomic systems. The concept of nonthermal fixed points has been discussed, without [52–58] and with [59–62] relation to topological defects, order parameters and ordering kinetics, advancing a comprehensive description of universal dynamics.

A standard analytical approach that is usually employed for studying scaling at nonthermal fixed points consists of deriving evolution equations governing the dynamics of correlation functions in a given model and then analyzing the scaling properties of these equations. A particularly approachable class of models is given by scalar theories with quartic interactions between N-component fields (either relativistic or nonrelativistic, real or complex), symmetric under some matrix group (e.g., U(N) or O(N)) in the space of field components. In this case, one can apply various techniques such as the $1/N$ expansion [54, 57, 63] or the low-energy effective description [64] to systematically derive approximate evolution equations, e.g., the quantum Boltzmann equation, and predict and explain the observed scaling. Though rather simple, such models can often be seen as approximations of the experimentally relevant systems. For example, a nonrelativistic U(N)-symmetric model can be considered a limiting case of a spin-1 Bose gas, in which a nonthermal fixed point was observed for the first time [15], see Fig. 1.1. This further emphasizes the importance of theoretical developments in this area. In this work, however, we decide to go beyond both such a class of models and the standard dynamical approach to scaling at nonthermal fixed points. Firstly, we consider a single-component Bose gas, in which a universal self-similar dynamics has been recently observed [17] and which lacks a $1/N$ expansion parameter. Secondly, instead of studying nonthermal fixed points through the lens of evolution equations, we develop a functional renormalization group approach to far-from-equilibrium scaling.

In the second part of this work, we concentrate on the dynamics preceding a fully developed self-similar evolution. In [13] and [14], it was proposed that already before achieving fully developed scaling the system may exhibit a dramatic reduction in complexity such that its dynamics can be described by a few slowly evolving quantities. In particular, numerically solving the leading-order QCD kinetic theory [65] it was observed that much before the scaling with universal exponents is established, the evolution is already governed by the fixed-point scaling function with time-dependent scaling exponents [14]. In this work, we consider a toy model of an expanding Yang-Mills plasma and derive approximate equations that govern the dynamics of its scaling exponents. More specifically, employing the Hamiltonian formulation of kinetic theory we derive the stability equations for scaling exponents, which can be interpreted as relaxation equations to a nonthermal fixed point, and demonstrate for the first time that the nonthermal fixed point is stable under small perturbations.

The thesis is organized as follows. We begin, in Ch. 2, with an introduction of the
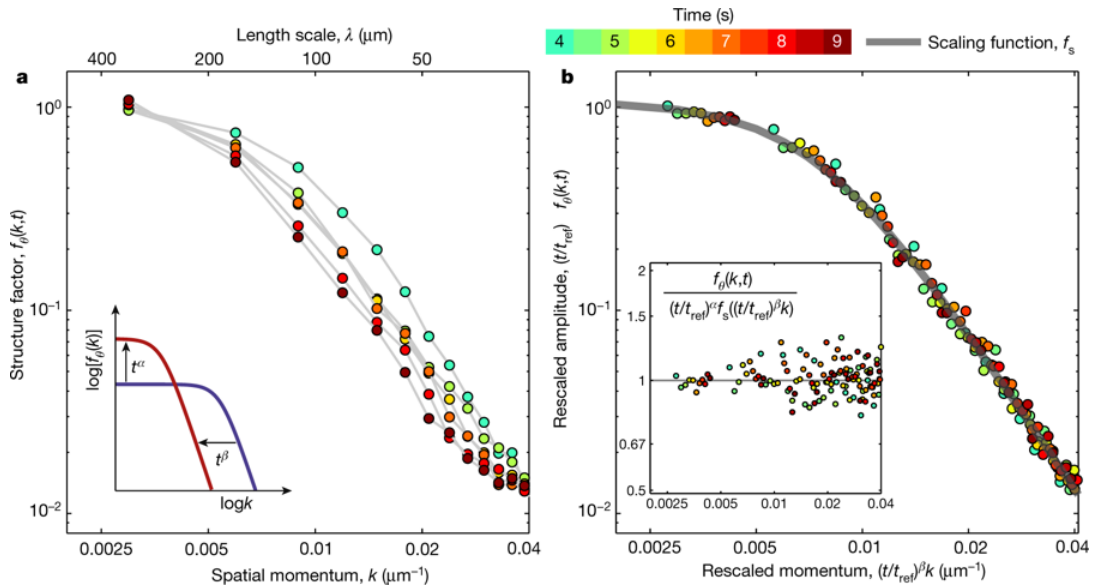
Figure 1.1. Self-similar evolution of a structure factor $f_\theta(k, t)$ in a quasi-one-dimensional spin-1 Bose gas after a quench. The curve rescales with the amplitude critical exponent $\alpha = 0.33 \pm 0.08$ and the momentum critical exponent $\beta = 0.54 \pm 0.06$. Figure taken from [15].

general concept of nonthermal fixed points and, in addition, outline the usual kinetic approach to studying them. Then, in Ch. 3, we provide an overview of functional methods of (nonequilibrium) quantum field theory by introducing most of the important definitions, techniques, and approximations necessary for the main part. In Ch. 4, we develop a functional renormalization group approach to nonthermal fixed points in a single-component Bose gas. To that end, we derive fixed-point equations that control their universal scaling properties. Adopting a certain approximation scheme we then solve these equations numerically and demonstrate how information about the scaling can be extracted from their solutions. After that, we switch our attention to high-energy physics, starting by outlining in Ch. 5 the physical picture of ultrarelativstic hadron-hadron collisions. We show how at extremely high energies a new universal state of matter, known as the color glass condensate (CGC), emerges as a description of the colliding nuclei. We then argue how a collision of two CGC sheets leads to the formation of a far-from-equilibrium longitudinally expanding non-Abelian plasma, which can be studied by means of kinetic theory. Finally, in Ch. 6, we use the Hamiltonian kinetic description in order to analyze stability properties of nonthermal fixed points in such systems and investigate the proposed preceding prescaling regime.

Publications

- Some results of this thesis are presently being prepared for publication or have been already published. Elements of text taken from the publications below are not marked explicitly. They are part of Chs. 4 and 6.

  ◇ A. N. Mikheev, A. Mazeliauskas, J. Berges, "Stability analysis of nonthermal fixed points in longitudinally expanding kinetic theory", Phys. Rev. D **105**, 116025 (2022).

  ◇ A. N. Mikheev, J. M. Pawlowski, T. Gasenzer, "A functional renormalization group approach to nonthermal fixed points in an ultracold Bose gas", in preparation.

- Beyond that, Ch. 2, which discusses some general concepts of nonthermal fixed points, follows almost word-to-word the overview article written by my collaborators and me:

  ◇ C.-M. Schmied, A. N. Mikheev, T. Gasenzer, "Non-thermal fixed points: Universal dynamics far from equilibrium", Int. J. Mod. Phys. A **34**, 1941006 (2019).

  Certain sections of that overview paper are verbatim of [57].

- In addition, Sec. 3.3.2 contains work that have never been published before and is currently not in preparation for any publication apart from this dissertation.

- Furthermore, two preprints have been recently uploaded to the arXiv e-print server:

  ◇ P. Heinen, A. N. Mikheev, C.-M. Schmied, and T. Gasenzer, "Non-thermal fixed points of universal sine-Gordon coarsening dynamics", arXiv:2212.01162 [cond-mat.quant-gas].

  ◇ P. Heinen, A. N. Mikheev, T. Gasenzer, "Anomalous scaling at non-thermal fixed points of the sine-Gordon model", arXiv:2212.01163 [cond-mat.quant-gas].

  Neither of these works is represented in this dissertation in any capacity.

- Finally, two more articles were published during my Master studies and are not included in the dissertation:

  ◇ A. N. Mikheev, C.-M. Schmied, T. Gasenzer, "Low-energy effective theory of nonthermal fixed points in a multicomponent Bose gas", Phys. Rev. A **99**, 063622 (2019).

  ◇ C.-M. Schmied, A. N. Mikheev, T. Gasenzer, "Prescaling in a far-from-equilibrium Bose gas", Phys. Rev. Lett. **122**, 170404 (2019).

Chapter 2

Nonthermal fixed points

2.1 Introduction to the concept of nonthermal fixed points

As already mentioned in the general introduction, the main subject of this work is a phenomenon of so-called nonthermal fixed points (NTFP), a concept motivated by the ideas of (near-)equilibrium *renormalization group* (RG) theory. In the RG framework, one essentially studies a physical system through a microscope at different resolutions. Close to a critical point one observes that the correlation functions take a self-similar form, i.e., they no longer depend on the resolution. As a simple example, consider a two-point correlation function in a homogeneous and isotropic system. Changing the value of a spatial resolution scale parameter s, the correlation function $C(x; s)$ describing the correlations between two points separated by the distance x should change accordingly. Self-similarity implies that $C(x; s)$ has to rescale as $C(x; s) = s^\zeta f(x/s)$. Hence, the correlations are solely characterized by a universal exponent ζ and the universal scaling function f. A *fixed point* of the RG flow equation corresponds to the case when the system becomes fully scale-independent, which happens when $f(x) \sim x^\zeta$. Typically, however, for a realistic physical system, the scaling function f retains some information of characteristic scales such as a *correlation length* ξ and thus does not have a pure power-law form. In this case, the system can only approximately approach the fixed point.

Taking the time t as the scale parameter, the renormalization-group idea can be extended to a time evolution of (strongly) nonequilibrium systems. The corresponding fixed point of the RG flow is called a *nonthermal fixed point*. In the scaling regime near a nonthermal fixed point, the evolution of, e.g., the time-dependent version of the correlations discussed above is determined by $C(x; t) = t^\alpha f(t^{-\beta}x)$, with now two universal exponents α and β that assume, in general, nonzero values. The associated correlation length of the system changes as a power of time, $\xi(t) \sim t^\beta$. Note that the time evolution taking power-law characteristics is equivalent to critical slowing down, here in real time. We remark that, depending on the

sign of β, increasing the time t can correspond to either a reduction or an increase of the microscope resolution. The scaling exponents α and β allow to determine the universality class associated with the fixed point [55].[1] Hence, the evolution of very different physical systems far from equilibrium can be categorized by means of their possible kinds of scaling behavior. A full classification of such *universality classes* remains an open problem. However, similar to the case of equilibrium critical phenomena, underlying symmetries of the system are expected to play a crucial role.

In contrast to the equilibrium case, however, initial conditions are not completely irrelevant. Whether a physical system is able to approach a nonthermal fixed point and show universal scaling dynamics or which fixed point can be reached in general may depend on the initial state. Going back to the RG analogy, one can imagine a space of all possible states. The evolution of one state to another can be then represented as a trajectory in this space. A set of all the trajectories forms a flow in the state space, similar to a flow of coupling constants in the RG theory or to a phase portrait of some dynamical system. While the asymptotic state is typically expected to correspond to the thermal equilibrium, there can be attractors near which the evolution is *critically slowed down*. These attractors are exactly the aforementioned nonthermal fixed points. Therefore, in general, the whole space can be divided into regions that are attracted to different nonthermal fixed points. At the same time, some initial conditions may not lead to a nonthermal fixed point at all but instead correspond to the *direct thermalization*, see Fig. 2.1. It is commonly accepted, however, that the key ingredient for the occurrence of self-similar dynamics is an *extreme out-of-equilibrium initial configuration*.

As a relevant example, consider the time evolution of a dilute Bose gas in three spatial dimensions after a strong cooling quench [57], see Fig. 2.2 as well as [55, 67–69]. An extreme version of such a quench can be achieved, e.g., by first cooling the system adiabatically such that its chemical potential is $0 < -\mu \ll k_B T$, where the temperature $T \gtrsim T_c$ is just above the critical temperature T_c separating the normal and the Bose condensed phase of the gas, and then removing all particles with energy higher than $\sim |\mu|$. This leads to a distribution that drops abruptly above a momentum scale Q,

$$n(t_0, \mathbf{k}) \approx n_0 \Theta(Q - |\mathbf{k}|) , \tag{2.1}$$

see Fig. 2.2. If the corresponding energy is on the order of the ground-state energy of the post-quench fully condensed gas, $(\hbar Q)^2/2m \simeq |\mu| \simeq g\rho$, where $g = 4\pi\hbar^2 a/m$, with the

---

[1]In this work, we restrict ourselves to two-point correlators only and furthermore assume that the corresponding statistical and spectral functions are related via simple proportionality, such that they encode the same scaling information. The latter assumption was recently tested and was shown to not hold in general [66].
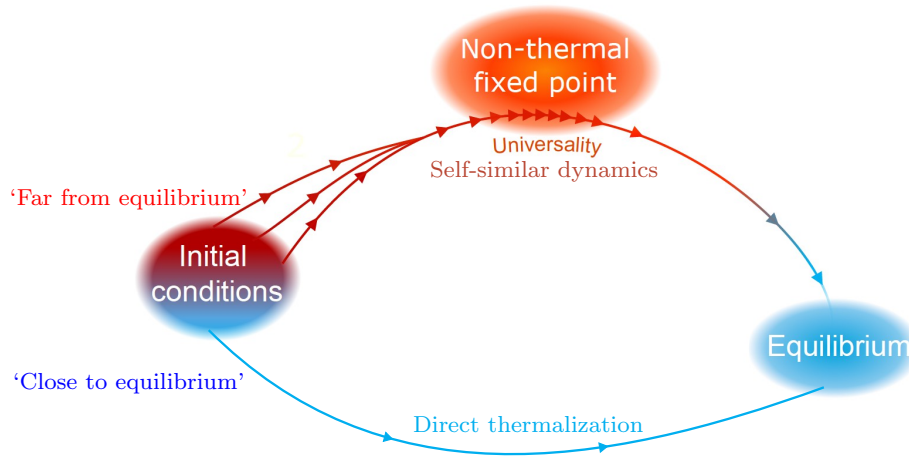
Figure 2.1. Schematics of different scenarios of thermalization. Within a subclass of far-from-equilibrium conditions all the states undergo the same self-similar evolution regime before reaching equilibrium. In contrast, a generic close-to-equilibrium initial state thermalizes directly without any universal scaling dynamics in-between. Figure adapted from [15].

scattering length a and the atom mass m, then the energy of the entire gas after the quench is concentrated at the scale $Q \simeq k_\xi$, with healing-length momentum scale $k_\xi = \sqrt{8\pi a\rho}$.

Most importantly, such a strong cooling quench leads to an extreme initial condition for the subsequent dynamics. The post-quench distribution is strongly overoccupied at momenta $k < Q$, as compared to the final equilibrium distribution. This initial overpopulation of modes with energies $\sim (\hbar Q)^2/2m$ induces inverse particle transport to lower momenta, while energy is transported to higher wavenumbers [55, 67, 68], as indicated by the arrows in Fig. 2.2. The rescaling is thus characterized by a bi-directional, in general nonlocal redistribution of particles and energy. Furthermore, in contrast to the case of a weak quench leading to a scaling evolution in which, typically, weak wave turbulence is induced [57, 70], where the inverse transport is characterized by a different, strongly nonthermal power-law form of the scaling function in the infrared (IR) region. While the spatio-temporal scaling provides the 'smoking gun' for the approach of a nonthermal fixed point, in all cases examined so far, this steep power-law scaling of the momentum distribution, $n(k) \sim k^{-\zeta}$, has been observed and reflects the character of the underlying transport, see Fig. 2.2. The evolution during this period is universal in the sense that it becomes mainly independent of the precise initial conditions set by the cooling quench as well as of the particular values of the physical parameters characterizing the system.

In the vicinity of a nonthermal fixed point, the momentum distribution of the Bose gas
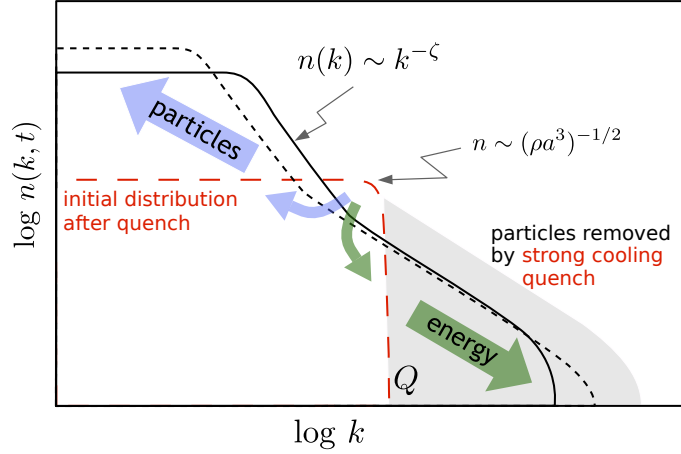
Figure 2.2. Self-similar scaling in time and space close to a nonthermal fixed point. The sketch shows, on a double-logarithmic scale, the time evolution of the single-particle momentum distribution $n(t, k)$ of a Bose gas for two different times t (solid and short-dashed line). Starting from an extreme initial distribution marked by the red long-dashed line, being the result of a strong cooling quench, a bi-directional redistribution of particles in momentum space occurs as indicated by the arrows. Particle transport towards zero momentum as well as energy transport to large momenta are characterized by self-similar scaling evolutions in space and time according to $n(t, k) = (t/t_{\text{ref}})^\alpha n(t_{\text{ref}}, [t/t_{\text{ref}}]^\beta k)$, with universal scaling exponents α and β, in general, different for both directions. Here, t_{ref} is an arbitrary reference time within the temporal scaling regime. The infrared transport (blue arrow) conserves the particle number which is concentrated at small momenta. In contrast, the energy, being concentrated at high momenta, is conserved in the redistribution of short-wavelength fluctuations (green arrow). See main text for details. Figure adapted from [69].

rescales self-similarly, within a certain range of momenta, according to

$$n(t, k) = (t/t_{\text{ref}})^\alpha n(t_{\text{ref}}, [t/t_{\text{ref}}]^\beta k) , \qquad (2.2)$$

with some reference time t_{ref}. The distribution shifts to lower momenta for $\beta > 0$, while transport to larger momenta occurs in the case of $\beta < 0$. A bi-directional scaling evolution is, in general, characterized by two different sets of scaling exponents. One set describes the inverse particle transport towards low momenta whereas the second set quantifies the transport of energy towards large momenta. Evaluated at a fixed reference time t_{ref}, the fixed-point solution (2.2) further defines the universal *scaling function* $n_S(k) = n(t_{\text{ref}}, k)$. Within a limited range of momenta, it satisfies the scaling hypothesis $n_S(k) = s^\zeta n_S(sk)$, with an additional, in general independent scaling exponent ζ. A frequently used simple Ansatz for the scaling function $n_S(Q)$ in the infrared region is given by $n_S(k) \sim \left[1 + (k/k_\Lambda)^\zeta\right]^{-1}$. It interpolates between the universal power-law behavior $n_S(k) \sim k^{-\zeta}$ for $k > k_\Lambda$ and the plateau region $n_S(k) \sim$ const. below the running scale k_Λ, see Fig. 2.2.

Global conservation laws – applying within a certain, extended regime of momenta – strongly constrain the redistribution underlying the self-similar dynamics in the vicinity of the nonthermal fixed point. Hence, they play a crucial role for the possible scaling evolution as they impose scaling relations between the scaling exponents. For example, particle number conservation in the infrared regime of long wavelengths, in d spatial dimensions, requires that $\alpha = d\beta$.

The resulting transport in momentum space can emerge from rather different underlying physical configurations and processes. For instance, the dynamics can be driven not only by the conserved redistribution of quasiparticle excitations such as in weak wave turbulence [55, 57] but also by the reconfiguration and annihilation of (topological) defects populating the system [62, 67]. The latter dynamics is often connected to the concept of superfluid turbulence [59, 60, 62]. If defects are subdominant or absent at all, the strongly occupied modes exhibiting scaling near the fixed point [55, 57] typically reflect strong phase fluctuations not subject to an incompressibility constraint. They can be described by the low-energy effective theory discussed in Ch. 4.1 or [64]. The associated scaling exponents are generically different for both types of dynamics, with and without defects [55, 61, 62].

The existence and significance of strongly nonthermal momentum power-laws, requiring a nonperturbative description reminiscent of wave turbulence, was proposed in the context of reheating after early-universe inflation [52, 71], then later generalized to scenarios of strong matterwave turbulence [53] and to the case of topological defects [59–61, 67, 72], see also [62, 73–78]. Universal scaling at a nonthermal fixed point in both space and time was studied for relativistic and nonrelativistic $O(N)$-symmetric models [55, 79], see also [56, 80], and discussed in the context of heavy-ion collisions [81–84] as well as axionic models [77].

As a final remark, we note that the concept of nonthermal fixed points includes scaling dynamics which exhibits coarsening and phase-ordering kinetics [24] following the creation of defects and nonlinear patterns after a quench, e.g., across an ordering phase transition. We emphasize, however, that coarsening and phase-ordering kinetics in most cases are being discussed within an open-system framework, considering the system to be coupled to a heat bath. Moreover, most theoretical treatments of these phenomena do not take nonlinear dynamics and transport into account.

2.2   Kinetic theory of nonthermal fixed points

In the previous section, we have introduced the basic ideas of nonthermal fixed points. For their theoretical investigation, one can make use of analytical as well as numerical tools. In this section, we will briefly overview a standard analytical approach to describe the scaling

behavior at such fixed points. Technical details at various levels of depth can be found in [56, 57, 85, 86].

For a general analytical treatment of nonthermal fixed points one needs to be able to calculate the time evolution of a quantum many-body system out-of equilibrium. Suitable techniques are provided by the framework of nonequilibrium quantum field theory (QFT), which will be properly described in Ch. 3. Using a path integral formulation, all information about the time-evolving quantum system is contained in the so-called Schwinger-Keldysh nonequilibrium generating functional [85]. Correlation functions, which show universal scaling at a nonthermal fixed point, can be obtained by functional differentiation of the generating functional with respect to corresponding sources. To calculate such observables at some instant in time, the system is evolved along a Schwinger-Keldysh closed time path which reflects the nature of nonequilibrium QFT as an initial value problem. This is in contrast to equilibrium QFT, where only asymptotic input and output states are used. The initial configuration of the out-of equilibrium system is contained in the initial density matrix which enters the generating functional. In the majority of cases it is sufficient to choose the initial density matrix to be Gaussian. Calculating the nonequilibrium generating functional in its most general formulation is highly nontrivial and generally cannot be done analytically.

To study the universal scaling behavior at nonthermal fixed points, we focus on the evolution of two-point correlators. From these, e.g., (quasi)particle occupation numbers in momentum space can be derived if the system is, on average, spatially translation invariant. Taking the Schwinger-Keldysh description one derives dynamical equations for unequal-time two-point correlators, called Kadanoff-Baym equations [87]. These functional integro-differential equations describe the nonequilibrium dynamics of a two-point correlation function exactly but are extremely nontrivial. In order to make some computations, at least numerically, one has to truncate the infinite series of diagrams entering the appropriate self-energy. Nevertheless, even in this case, the resulting equations are generically too complicated for an analytical treatment, and one is thus held to reduce the complexity of the problem and to obtain approximate dynamical equations that are capturing the physics relevant at a nonthermal fixed point. It turns out that a *kinetic theory* approach provides such an approximation, see, e.g., [56, 85, 88].

Using a kinetic-theory description enables us to perform a scaling analysis, from which the scaling exponents associated with the nonthermal fixed point can be predicted analytically. Within kinetic theory, the object of interest is the occupation number distribution $n(t, \mathbf{k}) = \left\langle \hat{\Psi}^\dagger(t, \mathbf{k}) \hat{\Psi}(t, \mathbf{k}) \right\rangle$, where for definiteness we consider a nonrelativistic Bose gas system, with $\hat{\Psi}$ being its field operator. Within he kinetic framework, the time evolution of $n(t, \mathbf{k})$ is described in terms of a generalized *quantum Boltzmann equation (QBE)*

$$\partial_t n(t, \mathbf{k}) = I[n](t, \mathbf{k}) \,, \tag{2.3}$$

where $I[n](t, \mathbf{k})$ is a scattering integral. Restricting ourselves to the case of elastic $2 \leftrightarrow 2$ scatterings, the latter takes the form

$$I[n](t, \mathbf{k}) = \int_{\mathbf{pqr}} |T_{\mathbf{kpqr}}|^2 \, \delta(\mathbf{k} + \mathbf{p} - \mathbf{q} - \mathbf{r}) \, \delta(\omega_{\mathbf{k}} + \omega_{\mathbf{p}} - \omega_{\mathbf{q}} - \omega_{\mathbf{r}})$$
$$\times \, [(n_{\mathbf{k}} + 1)(n_{\mathbf{p}} + 1)n_{\mathbf{q}}n_{\mathbf{r}} - n_{\mathbf{k}}n_{\mathbf{p}}(n_{\mathbf{q}} + 1)(n_{\mathbf{r}} + 1)] \,. \qquad (2.4)$$

with $T_{\mathbf{kpqr}}$ being the scattering T-matrix. The collision kernel (2.4) describes the redistribution of the occupations $n_{\mathbf{k}}$ of momentum modes $\mathbf{k}$ with eigenfrequency $\omega_{\mathbf{k}}$ due to elastic $2 \leftrightarrow 2$ collisions. In presence of a Bose condensate, the occupation numbers describe quasiparticle excitations. This modifies the scattering matrix and the mode eigenfrequencies. Here, we consider transport entirely within the range of a fixed scaling of the dispersion $\omega_{\mathbf{k}} \sim k^z$, with dynamical scaling exponent z, such that processes leading to a change in particle number are suppressed. The collective scattering effects beyond $2 \leftrightarrow 2$ processes can be captured in the T-matrix using, e.g., resummation techniques (see Sec. 2.2.1).

Two classical limits of the QBE scattering integral $I[n](t, \mathbf{k})$ exist. The usual Boltzmann integral for classical particles is obtained in the limit of $n(t, \mathbf{k}) \ll 1$. In case of large occupation numbers $n(t, \mathbf{k}) \gg 1$, termed *classical-wave limit*, the scattering integral reads

$$I[n](t, \mathbf{k}) = \int_{\mathbf{pqr}} |T_{\mathbf{kpqr}}|^2 \, \delta(\mathbf{k} + \mathbf{p} - \mathbf{q} - \mathbf{r}) \, \delta(\omega_{\mathbf{k}} + \omega_{\mathbf{p}} - \omega_{\mathbf{q}} - \omega_{\mathbf{r}})$$
$$\times \, [(n_{\mathbf{k}} + n_{\mathbf{p}})n_{\mathbf{q}}n_{\mathbf{r}} - n_{\mathbf{k}}n_{\mathbf{p}}(n_{\mathbf{q}} + n_{\mathbf{r}})] \,. \qquad (2.5)$$

The QBE then reduces to the *wave-Boltzmann equation (WBE)*, which is subject of the following discussion as we are interested in the universal dynamics of a near-degenerate Bose gas obeying $n(t, \mathbf{k}) \gg 1$ within the relevant momentum regime.

2.2.1   Properties of the scattering integral and the T-matrix

In the kinetic approximation, scaling features of the system at a nonthermal fixed point are directly encoded in the properties of the scattering integral. For a general treatment that governs the cases of presence and absence of a condensate density, we focus on the scaling of the distribution of quasiparticles, in the following denoted by $n_Q(\mathbf{k})$, instead of the single-particle momentum distribution $n(\mathbf{k})$. Note that in case of free particles, with dispersion $\omega(k) = k^2/2m \sim k^z$, i.e., dynamical exponent $z = 2$, we obtain $n_Q \equiv n$. For Bogoliubov sound with dispersion $\omega(k) = c_s k$ and thus $z = 1$, the scaling of n_Q differs from the scaling of n due to the k-dependent Bogoliubov mode functions characterizing the transformation between the particle and quasiparticle basis, $n(\mathbf{k}) \simeq (g\rho_0/c_s k)n_Q(\mathbf{k})$, for $k \to 0$, in general $n(\mathbf{k}) \sim k^{z-2+\eta}n_Q(\mathbf{k})$, with anomalous exponent η. Here, c_s denotes the speed of sound of the Bogoliubov excitations and ρ_0 is the condensate density.

Using a positive, real scaling factor s, the self-similar evolution of the quasiparticle distribution at a nonthermal fixed point reads

$$n_Q(t, \mathbf{k}) = s^{\alpha/\beta} n_Q \left(s^{-1/\beta} t, s\mathbf{k}\right). \tag{2.6}$$

We remark that by choosing the scaling parameter $s = (t/t_{\mathrm{ref}})^\beta$ one obtains the scaling form stated in the example in Sec. 2.1.

As the scattering integral, in the classical-wave limit, is a homogeneous function of momentum and time, it obeys scaling, provided the scaling of the quasiparticle distribution in (2.6), according to

$$I[n_Q](t, \mathbf{k}) = s^{-\mu} I[n_Q](s^{-1/\beta} t, s\mathbf{k}), \tag{2.7}$$

with scaling exponent $\mu = 2(d + m) - z - 3\alpha/\beta$. Here, m is the scaling dimension of the modulus of the T-matrix

$$|T(\mathbf{k}, \mathbf{p}, \mathbf{q}, \mathbf{r}; t)| = s^{-m} |T(s\mathbf{k}, s\mathbf{p}, s\mathbf{q}, s\mathbf{r}; s^{-1/\beta} t)|. \tag{2.8}$$

At a fixed instance in time, the T-matrix can have a purely spatial momentum scaling form. Consider a simple example of a universal quasiparticle distribution at a fixed time t_0, which, at least in a limited regime of momenta, shows power-law scaling,

$$n_Q(s\mathbf{k}) = s^{-\kappa} n_Q(\mathbf{k}), \tag{2.9}$$

with fixed-time momentum scaling exponent κ. The T-matrix is then expected to scale as

$$|T(\mathbf{k}, \mathbf{p}, \mathbf{q}, \mathbf{r}; t_0)| = s^{-m_\kappa} |T(s\mathbf{k}, s\mathbf{p}, s\mathbf{q}, s\mathbf{r}; t_0)|, \tag{2.10}$$

with m_κ being, in general, different from m. Note that Eq. (2.9) in realistic cases is regularized by an IR cutoff k_Λ or, respectively, a UV cutoff k_λ to ensure that the scattering integral stays finite in the limit $k \gg k_\Lambda$ or $k \ll k_\lambda$.

Generally, the scaling hypothesis for the T-matrix, Eq. (2.8), does not hold over the whole range of momenta. In fact, scaling, with different exponents, is found within separate limited scaling regions, which we discuss in the following.

Perturbative region: two-body scattering

For the non-condensed, weakly interacting Bose gas away from unitarity the T-matrix is well approximated by

$$|T_{\mathbf{kpqr}}|^2 = (2\pi)^4 g^2. \tag{2.11}$$

As the matrix elements are momentum independent we obtain $m_\kappa = m = 0$. It can be shown that Eq. (2.11) represents the leading perturbative approximation of the full momentum-dependent many-body coupling function.
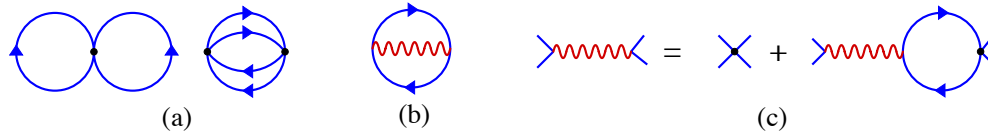
Figure 2.3. Graphical representation of the resummation scheme. (a) The two lowest-order diagrams of the loop expansion of the two-particle irreducible effective $\Gamma[\phi, G]$ (see Sec. 3.1.4) that lead to the quantum Boltzmann equation with perturbative T-matrix (2.11) or (2.12). Solid lines represent the full propagator $G(x, y)$, black dots the bare vertex $\sim g\delta(x - y)$. (b) Diagram representing the resummation approximation which replaces the diagrams in (a) within the IR regime of momenta and gives rise to the modified scaling of the T-matrix. (c) The wiggly line is the effective coupling function entering the T-matrix, which corresponds to a sum of bubble-chain diagrams. Figure taken from [57].

In presence of a condensate density $\rho_0 \leq \rho$, sound wave excitations become relevant below the healing-length momentum scale $k_\xi = \sqrt{2g\rho_0 m}$. Within leading-order perturbative approximation, the elastic scattering of these sound waves is described by the T-matrix

$$|T_{\mathbf{kpqr}}|^2 = (2\pi)^4 \frac{(mc_s)^4}{kpqr} \frac{3g^2}{2} . \tag{2.12}$$

Here, the speed of sound of the quasiparticle excitations c_s is given by $mc_s = k_\xi/\sqrt{2} = \sqrt{g\rho_0 m}$. For the Bogoliubov sound we obtain the scaling exponents $m_\kappa = m = -2$.

The above perturbative results are in general applicable to the UV range of momenta. However, scaling behavior in the far IR regime, where the momentum occupation numbers grow large, requires an approach beyond the leading-order perturbative approximation as contributions to the scattering integral of order higher than g^2 (i.e., collective phenomena) are no longer negligible.

Collective scattering: nonperturbative many-body T-matrix

To do so, one uses a nonperturbative s-channel loop resummation scheme, which is typically derived within a 2PI effective action formalism (see Sec. 3.1.4). The resummation procedure is schematically depicted in Fig. 2.3. It is equivalent to a large-N approximation at next-to-leading order and enables to calculate an effective momentum-dependent coupling constant $g_{\text{eff}}(k)$ which replaces the bare coupling g. The effective coupling also changes the scaling exponent m of the T-matrix within the IR regime of momenta. In particular, $g_{\text{eff}}(k)$ becomes suppressed in the IR to below its bare value g. This ultimately leads to an even steeper rise of the (quasi)particle spectrum.

For free particles ($z = 2$) in $d = 3$ dimensions one obtains

$$|T_{\mathbf{kpqr}}| = (2\pi)^4 g_{\text{eff}}^2(\varepsilon_{\mathbf{k}} - \varepsilon_{\mathbf{r}}, \mathbf{k} - \mathbf{r}), \tag{2.13}$$
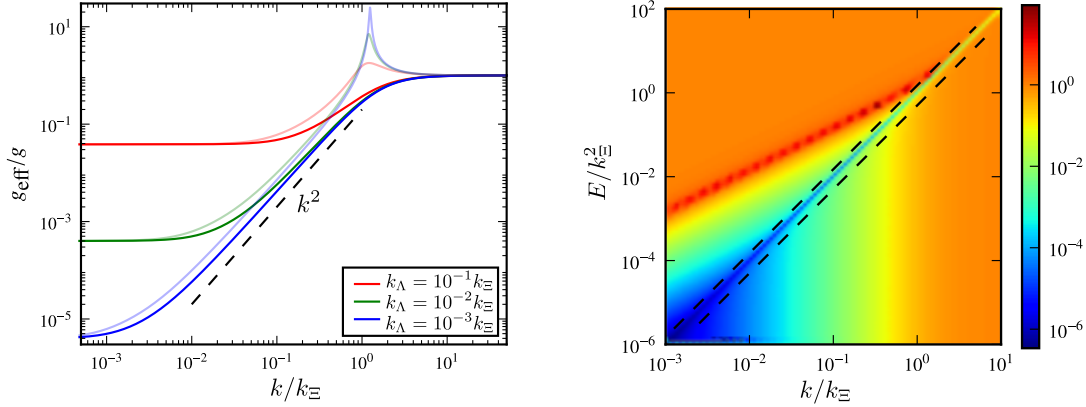
Figure 2.4. *Left panel:* Effective coupling $g_{\text{eff}}(k_0, k)/g$ in $d = 3$ dimensions as a function of the spatial momentum $k = |\mathbf{k}|$, on a double-logarithmic scale. The graph shows cuts along $k_0 = 0.5\varepsilon_{\mathbf{k}}$ (dark solid lines) and $k_0 = 1.5\varepsilon_{\mathbf{k}}$ (transparent solid lines), where $\varepsilon_{\mathbf{k}} = |\mathbf{k}|^2/2m$. Different colors correspond to different IR cutoffs k_Λ which are set by the scaling form of the occupation number distribution entering the nonperturbative coupling function. All momenta are measured in units of the 'healing'-length momentum scale $k_\Xi = (2g\rho_{\text{nc}}m)^{1/2}$ of the non-condensed particle density ρ_{nc} under $n(k)$. k_Ξ sets the scale separating the perturbative region at large momenta from the nonperturbative collective-scattering region within which the coupling assumes the form given in Eq. (2.15). *Right panel:* Contour plot of the effective coupling function $g_{\text{eff}}(k_0, k)/g$ as a function of $E = 2mk_0$ and momentum $k = |\mathbf{k}|$. The data is depicted for $k_\Lambda = 10^{-3}k_\Xi$. The two cuts shown in the left panel correspond to the black dashed lines. The quasiparticle distribution $n_Q(k) \equiv n(k)$ was chosen to scale with $\kappa = 3.5$ such that we are in a regime where the effective coupling assumes the universal scaling form (2.15). Figures adapted from [57].

where $\varepsilon_{\mathbf{k}} - \varepsilon_{\mathbf{r}}$ and $\mathbf{k} - \mathbf{r}$ are the energy ($\varepsilon_{\mathbf{k}} = |\mathbf{k}|^2/2m$) and momentum transfer in a scattering process, respectively.

The resulting momentum-dependent effective coupling function $g_{\text{eff}}(k_0, \mathbf{k})$ along two exemplary cuts $k_0 = 0.5\varepsilon_{\mathbf{k}}$ and $k_0 = 1.5\varepsilon_{\mathbf{k}}$ in frequency-momentum space, for three different IR cutoffs k_Λ, is shown in the left panel of Fig. 2.4.

At large momenta, the effective coupling is constant and agrees with the perturbative result, i.e., one finds $g_{\text{eff}} = g$. However, below the characteristic momentum scale $k_\Xi = \sqrt{2g\rho_{\text{nc}}m}$, the effective coupling deviates from the bare coupling g. Within a momentum range of

$$k_\Lambda \ll k \ll k_\Xi, \qquad (2.14)$$

the effective coupling is found to assume the universal scaling form

$$g_{\text{eff}}(k_0, \mathbf{k}) \simeq \frac{|\varepsilon_{\mathbf{k}}^2 - k_0^2|}{2\rho_{\text{nc}}\varepsilon_{\mathbf{k}}}, \qquad (\kappa > 3) \qquad (2.15)$$

independent of both, the microscopic interaction constant g, and the particular value of the scaling exponent κ of n_Q. Here, $\rho_{\mathrm{nc}} = \rho_{\mathrm{tot}} - \rho_0$ denotes the non-condensed particle density. Below the IR cutoff, i.e., for momenta $k < k_\Lambda$, the effective coupling becomes constant again. The dependence of the scaling form (2.15) on $E = 2mk_0$ and k is visualized in the right panel of Fig. 2.4.

It should be emphasized that the simple universal form of the effective coupling (2.15) only requires a sufficiently steep power-law scaling of the quasiparticle distribution $n_Q(k) \sim k^{-\kappa}$ and an IR regularization k_Λ ensuring finite particle number.

Making use of the scaling properties of the effective coupling,

$$g_{\mathrm{eff}}(k_0, \mathbf{k}) = s^{-\gamma_\kappa} g_{\mathrm{eff}}(s^z k_0, s\mathbf{k}) , \tag{2.16}$$

we obtain $\gamma_\kappa = 0$ in the perturbative regime and $\gamma_\kappa = 2$ in the collective-scattering regime for free particles with $z = 2$. Together with (2.13) this yields the corresponding scaling exponent of the T-matrix to be $m_\kappa = 2$. The same analysis of the effective coupling can be performed for the Bogoliubov dispersion with $z = 1$. In contrast to free particles the scaling exponent of the T-matrix reads $m_\kappa = 0$, see [57] for details.

2.2.2 Scaling analysis of the kinetic equation

We are now in the position to determine the scaling properties of the Bose gas at a nonthermal fixed point. Here, we focus on the case of a bi-directional self-similar evolution as obtained after performing a strong cooling quench, recall the example introduced in Sec. 2.1. For a detailed discussion of the scaling behavior occurring after weak cooling quenches, where only a few of the high-energy particles in the thermal tail are removed from the system, we also refer to [57].

To quantify the momentum exponent κ leading to a bi-directional scaling evolution we study the scaling of the quasiparticle distribution at a fixed evolution time as stated in (2.9). As the density of quasiparticles

$$\rho_Q = \int \frac{\mathrm{d}^d k}{(2\pi)^d} n_Q(\mathbf{k}) \tag{2.17}$$

and the energy density

$$\epsilon_Q = \int \frac{\mathrm{d}^d k}{(2\pi)^d} \omega_Q(\mathbf{k}) n_Q(\mathbf{k}) \tag{2.18}$$

are physical observables, they must be finite. Let us assume that the momentum distribution is isotropic, i.e., $n_Q(\mathbf{k}) \equiv n_Q(k)$, and given by a bare power-law scaling $n_Q \sim k^{-\kappa}$. The exponent κ then determines whether the IR or the UV regime dominates quasiparticle and energy densities. For a bi-directional self-similar evolution the quasiparticle density has to

dominate the IR and the energy density the UV, due to their different scaling with k. Hence, the scaling exponent κ has to fulfill

$$d \leq \kappa \leq d + z \,. \tag{2.19}$$

Note that, for ρ_Q and ϵ_Q to be finite, the quasiparticle distribution requires regularizations in the IR and the UV limits in that case as already introduced before in terms of k_Λ and k_λ, respectively.

According to the scaling hypothesis the time evolution of the quasiparticle distribution is captured by (2.6), with universal scaling exponents α and β. Global conservation laws strongly constrain the form of the correlations in the system and the ensuing dynamics and thus play a crucial role for the possible scaling phenomena as they imply scaling relations between the exponents α and β. Conservation of the total quasiparticle density (2.17) requires

$$\alpha = d\beta \,. \tag{2.20}$$

Analogously, if the dynamics conserves the energy density (2.18), the relation

$$\alpha = (d + z)\beta \tag{2.21}$$

has to be fulfilled.

Obviously, the scaling relations (2.20)) and (2.21) cannot both be satisfied for nonzero α and β if $z \neq 0$. This leaves us with two possibilities: Either $\alpha = \beta = 0$ or the scaling hypothesis (2.6) has to be extended to allow for different rescalings of the IR and the UV parts of the scaling function. In the following, we denote IR exponents with α, β and UV exponents with α', β', respectively. Making use of the global conservation laws as well as of the power-law scaling of the quasiparticle distribution, $n_Q \sim k^{-\kappa}$, one finds the scaling relations

$$\alpha = d\beta \,, \tag{2.22a}$$
$$(d + z - \kappa)\beta' = (d - \kappa)\beta \,. \tag{2.22b}$$

This implies $\beta\beta' \leq 0$, i.e., the IR and UV scales k_Λ and k_λ rescale in opposite directions. We remark that these relations hold in the limit of a large scaling region of momenta, i.e., for $k_\Lambda \ll k_\lambda$. Note that energy conservation only affects the UV shift with exponent β', (2.22b), while particle conservation gives the relation (2.22a) for the exponent β in the IR.

With this at hand we are finally able to derive analytical expressions for the scaling exponents based on the kinetic theory approach. Performing the s-channel loop-resummation, the effective coupling g_{eff} can be expressed by the retarded one-loop self-energy Π^R, which is defined in terms of the statistical and spectral function encoding the mode occupations

and, respectively, the dispersion relation as well as the density of states of the system. The aforementioned anomalous dimension η appears as a scaling dimension of the spectral function. The particle and quasiparticle distributions are obtained by frequency integrations over the statistical function. The resulting, most general scaling relations for the (quasi)particle distributions then read

$$n_Q(t, \mathbf{k}) = s^{\alpha/\beta} n_Q \left(s^{-1/\beta} t, s\mathbf{k} \right), \tag{2.23a}$$

$$n_Q(t_0, \mathbf{k}) = s^{\kappa} n_Q \left(t_0, s\mathbf{k} \right), \tag{2.23b}$$

$$n(t, \mathbf{k}) = s^{\alpha/\beta - \eta + 2 - z} n \left(s^{-1/\beta} t, s\mathbf{k} \right), \tag{2.23c}$$

$$n(t_0, \mathbf{k}) = s^{\kappa - \eta + 2 - z} n \left(t_0, s\mathbf{k} \right) = s^{\zeta} n \left(t_0, s\mathbf{k} \right). \tag{2.23d}$$

To show possible differences in the scaling behavior of the particle and quasiparticle distributions we added the relations for the particle distribution which scales as $n(\mathbf{k}) \sim k^{z-2+\eta} n_Q(\mathbf{k})$ relative to the quasiparticle number, see beginning of Sec. 2.2.1. Note that the momentum scaling of $n(\mathbf{k})$ is characterized by the scaling exponent ζ according to (2.23d).

Zeroes of the scattering integral in the kinetic equation correspond to fixed points of the time evolution. From a scaling analysis of the QBE one obtains the scaling relation

$$\alpha = 1 - \beta\mu. \tag{2.24}$$

Making use of the scaling of the T-matrix within the different momentum regimes as well as the global conservation laws of the system, one finds the scaling exponents by means of simple power counting to be

$$\alpha = d/z, \quad \beta = 1/z, \tag{2.25a}$$

$$\alpha' = \beta'(d + z), \quad \beta' = \beta(3z - 4 + 2\eta)(z - 4 - 2\eta)^{-1}, \tag{2.25b}$$

$$\kappa = d + (3z - 4)/2 + \eta, \quad \zeta = d + z/2. \tag{2.25c}$$

On the grounds of numerical simulations in [89], the IR scaling exponent $\beta = 1/z$ has been proposed. Note that the exponents stated in (2.25b) are usually not observed as the UV region is dominated by a near-thermalized tail. During the early-time evolution after a strong cooling quench, an exponent $\zeta \simeq d + 1$ was seen in semi-classical simulations for $d = 3$ in [55] and [64], for $d = 2$ in [67], and for $d = 1$ in .[2] Numerical implementation of the kinetic equation in $d = 3$ dimensions also resulted in $\kappa \simeq 4$, see [90]. For a single-component Bose gas in $d = 3$ dimensions, the IR scaling exponents have recently been numerically

---

[2]In fact, in numerical simulations, one often observes the exponent to be close to $d + 2$ rather than $d + 1$, see [60, 67]. At least for the case of a nonrelativistic single-component Bose gas, this can be related to vortex scaling (in $d = 2$ and 3 spatial dimensions), as discussed in [67]. In these studies, scaling with $d + 1$ was only observed in the compressible component when the incompressible component had become subdominant after the decay of the last vortex pair/ring.

determined to be $\alpha = 1.66(12)$, $\beta = 0.55(3)$, in agreement with the analytically predicted values [55].

For the Bose gas, the above stated exponents are expected to be valid in $d = 3$ dimensions as well as in $d = 2$. The one-dimensional case is rather different due to kinematic constraints on elastic $2 \leftrightarrow 2$ scattering from energy and particle-number conservation. As a final remark, it should be noted that the development of nonlinear and topological excitations in combination with strong phase coherence is likely to modify the results presented, potentially through an appropriate modification of the scaling exponents z and η.

As a closing remark, let us notice that, while in the above discussion collective phenomena that modify the properties of the scattering matrix were taken into account by means of a coupling resummation scheme, there are alternative approaches available. For example, one can think of an idea to reformulate the theory in terms of new degrees of freedom in the first place, such that the resulting description becomes more easy to treat in nonperturbative regions. Since the nonperturbative behavior appears at low momentum scales, it is suggestive to use a *low-energy effective field theory (LEEFT)* approach [91, 92]. This typically implies a choice of suitable degrees of freedom describing the physics occurring below a chosen energy scale. In [64], this idea was implemented to described nonthermal fixed points in a U(N)-symmetric multicomponent Bose gas. Remarkably, the IR scaling exponents derived within the effective-field-theory approach indeed reproduced the exponents (2.25a) and (2.25c) obtained by performing an s-channel ($1/N$) resummation.

Chapter 3

Introduction to functional methods in nonequilbrium quantum field theory

The aim of this section is to provide a brief overview of some theoretical tools that we will employ for studying universal scaling dynamics of far-from-equilibrium quantum many-body systems. We first give a quick introduction to the general framework of nonequilibrium quantum field theory. We recall how a general quantum-mechanical system can be described in terms of a functional integral over classical variables and show what specifics emerge in the nonequilibrium case. We then discuss the structure of correlation functions out of equilibrium and show how they can be extracted from various generating functionals. The second part is dedicated to constraints on the structure of these functionals that follow from symmetries and causality. Finally, we present the framework of the (functional) renormalization group, a natural language of scaling phenomena.

3.1 Nonequilibrium quantum field theory

The description of any nonequilbrium quantum system consists of two main ingredients. First, one typically needs to specify an *initial condition* at some fixed time t_0. This can be done via a *density operator* $\hat{\rho}(t_0) \equiv \hat{\rho}_0$, which, in general, can correspond to either a mixed ($\text{Tr}\{\hat{\rho}_0^2\} < 1$) or a pure ($\text{Tr}\{\hat{\rho}_0^2\} = 1$) state. An equivalent way of specifying the initial state can be achieved by providing all initial *correlation functions*: one-point $\text{Tr}\{\hat{\rho}_0\hat{\varphi}(t_0, \mathbf{x})\}$, two-point $\text{Tr}\{\hat{\rho}_0\hat{\varphi}(t_0, \mathbf{x})\hat{\varphi}(t_0, \mathbf{y})\}$, etc. Here, $\hat{\varphi}(t_0, \mathbf{x})$ denotes a bosonic (real) scalar field operator defined at the spacetime point $(t_0, \mathbf{x})$.

Typically, the initial state can be well-approximated by specifying only a few lowest correlators, while the higher ones may build up during the evolution at later times $t > t_0$. In practice, one often restricts the description of the initial state to only one- and two-point correlation function. In terms of density matrix this approximation is equivalent to
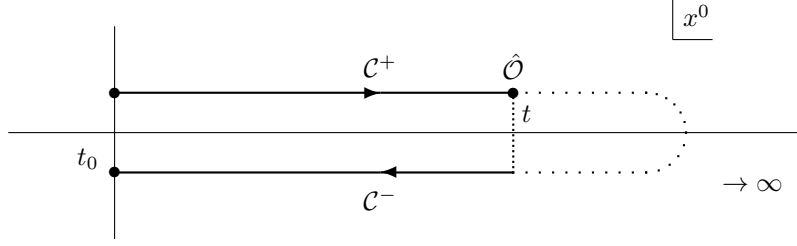
Figure 3.1. Schwinger–Keldysh contour $\mathcal{C}$. Note that, due to causality, for any n-point function with finite time arguments $t_1, \ldots, t_n$, contributions of a CTP cancel for times exceeding $t_{\max} = \max(t_1, \ldots, t_n)$.

assumption of *Gaussianity* of $\hat{\rho}_0$, see Sec. 3.1.2.

Given the initial state the subsequent time-evolution of a closed quantum system is *unitary* and entirely defined by the Hamiltonian. As we will see in the next section, this can be translated to the path-integral language with a (semi-)classical action defined on the closed time contour.

3.1.1 Path integral formalism and Schwinger–Keldysh contour

Perhaps, the main goal of any quantum field theory is providing the expectation values of observables. The latter typically take a form

$$\left\langle \hat{\mathcal{O}}(x_1) \ldots \hat{\mathcal{O}}(x_n) \right\rangle = \mathrm{Tr}\left\{ \hat{\rho}_0 \, \hat{\mathcal{O}}(x_1) \ldots \hat{\mathcal{O}}(x_n) \right\}, \tag{3.1}$$

with $\hat{\mathcal{O}}(x)$ being some local operator at the spacetime point $x = (x^0, \mathbf{x})$. Here, we have adopted the Heisenberg picture, in which observables are represented by time-dependent operators, whereas the density matrix does not evolve in time.

In most cases, observables of interest can be constructed from linear combinations of products of field operators $\hat{\varphi}$. The problem therefore reduces to finding the expectation value of such products. They, in turn, can be conveniently extracted from the so-called *generating functional* for correlation functions

$$Z[J; \hat{\rho}_0] = \mathrm{Tr}\left\{ \hat{\rho}_0 \mathcal{T}_{\mathcal{C}} \exp\left(\mathrm{i} \int_{x,\mathcal{C}} J(x)\hat{\varphi}(x) \right) \right\}, \tag{3.2}$$

where $J(x)$ represents a classical source and $\hat{\rho}_0$ is assumed to be properly normalized, $\mathrm{Tr}\{\hat{\rho}_0\} = 1$. The symbol $\mathcal{C}$ appearing in the integration limit indicates that the integration goes along the *closed time (Schwinger–Keldysh) contour*, which we will discuss shortly. One should furthermore note presence of the *time-ordering operator* $\mathcal{T}_{\mathcal{C}}$, which corresponds to the usual time ordering along the positive branch $\mathcal{C}^+$ and reversed ordering along the negative piece $\mathcal{C}^-$. As a result, (3.2) generates time-ordered correlation functions.

Let us first address the origin of the Schwinger–Keldysh contour. To that end, consider the expectation value

$$\left\langle \hat{\mathcal{O}}_{\mathcal{H}}(x) \right\rangle = \mathrm{Tr}\Big\{ \hat{\rho}_0 \hat{\mathcal{O}}_{\mathcal{H}}(x) \Big\}, \tag{3.3}$$

where we introduced the subscript $\mathcal{H}$ to emphasize that we work in the Heisenberg picture. The time dependence of operators is given by

$$\hat{\mathcal{O}}_{\mathcal{H}}(x) = U^{\dagger}(t, t_0)\hat{\mathcal{O}}(\mathbf{x})U(t, t_0), \tag{3.4}$$

with the time evolution operator $U(t, t_0) = \mathcal{T} \exp\left[-\mathrm{i}\int_{t_0}^{t} dt'\, \hat{H}(t')\right] = U^{\dagger}(t_0, t)$, so that (3.3) can be rewritten as

$$\left\langle \hat{\mathcal{O}}_{\mathcal{H}}(x) \right\rangle = \mathrm{Tr}\Big\{ \hat{\rho}_0 U^{\dagger}(t, t_0)\hat{\mathcal{O}}(\mathbf{x})U(t, t_0) \Big\}. \tag{3.5}$$

Inserting the identity operator $U(t, +\infty)U(+\infty, t) = \mathbb{1}$ and using $U(t_0, t)U(t, +\infty) = U(t_0, +\infty)$ one immediately finds

$$\left\langle \hat{\mathcal{O}}(x) \right\rangle = \mathrm{Tr}\Big\{ U(t_0, +\infty)\, U(+\infty, t)\, \hat{\mathcal{O}}(\mathbf{x})U(t, t_0)\, \hat{\rho}_0 \Big\}, \tag{3.6}$$

where we have suppressed the $\mathcal{H}$ subscript on the left-hand side since an expectation value of any observable is picture-independent. The expression under the trace in (3.6) describes (reading from right to left) the evolution from $t = t_0$, at which the initial state is specified, towards t, where the observable is computed, until $t = +\infty$, at which point it 'turns back' to $t = t_0$. Such a closed time path (CTP), known as the Schwinger–Keldysh contour, is schematically depicted in Fig. 3.1. In the literature, one can often find the definition of the CTP with $t = -\infty$ and/or $\hat{\rho}_0 = \hat{\rho}^{(eq)}$. In the latter case, the equilibrium density matrix $\rho^{(eq)} = Z_{\beta}^{-1}e^{-\beta\hat{H}}$ can be interpreted as an evolution along the imaginary time branch from t_0 to $t_0 - \mathrm{i}\beta$ leading to an additional piece of the Schwinger–Keldysh contour.

We are now set to derive a functional-integral representation of the generating functional $Z[J; \hat{\rho}_0]$. To that end, we define the eigenstates of the field operator $\hat{\varphi}^{\pm}$ at a reference time t_0,

$$\hat{\varphi}^{\pm}(t_0, \mathbf{x}) \left| \varphi^{\pm} \right\rangle = \varphi_0^{\pm}(\mathbf{x}) \left| \varphi^{\pm} \right\rangle, \tag{3.7}$$

where $\pm$ indicates on which piece $\mathcal{C}^{\pm}$ of the contour t_0 is located, i.e.,

$$\mathcal{O}(x) = \begin{cases} \mathcal{O}^{+}, & \text{if } x^0 \in \mathcal{C}^{+} \\ \mathcal{O}^{-}, & \text{otherwise.} \end{cases} \tag{3.8}$$

This allows to rewrite (3.2) as

$$Z[J; \hat{\rho}_0] = \int [d\varphi_0^{+}] \left\langle \varphi^{+} \right| \hat{\rho}_0 \mathcal{T}_{\mathcal{C}} \exp\left[\mathrm{i}\int_{x,\mathcal{C}} J(x)\hat{\varphi}(x) \right] \left| \varphi^{+} \right\rangle, \tag{3.9}$$

with the integration measure $[d\varphi_0^{\pm}] \equiv \prod_{\mathbf{x}} d\varphi_0^{\pm}(\mathbf{x})$. Inserting the identity operator $\mathbb{1} = \int [d\varphi_0^-] |\varphi^-\rangle\langle\varphi^-|$ one readily obtains

$$Z[J; \hat{\rho}_0] = \int [d\varphi_0^+][d\varphi_0^-] \langle\varphi^+| \hat{\rho}_0|\varphi^-\rangle \left(\varphi^-, t_0|\varphi^+, t_0\right)_J, \tag{3.10}$$

where

$$\left(\varphi^-, t_0|\varphi^+, t_0\right)_J = \langle\varphi^-| \mathcal{T}_{\mathcal{C}} \exp\left[\mathrm{i}\int_{x,\mathcal{C}} J(x)\hat{\varphi}(x)\right]|\varphi^+\rangle \tag{3.11}$$

is the transition amplitude in the presence of the source J. Same as in the standard vacuum quantum field theory, this amplitude can be written as a path integral over classical fields $\varphi(x)$ with the corresponding (semi-)classical action $S[\varphi]$:

$$\left(\varphi^-, t_0|\varphi^+, t_0\right)_J = \int_{\varphi_0^+}^{\varphi_0^-} \mathcal{D}'\varphi \exp\left[\mathrm{i}S[\varphi] + \mathrm{i}\int_{x,\mathcal{C}} J(x)\varphi(x)\right]. \tag{3.12}$$

Here, the prime symbol in $\mathcal{D}'\varphi$ represents the fact that integration over fields at t_0 is excluded, while the integration limits denote that the boundary condition $\varphi^{\pm}(t_0, \mathbf{x}) = \varphi_0^{\pm}(\mathbf{x})$ has to be satisfied. The (semi-)classical action is given by integrating the appropriate Lagrangian density over the closed time contour:

$$S[\varphi] = \int_{\mathcal{C}} \mathrm{d}x^0 \int \mathrm{d}^d\mathbf{x}\, \mathcal{L}[\varphi] = \int_{t_0} \mathrm{d}x^0 \int \mathrm{d}^d\mathbf{x}\, \left(\mathcal{L}\left[\varphi^+\right] - \mathcal{L}\left[\varphi^-\right]\right). \tag{3.13}$$

With that, we may finally express the generating functional $Z[J; \hat{\rho}_0]$ in terms of a path integral as

$$Z[J; \hat{\rho}_0] = \underbrace{\int [d\varphi_0^+][d\varphi_0^-] \langle\varphi^+| \hat{\rho}_0 |\varphi^-\rangle}_{\text{initial conditions}} \underbrace{\int_{\varphi_0^+}^{\varphi_0^-} \mathcal{D}'\varphi\, \mathrm{e}^{\mathrm{i}\left\{S[\varphi] + \int_{x,\mathcal{C}} J(x)\varphi(x)\right\}}}_{\text{quantum dynamics}}. \tag{3.14}$$

Note how this expression visualizes the two main ingredients of nonequilibrium quantum field theory: statistical fluctuations captured by averaging over the initial density matrix $\hat{\rho}_0$ and quantum fluctuations encoded in the functional integral with the action $S[\varphi]$.

As a final remark, let us mention that it is customary to introduce a 'metric' $c_{ab} = \mathrm{diag}(1, -1)$ that reflects the structure of the Schwinger-Keldysh contour. The source term then, for example, can be written as

$$\int_{x,\mathcal{C}} J(x)\varphi(x) = \int_{x,t_0} \left[J^+(x)\varphi^+(x) - J^-(x)\varphi^-(x)\right] = \int_{x,t_0} J_a(x)\varphi^a(x), \tag{3.15}$$

where we have used $J_+(x) = J^+(x)$ and $J_-(x) = -J^-(x)$.

3.1.2 Initial conditions

As it was already mentioned in the beginning, one of the key ingredients for describing the evolution of quantum many-body systems is a specification of the initial conditions. The most general density matrix reads

$$\left\langle \varphi^+ \right| \hat{\rho}_0 \left| \varphi^- \right\rangle = \mathcal{N} e^{i h_{\mathcal{C}}[\varphi]} , \tag{3.16}$$

where $\mathcal{N}$ is a normalization prefactor and $h[\varphi]$ can be expanded in fields as

$$h_{\mathcal{C}}[\varphi] = \int_{x,\mathcal{C}} \alpha_1(x)\, \varphi(x) + \frac{1}{2!} \int_{xy,\mathcal{C}} \alpha_2(x,y)\, \varphi(x)\varphi(y) + \dots \tag{3.17}$$

Since the initial conditions are specified at $t = t_0$, all the time integrals in (3.17) contribute only at the endpoints of $\mathcal{C}$. Therefore, the coefficients $\alpha_1(x), \alpha_2(x,y), \dots$ should vanish for $t \neq t_0$. In other words,

$$\int_{x,\mathcal{C}} \alpha_1(x)\, \varphi(x) = \int_{\mathbf{x}} \left\{ \alpha_1^+(\mathbf{x})\, \varphi_+(\mathbf{x}) + \alpha_1^-(\mathbf{x})\, \varphi_-(\mathbf{x}) \right\} , \tag{3.18a}$$

$$\int_{xy,\mathcal{C}} \alpha_2(x,y)\, \varphi(x)\, \varphi(y) = \int_{\mathbf{xy}} \left\{ \alpha_2^{++}(\mathbf{x},\mathbf{y})\, \varphi_+(\mathbf{x})\varphi_+(\mathbf{y}) + \alpha_2^{+-}(\mathbf{x},\mathbf{y})\, \varphi_+(\mathbf{x})\varphi_-(\mathbf{y}) \right.$$
$$\left. + \alpha_2^{-+}(\mathbf{x},\mathbf{y})\, \varphi_-(\mathbf{x})\varphi_+(\mathbf{y}) + \alpha_2^{--}(\mathbf{x},\mathbf{y})\, \varphi_-(\mathbf{x})\varphi_-(\mathbf{y}) \right\} , \tag{3.18b}$$

and so forth. For $\hat{\rho}_0$ to be hermitian, the coefficients $\{\alpha_i\}$ have to satisfy certain conditions: $i\alpha_{1,+} = (i\alpha_{1,-})^*$, $i\alpha_{2,++} = (i\alpha_{2,--})$, $i\alpha_{2,+-} = (i\alpha_{2,-+})^*$, etc. In addition, symmetry requirements of the initial state (both spacetime and internal) may give rise to further constraints on $\alpha_n(x_1, \dots, x_n)$.

Using the parameterization (3.17) one can rewrite the expression for generating functional (3.2) as

$$Z[J; \hat{\rho}_0] = \int \mathcal{D}\varphi\, e^{i\left\{ S[\varphi] + \int_{x,\mathcal{C}} J(x)\varphi(x) + \frac{1}{2}\int_{xy,\mathcal{C}} \varphi(x)\alpha_2(x,y)\varphi(y) + \frac{1}{3!}\int_{xyz,\mathcal{C}} \alpha_3(x,y,z)\varphi(x)\varphi(y)\varphi(z) + \dots \right\}} , \tag{3.19}$$

where we ignored the irrelevant normalization prefactor and shifted the source term $J(x) + \alpha_1(x) \to J(x)$.

A very important class of initial conditions is given by the family of Gaussian density matrices, for which $\alpha_n(x_1, \dots, x_n) \equiv 0$, $n \geq 3$. In this instance, the expression (3.19) is simplified significantly and reads

$$Z^{(\text{Gauss})}[J, R] = \int \mathcal{D}\varphi\, e^{i\left\{ S[\varphi] + \int_{x,\mathcal{C}} J(x)\varphi(x) + \frac{1}{2}\int_{xy,\mathcal{C}} \varphi(x)R(x,y)\varphi(y) \right\}} . \tag{3.20}$$

Dependence of the generating functional on the initial state then is completely determined by the initial-time linear (J) and bilinear (R) sources.

3.1.3 Correlation functions

Time-ordered correlation functions

The (nonequilibrium) generating functional introduced in the previous section plays a crucial role in (nonequilibrium) quantum field theory. It provides a very convenient way of computing time-ordered correlation functions of any order. For example, the one-point function – the *macroscopic field* $\phi(x)$ – can be obtained by differentiating $Z[J; \hat{\rho}_0]$ with respect to the source $J(x)$. Indeed,

$$\frac{\delta Z[J; \hat{\rho}_0]}{\mathrm{i}\delta J(x)}\bigg|_{J=0} = \mathrm{Tr}\{\hat{\rho}_0 \hat{\varphi}(x)\} \equiv \langle \hat{\varphi}(x) \rangle \equiv \phi(x)\,. \tag{3.21}$$

By taking further derivatives we can extract the time-ordered two-point correlator,

$$\frac{\delta^2 Z[J; \hat{\rho}_0]}{\mathrm{i}\delta J(x)\mathrm{i}\delta J(y)}\bigg|_{J=0} = \mathrm{Tr}\{\hat{\rho}_0 \mathcal{T}_C \hat{\varphi}(x)\hat{\varphi}(y)\} \equiv \langle \mathcal{T}_C \hat{\varphi}(x)\hat{\varphi}(y) \rangle\,, \tag{3.22}$$

or any higher-order correlation function $\langle \mathcal{T}_C \hat{\varphi}(x_1) \ldots \hat{\varphi}(x_n) \rangle$ in a similar fashion.

From the perspective of probability theory, the above correlation functions can be understood as the functional generalization of *moments* of a probability distribution. One disadvantage of such description is that higher-order correlators carry some information about the lower-order ones. In the diagrammatic language, this redundant information corresponds to *disconnected* diagrams contributing to higher-order correlation functions. A more economic description can be achieved by considering *connected* correlation functions, which are generated by the *Schwinger functional* $W[J; \hat{\rho}_0] = -\mathrm{i} \log Z[J; \hat{\rho}_0]$. Its first-order derivative results in a macroscopic field ϕ, as we had before:

$$\frac{\delta W[J; \hat{\rho}_0]}{\delta J(x)}\bigg|_{J=0} = -\frac{\mathrm{i}}{Z[J, \hat{\rho}_0]} \frac{\delta Z[J; \hat{\rho}_0]}{\delta J(x)}\bigg|_{J=0} = \phi(x)\,. \tag{3.23}$$

Taking one further derivative yields the *connected two-point correlator* (or the *propagator*)

$$\frac{1}{\mathrm{i}} \frac{\delta^2 W[J; \hat{\rho}_0]}{\delta J(x)\delta J(y)}\bigg|_{J=0} = \frac{\delta^2 Z[J; \hat{\rho}_0]}{\mathrm{i}\delta J(x)\mathrm{i}\delta J(y)} - \frac{\delta Z[J; \hat{\rho}_0]}{\mathrm{i}\delta J(x)} \frac{\delta Z[J; \hat{\rho}_0]}{\mathrm{i}\delta J(y)}$$
$$= \langle \mathcal{T}_C \hat{\varphi}(x)\hat{\varphi}(y) \rangle - \langle \hat{\varphi}(x) \rangle \langle \hat{\varphi}(y) \rangle \equiv G(x, y)\,, \tag{3.24}$$

which will be one of the central objects in the following discussion. By analogy, any n-point connected correlator (or the n-point *cumulant*) can be obtained by taking n functional derivatives of $W[J; \hat{\rho}_0]$ with respect to J.

Recalling the '$\pm$-notation' (3.8) established in the previous section, we can introduce additional nonequilibrium correlation functions by taking functional derivatives with respect to $J^+(x)$ and $J^-(x)$. For instance, the one-point function for vanishing sources,

$$\frac{\delta Z[J; \hat{\rho}_0]}{\mathrm{i}\delta J_\pm(x)}\bigg|_{J=0} = \mathrm{Tr}\{\hat{\rho}_0 \hat{\varphi}(x)\} \equiv \phi(x)\,, \tag{3.25}$$

is identical to the previous result (3.21) and does not depend on the choice of a branch. On contrary, the two-point correlator provides four distinct options:

$$
\frac{\delta^2 Z[J;\hat{\rho}_0]}{i\delta J_+(x) i\delta J_+(y)}\bigg|_{J=0} = \langle \hat{\varphi}(x)\hat{\varphi}(y)\rangle\, \Theta(x^0 - y^0) + \langle \hat{\varphi}(y)\hat{\varphi}(x)\rangle\, \Theta(y^0 - x^0)
$$

$$
\equiv G^{++}(x,y) + \phi(x)\phi(y)\,,
$$

$$
\frac{\delta^2 Z[J;\hat{\rho}_0]}{i\delta J_-(x) i\delta J_-(y)}\bigg|_{J=0} = \langle \hat{\varphi}(x)\hat{\varphi}(y)\rangle\, \Theta(y^0 - x^0) + \langle \hat{\varphi}(y)\hat{\varphi}(x)\rangle\, \Theta(x^0 - y^0)
$$

$$
\equiv G^{--}(x,y) + \phi(x)\phi(y)\,, \tag{3.26}
$$

$$
\frac{\delta^2 Z[J;\hat{\rho}_0]}{i\delta J_+(x) i\delta J_-(y)}\bigg|_{J=0} = \langle \hat{\varphi}(y)\hat{\varphi}(x)\rangle \equiv G^{+-}(x,y) + \phi(x)\phi(y)\,,
$$

$$
\frac{\delta^2 Z[J;\hat{\rho}_0]}{i\delta J_-(x) i\delta J_+(y)}\bigg|_{J=0} = \langle \hat{\varphi}(x)\hat{\varphi}(y)\rangle \equiv G^{-+}(x,y) + \phi(x)\phi(y)\,,
$$

where, analogously to (3.24), we adopted the notation $G^{\pm\pm}(x,y)$ to denote connected correlation functions.

In principle, any nonequilibrium two-point correlator, not only the time-ordered one, can be expressed in terms of the components (3.26). However, not all of them are independent. First of all, there is an obvious symmetry $G^{+-}(x,y) = G^{-+}(y,x)$. Furthermore, using the property $\Theta(x^0 - y^0) + \Theta(y^0 - x^0) = 1$ one can readily check that

$$
G^{++}(x,y) + G^{--}(x,y) = G^{+-}(x,y) + G^{-+}(x,y)\,. \tag{3.27}
$$

Therefore, a general propagator can be completely parameterized by two independent functions.

Statistical and spectral functions

It is often convenient to split the full propagator G into symmetric and anti-symmetric parts. To that end, we consider the expectation values of the commutator and the anti-commutator of $\hat{\varphi}$:

$$
\rho(x,y) = i\,\langle [\hat{\varphi}(x), \hat{\varphi}(y)]\rangle\,,
$$

$$
F(x,y) = \frac{1}{2}\,\langle \{\hat{\varphi}(x), \hat{\varphi}(y)\}\rangle - \phi(x)\phi(y)\,. \tag{3.28}
$$

The anti-symmetric function $\rho(x,y)$ is known as the *spectral function*, whereas the symmetric part $F(x,y)$ is called the *statistical function*. They have a simple physical interpretation: while the former carries information about the spectrum of a theory, the latter one encodes information about occupation numbers.

Since these functions play a prominent role in nonequilibrium quantum many-body dynamics, it is worth spending a bit of time discussing their properties. First, let us establish

their connection to the time-ordered propagator (3.24) introduced in the previous section:

$$\langle \mathcal{T}_C \hat{\varphi}(x) \hat{\varphi}(y) \rangle = \langle \hat{\varphi}(x) \hat{\varphi}(y) \rangle \, \Theta_C(x^0 - y^0) + \langle \hat{\varphi}(y) \hat{\varphi}(x) \rangle \, \Theta_C(y^0 - x^0)$$
$$= \frac{1}{2} \langle \{\hat{\varphi}(x), \hat{\varphi}(y)\} \rangle \left[\Theta_C(x^0 - y^0) + \Theta_C(y^0 - x^0) \right]$$
$$+ \frac{1}{2} \langle [\hat{\varphi}(x), \hat{\varphi}(y)] \rangle \left[\Theta_C(x^0 - y^0) - \Theta_C(y^0 - x^0) \right]. \tag{3.29}$$

This yields

$$G(x, y) = F(x, y) - \frac{\mathrm{i}}{2} \rho(x, y) \, \mathrm{sgn}_C(x^0 - y^0), \tag{3.30}$$

where we made use of the contour signum function $\mathrm{sgn}_C(x^0 - y^0)$. Secondly, from the definition of $\rho(x, y)$ and the commutation relations of a scalar field it readily follows that

$$\rho(x, y)|_{x^0 = y^0} = 0, \quad \partial_{x^0} \rho(x, y)|_{x^0 = y^0} = \delta(\mathbf{x} - \mathbf{y}). \tag{3.31}$$

Keldysh rotation

In the opening part of this chapter, we have demonstrated how description of a nonequilibrium quantum system gives rise to the Schwinger–Keldysh contour, effectively doubling the number of degrees of freedom: for instance, a single scalar field φ splits into two components $\varphi_\pm$ living on the opposite branches of the closed time path. In practice, however, it is often more convenient to work with another (rotated) pair of fields,

$$\begin{pmatrix} \varphi_{\mathrm{cl}} \\ \varphi_{\mathrm{q}} \end{pmatrix} = \begin{pmatrix} 1/2 & 1/2 \\ 1 & -1 \end{pmatrix} \begin{pmatrix} \varphi^+ \\ \varphi^- \end{pmatrix} \equiv A \begin{pmatrix} \varphi^+ \\ \varphi^- \end{pmatrix}, \tag{3.32}$$

called a *classical* φ_{cl} and a *quantum* φ_{q} *components* of the field, respectively. Consequently,

$$\begin{pmatrix} G_{\mathrm{clcl}} & G_{\mathrm{clq}} \\ G_{\mathrm{qcl}} & G_{\mathrm{qq}} \end{pmatrix} = A \begin{pmatrix} G^{++} & G^{+-} \\ G^{-+} & G^{--} \end{pmatrix} A^T = \begin{pmatrix} F & -\mathrm{i}G^R \\ -\mathrm{i}G^A & \tilde{F} \end{pmatrix}, \tag{3.33}$$

where $G^R(x, y) = \rho(x, y) \, \Theta(x^0 - y^0)$ and $G^A(x, y) = -\rho(x, y) \, \Theta(y^0 - x^0)$ are called the *retarded* and *advanced* propagators, respectively. Note that (3.27) implies $\tilde{F} \equiv 0$.

3.1.4 Quantum effective action

The generating functional $Z[J; \hat{\rho}_0]$ introduced in Sec. 3.1.1 is a nonequilibrium field-theoretic generalization of the thermodynamic partition function from statistical mechanics. Similarly, the Schwinger functional $W[J; \hat{\rho}_0]$ is a generalization of the Helmholtz free energy in the presence of an external source. Continuing with the ideas of statistical mechanics even

further it is then suggestive to consider the *Legendre transform* of $W[J; \hat{\rho}_0]$,[1]

$$\Gamma[\phi; \hat{\rho}_0] = W[J_\phi; \hat{\rho}_0] - \int_{x,\mathcal{C}} J_\phi(x)\phi(x), \tag{3.34}$$

which in thermodynamics would correspond to the Gibbs free energy. Here, $J_\phi(x)$ is defined as the source that extremizes the expression $W[J; \hat{\rho}_0] - \int_{x,\mathcal{C}} J(x)\phi(x)$. The resulting functional of the macroscopic field $\phi(x)$ is called the *one-particle irreducible* (1PI) *(quantum) effective action* $\Gamma[\phi; \hat{\rho}_0]$, for reasons that will become apparent shortly. It should be emphasized that, in the absence of approximations, computation of any of these generating functionals provides an exact description of the system. In this sense, they are all equivalent and any choice is only a matter of convenience.

From a physical viewpoint, the effective action can be understood as a generalization of the classical action that takes all the quantum-statistical fluctuations into account. To see this, we observe that a functional derivative of $\Gamma[\phi; \hat{\rho}_0]$ reads

$$\frac{\delta\Gamma[\phi; \hat{\rho}_0]}{\delta\phi(x)} = -J_\phi(x). \tag{3.35}$$

Here, we have used

$$J_\phi: \quad \frac{\delta W[J; \hat{\rho}_0]}{\delta J(x)}\bigg|_{J=J_\phi} = \phi(x), \tag{3.36}$$

which follows immediately from the definition (3.34). Inverting the dependence $J_\phi \to \phi_J$ we readily obtain

$$\frac{\delta\Gamma[\phi; \hat{\rho}_0]}{\delta\phi(x)}\bigg|_{\phi=\phi_J} = -J(x), \quad \frac{\delta W[J; \hat{\rho}_0]}{\delta J(x)} = \phi_J(x). \tag{3.37}$$

Therefore, ϕ_J can be identified as the expectation value $\langle\hat{\varphi}\rangle_J$ in the presence of a current J, while (3.37) can be understood as *quantum equation of motion* for a given background source J. In the following, we will often suppress the subscripts J and ϕ as well as the dependence of the generating functionals on the initial state $\hat{\rho}_0$.

Let us now discuss the objects generated by the 1PI effective action,

$$\Gamma^{(n)}(x_1, \ldots, x_n) \equiv \frac{\delta^n \Gamma[\phi]}{\delta\phi(x_1)\ldots\delta\phi(x_n)}, \tag{3.38}$$

known as the *vertex functions*, the *1PI functions* or the *1PI vertices*. To establish their relation to connected correlation functions, we first note

$$\int_y \frac{\delta^2\Gamma[\phi]}{\delta\phi(x_1)\delta\phi(y)}\frac{\delta^2 W[J]}{\delta J(y)\delta J(x_2)} = \int_y \frac{\delta}{\delta\phi(x_1)}\left(\frac{\delta\Gamma[\phi]}{\delta\phi(y)}\right)\frac{\delta}{\delta J(y)}\left(\frac{\delta W[J]}{\delta J(x_2)}\right)$$
$$= -\int_y \frac{\delta J(y)}{\delta\phi(x_1)}\frac{\delta\phi(x_2)}{\delta J(y)} = -\delta(x_1 - x_2). \tag{3.39}$$

---

[1]Following [56, 85] we adopt a slightly unusual convention of the Legendre transform when discussing nonequilibrium QFT, in which one subtracts the source term from the Schwinger functional, and not the other way around.

In other words, the two-point 1PI function is the inverse of the propagator (3.24):

$$\left(\Gamma^{(2)} \circ G\right)(x_1, x_2) \equiv \int_y \Gamma^{(2)}(x_1, y)\, G(y, x_2) = \mathrm{i}\delta(x_1 - x_2). \qquad (3.40)$$

Naturally, for multicomponent fields, spacetime arguments have to be supplemented with field-component indices. For example, a real scalar field in Keldysh basis would have a label $a \in \{\mathrm{cl}, \mathrm{q}\}$. Inverting (3.33) and using $\tilde{F} \equiv 0$ we can then read off

$$\begin{pmatrix} \Gamma^{(2)}_{\mathrm{clcl}} & \Gamma^{(2)}_{\mathrm{clq}} \\ \Gamma^{(2)}_{\mathrm{qcl}} & \Gamma^{(2)}_{\mathrm{qq}} \end{pmatrix} = \begin{pmatrix} 0 & \mathrm{i}G^{-1}_{\mathrm{qcl}} \\ \mathrm{i}G^{-1}_{\mathrm{clq}} & G^{-1}_{\mathrm{clq}} \circ F \circ G^{-1}_{\mathrm{qcl}} \end{pmatrix}. \qquad (3.41)$$

We will discuss the structure of the two-point function in more details in Sec. 3.3.1, but for now we simply note that $\Gamma^{(2)}_{\mathrm{clcl}} \equiv 0$.

For a general conversion between vertex functions and connected correlators, it is left to establish a connection between J-derivatives and ϕ-derivatives:

$$\frac{\delta}{\delta J(x)} = \int_y \frac{\delta\phi(y)}{\delta J(x)} \frac{\delta}{\delta\phi(y)} = \mathrm{i}\int_y G(x, y)\frac{\delta}{\delta\phi(y)}, \qquad (3.42)$$

where we have used that $\phi(x) = W^{(1)}(x)$ such that $\delta\phi(y)/\delta J(x) = W^{(2)}(x, y)$. Therefore,

$$W^{(n)}(x_1, \ldots, x_n) = \prod_{i=1}^{n-1} \int_{x_i'} \left(\mathrm{i}G(x_i, x_i')\frac{\delta}{\delta\phi(x_i')}\right)\phi(x_n). \qquad (3.43)$$

For example, the four-point function takes the form

$$W^{(4)}(x_1, \ldots, x_4) = \left(\prod_{i=1}^{4} \int_{x_i'} G(x_i, x_i')\right)\left\{ -\Gamma^{(4)}(x_1', \ldots, x_4') \right.$$
$$\left. + \mathrm{i}\left[\int_{y,z} \Gamma^{(3)}(x_1', x_2', y)\, G(y, z)\, \Gamma^{(3)}(z, x_3', x_4') + \begin{pmatrix} 2 \leftrightarrow 3 \\ 2 \leftrightarrow 4 \end{pmatrix}\right]\right\}. \qquad (3.44)$$

Note that the first term cannot be separated into two disconnected ones by cutting a single internal line, i.e., by removing one internal (bare) propagator. Such contributions are called one-particle irreducible (1PI). On the other hand, the second term is clearly one-particle reducible. In general, any connected correlation function can always be decomposed into one-particle irreducible and one-particle reducible parts. From this perspective, 1PI functions are even more economical way of storing information as compared to connected correlators as they do not contain any one-particle reducible data, which is already stored in lower-order correlators. In fact, one can show that the whole quantum effective action Γ is one-particle irreducible, i.e., its loop expansion contains only 1PI diagrams [93, 94]. Likewise, the vertex functions are 1PI.

In principle, one can go further and construct a functional whose loop expansion contains only n-particle irreducible diagrams. By analogy to the previous case, functionals of

this kind are called nPI effective actions. A particularly significant role in nonequilbrium QFT is played by the 2PI effective action $\Gamma[\phi, G]$, also known as the *Luttinger–Ward (or Cornwall–Jackiw–Tomboulis) functional* [95, 96], which can be obtained by performing a second Legendre transform with respect to an additional two-point source $R(x, y)$. A very attractive feature that makes $\Gamma[\phi, G]$ so appealing is that its expansion is self-consistent with respect to both the mean field ϕ and the propagator G. In particular, this allows one to avoid secular terms in the evolution equations for ϕ, F, and ρ at a finite loop order [85]. This property is crucial for obtaining a universal late-time dynamics that is insensitive to the initial condition (e.g., thermalization or nonthermal fixed points). However, since an approximation scheme for the effective action that will be adopted in this work does not involve any loop expansion in the first place and since we are also not going to use it for deriving evolution equations, we will not discuss $\Gamma[\phi, G]$ any further and refer to the literature instead ([85, 97] and references therein).

3.1.5   Wigner transform, spectral function, and the gradient expansion

In physics, it is often more convenient to work in Fourier space rather than in coordinate space. When spacetime-translation invariance is present, an arbitrary two-point function $G(x, x')$ will depend only on the difference of its arguments $x - x'$ implying that its Fourier image will be a function of a single momentum p only.

Out of equilibrium, however, time-translation invariance in general does not hold,[2] so a two-point function depends on both the difference $t - t'$ and the sum $t + t'$ of its temporal arguments. Likewise, in spatially inhomogeneous systems, it will depend on both $\mathbf{x} - \mathbf{x}'$ and $\mathbf{x} + \mathbf{x}'$. The *Wigner transform* of a two-point function is then defined as the Fourier transform with respect to its relative coordinates only:

$$G^W(X, p) = \int_{-2X}^{2X} \mathrm{d}^{d+1}\sigma \, \mathrm{e}^{\mathrm{i}p\cdot\sigma} G\left(X + \sigma/2, X - \sigma/2\right), \tag{3.45}$$

where the integration limits signify the fact that the integration over σ^μ is bounded by $\pm 2X^\mu$. However, in order to exploit usual properties of the standard Fourier transform it is common to extend the limits to $\pm\infty$ [56]. The inverse map of (3.45) is sometimes referred to as the *Weyl transform*.

Recall that in standard quantum field theory the system's spectrum is determined by the pole structure of the full propagator in Fourier space. In nonequilibrium, this role is assigned, as its name suggests, to the spectral function in Wigner space ρ^W. In general, poles of ρ^W may be complex. The real part then determines the excitation's dispersion relation, whereas the imaginary part sets its inverse lifetime.

---

[2]When it does hold, one says that the system is in *stationary nonequilibrium*.

Using an integral representation of the Heaviside function,

$$\Theta(\sigma) = \int_{-\infty}^{+\infty} \frac{\mathrm{d}\omega'}{2\pi\mathrm{i}} \frac{\mathrm{e}^{-\mathrm{i}\omega'\sigma}}{\omega' + \mathrm{i}0^+}, \tag{3.46}$$

one readily obtains that the retarded propagator admits the following integral representation in terms of the spectral function:

$$\mathrm{i}G_{\mathrm{clq}}^W(\tau, \omega, \mathbf{p}) = \int_{-\infty}^{+\infty} \frac{\mathrm{d}\omega'}{2\pi\mathrm{i}} \frac{\rho^W(\tau, \omega', \mathbf{p})}{\omega - \omega' + \mathrm{i}0^+} \equiv \mathcal{G}(\tau, \omega + \mathrm{i}0^+, \mathbf{p}), \tag{3.47}$$

where we have assumed spatial homogeneity. Likewise, the advanced propagator is given by $\mathcal{G}(\tau, \omega - \mathrm{i}0^+, \mathbf{p})$. Now, in general, ρ^W will have poles in both upper and lower complex planes in a symmetric manner. In contrast, the retarded (advanced) propagator is analytic in the upper (lower), while in the lower (upper) plane its poles are shifted by $\mathrm{i}0^+$ ($-\mathrm{i}0^+$) (see, e.g., [98]). In other words, the spectral information can be equally (and even more conveniently) extracted from the retarded/advanced propagator.

From (3.41), it follows that the retarded propagator can be obtained by virtue of inverting the q $-$ cl-component of the effective action:

$$\left(\Gamma_{\mathrm{qcl}}^{(2)} \circ G_{\mathrm{clq}}\right)(x, y) = \mathrm{i}\delta(x - y). \tag{3.48}$$

For spacetime-translation invariant systems, this convolution may be readily translated into a simple algebraic product in Fourier space. This, in turn, implies that the pole structure of the retarded propagator can be extracted by studying zeros of the q $-$ cl-component of the effective action. As will be more thoroughly discussed in Sec. 3.3.1, one may generally write $\Gamma_{\mathrm{qcl}}^{(2)}(t, t', \mathbf{p}) = D(t, t', \mathbf{p})\,\Theta(t - t')$, with D being an odd function in $t - t'$. Following the same logic as in (3.47) we thus conclude

$$\left(\Gamma_{\mathrm{qcl}}^{(2)}\right)^W(\tau, \omega, \mathbf{p}) = \int_{-\infty}^{+\infty} \frac{\mathrm{d}\omega'}{2\pi\mathrm{i}} \frac{D^W(\tau, \omega', \mathbf{p})}{\omega - \omega' + \mathrm{i}0^+} \equiv \Omega(\tau, \omega + \mathrm{i}0^+, \mathbf{p}). \tag{3.49}$$

Therefore, for stationary nonequilibrium, one can obtain information about the system's spectrum by examining zeros of Ω.

The situation, however, is more involved once we go beyond stationary nonequilibrium. An important result of the Wigner-Weyl calculus is that the Wigner transform of a convolution of two functions is given by (see, e.g., [99])

$$(A \circ B)^W(X, p) = A^W(X, p) \exp\left[\frac{\mathrm{i}}{2}\left(\overleftarrow{\partial_p}\overrightarrow{\partial_X} - \overleftarrow{\partial_X}\overrightarrow{\partial_p}\right)\right] B^W(X, p)$$

$$\equiv A^W(X, p) \star B^W(X, p). \tag{3.50}$$

where we have introduced the notation $\star$ for the bilinear map known as the *Moyal (or Weyl–Groenewold) product*. Therefore, for time-evolving nonequilibrium systems,

$$\Gamma_{\mathrm{qcl}}^W(\tau, \omega, \mathbf{p}) \star G_{\mathrm{clq}}^W(\tau, \omega, \mathbf{p}) = \mathrm{i}, \tag{3.51}$$

where, for the sake of brevity, we have dropped the derivative superscript in the Wigner transform of $\Gamma^{(2)}$.

In general, a $\star$-inverse needs not to share the singularity structure of a multiplicative inverse. Thus, strictly speaking, in time-evolving nonequilibrium, it does not suffice to study zeros of the inverse (retarded/advanced) propagator to analyze the system's spectrum.

In practice, however, one often encounters the case when the two-point functions of interest are relatively slow (fast) functions of the central (relative) coordinate. One can then treat $\partial_X \partial_p$ in (3.50) as a small parameter and expand:

$$(A \circ B)^W (X, p) = A^W(X, p) \, B^W(X, p) + \frac{\mathrm{i}}{2} \left\{ A^W(X, p), B^W(X, p) \right\}_{\mathrm{PB}} + \dots, \quad (3.52)$$

where $\{\cdot, \cdot\}_{\mathrm{PB}}$ denotes the standard Poisson bracket. Such an expansion in terms of ∂_X and ∂_p is known as the *gradient expansion* and plays a prominent role in the context of transport theory: in particular, the quantum kinetic equation, discussed in Sec. 2.2, is obtained in the lowest-order in the gradient expansion. Typically, after an initial stage of evolution characterized by rapid oscillations, the latter get effectively damped out and the subsequent dynamics becomes comparably smooth [88, 100–103]. Since the self-similar dynamics associated with nonthermal fixed points is an asymptotically late phenomenon, it is expected that the gradient expansion should be a reliable approximation during the scaling regime.

3.1.6 Fluctuation-dissipation relation and the quasiparticle Ansatz

In equilibrium, there is an addition relation between the statistical (F) and the spectral (ρ) functions, known as the *fluctuation-dissipation theorem*:

$$F^{(\mathrm{eq})}(\omega, \mathbf{p}) = -\mathrm{i} \left(f(\omega) + \frac{1}{2} \right) \rho^{(\mathrm{eq})}(\omega, \mathbf{p}), \quad (3.53)$$

where $f(\omega)$ is the distribution function. Out of equilibrium, on the other hands, such a proportionality does not generally hold [66]. Nevertheless, in practice, one often employs a similar Ansatz:

$$F^W(\tau, \omega, \mathbf{p}) = -\mathrm{i} \left(f(\tau, \omega) + \frac{1}{2} \right) \rho^W(\tau, \omega, \mathbf{p}). \quad (3.54)$$

To better understand the physics behind this parameterization, it is helpful to consider first the case of a free theory. In the absence of interactions, the equation that governs evolution of the spectral function takes a very simple form

$$\left(\partial^2 + m^2 \right) \rho^{(\mathrm{free})}(x, y) = 0, \quad (3.55)$$

where for concreteness and brevity we again consider the case of a real scalar theory. The solution of (3.55) reads

$$\rho^{(\mathrm{free})}(t, t', \mathbf{p}) = \frac{1}{\omega_{\mathbf{p}}^{(0)}} \sin \left[\omega_{\mathbf{p}}^{(0)} (t - t') \right], \quad (3.56)$$

where $\omega_{\mathbf{p}}^{(0)} = \sqrt{\mathbf{p}^2 + m^2}$ is the free-particle dispersion relation. Upon performing Wigner transform we readily find

$$-\mathrm{i}\rho^{(\mathrm{free})}(\tau, \omega, \mathbf{p}) = \frac{\sin\left[(\omega - \omega_{\mathbf{p}}^{(0)})2\tau\right]}{\omega_{\mathbf{p}}^{(0)}\left(\omega - \omega_{\mathbf{p}}^{(0)}\right)} - \frac{\sin\left[(\omega + \omega_{\mathbf{p}}^{(0)})2\tau\right]}{\omega_{\mathbf{p}}^{(0)}\left(\omega + \omega_{\mathbf{p}}^{(0)}\right)}. \tag{3.57}$$

At finite central time τ, the free spectral function in Wigner space shows a rapidly oscillating behavior, with it enveloped peaked at $\omega = \pm\omega_{\mathbf{p}}^{(0)}$. In the late-time limit $\tau \to \infty$, it reduces to the expected δ-like form:

$$-\mathrm{i}\rho^{(\mathrm{free})}(\tau, \omega, \mathbf{p}) = 2\pi\delta\left(\omega^2 - \left(\omega_{\mathbf{p}}^{(0)}\right)^2\right). \tag{3.58}$$

In other words, in the non-interacting case, the Ansatz (3.54) simply puts the occupation number $f(\tau, \omega)$ on the mass-shell.

Once interactions are included, the spectral function will in general have a more complicated form. Despite that, in many cases, it will still have a peaked structure, albeit with generally a modified dispersion relation $\omega_{\mathbf{p}}$ and peaks acquiring a nonzero 'width' $\gamma_{\mathbf{p}}$. Physically, this corresponds to the case of well-defined quasiparticles. The Ansatz (3.54) is therefore expected to be adequate in cases where the dynamics of a noenquilbrium system is dominated by quasiparticle excitations. While not all the observed nonthermal fixed points fall to this physical picture, in this work, we are going to restrict ourselves to such scenarios.

3.2   Equal-time formulation of nonequilibrium quantum field theory

An alternative formulation of nonequilibrium quantum field theory can be given solely in terms of equal-time quantities [104]. This formalism will prove useful when discussing symmetry constraints on equal-time propagators in Sec. 3.3.2, so let us briefly outline its key concepts here.

We begin by introducing the generating functional for equal-time correlation functions via

$$Z_t\left[K_\varphi, K_\pi\right] = \mathrm{Tr}\left\{\hat{\rho}_t \exp\left[\int_{\mathbf{x}} K_\varphi(\mathbf{x})\,\hat{\varphi}(\mathbf{x}) + K_\pi(\mathbf{x})\,\hat{\pi}(\mathbf{x})\right]\right\}. \tag{3.59}$$

Here, $\hat{\rho}_t$ is the system's density matrix in the Heisenberg picture at time t and $\hat{\phi}$ and $\hat{\pi}$ are canonically conjugate fields. Making use of the Baker–Campbell–Hausdorff formula it can be readily rewritten as

$$Z_t\left[K_\varphi, K_\pi\right] = \mathrm{Tr}\left\{\hat{\rho}_t \mathrm{e}^{\int_{\mathbf{x}} K_\varphi(\mathbf{x})\,\hat{\varphi}(\mathbf{x})}\mathrm{e}^{\int_{\mathbf{x}} K_\pi(\mathbf{x})\,\hat{\pi}(\mathbf{x})}\mathrm{e}^{-(\mathrm{i}/2)\int_{\mathbf{x}} K_\varphi(\mathbf{x})\,K_\pi(\mathbf{x})}\right\}. \tag{3.60}$$

Similarly to the conventional generating functional, its equal-time counterpart admits a path-integral representation:

$$Z_t\left[K_\varphi, K_\pi\right] = \int \mathcal{D}\varphi^+ \mathcal{D}\varphi^- \mathcal{D}\pi \left\langle \varphi^+ \right| \hat{\rho}_t \left| \varphi^- \right\rangle \left\langle \varphi^- \right| \exp\left[\int_{\mathbf{x}} K_\varphi(\mathbf{x})\, \hat{\varphi}(\mathbf{x})\right] \left| \pi \right\rangle$$

$$\times \left\langle \pi \right| \exp\left[\int_{\mathbf{x}} K_\pi(\mathbf{x})\, \hat{\pi}(\mathbf{x})\right] \left| \varphi^+ \right\rangle \exp\left[-\frac{\mathrm{i}}{2}\int_{\mathbf{x}} K_\varphi(\mathbf{x})\, K_\pi(\mathbf{x})\right]$$

$$= \int \mathcal{D}\varphi \mathcal{D}\pi\, \mathcal{W}_t\left[\varphi, \pi\right] \exp\left[\int_{\mathbf{x}} K_\varphi(\mathbf{x})\, \varphi(\mathbf{x}) + K_\pi(\mathbf{x})\, \pi(\mathbf{x})\right]. \tag{3.61}$$

Here, we have used $\langle \varphi | \pi \rangle = \exp\left[\mathrm{i}\int_{\mathbf{x}} \varphi(\mathbf{x})\pi(\mathbf{x})\right]$ and shifted the integration variable $\pi \to \pi + \mathrm{i}K_\varphi/2$. The weight functional $\mathcal{W}_t$, defined as

$$\mathcal{W}_t\left[\varphi, \pi\right] = \int \mathcal{D}\tilde{\varphi} \left\langle \varphi - \frac{\tilde{\varphi}}{2} \right| \hat{\rho}_t \left| \varphi + \frac{\tilde{\varphi}}{2} \right\rangle \exp\left[-\mathrm{i}\int_{\mathbf{x}} \pi(\mathbf{x})\tilde{\varphi}(\mathbf{x})\right], \tag{3.62}$$

is known as the *Wigner functional* in the literature and plays a central role in the phase-space formulation of quantum mechanics/field theory [105, 106]. Being its corresponding characteristic functional, Z_t is known to generate *symmetric* (or *Weyl*) *ordered* correlation functions [107]. For example, the two-point functions take the form:

$$\left.\frac{\delta^2 Z_t\left[K_\varphi, K_\pi\right]}{\delta K_\varphi(\mathbf{x})\, \delta K_\varphi(\mathbf{y})}\right|_{K_\varphi, K_\pi = 0} = \frac{1}{2}\left\langle \hat{\varphi}(\mathbf{x})\, \hat{\varphi}(\mathbf{y}) + \hat{\varphi}(\mathbf{y})\, \hat{\varphi}(\mathbf{x})\right\rangle = \left\langle \hat{\varphi}(\mathbf{x})\hat{\varphi}(\mathbf{y})\right\rangle,$$

$$\left.\frac{\delta^2 Z_t\left[K_\varphi, K_\pi\right]}{\delta K_\varphi(\mathbf{x})\, \delta K_\pi(\mathbf{y})}\right|_{K_\varphi, K_\pi = 0} = \frac{1}{2}\left\langle \hat{\varphi}(\mathbf{x})\, \hat{\pi}(\mathbf{y}) + \hat{\pi}(\mathbf{y})\, \hat{\varphi}(\mathbf{x})\right\rangle = \frac{1}{2}\left\langle \{\hat{\varphi}(\mathbf{x}), \hat{\pi}(\mathbf{y})\}\right\rangle, \tag{3.63}$$

$$\left.\frac{\delta^2 Z_t\left[K_\varphi, K_\pi\right]}{\delta K_\pi(\mathbf{x})\, \delta K_\pi(\mathbf{y})}\right|_{K_\varphi, K_\pi = 0} = \frac{1}{2}\left\langle \hat{\pi}(\mathbf{x})\, \hat{\pi}(\mathbf{y}) + \hat{\pi}(\mathbf{y})\, \hat{\pi}(\mathbf{x})\right\rangle = \left\langle \hat{\pi}(\mathbf{x})\hat{\pi}(\mathbf{y})\right\rangle.$$

To generate connected correlation functions, one can invoke an equal-time equivalent of the Schwinger functional:

$$E_t\left[K_\varphi, K_\pi\right] = \log Z_t\left[K_\varphi, K_\pi\right]. \tag{3.64}$$

Comparing to (3.28) we note that the second derivative of E_t with respect to the φ-source generates an equal-time statistical propagator:

$$E_t^{(2,0)}(\mathbf{x}, \mathbf{y}) = F(t, \mathbf{x}, t, \mathbf{y}). \tag{3.65}$$

Here, $E_t^{(n,m)}$ means taking n derivatives with respect to the source K_φ and m derivatives with respect to the source K_π.

Likewise, the generator for 1PI vertices can be obtained via the usual Legendre transform

$$\Gamma_t\left[\Pi, \Phi\right] = \sup_{K_\varphi, K_\pi} \left\{\int_{\mathbf{x}}\left[K_\varphi(\mathbf{x})\, \Phi(\mathbf{x}) + K_\pi(\mathbf{x})\, \Pi(\mathbf{x})\right] - E_t\left[K_\varphi, K_\pi\right]\right\}. \tag{3.66}$$

Relations between connected correlators and vertex functions match those derived in Sec. 3.1.4. In particular,

$$\int_{\mathbf{y}} \Gamma_{t,ac}^{(2)}(\mathbf{x}_1, \mathbf{y})\, G_{t,cb}(\mathbf{y}, \mathbf{x}_2) = \delta_{ab}\delta(\mathbf{x}_1 - \mathbf{x}_2), \tag{3.67}$$

where the Latin subscripts label the phase-space components Φ and Π.

The dynamics in this framework is covered by the *von Neumann equation* for the density matrix $\hat{\rho}_t$, which can be recast into the evolution equation for the Wigner functional,

$$\partial_t \mathcal{W}_t = \{\{H, \mathcal{W}_t\}\}, \tag{3.68}$$

called the *Moyal equation*. Here, $\{\{\cdot, \cdot\}\}$ denotes the (functional) *Moyal bracket*

$$\{\{A, B\}\} = 2A[\varphi, \pi] \sin\left[\frac{1}{2}\int_{\mathbf{x}}\left(\frac{\overleftarrow{\delta}}{\delta\varphi(\mathbf{x})}\frac{\overrightarrow{\delta}}{\delta\pi(\mathbf{x})} - \frac{\overleftarrow{\delta}}{\delta\pi(\mathbf{x})}\frac{\overrightarrow{\delta}}{\delta\varphi(\mathbf{x})}\right)\right] B[\varphi, \pi]. \tag{3.69}$$

These equations can be further recast into the exact evolution equations for the equal-time generating functionals [104]. For a deeper discussion on the equal-time approach to nonequilibrium QFT, we refer to [108]. An experimental extraction of the equal-time vertex functions was performed in [109, 110].

3.3   Structure of a nonequilibrium effective action

3.3.1   Causal properties and associated constraints

In this section, we briefly recall some exact causal features of a 1PI effective action defined on a Schwinger–Keldysh contour. For more details, see [97, 111].

We begin by recalling that a nonequilibrium generating functional admits the representation

$$Z\left[J^+, J^-; \hat{\rho}_0\right] \equiv \exp\left(iW\left[J^+, J^-; \hat{\rho}_0\right]\right) = \text{Tr}\left[\hat{U}_{J^-}(t_0, t)\,\hat{U}_{J^+}(t, t_0)\,\hat{\rho}_0\right]_{t\to\infty}, \tag{3.70}$$

cf. (3.2), with the evolution operator $\hat{U}_J(t_1, t_2)$ given by

$$\hat{U}_J(t_2, t_1) = \mathcal{T}\exp\left[-i\int_{t_1}^{t_2} dt \int d^d\mathbf{x}\left(\hat{H} - J\hat{\varphi}\right)\right]. \tag{3.71}$$

Provided that the initial density matrix is Hermitian and the evolution operator is unitary – which is the case for closed quantum systems – one readily obtains

$$\exp\left(-iW^*\left[J^+, J^-; \hat{\rho}_0\right]\right) = \text{Tr}\left[\hat{U}_{J^+}(t_0, t)\,\hat{U}_{J^-}(t, t_0)\,\hat{\rho}_0\right]_{t\to\infty} = \exp\left(iW\left[J^-, J^+; \hat{\rho}_0\right]\right), \tag{3.72}$$

implying

$$W\left[J^+, J^-; \hat{\rho}_0\right] = -W\left[J^-, J^+; \hat{\rho}_0\right]^*. \tag{3.73}$$

Taking derivatives with respect to the sources,

$$\phi_+\left[J^+, J^-\right] = \frac{\delta W\left[J^+, J^-; \hat{\rho}_0\right]}{\delta J^+}, \quad \phi_-\left[J^+, J^-\right] = \frac{\delta W\left[J^+, J^-; \hat{\rho}_0\right]}{\delta J^-}, \tag{3.74}$$

we readily derive a constraint on the field expectation value:

$$\phi_+[J^+, J^-] = -\phi_-[J^-, J^+]^*, \quad \phi_-[J^+, J^-] = -\phi_+[J^-, J^+]^*. \tag{3.75}$$

It is worth emphasizing that, even for a real scalar theory, the mean fields ϕ_a are not in general real. As one can see from (3.75), the latter must only hold in the coincidence limit $J^+ = J^- = J$, in which there is a single real mean field $\phi[J, J] = \phi^+[J, J] = \phi^-[J, J]$,[3] as one would expect from a real scalar field theory.

Introducing further, as usual, the 1PI effective action via Legendre transform (3.34), one finds

$$\Gamma\left[\phi^{+*}, \phi^{-*}; \hat{\rho}_0\right] = -\Gamma\left[\phi^-, \phi^+; \hat{\rho}_0\right]^*. \tag{3.76}$$

We thus conclude that the diagonal entries of the generating functionals vanish: $W[J, J] \equiv 0$ and $\Gamma[\phi, \phi] \equiv 0$. Hence, in terms of Keldysh-rotated fields (3.33), we discover two important constraints on the effective action:

$$\Gamma\left[\phi_{cl}, \phi_q = 0; \hat{\rho}_0\right] \equiv 0, \quad \Gamma\left[\phi_{cl}^*, \phi_q^*; \hat{\rho}_0\right] = -\Gamma\left[\phi_{cl}, -\phi_q; \hat{\rho}_0\right]^*. \tag{3.77}$$

Note that for real configurations, the second constraint can be reformulated as

$$\text{Re}\,\Gamma[\phi_{cl}, \phi_q] = -\text{Re}\,\Gamma[\phi_{cl}, -\phi_q], \quad \text{Im}\,\Gamma[\phi_{cl}, \phi_q] = \text{Im}\,\Gamma[\phi_{cl}, -\phi_q]. \tag{3.78}$$

Therefore, a Taylor expansion of $\Gamma\left[\phi_{cl}, \phi_q; \hat{\rho}_0\right]$ takes the form

$$\Gamma\left[\phi_{cl}, \phi_q; \hat{\rho}_0\right] = \int_x \phi_q(x)\,\mathcal{D}[\phi_{cl}](x) + \frac{1}{2}\int_{x,x'} \phi_q(x)\,N(x, x')\,\phi_q(x') + \dots \tag{3.79}$$

Using that, we can readily write the quantum equation of motion as

$$\left.\frac{\delta\Gamma\left[\phi_{cl}, \phi_q; \hat{\rho}_0\right]}{\delta\phi_q(x)}\right|_{\phi_{cl}=\phi, \phi_q=0} = \mathcal{D}[\phi_{cl}](x) = -J(x). \tag{3.80}$$

Assuming $\mathcal{D}[\phi = 0] = 0$[4] and that the action is analytic in the fields near $(0,0)$, one realizes that $\mathcal{D}[\phi_{cl}]$ admits its own Taylor expansion,

$$\mathcal{D}[\phi_{cl}](x) = \int_{x'} D(x, x')\,\phi_{cl}(x') + \dots, \tag{3.81}$$

so that the linearized quantum equation of motion is given by

$$\int_{x'} D(x, x')\,\phi_{cl}(x') = -J(x). \tag{3.82}$$

---

[3]Notice the change of sign due to raising the indices, cf. (3.15).
[4]Otherwise, one shall simply shift the expansion point.

Together with (3.78) this implies that $D(x, x')$ is real and causal (in particular, it has no support for $t < t'$), whilst $N(x, x')$ is purely imaginary. Finally, we translate these constraints to the two-point functions by noticing

$$\left.\frac{\delta^2\Gamma[\phi_{\mathrm{cl}}, \phi_{\mathrm{q}}]}{\delta\phi_{\mathrm{q}}(x)\delta\phi_{\mathrm{cl}}(x')}\right|_{\phi_{\mathrm{cl}}=\phi,\phi_{\mathrm{q}}=0} \equiv \Gamma^{(2)}_{\mathrm{qcl}}[\phi, 0](x, x') = \Gamma^{(2)}_{\mathrm{clq}}[\phi, 0](x', x) = D(x, x'), \quad (3.83\mathrm{a})$$

$$\left.\frac{\delta^2\Gamma[\phi_{\mathrm{cl}}, \phi_{\mathrm{q}}]}{\delta\phi_{\mathrm{q}}(x)\delta\phi_{\mathrm{q}}(x')}\right|_{\phi_{\mathrm{cl}}=\phi,\phi_{\mathrm{q}}=0} \equiv \Gamma^{(2)}_{\mathrm{qq}}[\phi, 0](x, x') = N(x, x'), \quad (3.83\mathrm{b})$$

$$\left.\frac{\delta^2\Gamma[\phi_{\mathrm{cl}}, \phi_{\mathrm{q}}]}{\delta\phi_{\mathrm{cl}}(x)\delta\phi_{\mathrm{cl}}(x')}\right|_{\phi_{\mathrm{cl}}=\phi,\phi_{\mathrm{q}}=0} \equiv \Gamma^{(2)}_{\mathrm{clcl}}[\phi, 0](x, x') \equiv 0. \quad (3.83\mathrm{c})$$

3.3.2   Aspects of symmetry

Schwinger–Keldysh formulation and spontaneous symmetry breaking

Just like in equilibrium, the existence of a global continuous symmetry G has great consequences on the structure of the nonequilibrium effective action and correlation functions. These symmetry constraints can be most easily derived in the path-integral formulation introduced in Sec. 3.1.1. To that end, consider an infinitesimal symmetry transformation:

$$x^\mu \to \tilde{x}^\mu = x^\mu + \epsilon_k(x)Y_k^\mu(x), \quad \varphi^a(x) \to \tilde{\varphi}^a(\tilde{x}) = \varphi^a(x) + \epsilon_k(x)X_k^a[x; \varphi]. \quad (3.84)$$

Here, the superscript a labels whether the field belongs to an upper '+' or lower '−' branch of the Schwinger–Keldysh contour as well as other possible internal indices. Even though $\epsilon_k = \mathrm{const}$ for global symmetries, for deriving symmetry identities it is convenient to suppose them spacetime-dependent. It is customary to also define generators $\mathcal{F}_k$ of a symmetry via an infinitesimal transformation at the same spacetime point,

$$\tilde{\varphi}^a(x) \equiv \varphi^a(x) + \mathrm{i}\epsilon_k(x)\mathcal{F}_k^a[x; \varphi], \quad (3.85)$$

which can be easily related to (3.84) upon performing a Taylor expansion of $\tilde{\varphi}^a(\tilde{x})$ to linear order:

$$\mathrm{i}\mathcal{F}_k^a[x; \varphi] = X_k^a[x; \varphi] - Y_k^\mu(x)\partial_\mu\varphi^a(x). \quad (3.86)$$

We are now set to discuss the effect of symmetries on the structure of correlation functions. In the path integral formalism, the latter take a form

$$\left\langle \prod_{i=1}^n \varphi^{a_i}(x_i) \right\rangle_K = \int \mathrm{d}\varphi_0^+ \, \mathrm{d}\varphi_0^- \, \rho_0\left[\varphi_0^+, \varphi_0^-\right] \int_{\varphi_0^+}^{\varphi_0^-} \mathcal{D}'\varphi^+ \mathcal{D}'\varphi^- \left(\prod_{i=1}^n \varphi^{a_i}(x_i)\right) \mathrm{e}^{\mathrm{i}(S[\varphi]+K\cdot\varphi)},$$
$$(3.87)$$

where the subscript denotes the expectation value in the presence of the source K and contour time-ordering is implied. Let us now change the dummy integration variable on the

right-hand side to $\tilde{\varphi}$ from (3.85). The variation in the field operators product is explicitly given by

$$\prod_{i=1}^{n} \tilde{\varphi}^{a_i}(x_i) = \mathrm{i} \sum_{i} \epsilon_k(x_i) \mathcal{F}_k^{a_i}[x;\varphi] \prod_{j\neq i} \varphi^{a_j}(x_j) + O\left(\epsilon^2\right)$$

$$= \mathrm{i} \int_{x,t_0} \epsilon_k(x) \sum_{i=1}^{n} \left[\mathcal{F}_k^{a_i}[x;\varphi] \prod_{j\neq i} \varphi^{a_j}(x_j) \right] \delta(x - x_i) + O\left(\epsilon^2\right), \qquad (3.88)$$

with the short-hand notation $\in_{x,t_0}$ defined in (7.4). Next, recalling the celebrated *Noether theorem*, we note that for a continuous global symmetry the change in action can be written as

$$\delta S = - \int_{x,t_0} \epsilon_k \partial_\mu J_k^\mu, \qquad (3.89)$$

where the (classically conserved) current J is given by [112, 113]

$$J_k^\mu = \frac{\partial \mathcal{L}}{\partial\left(\partial_\mu \varphi^a\right)} X_k^a - \left(\frac{\partial \mathcal{L}}{\partial\left(\partial_\mu \varphi^a\right)} \partial_\nu \varphi^a - \delta_\nu^\mu \mathcal{L} \right) Y_a^\nu. \qquad (3.90)$$

We are also going to assume that the measure is invariant under the symmetry transformation:[5]

$$\mathrm{d}\tilde{\varphi}_0^+ \, \mathrm{d}\tilde{\varphi}_0^- = \mathrm{d}\varphi_0^+ \, \mathrm{d}\varphi_0^- , \quad \mathcal{D}'\tilde{\varphi}^+ \mathcal{D}'\tilde{\varphi}^- = \mathcal{D}'\varphi^+ \mathcal{D}'\varphi^-. \qquad (3.91)$$

A final – and new as compared to the usual equilibrium case – ingredient is the initial density matrix ρ_0. Under the infinitesimal transformation (3.85) it changes according to

$$\rho_0[\tilde{\varphi}_0^+, \tilde{\varphi}_0^-] = \rho_0[\varphi_0^+, \varphi_0^-] \left\{ 1 - \int_{x,t_0} \frac{\delta h_{\mathcal{C}}[\varphi_0]}{\delta \varphi_0^a(x)} \mathcal{F}_k^a[x;\varphi_0] \delta\left(x^0 - t_0\right) \epsilon_k(x) \right\} + O\left(\epsilon^2\right), \qquad (3.92)$$

where we have made use of the parameterization (3.17) and introduced a dummy δ-function to have integration over temporal axis as in other terms. Taking into account that the source term transforms as $\exp\left(\mathrm{i}K \cdot \varphi\right) \rightarrow \exp\left[\mathrm{i}K \cdot \left(\varphi + \mathrm{i}\epsilon_k \mathcal{F}_k\right)\right]$, expanding everything to first order in ϵ, using that it is arbitrary, and finally setting $K = 0$ we get

$$\left\langle \partial_\mu J_k^\mu(x) \prod_{i=1}^{n} \varphi^{a_i}(x_i) \right\rangle = \sum_{i=1}^{n} \delta(x - x_i) \left\langle \mathcal{F}_k^{a_i}[x_i;\varphi] \prod_{j\neq i} \varphi^{a_j}(x_j) \right\rangle$$

$$+ \mathrm{i} \left\langle \frac{\delta h_{\mathcal{C}}[\varphi_0]}{\delta \varphi_0^a(x)} \mathcal{F}_k^a[x;\varphi_0] \prod_{i=1}^{n} \varphi^{a_j}(x_j) \right\rangle \delta\left(x^0 - t_0\right). \qquad (3.93)$$

Expressions of these kind are collectively known as *Ward–Takahashi identities (WTIs)*. It is easy to see that the above derivation can be easily generalized to the case of product of any local operators $\mathcal{O}[x;\varphi]$. Assuming they transform under (3.85) as

$$\mathcal{O}^a[x;\tilde{\varphi}] = \mathcal{O}^a[x;\varphi] + \mathrm{i}\epsilon_k(x)\mathcal{G}_k^a[x;\varphi], \qquad (3.94)$$

---

[5]In other words, we assume that the symmetry in question is free of *quantum anomalies*.

with $\mathcal{G}_k = \delta\mathcal{O}/\delta\varphi \cdot \mathcal{F}_k$, the generalized WTIs then read

$$\left\langle \partial_\mu J_k^\mu(x) \prod_{i=1}^n \mathcal{O}^{a_i}(x_i) \right\rangle = \sum_{i=1}^n \delta(x - x_i) \left\langle \mathcal{G}_k^{a_i}[x_i; \varphi] \prod_{j \neq i} \mathcal{O}^{a_j}(x_j) \right\rangle$$
$$+ \, \mathrm{i} \left\langle \frac{\delta h_\mathcal{C}[\varphi_0]}{\delta\varphi_0^a(x)} \mathcal{F}_k^a[x; \varphi_0] \prod_{i=1}^n \mathcal{O}^{a_j}(x_j) \right\rangle \delta\left(x^0 - t_0\right). \quad (3.95)$$

In particular, for the trivial case $\mathcal{O} = 1$ one readily obtains

$$\langle \partial_\mu J_k^\mu(x) \rangle = \mathrm{i} \left\langle \frac{\delta h_\mathcal{C}[\varphi_0]}{\delta\varphi_0^a(x)} \mathcal{F}_k^a[x; \varphi_0] \right\rangle \delta\left(x^0 - t_0\right). \quad (3.96)$$

This highlights a simple observation that out of equilibrium, even when the Hamiltonian enjoys some continuous symmetry, the associated current (operator) may be not fully conserved if the initial density matrix does not respect the symmetry, i.e., $\delta h_\mathcal{C} \neq 0$. Apart from that, however, nonequilibrium Ward–Takahashi identities match their equilibrium counterparts for virtually any case of continuous symmetry, with the exception that the temporal arguments may take any value on the Schwinger–Keldysh contour [114]. A possible exception would be a class of exotic symmetries that mix $\pm$ components.

After covering consequences of continuous symmetries on correlation functions, let us shift our attention to constraints that symmetries impose on the structure of the quantum effective action itself. To that end, we first note that in the presence of the external source K the equation (3.96) reads

$$\langle \partial_\mu J_k^\mu(x) \rangle_K = \mathrm{i} \left\langle \frac{\delta h_\mathcal{C}[\varphi_0]}{\delta\varphi_0^a(x)} \mathcal{F}_k^a[x; \varphi_0] \right\rangle_K \delta\left(x^0 - t_0\right) + \mathrm{i} K_a(x) \langle \mathcal{F}_k^a[x; \varphi] \rangle_K. \quad (3.97)$$

Taking the integral of both sides and applying Stokes' theorem,

$$\int_{x,t_0} \langle \partial_\mu J_k^\mu(x) \rangle_K = \int_{\partial\Omega} \langle J_k^\mu(x) \rangle_K = 0, \quad (3.98)$$

we readily obtain

$$\int_{x,t_0} K_a(x) \langle \mathcal{F}_k^a[x; \varphi] \rangle_K = - \int_{\mathbf{x}} \left\langle \frac{\delta h}{\delta\varphi_0^a(\mathbf{x})} \mathcal{F}_k^a[\mathbf{x}; \varphi_0] \right\rangle_K. \quad (3.99)$$

Here, we have assumed that the current decays quickly enough at the boundaries. For simplicity, we are also going to assume that the initial density matrix respects the symmetry in question, so that the right-hand side of (3.99) vanishes. Then, upon invoking the quantum equation of motion (3.35), one finds

$$\int_{x,t_0} \frac{\delta\Gamma[\phi]}{\delta\phi^a(x)} \langle \mathcal{F}_k^a(\varphi) \rangle_{K_\phi} = 0. \quad (3.100)$$

In other words, the quantum effective action is invariant under the transformation

$$\tilde{\phi}^a(x) = \phi^a(x) + \epsilon_k \langle \mathcal{F}_k^a[x; \varphi] \rangle_{K_\phi}. \quad (3.101)$$

A very important and rather common case is when the symmetry transformations act linearly on the fields,

$$\mathcal{F}_k^a[x;\varphi] = c_k^a(x) + \int_{y,t_0} T_{kb}^a(x,y)\varphi^b(y)\,,\tag{3.102}$$

for which

$$\langle \mathcal{F}_k^a[x;\varphi]\rangle_{K_\phi} = c_k^a(x) + \int_{y,t_0} T_{kb}^a(x,y)\phi^b(y) = \mathcal{F}_k^a[x;\phi]\,.\tag{3.103}$$

Hence, for linearly realized symmetries the quantum effective action has the same symmetry properties as the classical one:

$$\int_{x,t_0} \frac{\delta\Gamma[\phi]}{\delta\phi^a(x)}\mathcal{F}_k^a[x;\phi] = 0.\tag{3.104}$$

Taking further field derivatives will generate relations between higher n-point 1PI vertices. For instance, taking one field derivative yields

$$\int_{x,t_0} \left[T_{kb}^a \frac{\delta^2\Gamma[\phi]}{\delta\phi^a(x)\delta\phi^c(y)}\phi^b(x) + T_{kc}^a \frac{\delta\Gamma[\phi]}{\delta\phi^a(x)}\delta(x-y) \right] = 0,\tag{3.105}$$

where, for brevity, we assumed $T_{kb}^a(x,y) = T_{kb}^a\delta(x-y)$ and $c_k^a = 0$, which is often the case. Symmetry identities of these kind, relating vertex functions to one another, are commonly known as *Slavnov–Taylor identities (STIs)*.

In equilibrium, STIs for the two-point function play an important role in the case of *spontaneously broken symmetries (SSB)*. In particular, they allow to establish that for each broken symmetry there is a massless *(Nambu–)Goldstone mode*. We close this section by making a sketch of how this statement translates to nonequilbrium.

To that end, we evaluate (3.105) at the solution of the quantum equation of motion. For our purposes, it is more convenient to work in the Keldysh-rotated basis, in which only the classical component of the mean field can take a nonzero value. In addition to that, for conventional symmetries that do not mix $\pm$ components, it is easy to see that T_{kb}^a is diagonal in Keldysh space. Hence, since ϕ^b in (3.105) is classical, so is ϕ^a in the derivative. But as discussed in Sec. 3.3.1, $\Gamma_{\text{clcl}}^{(2)} \equiv 0$ for causal reasons, so ϕ^c in the derivative has to be quantum. Finally, in the absence of an external field, the second term vanishes. We thus conclude that for spatially translation-invariant systems with spontaneous symmetry breaking the equation (3.105) reduces to

$$\int_t T_{k\beta}^\alpha \Gamma_{\text{cl}\alpha,\text{q}\gamma}^{(2)}[\phi,0](t,t',\mathbf{p}=0)\phi^\beta(t) = 0,\tag{3.106}$$

where we have also assumed that the mean field ϕ is spatially translation-invariant. An important class of configurations that break translation invariance are *topological defects*, such as solitons, skyrmions, vortices, etc. In the following, we distance ourselves from subtleties associated with such configurations and suppose that the field expectation value is homogeneous.

Let us first consider the case of stationary nonequilbrium, in which one considers states that are not in equilibrium, yet not evolving in time. The two-point function is then time-translation invariant, so that the equation further simplifies to

$$\Omega_{\alpha\gamma}(\omega = \mathrm{i}0^+, \mathbf{p} = 0) T^\alpha_{k\beta} \phi^\beta = 0, \tag{3.107}$$

cf. (3.49). At this point, the proof goes exactly the same way as in the standard quantum field theory [115]. As argued in Sec. 3.1.5, Ω encodes the system's spectrum. Evaluated at zero momenta, it (or rather its real part) can be identified with the mass matrix. From the equation (3.107), it follows that $T_k\phi$ are its eigenvectors with zero eigenvalue. The corresponding geometric – and since the mass matrix is symmetric,[6] also algebraic – multiplicity is given by the number of such eigenvectors. Finally, since for unbroken generators $T_k\phi$ vanishes, the number of zero modes is given by the number of broken symmetries, which closes the proof. Note that, according to the above argument, also imaginary parts of the eigenvalues vanish, which might seem to suggest that these gapless modes are stable. However, the prove only states that their decay rates go to zero as $p \to 0$.

Coming back to the case of a time-evolving nonequilbrium system, where time-translation invariance no longer holds, we instead rewrite (3.106) in Wigner space by means of (3.45). After some simple algebra, one then finds

$$\int_{\sigma,\omega} \Omega_{\alpha\gamma}(\tau, \omega + \mathrm{i}0^+, \mathbf{p} = 0) \exp\left[\sigma\left(\frac{1}{2}\overleftarrow{\partial}_\tau - \mathrm{i}\omega + \overrightarrow{\partial}_\tau\right)\right] T^\alpha_{k\beta} \phi^\beta(\tau) = 0. \tag{3.108}$$

where $\sigma = t - t'$ and, for aesthetic reasons, we have changed t' to τ. In principle, not much can be generally done to further simplify this equation. However, as argued in Sec. 3.1.5, one expects later stages of evolution to be comparatively smooth with respect to central time. Therefore, to leading order (in the gradient expansion), one may neglect ∂_τ-derivatives, which yields

$$\Omega_{\alpha\gamma}\left(\tau, \omega = \mathrm{i}0^+, \mathbf{p} = 0\right) T^\alpha_{k\beta} \phi^\beta(\tau) \approx 0. \tag{3.109}$$

Following the same line of reasoning as above, we readily conclude that $\Omega_{\alpha\beta}(\tau, p = 0)$ contains zero modes. At this point, we further recall that to lowest order in the gradient expansion also the Moyal inverse reduces to the ordinary multiplicative one, see (3.50) and (3.52). Hence, the pole structure of the retarded/advanced propagator is again encoded in the zeros of Ω. The presence of zero eigenvalues in the mass matrix $\Omega_{\alpha\beta}(\tau, p = 0)$ therefore signals that there are gapless modes in the spectrum. While hand-waving at best, this argument suggests that, at least during later stages of the evolution, the Goldstone theorem should work in the usual manner even for time-evolving nonequilibrium systems.

---

[6]It is straightforward to show that $\Omega_{\alpha\beta}(\tau, \omega + \mathrm{i}0^+, \mathbf{p}) = \Omega_{\beta\alpha}(\tau, -\omega - \mathrm{i}0^+, -\mathbf{p})$, so that $\Omega_{\alpha\beta}(\tau, \omega = \mathrm{i}0^+, \mathbf{p} = 0) = \Omega_{\beta\alpha}(\tau, \omega = -\mathrm{i}0^+, \mathbf{p} = 0)$. The $\pm \mathrm{i}0^+$ part, which stems from the causal structure of the effective action, is not relevant in this context and can be ignored.

We close this discussion by noting that the question of the number of Goldstone modes is in fact more subtle in nonrelativistic systems. In that case, some of the ostensible zero modes can actually be null-vectors.[7] This was first explored in [116] and then not too long ago thoroughly examined in [117]. The result is that, in nonrelativistic systems with N spontaneously broken generators, gapless excitations in general come in two kinds: the so-called type-A modes with $\omega(\mathbf{p}) \sim |\mathbf{p}|^{2l+1}$ and the type-B modes with $\omega(\mathbf{p}) \sim |\mathbf{p}|^{2l}$. In total, there are $n + 2m = N$ of them, where n (m) is the number of type-A (type-B) modes.

Out of equilibrium, the status of Goldstone's theorem for open classical and quantum systems has been recently studied in detail in [118]. As far as the author knows, the case of time-evolving nonequilibrium in closed systems is yet to be systematically investigated.

Equal-time correlation functions and symmetries

As we have just seen, symmetry identities provide powerful constraints on the structure of correlation functions. In cases when a system exhibits spontaneous breaking of a continuous symmetry, we were able to argue that the spectrum contains gapless modes, which sets limitations on the system's spectral function. Recall, however, that the latter vanishes for coinciding temporal arguments, cf. (3.31). Therefore, this condition does not, in general, impose any constraints on the equal-time (statistical) correlator. To study what effect do symmetries have on the structure of the time-diagonal part of the propagator, it is suggestive to make use of the framework introduced in Sec. 3.2.

We again begin by considering an infinitesimal continuous transformation:

$$\tilde{\varphi}^a(\mathbf{x}) = \varphi^a(\mathbf{x}) + \mathrm{i}\epsilon_k(\mathbf{x})\mathcal{F}_k^a[\mathbf{x}; \Phi]\,, \quad \tilde{\pi}^a(\mathbf{x}) = \pi^a(\mathbf{x}) + \mathrm{i}\epsilon_k(\mathbf{x})\mathcal{P}_k^a[\mathbf{x}; \Phi]\,. \qquad (3.110)$$

Here, for brevity, we have introduced the superfield $\Phi = (\varphi^1, \ldots, \varphi^n; \pi^1, \ldots, \pi^n)$ to denote the collection of both all the fields and their canonically conjugate momenta. As the next step, we change the dummy integration variable in (3.61),

$$Z_t\left[K_\varphi, K_\pi\right] = \int \mathcal{D}\tilde{\varphi}\mathcal{D}\tilde{\pi}\, W_t\left[\tilde{\varphi}, \tilde{\pi}\right] \exp\left[\int_{\mathbf{x}} K_\varphi^a(\mathbf{x})\tilde{\varphi}_a(\mathbf{x}) + K_\pi^a(\mathbf{x})\tilde{\pi}_a(\mathbf{x})\right]\,, \qquad (3.111)$$

and take $\tilde{\varphi}$ with $\tilde{\pi}$ to be of (3.110). Assuming, as before, that the measure is invariant under the transformations in question, expanding to linear order, and using that ϵ is arbitrary we then get

$$\left\langle \left[\frac{\delta \log W_t}{\delta\varphi(\mathbf{x})} + K_\varphi^a(\mathbf{x})\right] \mathcal{F}_{k,a}[\mathbf{x}; \Phi] + \left[\frac{\delta \log W_t}{\delta\pi(\mathbf{x})} + K_\pi^a(\mathbf{x})\right] \mathcal{P}_{k,a}[\mathbf{x}; \Phi] \right\rangle_{W_t, K_\varphi, K_\pi} = 0,$$
$$(3.112)$$

---

[7]Physically, this happens if the symmetry-breaking field corresponds to one of the conserved charges. A textbook example is the O(3) Heisenberg ferromagnetic model. There is only a single gapless mode associated with the O(3) $\to$ O(2) symmetry-breaking pattern, known as the magnon.

cf. (3.97). In the integrated form, the terms with W_t constitute nothing but the change $\delta \log W_t$ under infinitesimal symmetry transformations. If, as presumed in the previous section, the initial condition does not explicitly break the symmetry in question (i.e., $\delta W_{t_0} = 0$), the Wigner functional W_t will remain symmetry-invariant also at any $t > t_0$. For a prove of this (rather self-evident) fact, see App. 3.A. Upon performing the Legendre transform one then ends up with the usual Slavnov–Taylor identities:

$$\int_{\mathbf{x}} \left(\frac{\delta \Gamma[\Phi]}{\delta \phi^a(\mathbf{x})} \mathcal{F}_k^a[\mathbf{x}; \Phi] + \frac{\delta \Gamma[\Phi]}{\delta \Pi^a(\mathbf{x})} \mathcal{F}_k^a[\mathbf{x}; \Phi] \right) = 0. \tag{3.113}$$

Here, for lack of a better notation, Φ denotes the collection $(\phi^1, \ldots, \phi^n; \Pi^1, \ldots, \Pi^n)$ of the full mean fields and conjugate momenta. We have also again supposed that the symmetry is linearly realized.

For concreteness and in light of further relevance, let's consider the case of a simple U(1) symmetry in a nonrelativistic system. Adopting the field representation $\psi = \sqrt{n}\exp(i\varphi)$, the canonically conjugate variables are now the density n and the phase φ [113]. Under an infinitesimal U(1) transform they change as

$$\tilde{\varphi}(\mathbf{x}) = \varphi(\mathbf{x}) + \epsilon, \quad \tilde{n}(\mathbf{x}) = n(\mathbf{x}). \tag{3.114}$$

The master Slavnov–Taylor identity generated by this symmetry transformation reads $\int_{\mathbf{x}} \Gamma_{t,\phi}^{(1)}(\mathbf{x}) = 0$, where ϕ is the full mean phase field (the full density field is denoted by ρ). Upon taking ϕ and ρ derivatives one gets

$$\int_{\mathbf{x}} \Gamma_{t,\phi\phi}^{(2)}(\mathbf{x}, \mathbf{y}) = \int_{\mathbf{x}} \Gamma_{t,\phi\rho}^{(2)}(\mathbf{x}, \mathbf{y}) = 0, \tag{3.115}$$

which for a spatially translation-invariant case means $\Gamma_{t,\phi\phi}^{(2)}(\mathbf{p} = 0) = \Gamma_{t,\phi\rho}^{(2)}(\mathbf{p} = 0) = 0$.

The equal-time propagators $G_{t,\alpha\beta}$ can be readily obtained by virtue of inverting the $\Gamma^{(2)}$ matrix:

$$\begin{pmatrix} G_{t,\phi\phi}(\mathbf{p}) & G_{t,\phi\rho}(\mathbf{p}) \\ G_{t,\rho\phi}(\mathbf{p}) & G_{t,\rho\rho}(\mathbf{p}) \end{pmatrix} = \frac{1}{\Gamma_{t,\phi\phi}^{(2)}(\mathbf{p})\Gamma_{t,\rho\rho}^{(2)}(\mathbf{p}) - \Gamma_{t,\phi\rho}^{(2)}(\mathbf{p})\Gamma_{t,\rho\phi}^{(2)}(\mathbf{p})} \begin{pmatrix} \Gamma_{t,\rho\rho}^{(2)}(\mathbf{p}) & -\Gamma_{t,\phi\rho}^{(2)}(\mathbf{p}) \\ -\Gamma_{t,\rho\phi}^{(2)}(\mathbf{p}) & \Gamma_{t,\phi\phi}^{(2)}(\mathbf{p}) \end{pmatrix}, \tag{3.116}$$

or explicitly,

$$G_{t,\rho\phi}(\mathbf{p}) = \frac{\Gamma_{t,\rho\phi}^{(2)}(\mathbf{p})}{\Gamma_{t,\phi\phi}^{(2)}(\mathbf{p})\Gamma_{t,\rho\rho}^{(2)}(\mathbf{p}) - \Gamma_{t,\rho\phi}^{(2)}(\mathbf{p})\Gamma_{t,\phi\rho}^{(2)}(\mathbf{p})}, \tag{3.117a}$$

$$G_{t,\rho\rho}(\mathbf{p}) = \frac{1}{\Gamma_{t,\rho\rho}^{(2)}(\mathbf{p}) - \Gamma_{t,\rho\phi}^{(2)}(\mathbf{p})\Gamma_{t,\phi\rho}^{(2)}(\mathbf{p})/\Gamma_{t,\phi\phi}^{(2)}(\mathbf{p})}, \tag{3.117b}$$

$$G_{t,\phi\phi}(\mathbf{p}) = \frac{1}{\Gamma_{t,\phi\phi}^{(2)}(\mathbf{p}) - \Gamma_{t,\rho\phi}^{(2)}(\mathbf{p})\Gamma_{t,\phi\rho}^{(2)}(\mathbf{p})/\Gamma_{t,\rho\rho}^{(2)}(\mathbf{p})}. \tag{3.117c}$$

With this, we can analyze the $\mathbf{p} \to 0$ limit. To that end, we first note that, for a homogeneous full mean field to be stable, the second order derivative of the effective action $\Gamma^{(2)}_{\alpha\beta}(\mathbf{p} \to 0)$ evaluated in said configuration has to be positive definite. In our case, this simply implies $\Gamma^{(2)}_{t,\rho\rho}(\mathbf{p} \to 0) = \text{const.} > 0$. Plugging this into (3.117c) we then readily deduce that $G_{t,\phi\phi}$ does not have a finite $\mathbf{p} \to 0$ limit. In contrast, the density-density correlator $G_{t,\rho\rho}$ approaches a finite constant value. Generalizing this argument to other cases of spontaneous symmetry breaking, we say that equal-time propagators of soft (Goldstone) modes are expected to diverge in the limit of vanishing momentum, whereas the massive modes should have a finite $\mathbf{p} \to 0$ limit.

Recalling the discussion in Sec. 2.1 one can speculate that the IR plateau observed in Fig. 2.2 is due to densities, while the phase correlator is expected to have a pure power-law form all the way up to the IR cutoff scale. Note that in this case one can no longer distinguish between the dynamical scaling exponents α and β. Instead, one has a very simple scaling form $F(t, t, \mathbf{p}) \sim t^{-\gamma} p^{-\kappa}$, with a single temporal exponent γ.

A remark is in order. Note that a typical initial condition is not translationally invariant. For example, the box initial condition (2.1) explicitly introduces a scale Q and a plateau to the system. Intuitively, based on the above discussion, one expects this scale to decouple from the late-time IR behavior of the Goldstone propagators. Such an absence of an IR plateau in phase correlators during the scaling regime after quenches has been indeed observed in classical-statistical simulations [119], although a thorough investigation is still lacking. It would be therefore interesting to systematically study the IR behavior of soft-mode propagators in various systems (having different symmetry groups, relativistic and nonrelativistic), with and without transnationally-invariant initial conditions, to test the above formulated intuitive picture.

Finally, of great theoretical and experimental relevance is also the topic of small explicit symmetry violations. They can come either from a Hamiltonian itself, or from initial conditions, or both. In App. 3.A, we show that in the second case, the symmetry violation at time $t > t_0$ can be expressed as

$$\delta W_t [\varphi, \pi] = \sum_{n=0}^{\infty} \frac{(\mathrm{i}t)^n}{n!} \left\{ \left\{ (H [\varphi, \pi])^n, \delta W_{t_0} [\varphi, \pi] \right\} \right\}. \tag{3.118}$$

This raises a series of natural questions. First, one may ask if there is a class of Hamiltonians and symmetry violation scenarios (e.g., linear or quadratic), for which the above expression can be brought to a closed form. Secondly, what can be said about the general fate of initial symmetry violations: when do they grow and when do they decay? Lastly, what is the effect of such symmetry violations? Could they generate an IR plateau for soft modes?[8] To the

---

[8] As a suggestive analogy, recall how in QCD, would-be-Goldstone pions acquire small but finite masses due to a minor explicit chiral symmetry violation.

best of author's knowledge, none of these question have been so far properly addressed in the literature.

3.4   Basics of functional renormalization group

In the following part, we will provide a quick overview of the (functional) renormalization group framework and its connection to critical phenomena and scaling. In contrast to the previous sections, here we consider the case of a real scalar field in d-dimensional *Euclidean space*. Compared to the Minkowski case, it has the advantage that unfavorable field configurations are strongly exponentially damped via $\exp(-S)$ rather than being suppressed by a rapidly oscillating phase factor $\exp(\mathrm{i}S)$, which makes the convergence properties more evident and clear. A formal generalization to the Minkowski spacetime, however, is straightforward.

3.4.1   Wilsonian renormalization group

In the path-integral language, the generating functionals introduced in Sec. 3.1 are equivalent to integrating out all quantum fluctuations at once:

$$Z[J;\Lambda] = \int [\mathcal{D}\varphi]_{\text{reg}}\, \mathrm{e}^{-S_\Lambda[\varphi;\mathbf{g}]+J\cdot\varphi}. \tag{3.119}$$

Here, we have punctiliously assumed a properly regularized measure $[\mathcal{D}\varphi]_{\text{reg}}$, which, in particular, instructs one that only field configurations with momenta smaller than Λ are involved. In the following, we will drop both the subscript 'reg' as well as the indication of the implicit dependence of $Z[J]$ on Λ.

The *ultraviolet (UV) cutoff* scale Λ serves as a maximally allowed energy, which only for UV-complete theories can be sent to infinity. This scale may have a physical origin, in which case it usually marks the breakdown of a model: for example, it can be an inverse lattice spacing $1/a$ when studying discrete models using field-theoretic methods or the electroweak scale in quantum electrodynamics. On the other hand, it might also be a mere technical tool to regulate short-distance divergences and render computations finite. In either case, the *microscopic action* $S_\Lambda[\phi;\mathbf{g}]$ describes the system in terms of degrees of freedom – represented by the field φ – that are appropriate at this scale Λ.

Usually, the action can be written as an integral of a polynomial of the field and derivatives thereof, with the coefficients $\mathbf{g} = (g_1, g_2, \ldots)$ called *coupling constants*. If the action is quadratic in the field, it is called *Gaussian* and the integration (3.119) can be performed exactly. Unfortunately, in virtually all cases of interest, the action involves higher-order (interaction) terms hindering the exact integration. One therefore has to rely on approximations. Among the simplest of them are *mean-field theory*, in which one evaluates the path

integral using a saddlepoint method, and the *Gaussian approximation*, where one retains fluctuations around the saddle point to the quadratic order. As we will see, however, in low-dimensional systems (more specifically, below the so-called *upper critical dimension* of the system) these approximation schemes become unreliable. The Wilsonian *renormalization group* method will allow us to not only overcome this problem, but will also provide us with a natural framework to study scaling phenomena.

The basic idea of Wilson is, instead of integrating all the fluctuations in one go, to do it iteratively, integrating out high-energy fluctuations step by step. After each iteration, one obtains an effective theory for the remaining low-energy modes. To achieve this, we first split the degrees of freedom into slow ($\varphi_<$) and fast ($\varphi_>$) modes by writing the field as a sum

$$\varphi(\mathbf{p}) = \varphi_>(\mathbf{p}) + \varphi_<(\mathbf{p}) \,, \tag{3.120}$$

where

$$\operatorname{supp}(\varphi_<) = \left\{ \mathbf{p} \in \mathbb{R}^d : |\mathbf{p}| \leq \Lambda/b \right\}, \quad \operatorname{supp}(\varphi_>) = \left\{ \mathbf{p} \in \mathbb{R}^d : \Lambda \geq |\mathbf{p}| \geq \Lambda/b \right\}, \tag{3.121}$$

with $b > 1$. Let us choose the source J such that it only couples to the slow modes. The generating functional $Z[J]$ can then be rewritten as

$$Z[J] = \int \mathcal{D}\varphi_< \, \mathrm{e}^{J \cdot \varphi_<} \int \mathcal{D}\varphi_> \, \mathrm{e}^{-S_\Lambda[\varphi_< + \varphi_>; \mathbf{g}]} \equiv \int \mathcal{D}\varphi_< \, \mathrm{e}^{-S_{\Lambda'}^<[\varphi_<; \mathbf{g}_<] + J \cdot \varphi_<} \,. \tag{3.122}$$

Here, $\Lambda' \equiv \Lambda/b$ and the couplings $\mathbf{g}_<$ in the new effective action $S_{\Lambda'}^<$ will in general differ from the original ones. In fact, such a *coarse-graining* procedure will always generate all possible terms (couplings) that are compatible with the system's symmetries. As we will shortly see, however, for many purposes it suffices to keep track on only a handful of them.

After completing the *mode elimination* step, one still cannot directly compare the original action S_Λ with its coarse-grained counterpart $S_{\Lambda'}^<$. To bring everything to the same form as before the mode integration, one has to rescale all momenta and fields. This point is best illustrated in the *Kadanoff block-spin picture*, which can be thought as both the precursor and the real-space analogue of the Wilsonian momentum-shell renormalization, see Fig. 3.2 and the caption therein. Stated mathematically, we define rescaled momenta $\mathbf{p}'$ and fields φ' via

$$\mathbf{p}' = b\mathbf{p}, \quad \varphi'(\mathbf{p}') = \zeta_b^{-1} \phi^<(\mathbf{p}'/b) \,. \tag{3.123}$$

Here, ζ_b is the field rescaling factor to be determined shortly. Although there is a certain freedom in its choice, it is customary to define it such that the kinetic term of the renormalized action $S'[\varphi']$ retains its canonical form. As an example, consider a simple $\mathbb{Z}_2$-symmetric scalar field. As has been already mentioned, in general a mode elimination step will generate all possible terms consistent with the system's symmetries, so the quadratic part of the
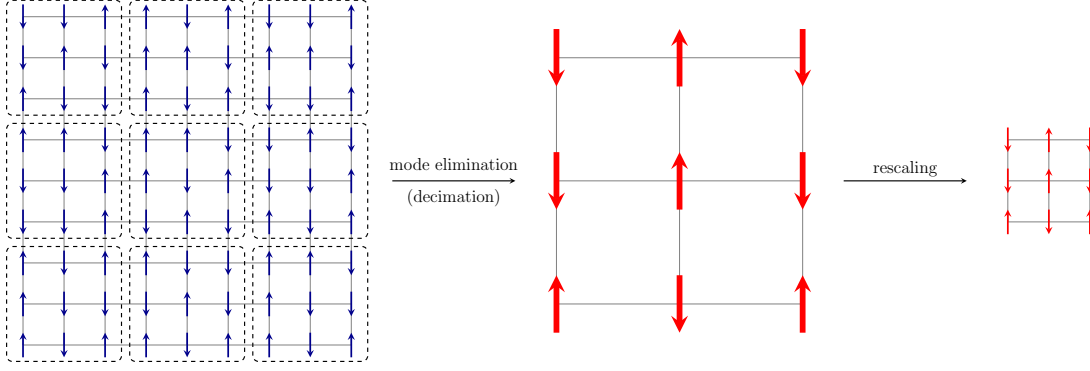
Figure 3.2. Kadanoff's mode elimination and rescaling procedures for the two-dimensional Ising model. In the first step (left), the microscopic spins are grouped forming 'mesoscopic' block spins (middle) for $b = 3$. After this step, the lattice spacing a' is $b = 3$ as big as the original one a. By rescaling the distances and fields by a' one comes back to the situation where all the distances are measured by the intrinsic unit a'. Note that the new lattice is then identical to the original one, except the number of spins has reduced by the factor of b^2. In thermodynamic limit, however, which is always implicitly assumed, the latter does not play a significant role.

action will take a form

$$
\begin{aligned}
&\frac{1}{2} \int\limits_{|\mathbf{p}|<\Lambda/b} \frac{\mathrm{d}^d\mathbf{p}}{(2\pi)^d}\, \varphi_<(-\mathbf{p}) \left[m_<^2 + a_{2,<}\mathbf{p}^2 + a_{4,<}\mathbf{p}^4 + \ldots\right] \varphi_<(\mathbf{p}) \\
&= \frac{1}{2} \int\limits_{|\mathbf{p}|<\Lambda} \frac{\mathrm{d}^d\mathbf{p}'}{(2\pi)^d}\, \varphi'(-\mathbf{p}') \left[m'^2 + \mathbf{p}'^2 + a_4'\mathbf{p}'^4 + \ldots\right] \varphi'(\mathbf{p}').
\end{aligned}
\tag{3.124}
$$

From the second line, we can read off the scaling factor as

$$
\zeta_b = b^{1+d/2}\sqrt{a_{2,<}} \equiv b^{1+d/2}\sqrt{Z_b}.
\tag{3.125}
$$

We observe that it consists of two pieces: the simple part $b^{1+d/2} \equiv b^{d_\varphi}$, which is present even in the absence of interactions, follows readily from the microscopic action by means of dimensional analysis. It defines the *engineering dimension* d_φ of the field $\varphi(\mathbf{p})$. The nontrivial part Z_b, known as the *wave function renormalization*, on the other hand, is due to interactions and can modify the field's simple scaling properties near a critical point (see below).

Upon performing both steps (mode elimination and rescaling) the renormalized action takes the same form as the original one, but with modified coupling constants $\mathbf{g}'$, which defines a mapping

$$
\mathbf{g}' = \mathcal{R}(b; \mathbf{g}).
\tag{3.126}
$$

One can then proceed by iterating the same procedure again, but now with $\mathbf{g}'$ as the initial

couplings. By construction,

$$\mathbf{g}'' = \mathcal{R}(b'; \mathbf{g}') = \mathcal{R}(b'; \mathcal{R}(b; \mathbf{g})) = \mathcal{R}(b'b; \mathbf{g}), \quad \mathcal{R}(1; \mathbf{g}) = \mathbf{g}, \tag{3.127}$$

which implies that the set of transformations $\mathcal{R}$ form a one-parameter semigroup, known as the *renormalization group (RG)*. Upon iterating RG transformations over and over again, one probes more and more macroscopic (infrared) physics. In practice, it is more convenient to do this in infinitesimal steps, $b = \exp(l)$, $l \ll 1$, and recast the map (3.126) into a set of ordinary differential equations:

$$\partial_l g_i = \beta_{g_i}(\mathbf{g}), \tag{3.128}$$

where on the right-hand side we have introduced the *(Gell-Mann–Low) β-functions* $\beta_{g_i}(\mathbf{g}) = \lim_{l \to 0} \left[\mathcal{R}_i \left(e^l; \mathbf{g} \right) - \mathbf{g} \right] / l$.

Of great importance are fixed points $\mathbf{g}^*$ of the map (3.126) or, equivalently, of the *RG flow* (3.128):

$$\mathbf{g}^* : \quad \mathbf{g}^* = \mathcal{R}(b; \mathbf{g}^*) \iff \beta_i(\mathbf{g}^*) = 0. \tag{3.129}$$

Once the system reaches an RG fixed point, it no longer changes under subsequent RG transformations: the coarse-grained (and appropriately rescaled) picture looks exactly the same as the original one. Such systems are called *self-similar* or *scale-invariant*. To better illustrate this point, recall that for any system there is always an intrinsic scale ξ characterizing an exponential decay of correlations.[9] It is straightforward to show that, under an RG step, the latter transforms as $\xi' \equiv \xi(\mathbf{g}') = \xi(\mathbf{g})/b$. At a fixed point, one has $\xi(\mathbf{g}^*) = \xi(\mathbf{g}^*)/b$, which can be only satisfied if either $\xi = \infty$ (*critical fixed points*), in which case the (two-point) correlator is expected to have a power-law form, or $\xi = 0$ (*trivial fixed points*), so that the correlator is simply constant.

In fact, it is easy to see that $\xi = \infty$ not only for the specific values $\mathbf{g}^*$ of the couplings, but also for the entire basin of attraction of the critical point, i.e., for all the couplings that are mapped to $\mathbf{g}^*$ by the RG flow. Such a subspace of couplings $\{\mathbf{g} : \boldsymbol{R}^{(n \to \infty)}(b; \mathbf{g}) = \mathbf{g}^*\}$ is called the fixed point's *critical surface*. The existence of such basins of attraction explains the notion of the *universality* of critical phenomena: all theories with microscopic couplings lying on a critical surface flow to the same critical point and thus demonstrate the same macroscopic behavior. The codimension of a critical manifold defines the number of couplings that have to be fine-tuned in order to observe universal scaling behavior. In practice, however, it suffices to set fine-tuning parameters close, but not exactly on the critical surface (which is anyway experimentally impossible). In this case, the RG trajectory will move toward $\mathbf{g}^*$ and stay in its vicinity until eventually departing away. However, because

---

[9]Of course, for anisotropic/nonequilibrium/etc. systems, there could be more than one such scale, each characterizing exponential decay along their respective coordinate.

the flow almost vanishes in the neighborhood of a fixed point, this 'nearly critical' RG trajectory will stuck around the fixed point for a long 'RG time'. The correlation length then will be finite, yet exceeding the physical dimension L, which also determines the maximum RG time in this scenario.

Since, as just discussed, scaling behavior is controlled by a given fixed point $\mathbf{g}^*$ and its surroundings, it is suggestive to consider it more closely by studying the linearized flow (3.128) in the vicinity of $\mathbf{g}^*$:

$$\partial_l \delta g_i = \mathcal{B}_{ij}(\mathbf{g}^*)\delta g_j + O(\delta g^2)\,, \tag{3.130}$$

where $\delta \mathbf{g} \equiv \mathbf{g} - \mathbf{g}^*$ and $\mathcal{B}_{ij} \equiv \partial \beta_{g_i}/\partial g_j$. Near the fixed point, the flow is determined by the *stability matrix* $\mathcal{B}_{ij}$. Let $\mathbf{v}_\alpha$ be its (left) eigenvector with eigenvalue λ_α. The linear combinations $u_\alpha = \mathbf{v}_\alpha^T \cdot \delta \mathbf{g}$ are called *scaling variables*. By construction, their RG flow takes a particularly simple form $\partial_l u_\alpha = \lambda_\alpha y_\alpha$. Scaling variables with $\mathrm{Re}\{\lambda_\alpha\} < 0$ are called *irrelevant* since, even if one tunes them away from the critical surface, the RG flow will bring them back as if they never existed. Likewise, variables with $\mathrm{Re}\{\lambda_\alpha\} > 0$ are called *relevant*: they are the fine-tuning parameters one has to adjust in order to get on the critical surface and their corresponding eigenvectors span the tangent plane to the critical surface at the fixed point. Finally, there are *marginal* scaling variables with $\mathrm{Re}\{\lambda_\alpha\} = 0$, whose stability cannot be determined by a linearized RG flow.

In general, scaling variables need not to coincide with any of the coupling constants. One important exception is the Gaussian fixed point, where all the eigenvectors are aligned along the 'couplings axes' and their eigenvalues can be deduced by virtue of simple power counting. Above the aforementioned upper critical dimension d_{up}, all the eigenvalues corresponding to interaction couplings turn out to be negative implying that the system flows in the direction of a free field theory. Consequently, large-scale physics is described by the mean-field approximation. Below d_{up}, however, some of the interaction terms will star flowing away from the Gaussian fixed point, thus spoiling the mean-field description. New – non-Gaussian – fixed points may then emerge, controlling macroscopic physics in their vicinity. When fixed-point values of the interaction couplings at such critical points are small, one may employ weak-coupling methods to study them. For more details on the perturbative Wilsonian renormalization group and its application to critical phenomena, we refer to [93, 120, 121].

3.4.2 Functional renormalization group and the Wetterich equation

In the previous section, we have seen how scaling behavior of a self-similar system is controlled by the corresponding RG fixed point and its vicinity. It is therefore tempting to apply the same RG framework to study far-from-equilibrium scaling dynamics associated

with nonthermal fixed points. We face, however, two obstacles. Firstly, the original Wilsonian momentum-shell RG, which we discussed above, is perturbative in nature. Nonthermal fixed points, on the other hand, are typically characterized by strong fluctuations/large occupancies, making perturbative approaches generally not suitable. We shall thus seek for nonperturbative RG schemes. Secondly, since NTFP scaling is formulated in terms of correlation functions, it is desirable to have an RG framework that operates directly with such objects. Both of these goals are achieved by the *functional renormalization group*, which we outline in the following.

The idea that one can write down an exact equation for the Wilsonian effective action S_Λ (or Hamiltonian) goes as back as 1970s, with the first attempts due to Wegner and Houghton [122] and Wilson and Kogut [123]. It was later understood that the sharp separation into fast and slow modes makes such equations hard to work with in practice and even leads to spurious effects. An exact RG equation with a smoothly implemented cutoff was then proposed by Polchinski [124]. Finally, it was realized by Wetterich [125] and slightly later by Morris [126] that a more convenient formulation of an exact flow equation can be obtained in terms of the effective action, whose derivation will be outlined in what follows.

We begin by introducing a cutoff. A versatile and analytically stable way of implementing a smooth cutoff is achieved by adding a quadratic mass-like term $\Delta S_k[\varphi]$ to the action:

$$\Delta S_k[\varphi] = \frac{1}{2} \int_{x,y} \varphi(\mathbf{x})\, R_k(\mathbf{x},\mathbf{y})\, \varphi(\mathbf{y})\,. \tag{3.131}$$

The *regulator* function R_k is chosen such that it suppresses modes with momenta $\mathbf{p}^2 \lesssim k^2$ and does not affect modes with momenta $\mathbf{p}^2 \gtrsim k^2$. This imposes a set of requirements on the regulator:

$$\text{IR suppression}: \qquad \lim_{k^2/\mathbf{p}^2 \to \infty} R_k(\mathbf{p}^2) > 0, \tag{3.132a}$$

$$\text{physical limit}: \qquad \lim_{\mathbf{p}^2/k^2 \to \infty} R_k(\mathbf{p}^2) = 0, \tag{3.132b}$$

$$\text{UV limit}: \qquad \lim_{k \to \Lambda} R_k(\mathbf{p}^2) = \infty. \tag{3.132c}$$

The first condition simply implements an IR regularization. The second one ensures that we recover full generating functionals once the regulator is removed as $k \to 0$. Finally, one can show that the last property implies that the scale-dependent effective action reduces to the bare/microscopic one in the UV limit $k \to \Lambda$.

For simple scalar theories, the regulator is often written as

$$R_k\left(\mathbf{p}^2\right) = \mathbf{p}^2 r\left(\mathbf{p}^2/k^2\right), \tag{3.133}$$

where $r(y)$ is a dimensionless regulator *shape function*. The requirements (3.132) on the regulator R_k translate in an obvious manner into conditions on the shape function. Explicitly,
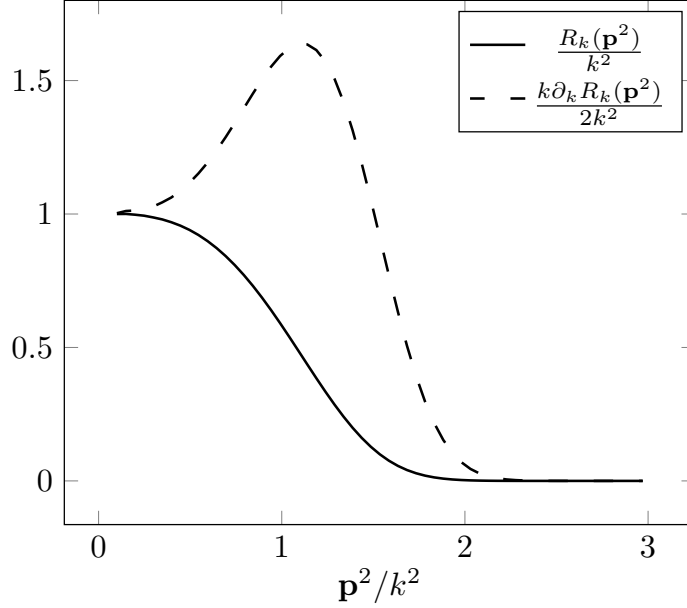
Figure 3.3. A sketch of a typical regulator and its derivative. In this example, we used the exponential shape function (3.136) with $a = c = 1$, $b = 3$. The derivative having a peak around $\mathbf{p}^2/k^2$ implements the Wilsonian momentum-shell idea.

the latter can be summarized as [127]

$$\lim_{y \to \infty} y^{d/2} r(y) = 0, \tag{3.134a}$$

$$\lim_{y \to 0} r(y) \propto y^{-n}, \quad n \geq 1. \tag{3.134b}$$

For analytical calculations, popular choices for the shape function include

$$\text{Litim regulator}: \quad r(y) = \left(\frac{1}{y} - 1\right) \Theta(1 - y),$$
$$\text{sharp regulator}: \quad r(y) = \frac{1}{\Theta(y - 1)} - 1, \tag{3.135}$$

with $\Theta(x)$ being the Heaviside step function. However, non-analytic nature of these regulators make them not-too-suited for numerical implementations. For the latter purposes, a better choice is a family of smooth exponential regulators,

$$r(y) = \frac{a y^{b-c}}{\exp(y^b) - 1}, \tag{3.136}$$

with a, b, and c being parameters to be chosen by hand. A sketch of a typical regulator is shown in Fig. 3.3.

We are now set to derive a functional RG equation. In the presence of a regulator, the generating functional takes the form

$$Z_k[J] = \int \mathcal{D}\varphi \, e^{-S[\varphi] - \Delta S_k[\varphi] + J \cdot \varphi}, \tag{3.137}$$

where the source is taken to be k-independent. Assuming the existence of $Z_{k=0}$ we can write

$$Z_k[J] = \mathrm{e}^{-\Delta S_k[\delta/\delta J]} Z_{k=0}[J]\,, \tag{3.138}$$

from which one infers the equation that governs the generating functional's k-dependence:

$$k\partial_k Z_k[J] = -k\partial_k \Delta S_k[\delta/\delta J] Z_k[J] = -\frac{1}{2}\int_{\mathbf{p}} Z_k^{(2)}[J]\,(\mathbf{p}, -\mathbf{p})\, k\partial_k R_k(\mathbf{p}^2)\,. \tag{3.139}$$

where $\dot{\mathcal{O}}_k \equiv k\partial_k \mathcal{O}_k$. The $k\partial_k$-derivative is used for convenience as it does not alter the dimension of the generating functional.

Introducing the regularized Schwinger functional $W_k = \log Z_k[J]$, the flow equation can be readily rewritten in terms of connected correlation functions:

$$k\partial_k W_k[J] = -\frac{1}{2}\int_{\mathbf{p}} \left[W_k^{(2)}[J](\mathbf{p}, -\mathbf{p}) + W_k^{(1)}[J](\mathbf{p})W_k^{(1)}[J](-\mathbf{p}) \right] k\partial_k R_k(\mathbf{p}^2)\,. \tag{3.140}$$

In this form, it is known as the *(Wilson–)Polchinski equation.* Before we proceed with the flow equation for the quantum effective action, let us take a closer look at the structure of the Polchinski equation. Recalling that $W^{(1)} = \phi$ we recognize resemblance of the second term to the derivative of the regulator $\Delta S_k[\phi]$ evaluated on the mean field. This term is therefore trivial in terms of ϕ, which suggests subtracting it from the flow equation for the effective action for convenience. This can be achieved by modifying the Legendre transform when defining the scale-dependent effective action $\Gamma_k[\phi]$:

$$\Gamma_k[\phi] = \sup_J \left(\int_{\mathbf{p}} J(\mathbf{x})\,\phi(\mathbf{x}) - W_k[J] \right) - \Delta S_k[\phi] = \int_{\mathbf{p}} J_{k,\phi}(\mathbf{x})\,\phi(\mathbf{x}) - W_k[J_{k,\phi}] - \Delta S_k[\phi], \tag{3.141}$$

cf. (3.34). Note that one recovers the usual Legendre transform in the limit $k \to 0$, as it should be. Since we eventually want to study Γ_k as a functional of a k-independent mean field ϕ, the supremum source $J_{k,\phi}$ is necessarily k-dependent, which explains the subscript. As usual, from the definition (3.141),

$$\phi(\mathbf{x}) = W_k^{(1)}[J_{k,\phi}](\mathbf{x})\,, \tag{3.142}$$

while the quantum equation of motion gets slightly modified:

$$\begin{aligned}\Gamma_k^{(1)}[\phi](\mathbf{x}) &= J_{k,\phi}(\mathbf{x}) + \int_{\mathbf{y}} \frac{\delta J_{k,\phi}(\mathbf{y})}{\delta\phi(\mathbf{x})} \left[\phi(\mathbf{y}) - W_k^{(1)}[J_{k,\phi}](\mathbf{y}) \right] - \int_{\mathbf{y}} R_k(\mathbf{x}, \mathbf{y})\phi(\mathbf{y}) \\ &= J_{k,\phi}(\mathbf{x}) - \int_{\mathbf{y}} R_k(\mathbf{x}, \mathbf{y})\phi(\mathbf{y})\,, \end{aligned} \tag{3.143}$$

from which we deduce

$$\frac{\delta J_{k,\phi}(\mathbf{x})}{\delta\phi(\mathbf{y})} = \Gamma_k^{(2)}[\phi](\mathbf{x}, \mathbf{y}) + R_k(\mathbf{x}, \mathbf{y})\,. \tag{3.144}$$

Following the same logic as in Sec. 3.1.4 one then readily obtains

$$G_k[\phi] \equiv W_k^{(2)}[J_{k,\phi}] = \left(\Gamma_k^{(2)}[\phi] + R_k\right)^{-1}. \tag{3.145}$$

We are now set to derive the flow equation for Γ_k:

$$
\begin{aligned}
k\partial_k \Gamma_k[\phi] &= \int_{\mathbf{x}} k\partial_k J_{k,\phi}(\mathbf{x}) \left[\phi(\mathbf{x}) - W_k^{(1)}[J_{k,\phi}](\mathbf{x})\right] - k\partial_k W_k[J]\big|_{J=J_{k,\phi}} - k\partial_k \Delta S_k[\phi] \\
&\stackrel{(3.142),\,(3.140)}{=} \frac{1}{2} \int_{\mathbf{x},\mathbf{y}} W_k^{(2)}[J_{k,\phi}] (\mathbf{x},\mathbf{y})\, k\partial_k R_k(\mathbf{x},\mathbf{y}) \\
&\stackrel{(3.145)}{=} \frac{1}{2} \int_{\mathbf{x},\mathbf{y}} \left(\Gamma_k^{(2)}[\phi] + R_k\right)^{-1} (\mathbf{x},\mathbf{y})\, k\partial_k R_k(\mathbf{x},\mathbf{y}).
\end{aligned}
\tag{3.146}
$$

In the compact notation, this flow equation for the effective action, known as the *Wetterich equation*, can be written as

$$k\partial_k \Gamma_k[\phi] = \frac{1}{2} \operatorname{Tr}\left[\left(\Gamma_k^{(2)}[\phi] + R_k\right)^{-1} \cdot k\partial_k R_k\right]. \tag{3.147}$$

Written in this form, it may be easily generalized to more complicated theories. Here, the trace sums/integrates over spacetime variables, internal indices, and, in general, different fields (if fermions are present, the trace has to be replace with the supertrace). It is worth emphasizing that both the Polchinski and the Wetterich equations are exact and equivalent to one another. The former has a very appealing mathematical structure of a heat equation and is preferred in mathematical physics [128]. In particular, it is widely used for proofs of perturbative renormalizability. On the other hand, the Wetterich equation has better stability properties and is more suitable for practical applications.

By taking field derivatives one readily obtains the flow equations governing k-dependence of the n-point functions $\Gamma_k^{(n)}$. For example,

$$k\partial_k \Gamma_k^{(1)} = -\frac{1}{2} \operatorname{Tr}\left[\Gamma_k^{(3)}[\phi] \cdot (G_k[\phi] \cdot k\partial_k R_k \cdot G_k[\phi])\right], \tag{3.148a}$$

$$k\partial_k \Gamma_k^{(2)} = \frac{1}{2} \operatorname{Tr}\left[\left(-\Gamma_k^{(4)}[\phi] + 2\Gamma_k^{(3)}[\phi] \cdot G_k[\phi] \cdot \Gamma_k^{(3)}[\phi]\right) \cdot (G_k[\phi] \cdot k\partial_k R_k \cdot G_k[\phi])\right], \tag{3.148b}$$

an so forth. For a diagrammatic representation, see Fig. 3.4. Note that all of the equations have a one-loop structure.

One furthermore observes that, e.g., the flow equation for the two-point function $\Gamma_k^{(2)}$ involves 3- and 4-point vertices $\Gamma_k^{(3)}$ and $\Gamma_k^{(4)}$, respectively. In general, the flow of the n-point function will involve propagators up to $\Gamma_k^{(n+2)}$ and have a form

$$k\partial_k \Gamma_k^{(n)}[\phi] = -\frac{1}{2} \operatorname{Tr}\left[\Gamma_k^{(n+2)}[\phi] \cdot (G_k[\phi] \cdot k\partial_k R_k \cdot G_k[\phi]) + \Gamma_k^{(m<n+2)}[\phi] - \text{terms}\right], \tag{3.149}$$

$$k\partial_k \Gamma_k \;=\; \frac{1}{2} \;\bigcirc\;, \qquad k\partial_k \Gamma_k^{(1)} \;=\; -\frac{1}{2} \;\bigcirc\;,$$

$$k\partial_k \Gamma_k^{(2)} \;=\; -\frac{1}{2} \;\bigcirc\; + \;\bigcirc\;$$

Figure 3.4. Diagrammatic representation of the flow equations (3.147) and (3.148). Bold dots denote the propagators and the vertices, whereas the circled cross stands for the insertion of the regulator derivative: $\otimes = k\partial_k R_k$.

In other words, the flow equations result in an infinite hierarchy of coupled integro-differential equations and therefore require a choice of an expansion/truncation scheme that will allow to close it. For an overview of such systematic expansion schemes and their applications in a wide range of physical problems (as well as for a broader introduction to the topic of nonperturbative RG), one is invited to read [129–133]. A deep discussion on the general structure of functional RG flows can be found in [127].

APPENDIX

3.A   Wigner functional and initial conditions

Suppose the Hamiltonian H of a system is invariant under some symmetry group G, while the initial condition may violate the symmetry in question. Infinitesimally then,

$$W_{t_0} \to W_{t_0} + \delta W_{t_0}, \quad H \to H, \tag{3.A.1}$$

where δW_{t_0} is not necessarily vanishing. With the help of the functional Moyal product,

$$A \star B = A[\varphi, \pi] \exp\left[\frac{\mathrm{i}}{2} \int_{\mathbf{x}} \left(\frac{\overleftarrow{\delta}}{\delta \varphi(\mathbf{x})} \frac{\overrightarrow{\delta}}{\delta \pi(\mathbf{x})} - \frac{\overleftarrow{\delta}}{\delta \pi(\mathbf{x})} \frac{\overrightarrow{\delta}}{\delta \varphi(\mathbf{x})} \right) \right] B[\varphi, \pi], \tag{3.A.2}$$

cf. (3.50), a formal solution to the Moyal equation (3.68) can be written as [105]

$$W_t[\varphi, \pi] = U_{t,\star}^{-1}[\varphi, \pi] \star W_{t_0}[\varphi, \pi] \star U_{t,\star}[\varphi, \pi], \tag{3.A.3}$$

Here, we have also introduced a $\star$-unitary evolution operator

$$U_{t,\star} = \exp_\star(\mathrm{i}tH) \equiv 1 + \mathrm{i}tH - \frac{t^2}{2} H \star H - \frac{\mathrm{i}t^3}{3!} H \star H \star H + \dots \tag{3.A.4}$$

and set $t_0 = 0$ for brevity. Since $\star$-map is bilinear and H is invariant, we deduce that under the infinitesimal symmetry transformation

$$W_t[\varphi, \pi] \to W_t[\varphi, \pi] + \underbrace{U_{t,\star}^{-1}[\varphi, \pi] \star \delta W_{t_0}[\varphi, \pi] \star U_{t,\star}[\varphi, \pi]}_{\equiv \delta W_t[\varphi, \pi]}. \tag{3.A.5}$$

For $\delta W_{t_0} = 0$, we immediately obtain that also $\delta W_{t > t_0} \equiv 0$, as expected.

Let us also briefly discuss the case $\delta W_{t_0} \neq 0$. Invoking the Baker–Campbell–Hausdorff formula for the Moyal product,

$$\mathrm{e}^X \star Y \star \mathrm{e}^{-X} = \sum_{n=0}^\infty \frac{1}{n!} \left\{\{(X)^n, Y\}\right\}, \tag{3.A.6}$$

where

$$\left\{\{(X)^n, Y\}\right\} \equiv \underbrace{\left\{\{X, \dots \{\{X, \{\{X, Y\}\}\}\} \dots\}\right\}}_{n \text{ times}}, \tag{3.A.7}$$

one immediately finds

$$\delta W_t[\varphi, \pi] = \sum_{n=0}^\infty \frac{(\mathrm{i}t)^n}{n!} \left\{\{(H[\varphi, \pi])^n, \delta W_{t_0}[\varphi, \pi]\}\right\}. \tag{3.A.8}$$

Chapter 4

A functional renormalization group approach to nonthermal fixed points in an ultracold Bose gas

In Ch. 2, we have presented the general concept of a far-from-equilibrium scaling near nonthermal fixed points. In addition, we have shown how nonthermal fixed points can be described as self-similar solutions to evolution equations governing the dynamics of correlation functions. In Sec. 3.4, on the other hand, we have seen how a general scaling has a natural interpretation in terms of fixed points of the renormalization group flow. In particular, we saw that all the universal scaling properties can be extracted from the vicinity of a given infrared fixed point. It is therefore suggestive to try to extend this idea to the case of a far-from-equilibrium self-similar dynamics and demonstrate how nonthermal fixed points can be understood from the renormalization-group perspective. To a certain degree, this goal has been already achieved for the case of (strong) stationary nonequilibrium, see, e.g., [71, 134, 135]. In addition, an alternative renormalization scheme involving a temporal regulator has been proposed as a suitable description of far-from-equilibrium systems even beyond the stationary case [136–138]. However, a complete satisfactory RG description of nonthermal fixed points is still lacking. In this work, we attempt to implement this program for a specific example of a single-component Bose gas. The employed method follows closely the works [139] and [135], in which the fixed-point fRG equations were used to analyze infrared scaling properties in Landau gauge QCD and the stochastic driven-dissipative Burgers' equation, respectively.

4.1 Model

We consider a system of a uniform single-component Bose gas described by the Hamiltonian

$$\hat{H} = \int d^d\mathbf{x} \left[-\hat{\Psi}^\dagger \frac{\nabla^2}{2m} \hat{\Psi} + \frac{g}{2} \left(\hat{\Psi}^\dagger \hat{\Psi} \right)^2 \right], \tag{4.1}$$

where m is the particle mass and the nonrelativistic bosonic field operators satisfy the usual commutation relations,

$$[\hat{\Psi}(\mathbf{x}), \hat{\Psi}^\dagger(\mathbf{y})] = \delta(\mathbf{x} - \mathbf{y}), \quad [\hat{\Psi}(\mathbf{x}), \hat{\Psi}(\mathbf{y})] = [\hat{\Psi}^\dagger(\mathbf{x}), \hat{\Psi}^\dagger(\mathbf{y})] = 0, \tag{4.2}$$

in the Schrödinger picture. As has been mentioned in Ch. 1, nonequilibrium scaling associated with nonthermal fixed points has been recently observed in such systems in the experiment [17].

From this Hamiltonian, using the coherent-state path integral formalism [140] one may obtain the microscopic action

$$S[\psi, \psi^*] = \int d^d\mathbf{x}\, dt \left[\frac{i}{2} \left(\psi^* \partial_t \psi - \psi \partial_t \psi^* \right) - \frac{1}{2m} \nabla\psi^* \cdot \nabla\psi - \frac{g}{2} \left(\psi^* \psi \right)^2 \right]. \tag{4.3}$$

This action is clearly invariant under global U(1) transformations,

$$\psi(x) \to e^{i\alpha}\psi(x), \quad \psi^*(x) \to e^{-i\alpha}\psi^*(x), \tag{4.4}$$

implying the particle-number conservation. This symmetry may be (spontaneously) broken forming a (quasi)condensate

$$\left\langle \hat{\Psi}(x) \right\rangle = \psi_0(x) = \sqrt{n_0(x)} \exp\left[i\mathcal{K}(x) \right] \neq 0. \tag{4.5}$$

In this case, it is often convenient to adopt the density-phase representation of the field,

$$\psi(x) = \sqrt{n(x)} \exp\left[i\theta(x) \right], \tag{4.6}$$

and consider the dynamics of density-phase fluctuations on top of the background solution: $n(x) = n_0(x) + \delta n(x)$, $\theta(x) = \mathcal{K}(x) + \varphi(x)$. In the Bogoliubov approximation and in the absence of external potential, $\mathcal{K}^{\mathrm{B}}(x) = -\mu t$ and $n_0^{\mathrm{B}} = \mu/g$, with μ being the chemical potential generally defined through the condition

$$\int d^d\mathbf{x} \left\langle \hat{\Psi}^\dagger(x)\, \hat{\Psi}(x) \right\rangle = N, \tag{4.7}$$

where N is the total particle number [111].

At sufficiently low energies/temperatures (below the healing-length momentum scale), density fluctuations are suppressed and the interesting physics is mostly encoded in the dynamics of phase fluctuations. As first argued in [141, 142] and [143] based on Galilean

invariance and later further explored in [144], the leading-order Lagrangian of the phase excitations in superfluids is given by

$$\mathcal{L}_{\text{eff}}^{\text{LO}} = P\left(D_t\theta\right), \tag{4.8}$$

where P is a polynomial function and $D_t\theta$ is a Galilei-invariant combination (see App. 4.A.1):

$$D_t\theta = \partial_t\theta - \frac{1}{2m}\left(\nabla\theta\right)^2 = -\mu + \partial_t\varphi - \frac{(\nabla\varphi)^2}{2m}. \tag{4.9}$$

In equilibrium, the simplest nontrivial Lagrangian of the form (4.8),

$$\mathcal{L} = a_1 D_t\theta + a_2\left(D_t\theta\right)^2 \tag{4.10}$$

gives qualitatively correct results, such as the Beliaev damping rate, already at one loop [145]. It is therefore suggestive to employ such an effective-field-theoretic (EFT) description also for nonequilibrium studies. In [64], an EFT approach was successfully applied for the description of nonthermal fixed points in a $U(N)$-symmetric Bose gas. Scaling properties derived within the EFT formalism were shown to be equivalent to those obtained using the large-N resummed kinetic theory. This further reinforces the idea of adopting the EFT description for studying scaling dynamics far from thermal equilibrium.

Out of equilibrium, however, the approximation $\mathcal{K} = -\mu t$ no longer holds. Nevertheless, if there is a nontrivial static equilibrium solution to the Gross–Pitaevskii equation,

$$\left[i\partial_t + \frac{\nabla^2}{2m} - g|\psi_0|^2 - 2g\rho_{\text{qp}} - \partial_t\mathcal{K}\right]\psi_0 = 0, \tag{4.11}$$

with $\rho_{\text{qp}}(x)$ being a quasiparticle density at $x = (t, \mathbf{x})$, then the background phase $\mathcal{K}(x)$ can be expressed through the slowly varying densities of the condensate $\rho_0 = |\psi_0|^2$ and the quasiparticles as [111]

$$-\partial_t\mathcal{K} = g\rho_0 + 2g\rho_{\text{qp}} = \mu. \tag{4.12}$$

The nonequilibrium chemical potential may then be fixed by the condition $\int d^d\mathbf{x}\left(\rho_0 + \rho_{\text{qp}}\right) = N$. Hence, even out of equilibrium, in the presence of a (quasi)condensate, one expects that the leading-order phase dynamics may be captured by the Lagrangian (4.8). The existence of such a quasicondensate during the scaling regime of a single-component Bose gas at the NTFP has been observed in, e.g., [66].

4.2 Fixed point equations

4.2.1 Nonperturbative RG flow equation action and parameterization of the propagators

In Sec. 3.4.2, we have derived the exact renormalization-group equation for the quantum effective action in Euclidean space. This equation can be straightforwardly generalized to

the case of Minkowski spacetime:

$$k\partial_k \Gamma_k[\phi] = \frac{\mathrm{i}}{2}\mathrm{Tr}\left[\left(\Gamma_k^{(2)}[\phi] + R_k\right)^{-1} \cdot k\partial_k R_k\right],\tag{4.13}$$

where, as usual, the trace sums/integrates over spacetime variables, internal indices, and, in general, different fields. In our case of a single-component scalar field out of equilibrium, the role of an internal index is played by $a \in \{\mathrm{cl}, \mathrm{q}\}$.

The central object of interest in this work will be a two-point function $\Gamma_k^{(2)}$ whose flow equation can be readily obtained by taking two field derivatives of (4.13):

$$k\partial_k \Gamma_{k,\mathbf{ab}}^{(2)} = \frac{\mathrm{i}}{2}G_{k,\mathbf{cd}}\Gamma_{k,\mathbf{dabe}}^{(4)}G_{k,\mathbf{ef}}k\partial_k R_{k,\mathbf{cf}}$$

$$- \frac{1}{2}\left(G_{k,\mathbf{cd}}\Gamma_{k,\mathbf{dae}}^{(3)}G_{k,\mathbf{eh}}\Gamma_{k,\mathbf{hbj}}^{(3)}G_{k,\mathbf{jf}}k\partial_k R_{k,\mathbf{cf}} + \underbrace{\mathrm{perm.}}_{\mathbf{a}\leftrightarrow\mathbf{b}}\right) \equiv I_{k,\mathbf{ab}}.\tag{4.14}$$

cf. (3.148). Here, perm. stands for permutation of the external legs and the DeWitt notation $\mathbf{a} = (t, \mathbf{x}, \mathrm{cl}/\mathrm{q})$ as well as the Einstein summation convention are assumed. The regularized propagator is directly related to the second derivative of the modified effective action:

$$G_{k,\mathbf{ab}}[\phi] = \mathrm{i}\left(\Gamma_k^{(2)}[\phi] + R_k\right)^{-1}_{\mathbf{ab}},\tag{4.15}$$

cf. (3.40) and (3.145).

4.2.2 Parametrization

As has been discussed in Sec. 3.4, information about the universal scaling properties, such as the scaling exponents, is encoded in the IR fixed points and their vicinities. This suggests to parameterize the inverse propagator, as we approach a fixed point at vanishing cutoff $k = 0$, in terms of the scaling form as [135, 139]

$$\Gamma_{k,\mathrm{clq}}^{(2)}(t, t', \mathbf{p}) = \Gamma_{\mathrm{clq}}^{(2)}(t, t', \mathbf{p}) - \mathrm{i}\left(\Gamma_{\mathrm{clq}}^{(2)} \circ [G_{\mathrm{qcl}}\delta Z_{k,\rho}] \circ \Gamma_{\mathrm{clq}}^{(2)}\right)(t, t', \mathbf{p}),$$

$$\Gamma_{k,\mathrm{qcl}}^{(2)}(t, t', \mathbf{p}) = \Gamma_{\mathrm{qcl}}^{(2)}(t, t', \mathbf{p}) - \mathrm{i}\left(\Gamma_{\mathrm{qcl}}^{(2)} \circ [\delta Z_{k,\rho}G_{\mathrm{clq}}] \circ \Gamma_{\mathrm{qcl}}^{(2)}\right)(t, t', \mathbf{p}),\tag{4.16a}$$

$$\Gamma_{k,\mathrm{qq}}^{(2)}(t, t', \mathbf{p}) = \Gamma_{\mathrm{qq}}^{(2)}(t, t', \mathbf{p}) + \mathrm{i}\left(\Gamma_{\mathrm{qcl}}^{(2)} \circ [F\delta Z_{k,F}] \circ \Gamma_{\mathrm{clq}}^{(2)}\right)(t, t', \mathbf{p}),\tag{4.16b}$$

where δZ_ρ and δZ_F are the deviations of the two-point correlators from those at vanishing cutoff. Here, $\circ$ denotes a convolution in temporal arguments, products in the square brackets denote a simple algebraic multiplication, and we have already assumed spatial isotropy.

Recall that for systems with a unitary evolution operator (see Sec. 3.3.1),

$$\Gamma_{\mathrm{clcl}}^{(2)}(t, t', \mathbf{p}) \equiv 0, \quad \Gamma_{\mathrm{clq}}^{(2)}(t, t', \mathbf{p}) = \Gamma_{\mathrm{qcl}}^{(2)}(t', t, -\mathbf{p}).\tag{4.17}$$

If the regulator $R_{k,\mathbf{ab}}$ is chosen such that it does not break the unitarity, relations (4.17) hold also at any finite cutoff k. In particular, this implies $\delta Z_k(t, t', \mathbf{p}) = \delta Z_k(t', t, -\mathbf{p})$ is an even function.

In general, δZ_k is a function of dimensionless variables only. In other words, if scales such as k or m are present, δZ_k will only depend on dimensionless combinations such as $\mathbf{p}^2/k^2$, $\mathbf{p}^2/m^2$, etc. On the other hand, at the vicinity of an infrared fixed point, the only remaining relevant scale is k implying that δZ_k depends on k only implicitly through dimensionless arguments:

$$\delta Z_k(\tau, \sigma, \mathbf{p}) = \delta Z(\hat{\tau}, \hat{\sigma}, x), \tag{4.18}$$

with

$$x \equiv \mathbf{p}^2/k^2 \equiv \hat{\mathbf{p}}^2, \quad \hat{\tau} \equiv k^{1/\beta}\tau, \quad \hat{\sigma} \equiv k^z\sigma. \tag{4.19}$$

Here, as always, $\tau \equiv (t+t')/2$ and $\sigma \equiv t-t'$ are central and relative times, respectively. In the most general case, their scaling dimensions $1/\beta$ and z need not to coincide. However, in all studies known to the author that investigated the relation between β and z, their scaling dimensions were observed to coincide to a good approximation, see, e.g., [57, 89]. For that reason, one often supposes the constraint $\beta = 1/z$, which we are also going to assume in this work.

4.2.3   Asymptotic behavior of δZ

Let us now discuss the asymptotic behavior of δZ. In the scaling limit $k \to 0$, we shall recover the full inverse propagator $\Gamma_{\mathbf{ab}}^{(2)}$, which immediately implies

$$\delta Z(\hat{\tau} \to 0, \hat{\sigma} \to 0, x \to \infty) = 0. \tag{4.20}$$

In Wigner space (3.45), we therefore expect

$$\delta Z^W(\hat{\tau} \to 0, \hat{\omega} \to \infty, x \to \infty) = 0. \tag{4.21}$$

Note, however, that for UV-divergent fixed points this may only be achieved if the scaling range is restricted to momenta smaller than some upper cutoff Λ and

$$\delta Z^W\left(\hat{\Lambda}^{-1/\beta} < \hat{\tau} \ll 1, 1 \ll \hat{\omega} \ll \hat{\Lambda}^z, 1 \ll x < \hat{\Lambda}^2\right) \simeq 0, \tag{4.22}$$

where $\hat{\Lambda} \equiv \Lambda/k$. In this situation of a UV-divergent fixed point, the theory is not well defined exactly at the fixed point, but the latter can be approached arbitrarily by choosing Λ accordingly large [135]. Since we consider an effective field theory,[1] there is no reason to anticipate for the fixed point in question to be UV-finite.

---

[1]And even for a UV complete theory, in the case of a nonthermal fixed point solution, one would typically expect a UV scale characterizing transition to an energy cascade.

In the opposite (regulator-dominated) limit $k \to \infty$, according to (4.16),

$$\delta Z_F \left(\hat{\tau} \to \infty, \hat{\sigma} \to \infty, x \to 0\right) = -1 + \frac{\left(G_{\mathrm{clq}} \circ \Gamma^{(2)}_{k \to \infty, \mathrm{qq}} \circ G_{\mathrm{qcl}}\right) (t, t', \mathbf{p})}{\mathrm{i} F(t, t', \mathbf{p})} ,$$

$$\delta Z_\rho \left(\hat{\tau} \to \infty, \hat{\sigma} \to \infty, x \to 0\right) = -1 + \frac{\left(G_{\mathrm{clq}} \circ \Gamma^{(2)}_{k \to \infty, \mathrm{qcl}} \circ G_{\mathrm{clq}}\right) (t, t', \mathbf{p})}{\mathrm{i} G_{\mathrm{clq}}(t, t', \mathbf{p})} .$$

(4.23)

The '-1 term' ensures cancellation of the scaling part in the parameterization (4.16) such that the trivial spatio-temporal dependence $\Gamma^{(2)}_{k \to \infty}$ is recovered as a consequence of the cutoff. It is worth noting that one should be careful with associating $\Gamma^{(2)}_{k \to \infty}$ with the classical propagator. This point is nicely illustrated in [139], where the gluon propagator contains a k-dependent mass term in the regulator-dominated regime $k \to \infty$. The bare propagator, one the other hand, is manifestly massless due to gauge invariance. This can be explained by the fact that the regulator term is not gauge-invariant and therefore terms not present in the bare action can be generated in the regulator-dominated regime. Likewise, Goldstone fields may acquire nonzero masses if the chosen regulator does not respect the system's symmetries. In the following, however, we are going to choose the regulator in such a manner that it respects all the symmetries of the full quantum effective action by construction, see Sec. 4.2.6.

4.2.4 Integrated flow equations

Using the parameterization (4.16) the flow equation (4.14) can be straightforwardly recast into a more convenient form of a set of integral equations for δZ_ρ and δZ_F. To achieve that, one integrates the flow for $\Gamma^{(2)}_{k,\mathrm{qcl}}$ ($\Gamma^{(2)}_{k,\mathrm{clq}}$) from k_1 to k_2 and then contracts it with G_{clq} (G_{qcl}) from the left and from the right. Likewise, we integrate the flow equation for $\Gamma^{(2)}_{k,\mathrm{qq}}$ and contract it with G_{clq} from the left and G_{qcl} from the right. The result reads

$$-\mathrm{i} \left(G_{\mathrm{clq}} \circ \Gamma^{(2)}_{\mathrm{qcl}} \circ [G_{\mathrm{qcl}} \delta Z_{k_2,\rho}] \circ \Gamma^{(2)}_{\mathrm{qcl}} \circ G_{\mathrm{clq}}\right) - (k_1 \leftrightarrow k_2) = \int_{k_1}^{k_2} \frac{\mathrm{d}k'}{k'} \left(G_{\mathrm{clq}} \circ I_{k',\mathrm{qcl}} \circ G_{\mathrm{clq}}\right),$$

$$-\mathrm{i} \left(G_{\mathrm{qcl}} \circ \Gamma^{(2)}_{\mathrm{clq}} \circ [\delta Z_{k_2,\rho} G_{\mathrm{clq}}] \circ \Gamma^{(2)}_{\mathrm{clq}} \circ G_{\mathrm{qcl}}\right) - (k_1 \leftrightarrow k_2) = \int_{k_1}^{k_2} \frac{\mathrm{d}k'}{k'} \left(G_{\mathrm{qcl}} \circ I_{k',\mathrm{clq}} \circ G_{\mathrm{qcl}}\right),$$

$$\mathrm{i} \left(G_{\mathrm{clq}} \circ \Gamma^{(2)}_{\mathrm{qcl}} \circ [F \delta Z_{k_2,F}] \circ \Gamma^{(2)}_{\mathrm{clq}} \circ G_{\mathrm{qcl}}\right) - (k_1 \leftrightarrow k_2) = \int_{k_1}^{k_2} \frac{\mathrm{d}k'}{k'} \left(G_{\mathrm{clq}} \circ I_{k',\mathrm{qq}} \circ G_{\mathrm{qcl}}\right).$$

(4.24)

Finally, employing (3.41) and $\rho = \mathrm{i} \left(G_{\mathrm{clq}} - G_{\mathrm{qcl}}\right)$ we obtain

$$[\delta Z_{k_2,\rho} - \delta Z_{k_1,\rho}] (t, t', \mathbf{p}) = \frac{1}{\rho(t, t', \mathbf{p})} \int_{k_1}^{k_2} \frac{\mathrm{d}k'}{k'} \left[\left(G_{\mathrm{clq}} \circ I_{k',\mathrm{qcl}} \circ G_{\mathrm{clq}}\right)(t, t', \mathbf{p}) - (\mathrm{q} \leftrightarrow \mathrm{cl})\right],$$

(4.25a)

$$[\delta Z_{k_2,F} - \delta Z_{k_1,F}] (t, t', \mathbf{p}) = \frac{\mathrm{i}}{F(t, t', \mathbf{p})} \int_{k_1}^{k_2} \frac{\mathrm{d}k'}{k'} \left(G_{\mathrm{clq}} \circ I_{k',\mathrm{qq}} \circ G_{\mathrm{qcl}}\right)(t, t', \mathbf{p}).$$

(4.25b)

Note that δZ_ρ and δZ_F enter the right-hand side of the equations (4.25) through the kernels $I_{k,\mathbf{ab}}$ since the latter contain regularized propagators. In other words, (4.25) is a set of coupled nonlinear integral equations.

In addition, the fixed-point equations have an explicit dependence on the full propagators F and ρ. At the fixed point, the latter are fully specified by their *scaling forms* and values of the critical exponents. This suggests the following strategy for searching for possible scaling solutions:

1. Solve the fixed point equations for a given choice of the scaling forms F_s and ρ_s and values of the critical exponents $\boldsymbol{\kappa}$.

2. Extract the asymptotic behavior of the solutions δZ_F and δZ_ρ. Importantly, in the regulator-dominated limit, the regular (constant) part of the solution, which we will denote for a second by c_F and c_ρ, is given by -1.

3. As a result, one derives two equations for F_s, ρ_s, and $\boldsymbol{\kappa}$: $c_F(F_s, \rho_s, \boldsymbol{\kappa}) = -1$ and $c_\rho(F_s, \rho_s, \boldsymbol{\kappa}) = -1$. In the following, we will argue how one can narrow down the number of unknowns such that the two equations are sufficient to fix the scaling.

In principle, the expressions for c_F and c_ρ could be found analytically, in which case the problem would reduce to solving a set of simple algebraic equations. However, given the complexity of the equations (4.25) such prospect does not look feasible. A more realistic approach is therefore to probe promising scaling solutions and check if they satisfy the above conditions.

4.2.5 Scaling forms

Since the parameter space of all possible scaling forms is, in general, infinitely large, we are going to fix the scaling forms treating them as an input to our problem. In this work, our choice of scaling forms for the spectral and statistical functions is motivated by the quasi-particle Ansatz discussed in Sec. 3.1.6. In addition, we make use of the symmetry considerations from Sec. 3.3.2. First, since ϕ corresponds to Goldstone excitations (phonons), the dispersion relation is expected to be gapless. Furthermore, the equal-time propagator should not have a finite $p \to 0$ limit. Putting all these conditions together, we then come up with

$$\rho(\tau, \sigma, \mathbf{p}) = \rho_0 \frac{\sin[\omega(\tau, \mathbf{p})\,\sigma]}{\omega(\tau, \mathbf{p})}\,, \tag{4.26a}$$

$$F(\tau, \sigma, \mathbf{p}) = \frac{f_0\,\tau^{-\gamma}}{p^\kappa} \cos[\omega(\tau, \mathbf{p})\,\sigma]\,, \tag{4.26b}$$

where the dispersion relation is generally given by

$$\omega(\tau, \mathbf{p}) = c_0 \tau^{-\beta(z-z_0)} |\mathbf{p}|^{z_0}. \tag{4.27}$$

We note that a time-dependent dispersion relation of the kind (4.27) was indeed observed in classical-statistical simulations of a single-component Bose gas [66] and a real scalar field in the nonrelativistic limit [146]. In both cases the observed excitations had approximately linear dispersion relation, $z_0 = 1$, and $z = 1/\beta = 2$. On the other hand, in both studies the observed scaling forms were more complicated than (4.26): the spectral function had a finite width $\gamma(\tau, \mathbf{p})$, the peak structure was more involved,[2] and both the spectral as well the statistical functions were not of Breit–Wigner (Lorentzian) form. Though it goes beyond the scope of this work, it may be an interesting direction to consider more complex scaling forms motivated by phenomenological studies.

Note also that, reflecting the adopted generalized fluctuation-dissipation relation (3.54), the statistical function (4.26b) may be written as

$$F(\tau, \sigma, \mathbf{p}) = f\left(\tau, \omega(\tau, \mathbf{p})\right) \rho_0 \frac{\cos[\omega(\tau, \mathbf{p})\,\sigma]}{\omega(\tau, \mathbf{p})}, \tag{4.28}$$

where

$$f\left(\tau, \omega(\tau, \mathbf{p})\right) = \frac{f_0 c^{\kappa/z_0}}{\rho_0} \frac{\tau^{-\gamma - \beta\kappa(z/z_0 - 1)}}{\omega(\tau, \mathbf{p})^{\kappa/z_0 - 1}} \tag{4.29}$$

plays the role of an (on-shell) quasiparticle distribution function, in the limit of large occupancies when one may neglect the quantum $1/2$.

After we have covered the form aspect of the propagators, let us quickly discuss their scaling properties. The scaling dimensions of the propagators F and ρ are defined as

$$\begin{aligned}
\rho(\tau, \sigma, \mathbf{p}) &= s^{\Delta_\rho}\, \rho(s^{-1/\beta}\tau, s^{-z}\sigma, s\mathbf{p})\,, \\
F(\tau, \sigma, \mathbf{p}) &= s^{\Delta_F}\, F(s^{-1/\beta}\tau, s^{-z}\sigma, s\mathbf{p})\,.
\end{aligned} \tag{4.30}$$

Using (4.26) the scaling dimensions Δ_ρ and Δ_F can be expressed as

$$\Delta_\rho = z, \quad \Delta_F = \kappa - \gamma/\beta. \tag{4.31}$$

In the language of NTFP scaling, $\Delta_F = \alpha/\beta$. In the following, we will impose the constraint $\Delta_F = d$, which can be considered as stemming from the particle number conservation law of the underlying 'fundamental bosons', cf. (2.20). In addition, we will assume that the excitations have a strictly linear dispersion relation, which fixes the scaling exponent $z_0 = 1$. Finally, as have been mentioned at the end of Sec. 4.2.2, we will also employ the constraint $\beta = 1/z$, which leaves us with only two independent scaling exponents.

To close the discussion, we check how our choice of the scaling forms fits the EFT considerations of Sec. 4.1. Recall that the leading-order microscopic action governing the

---

[2]Presumably, due to the presence of topological excitations, which, however, we exclude in the present work.

dynamics of phonon excitations is given by (4.10). The simplest extension to the Schwinger-Keldysh contour then reads

$$S[\theta_+, \theta_-] = \int_{x,t_0} \left\{ a_1 \left(D_t \theta_+ - D_t \theta_- \right) + a_2 \left[\left(D_t \theta_+ \right)^2 - \left(D_t \theta_- \right)^2 \right] \right\}.$$

Upon performing the Keldysh rotation and ignoring the boundary term we obtain

$$S[\phi_{\rm cl}, \phi_{\rm q}] = \int_{x,t_0} \left\{ \frac{a}{2} \partial_t \phi_{\rm cl} \partial_t \phi_{\rm q} - \frac{b}{2} \nabla \phi_{\rm cl} \nabla \phi_{\rm q} - \frac{a}{4m} \partial_t \phi_{\rm q} \left(\nabla \phi_{\rm cl} \right)^2 - \frac{a}{2m} \partial_t \phi_{\rm cl} \nabla \phi_{\rm cl} \nabla \phi_{\rm q} \right.$$

$$\left. - \frac{a}{16m} \partial_t \phi_{\rm q} \left(\nabla \phi_{\rm q} \right)^2 + \frac{a}{4m^2} \left(\nabla \phi_{\rm cl} \right)^3 \nabla \phi_{\rm q} + \frac{a}{16m^2} \nabla \phi_{\rm cl} \left(\nabla \phi_{\rm q} \right)^3 + (\rm qq - term) \right\}, \quad (4.32)$$

with $a \equiv 4a_2$ and $b/2 \equiv (a_1 - 2\mu a_2)/m$. Note that the m^{-1} and m^{-2} ratios between the couplings involving a are ensured by symmetry identities even beyond the classical level (see App. 4.A.2). Since we consider a closed system, the $\rm q - q$-component is a pure regularization, which is, however, necessary in order to have a nonzero occupation number. To ensure the scaling Ansatz (4.28), the $\rm q - q$-term then has to take the form

$$S_{\rm qq}^{(2)}(t, t', \mathbf{x}) = \int_{t_1} \left[f(t, t_1) S_{\rm clq}^{(2)}(t_1, t', \mathbf{x}) - S_{\rm qcl}^{(2)}(t, t_1, \mathbf{x}) f(t_1, t') \right], \quad (4.33)$$

up to subleading terms in the gradient expansion. Here, $f(t, t')$ is the inverse Wigner transform of $f(\tau, \omega)$ in (4.29).

From (4.32) we may readily infer the dispersion relation, $\omega_{\mathbf{p}}^2 = (b/a) \mathbf{p}^2 \equiv c_s^2 \mathbf{p}^2$, identifying c_s with the sound velocity. Using the above microscopic action as an Ansatz for the full nonequilibrium quantum effective action we allow a and b to depend on time. The simplest nontrivial generalization is then to let b be time-dependent, whilst keeping a time-independent. To match the scaling forms (4.26), we then set

$$a = \frac{a_0(t_0)}{m^2}, \quad b = \frac{b_0(t_0) \, t^{\beta-1}}{m^2}, \quad f(t, t') = f_0(t_0) \, g(t, t'), \quad (4.34)$$

with $g(t, t')$ being a parameter-free function. By appropriately rescaling the fields and choosing the right units of momentum one may get rid of all but two parameters,

$$g_{\rm cl} = \frac{a_0 f_0^{1/2}}{b_0 c_0^{d/2}}, \quad g_{\rm q} = \frac{g_{\rm cl}}{f_0^2}, \quad (4.35)$$

which serve as effective coupling constants. The resulting rescaled microscopic action reads

$$S[\phi_{\rm cl}, \phi_{\rm q}] = \int_{x,t_0} \left\{ \frac{1}{2} \left[\partial_t \phi_{\rm cl} \partial_t \phi_{\rm q} - t^{\beta-1} \nabla \phi_{\rm cl} \nabla \phi_{\rm q} \right] - \frac{g_{\rm cl}}{4} \partial_t \phi_{\rm q} \left(\nabla \phi_{\rm cl} \right)^2 - \frac{g_{\rm cl}}{2} \partial_t \phi_{\rm cl} \nabla \phi_{\rm cl} \nabla \phi_{\rm q} \right.$$

$$\left. + \frac{g_{\rm cl}^2}{4} \left(\nabla \phi_{\rm cl} \right)^3 \nabla \phi_{\rm q} - \frac{g_{\rm q}}{16} \partial_t \phi_{\rm q} \left(\nabla \phi_{\rm q} \right)^2 + \frac{g_{\rm q} g_{\rm cl}}{16} \nabla \phi_{\rm cl} \left(\nabla \phi_{\rm q} \right)^3 + (\rm qq - term) \right\}, \quad (4.36)$$

where the $\rm q - q$-component no longer contains any parameters, see App. 4.B for details. In terms of the scaling forms (4.26) and (4.27) this implies that one can set $\rho_0, f_0, c_0 \to 1$ by appropriately choosing the units and rescaling the fields.

4.2.6 Choice of the regulator

To fully fix the quadratic part of Γ_k, we still have to specify the regulator R_k. In the $\pm$ notation, it is given by

$$\Delta S_k = \frac{1}{2} \int (\varphi_+, \varphi_-) \begin{pmatrix} R_k^{++} & -R_k^{+-} \\ -R_k^{-+} & R_k^{--} \end{pmatrix} \begin{pmatrix} \varphi_+ \\ \varphi_- \end{pmatrix}, \tag{4.37}$$

and the regulators before and after Keldysh rotation are related via

$$\begin{pmatrix} R_{k,\mathrm{clcl}} & -R_{k,\mathrm{clq}} \\ -R_{k,\mathrm{qcl}} & R_{k,\mathrm{qq}} \end{pmatrix} = A \begin{pmatrix} R_k^{++} & -R_k^{+-} \\ -R_k^{-+} & R_k^{--} \end{pmatrix} A^T, \tag{4.38}$$

cf. (3.33). The simplest choice motivated by the standard form of a mass term is $R_k^{++} = -R_k^{--}$, $R_k^{+-} = R_k^{-+} \equiv 0$ or, equivalently, $R_{k,\mathrm{clq}} = R_{k,\mathrm{qcl}}$, $R_{\mathrm{clcl}} = R_{\mathrm{qq}} \equiv 0$. In this work, we employ a regulator of the form

$$R_{k,\mathrm{ab}}(t, t', \mathbf{p}) = \Gamma_{\mathrm{ab}}^{(2)}(t, t', \mathbf{p}) \, r_{\mathrm{ab}} \left(\mathbf{p}^2/k^2 \right), \tag{4.39}$$

with $r_{\mathrm{clcl}} = r_{\mathrm{qq}} \equiv 0$ and $r_{\mathrm{clq}} = r_{\mathrm{qcl}} \equiv r$. This choice has a nice advantage that, by construction, it enjoys the correct symmetry properties and causal structure of the full effective action. Therefore, any constraints imposed by symmetry or causality arguments (see Sec. 3.3) shall hold also for any finite cutoff k.

It remains to choose the shape function $r(y)$. As discussed in Sec. 3.4.2, a suitable candidate for numerical purposes is the exponential regulator

$$r(y) = \frac{a y^{b-c}}{\exp\left(y^b\right) - 1}, \tag{4.40}$$

where a, b, and c are parameters to be chosen by hand. The most common choice is $a = b = c = 1$, for which $r(y \to 0) \sim y^{-1}$ reflecting the usual p^2 form of the inverse propagator. However, in our case, to better match the momentum-dependence structure of the scaling forms (4.26), it might be helpful to instead take a κ-dependent c.

Note that the above regulator does not concern temporal fluctuations. Together with our Ansatz for the scaling forms, this implies that temporal scaling persists even in the limit $k \to \infty$. In principle, one may overcome this 'issue' by implementing a temporal cutoff. Regulators of this kind have been discussed in, e.g., [147]. However, for the purpose of finding scaling solutions, it will turn out to be unnecessary. This will be discussed in more detail in Sec. 4.4.

4.2.7 Vertices

In the previous sections, we covered the Ansatz for the quadratic part of the regularized effective Γ_k within our approximation. To complete our approximation scheme, we still have

to specify the choice of vertices $\Gamma^{(n \geq 3)}_{k,\mathbf{a}_1 \dots \mathbf{a}_n}$. In the present truncation scheme, they schematically read

$$\Gamma^{(n \geq 3)}_k = z_n S^{(n \geq 3)}_k, \tag{4.41}$$

with the classical vertices $S^{(n \geq 3)}_k$, which can be derived from the action (4.36) that we again use as a guiding Ansatz, taken with running couplings $g_{n,k}$. Together with the k-dependent prefactors z_n the latter form dimensionless couplings

$$\hat{g}_{n,k} = z_n g_{n,k} \equiv k^{-[g_n]} g_{n,k}, \tag{4.42}$$

with the scaling dimensions $[g_n]$ to be fixed in Sec. 4.3. Since we consider the IR critical region,

$$k \partial_k \hat{g}_{n,k} = 0, \tag{4.43}$$

so that dimensionless couplings approach their respective IR fixed-point values. Therefore, e.g., $\hat{g}_{n,k'}$ in the loop is k'-independent and can be replaced by $\hat{g}^*_n$. Thus, in the vicinity of the IR fixed point

$$k \partial_k \Gamma^{(n \geq 3)}_k = 0 \tag{4.44}$$

in the chosen truncation scheme.

4.2.8   Approximate equations for δZ

We are now set up to discuss the equations (4.25) for δZ outlined in Sec. 4.2.4. As we have already mentioned there, in order to find δZ one has to solve a set of coupled nonlinear integral equations. Therefore, the full solution is out of reach even numerically.

On the other hand, as argued in [139], the equations for δZ can be significantly simplified in the limit $k \to \infty$, which we are primarily interested in. In this case, the regions $\mathbf{q}^2/k^2 \lesssim 1$ and $(\mathbf{p}+\mathbf{q})^2/k^2 \lesssim 1$ in the loops are suppressed due to the regulator. According to (4.20), we can thus set $\delta Z \to 0$ in the loops to a good approximation. Equivalently, when computing the flow one may take

$$\widetilde{G}_{k,\mathbf{ab}}[\phi] \equiv \mathrm{i} \left(\Gamma^{(2)}[\phi] + R_k \right)^{-1}_{\mathbf{ab}} \tag{4.45}$$

instead of the full regularized propagators (4.15). For the choice of the regulator (4.39), these *'deformed propagators'* take a simple form $\tilde{G}_k(t,t',\mathbf{p}) = P(\mathbf{p}^2/k^2)\, G(t,t,\mathbf{p})$, with the functions

$$P_\rho(\mathbf{p}^2/k^2) = \frac{1}{1 + r(\mathbf{p}^2/k^2)}, \quad P_F(\mathbf{p}^2/k^2) = \frac{1}{[1 + r(\mathbf{p}^2/k^2)]^2} = P_\rho(\mathbf{p}^2/k^2)^2, \tag{4.46}$$
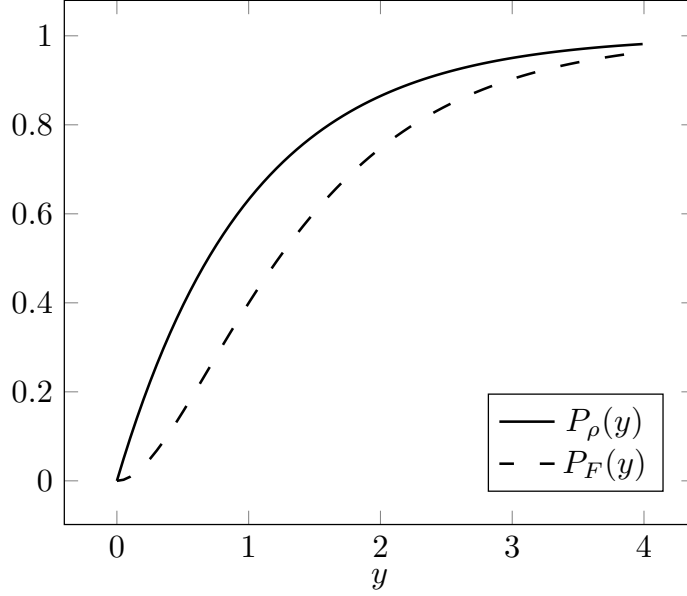
which we depict in Fig. 4.1.

Figure 4.1. The suppressing prefactors (4.46) entering the deformed propagators. Here, we have used the exponential regulator (4.40) with $a = b = c = 1$. Note that P and δZ always appear in the flow equation together as they both enter through the regularized propagator G_k. Hence, δZ always has a limited support in the infrared region of the loop, as claimed in the main text.

Together with (4.44) this dramatically simplifies the equations for δZ. Indeed, noting that $\widetilde{G}_k[\phi] \cdot \partial_k R_k \cdot \widetilde{G}_k[\phi] = -i\partial_k \widetilde{G}_k[\phi]$ we readily obtain

$$
\begin{aligned}
I_{k,\mathbf{ab}} &\simeq \frac{1}{2}\Gamma^{(4)}_{k,\mathbf{dabe}}k\partial_k\widetilde{G}_{k,\mathbf{ed}} + \frac{i}{2}k\partial_k\widetilde{G}_{k,\mathbf{jd}}\Gamma^{(3)}_{k,\mathbf{dae}}\widetilde{G}_{k,\mathbf{eh}}\Gamma^{(3)}_{k,\mathbf{hbj}} + \frac{i}{2}k\partial_k\widetilde{G}_{k,\mathbf{jd}}\Gamma^{(3)}_{k,\mathbf{dbe}}\widetilde{G}_{k,\mathbf{eh}}\Gamma^{(3)}_{k,\mathbf{hej}} \\
&= \frac{1}{2}\Gamma^{(4)}_{k,\mathbf{dabe}}k\partial_k\widetilde{G}_{k,\mathbf{ed}} + \frac{i}{2}\Gamma^{(3)}_{k,\mathbf{dae}}\left(k\partial_k\widetilde{G}_{k,\mathbf{jd}}\widetilde{G}_{k,\mathbf{eh}} + k\partial_k\widetilde{G}_{k,\mathbf{eh}}\widetilde{G}_{k,\mathbf{jd}}\right)\Gamma^{(3)}_{k,\mathbf{hbj}} \\
&= \frac{1}{2}\Gamma^{(4)}_{k,\mathbf{dabe}}k\partial_k\widetilde{G}_{k,\mathbf{ed}} + \frac{i}{2}\Gamma^{(3)}_{k,\mathbf{dae}}k\partial_k\left(\widetilde{G}_{k,\mathbf{jd}}\widetilde{G}_{k,\mathbf{eh}}\right)\Gamma^{(3)}_{k,\mathbf{hbj}}.
\end{aligned}
\tag{4.47}
$$

Using the assumption (4.44) we thus conclude

$$
\begin{aligned}
I_{k,\mathbf{ab}} &\simeq \frac{1}{2}k\partial_k\left[\Gamma^{(4)}_{k,\mathbf{dabe}}\widetilde{G}_{k,\mathbf{ed}} + i\widetilde{G}_{k,\mathbf{jd}}\Gamma^{(3)}_{k,\mathbf{dae}}\widetilde{G}_{k,\mathbf{eh}}\Gamma^{(3)}_{k,\mathbf{hbj}}\right] \\
&\equiv \frac{1}{2}k\partial_k\Sigma_{k,\mathbf{ab}} = \frac{1}{2}k\partial_k\Sigma_{\mathbf{ab}}\left[\tilde{G}_k, \Gamma^{(n\geq 3)}_*\right],
\end{aligned}
\tag{4.48}
$$

where in the last line we have denoted the vertex functions by $\Gamma^{(n\geq 3)}_*$ to emphasize their k-independence in the chosen truncation scheme. For a diagrammatic representation of the simplified flow equations, see App. 4.C.

To summarize, within the chosen truncation scheme, the k-dependence of the flow reduces to a total-derivative form. This, in turn, allows us to perform the integration in (4.25)

explicitly:

$$\delta Z_{k,\rho}\left(t, t', \mathbf{p}\right) \overset{\circ}{\simeq} \frac{1}{2\rho\left(t, t', \mathbf{p}\right)} \left[\left(G_{\text{clq}} \circ \Sigma_{k,\text{qcl}} \circ G_{\text{clq}}\right)\left(t, t', \mathbf{p}\right) - \left(\text{q} \leftrightarrow \text{cl}\right)\right], \qquad \text{(4.49a)}$$

$$\delta Z_{k,F}\left(t, t', \mathbf{p}\right) \overset{\circ}{\simeq} \frac{\mathrm{i}}{2F\left(t, t', \mathbf{p}\right)} \left(G_{\text{clq}} \circ \Sigma_{k,\text{qq}} \circ G_{\text{qcl}}\right)\left(t, t', \mathbf{p}\right), \qquad \text{(4.49b)}$$

cf. with Eqs. (13) in [139]. Here, to shorten the equations, we have introduced the following short-hand notation:

$$A_k \overset{\circ}{=} B_k \iff A_{k_2} - A_{k_1} = B_{k_2} - B_{k_1}. \qquad \text{(4.50)}$$

4.2.9   Causal structure of the equations

In their present form, the equations (4.49) involve integrals of functions that have a limited support in the temporal domain, e.g., G_{clq} or G_{qcl}. Performing integration for such integrands is numerically problematic, so we shall examine the implications of causal properties of the propagators on the temporal structure of the integrals to bring (4.49) to a more suitable form.

Tadpole contributions

We begin by considering the four-point (tadpole) contributions (III) and (VI), see Fig. 4.14. For $\Sigma_{k,\text{qq}}$, this contribution has the form $\int_{\mathbf{q}} \Gamma^{(4)}_{*,\text{clqqq}}\left(t, \mathbf{q}, \mathbf{p}, -\mathbf{p}, -\mathbf{q}\right) \tilde{G}_k^{R/A}\left(t, t, \mathbf{q}\right)$. Since $\tilde{G}_k^{R/A}\left(t, t, \mathbf{q}\right) \equiv 0$, this term does not contribute to $\Sigma_{k,\text{qq}}$. In contrast, the four-point contributions to $\Sigma_{k,\text{clq}}$ and $\Sigma_{k,\text{qcl}}$ are non-vanishing:

$$\Sigma^{(\text{t})}_{k,\text{clq}}\left(t_1, t_2, \mathbf{p}\right) = \delta\left(t_1 - t_2\right) \int_{\mathbf{q}} \Gamma^{(4)}_{*,\text{clclclq}}\left(t_1, \mathbf{q}, \mathbf{p}, -\mathbf{p}, -\mathbf{q}\right) \tilde{F}_k\left(t_1, t_1, \mathbf{q}\right)$$

$$\equiv \Sigma^{(\text{t})}_{k,\rho}\left(t_1, \mathbf{p}\right) \delta\left(t_1 - t_2\right), \qquad \text{(4.51)}$$

and likewise for $\Sigma^{(\text{t})}_{k,\text{qcl}}$. Plugging this into the fixed-point equation (4.49a) results in the following contribution to δZ_{ρ}:

$$\delta Z^{(\text{t})}_{k,\rho}\left(t, t', \mathbf{p}\right) \overset{\circ}{\simeq} \frac{1}{\rho\left(t, t', \mathbf{p}\right)} \int_t^{t'} \mathrm{d}t_1 \, \rho\left(t, t_1, \mathbf{p}\right) \Sigma^{(\text{t})}_{k,\rho}\left(t_1, \mathbf{p}\right) \rho\left(t_1, t', \mathbf{p}\right). \qquad \text{(4.52)}$$
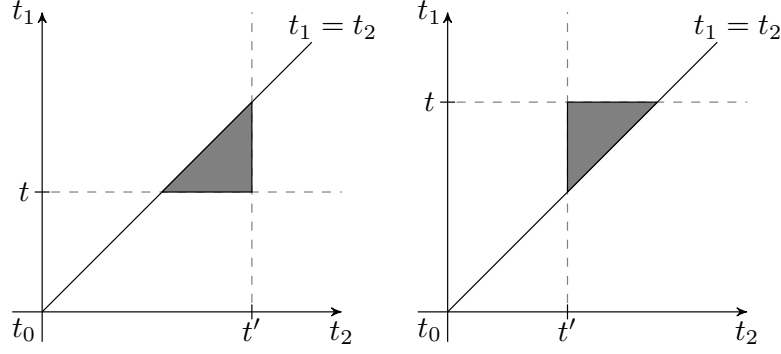
Figure 4.2. Integration domain for δZ_ρ when $t < t'$ (left) and $t > t'$ (right).

Non-tadpole contributions

Next, let us examine the non-tadpole diagrams (I), (II), (IV), and (V) depicted in Fig. 4.14. We first observe that there is only one contribution of this kind for δZ_ρ:

$$
\Sigma_{k,\text{clq}}^{(\text{nt})} (t_1, t_2, \mathbf{p}) = \int_{\mathbf{q}} \Gamma_{*,\text{clclq}}^{(3)} (t_1, \mathbf{q}, \mathbf{p}, -\mathbf{p} - \mathbf{q}) \, \tilde{F}_k (t_2, t_1, \mathbf{q})
$$
$$
\times \tilde{G}_k^A (t_1, t_2, \mathbf{p} + \mathbf{q}) \, \Gamma_{*,\text{clqcl}}^{(3)} (t_2, \mathbf{p} + \mathbf{q}, -\mathbf{p}, -\mathbf{q}), \tag{4.53a}
$$
$$
\Sigma_{k,\text{qcl}}^{(\text{nt})} (t_1, t_2, \mathbf{p}) = \int_{\mathbf{q}} \Gamma_{*,\text{clqcl}}^{(3)} (t_1, \mathbf{q}, \mathbf{p}, -\mathbf{p} - \mathbf{q}) \, \tilde{F}_k (t_2, t_1, \mathbf{q})
$$
$$
\times \tilde{G}_k^R (t_1, t_2, \mathbf{p} + \mathbf{q}) \, \Gamma_{*,\text{clclq}}^{(3)} (t_2, \mathbf{p} + \mathbf{q}, -\mathbf{p}, -\mathbf{q}). \tag{4.53b}
$$

Making use of some basic symmetry properties of the propagators and vertex functions one easily finds

$$
\begin{aligned}
\Sigma_{k,\text{qcl}}^{(\text{nt})} (t_1, t_2, \mathbf{p}) &= \Sigma_{k,\rho}^{(\text{nt})} (t_1, t_2, \mathbf{p}) \, \Theta (t_1 - t_2), \\
\Sigma_{k,\text{clq}}^{(\text{nt})} (t_1, t_2, \mathbf{p}) &= -\Sigma_{k,\rho}^{(\text{nt})} (t_1, t_2, \mathbf{p}) \, \Theta (t_2 - t_1),
\end{aligned} \tag{4.54}
$$

which reflects the causal structure of the kernel. We thus conclude

$$
\delta Z_{k,\rho}^{(\text{nt})} (t, t', \mathbf{p}) \overset{\circ}{\simeq} \frac{1}{\rho (t, t', \mathbf{p})} \int_t^{t_2} \mathrm{d}t_1 \int_t^{t'} \mathrm{d}t_2 \, \rho (t, t_1, \mathbf{p}) \, \Sigma_{k,\rho}^{(\text{nt})} (t_1, t_2, \mathbf{p}) \, \rho (t_2, t', \mathbf{p}). \tag{4.55}
$$

The temporal integration domain for cases $t < t'$ and $t > t'$ is summarized in Fig. 4.2. For

δZ_F, on the other hand, there are two distinct non-tadpole contributions:

$$\Sigma_{k,\text{qq}}^{(\text{cl})}(t_1, t_2, \mathbf{p}) = \text{i} \int_{\mathbf{q}} \Gamma_{*,\text{clqcl}}^{(3)}(t_1, \mathbf{q}, \mathbf{p}, -\mathbf{p}-\mathbf{q}) \, \tilde{F}_k(t_2, t_1, \mathbf{q})$$

$$\times \tilde{F}_k(t_1, t_2, \mathbf{p}+\mathbf{q}) \, \Gamma_{*,\text{clqcl}}^{(3)}(t_2, \mathbf{p}+\mathbf{q}, -\mathbf{p}, -\mathbf{q}), \qquad (4.56\text{a})$$

$$\Sigma_{k,\text{qq}}^{(\text{q})}(t_1, t_2, \mathbf{p}) = \text{i} \int_{\mathbf{q}} \Gamma_{*,\text{clqcl}}^{(3)}(t_1, \mathbf{q}, \mathbf{p}, -\mathbf{p}-\mathbf{q}) \, \tilde{G}_k^A(t_2, t_1, \mathbf{q})$$

$$\times \tilde{G}_k^R(t_1, t_2, \mathbf{p}+\mathbf{q}) \, \Gamma_{*,\text{qqq}}^{(3)}(t_2, \mathbf{p}+\mathbf{q}, -\mathbf{p}, -\mathbf{q})$$

$$+ \text{i} \int_{\mathbf{q}} \Gamma_{*,\text{qqq}}^{(3)}(t_1, \mathbf{q}, \mathbf{p}, -\mathbf{p}-\mathbf{q}) \, \tilde{G}_k^R(t_2, t_1, \mathbf{q})$$

$$\times \tilde{G}_k^A(t_1, t_2, \mathbf{p}+\mathbf{q}) \, \Gamma_{*,\text{clqcl}}^{(3)}(t_2, \mathbf{p}+\mathbf{q}, -\mathbf{p}, -\mathbf{q})$$

$$= \text{i} \int_{\mathbf{q}} \Gamma_{*,\text{qqq}}^{(3)}(t_1, \mathbf{q}, \mathbf{p}, -\mathbf{p}-\mathbf{q}) \, \tilde{\rho}_k(t_2, t_1, \mathbf{q})$$

$$\times \tilde{\rho}_k(t_1, t_2, \mathbf{p}+\mathbf{q}) \, \Gamma_{*,\text{clqcl}}^{(3)}(t_2, \mathbf{p}+\mathbf{q}, -\mathbf{p}, -\mathbf{q}), \qquad (4.56\text{b})$$

cf. Fig. 4.14, (I) and (II). We note that $\Sigma_{k,\text{qq}}^{(\text{cl})} \propto \tilde{F}_k^2$, whereas $\Sigma_{k,\text{qq}}^{(\text{q})} \propto \tilde{\rho}_k^2$. Therefore, one expects that the contribution coming from $\Sigma_{k,\text{qq}}^{(\text{cl})}$ dominates over the one from $\Sigma_{k,\text{qq}}^{(\text{q})}$ if

$$\left| \tilde{F}_k(t, t', \mathbf{q}) \, \tilde{F}_k(t, t', \mathbf{k}) \right| \gg \left| \tilde{\rho}_k(t, t', \mathbf{q}) \, \tilde{\rho}_k(t, t', \mathbf{k}) \right|, \qquad (4.57)$$

known as the *classicality condition* [56, 85, 148]. One expects it to hold if the number of field quanta in each mode is sufficiently high, i.e., if the occupation number is large, which is one of the trademarks of nonthermal fixed points. Plugging (4.56) into (4.49b) we finally arrive at

$$\delta Z_{k,F}(t, t', \mathbf{p}) \overset{\circ}{\simeq} \frac{-1}{2F(t, t', \mathbf{p})} \int_{t_0}^{t} \text{d}t_1 \int_{t_0}^{t'} \text{d}t_2 \, \rho(t, t_1, \mathbf{p}) \, \Sigma_{k,F}(t_1, t_2, \mathbf{p}) \, \rho(t_2, t', \mathbf{p}), \quad (4.58)$$

where $\text{i}\Sigma_{k,F} \equiv \Sigma_{k,qF}^{(\text{cl})} + \Sigma_{k,qq}^{(\text{q})}$.

4.3   Dimensionless form of the fixed point equations and preliminary dimensional analysis

4.3.1   Dimensionless form of the fixed point equations

As we noted in Sec. 4.2.2, near the IR fixed point, k is the only relevant scale. It is therefore suggestive to rewrite the equations for δZ in terms of dimensionless functions and variables (4.19). To that end, we first employ the definition (4.30) with $s = 1/k$:

$$\rho(\tau, \sigma, \mathbf{p}) \equiv k^{-\Delta_\rho} \hat{\rho}(\hat{\tau}, \hat{\sigma}, x) \,,$$
$$F(\tau, \sigma, \mathbf{p}) \equiv k^{-\Delta_F} \hat{F}(\hat{\tau}, \hat{\sigma}, x) \,. \qquad (4.59)$$

Because we adopt the approximation $\beta = 1/z$, relative and central times have the same scaling properties. This implies that it suffices to introduce $\eta \equiv k^{1/\beta}t$, $\eta' \equiv k^{1/\beta}t'$ and work with the functions $\hat{F}(\eta, \eta', x) \equiv \hat{F}(\hat{\tau}, \hat{\sigma}, x)$, $\hat{\rho}(\eta, \eta', x) \equiv \hat{\rho}(\hat{\tau}, \hat{\sigma}, x)$. Similarly, we define dimensionless vertex functions, which in our truncation scheme read

$$\Gamma_{k,\text{clqcl}}^{(3)}(t, \mathbf{q}, \mathbf{p}, -\mathbf{p} - \mathbf{q}) = k^{\Delta_3}\hat{S}_{3,\text{cl}}(\eta, y, x, -u),$$
$$\Gamma_{k,\text{clqcl}}^{(3)}(t, \mathbf{q}, \mathbf{p}, -\mathbf{p} - \mathbf{q}) = k^{\tilde{\Delta}_3}\hat{S}_{3,\text{q}}(\eta, y, x, -u),$$
(4.60)

and likewise for the four-point vertices $\Gamma_k^{(4)}$. Here, we have further introduced the notations

$$y \equiv \mathbf{q}^2/k^2, \quad u = x + y + 2\zeta\sqrt{xy}, \quad \zeta = \frac{\mathbf{p} \cdot \mathbf{q}}{|\mathbf{p}||\mathbf{q}|},$$
(4.61)

together with $\hat{S}_{3,\text{cl/q}}(\eta, y, x, -u) = \hat{g}_{\text{cl/q},k}[\ldots]$, $\hat{S}_{4,\text{cl}}(\eta, y, x, -u) = \hat{g}_{\text{cl/q},k}^2[\ldots]$, and $\hat{S}_{4,\text{q}}(\eta, y, x, -u) = \hat{g}_{\text{cl},k}\hat{g}_{\text{cl},k}[\ldots]$, where $[\ldots]$ schematically denote the dimensionless versions of the vertex structures in (4.36) and $\hat{g}_{\text{cl/q}}$ being the dimensionless couplings defined in Sec. 4.2.7. From this definition, one may infer the scaling dimensions of the vertices:

$$\Delta_3 = [g_{\text{cl}}] + 2 + 1/\beta, \quad \Delta_4 = 2[g_{\text{cl}}] + 4,$$
(4.62a)
$$\tilde{\Delta}_3 = [g_{\text{q}}] + 2 + 1/\beta, \quad \tilde{\Delta}_4 = [g_{\text{q}}] + [g_{\text{cl}}] + 4.$$
(4.62b)

Assembling the above definitions we can bring the equations (4.49) to their dimensionless form:

$$\delta Z_F(\eta, \eta', x) - \delta Z_F\left(\varepsilon^{1/\beta}\eta, \varepsilon^{1/\beta}\eta', x/\varepsilon^2\right) \simeq -\frac{k_2^{\mu_F}}{2\hat{F}(\eta, \eta', x)}\int_{\eta_0}^{\eta}d\eta_1\int_{\eta_0}^{\eta'}d\eta_2\,\hat{\rho}(\eta, \eta_1, x)$$
$$\times \left[\hat{\Sigma}_F^{(\text{cl})}(\eta_1, \eta_2, x) - \varepsilon^{-\Delta_{\Sigma_F}}\hat{\Sigma}_F^{(\text{cl})}\left(\varepsilon^{1/\beta}\eta_1, \varepsilon^{1/\beta}\eta_2, x/\varepsilon^2\right)\right]\hat{\rho}(\eta_2, \eta', x)$$
$$-\frac{k_2^{\tilde{\mu}_F}}{2\hat{F}(\eta, \eta', x)}\int_{\eta_0}^{\eta}d\eta_1\int_{\eta_0}^{\eta'}d\eta_2\,\hat{\rho}(\eta, \eta_1, x)$$
$$\times \left[\hat{\Sigma}_F^{(\text{q})}(\eta_1, \eta_2, x) - \varepsilon^{-\tilde{\Delta}_{\Sigma_F}}\hat{\Sigma}_F^{(\text{q})}\left(\varepsilon^{1/\beta}\eta_1, \varepsilon^{1/\beta}\eta_2, x/\varepsilon^2\right)\right]\hat{\rho}(\eta_2, \eta', x),$$
(4.63a)

$$\delta Z_\rho(\eta, \eta', x) - \delta Z_\rho\left(\varepsilon^{1/\beta}\eta, \varepsilon^{1/\beta}\eta', x/\varepsilon\right) \simeq \frac{k_2^{\mu_\rho}}{\hat{\rho}(\eta, \eta', x)}\int_{\eta}^{\eta_2}d\eta_1\int_{\eta}^{\eta'}d\eta_2\,\hat{\rho}(\eta, \eta_1, x)$$
$$\times \left[\hat{\Sigma}_\rho^{(\text{nt})}(\eta_1, \eta_2, x) - \varepsilon^{-\Delta_{\Sigma_\rho}}\hat{\Sigma}_\rho^{(\text{nt})}\left(\varepsilon^{1/\beta}\eta_1, \varepsilon^{1/\beta}\eta_2, x/\varepsilon^2\right)\right]\hat{\rho}(\eta_2, \eta', x)$$
$$+\frac{k_2^{\tilde{\mu}_\rho}}{\hat{\rho}(\eta, \eta', x)}\int_{\eta}^{\eta'}d\eta_1\,\hat{\rho}(\eta, \eta_1, x)\left[\hat{\Sigma}_\rho^{(\text{t})}(\eta_1, x) - \varepsilon^{-\tilde{\Delta}_{\Sigma_\rho}}\hat{\Sigma}_\rho^{(\text{t})}\left(\varepsilon^{1/\beta}\eta_1, x/\varepsilon^2\right)\right]\hat{\rho}(\eta_1, \eta', x),$$
(4.63b)

where $x = \mathbf{p}^2/k_2^2$ and we have introduced $\varepsilon \equiv k_1/k_2 < 1$ and

$$\mu_F = -\Delta_F - 2\Delta_\rho + 2\Delta_3 + d - 2/\beta, \quad \tilde{\mu}_F = \Delta_F - 4\Delta_\rho + \Delta_3 + \tilde{\Delta}_3 + d - 2/\beta,$$
$$\mu_\rho = -\Delta_F - 2\Delta_\rho + 2\Delta_3 + d - 2/\beta, \quad \tilde{\mu}_\rho = -\Delta_F - \Delta_\rho + \Delta_4 + d - 1/\beta.$$
(4.64)

Upon inspecting the dimensionless equations (4.63) one may notice a troubling explicit dependence on the dimensionless 'initial' time η_0 in the equation for δZ_F. It is therefore important to realize that this dependence is only seeming. Indeed, a fully developed self-similar evolution has no notion of past or future time, so the scale t_0 is arbitrary. In particular, it may be chosen as the reference scale in the usual NTFP definition (2.2). From this perspective, the scaling forms (4.26) should have been understood as functions of $t/t_{\text{ref}} = t/t_0$ from the very beginning. In this light, all the temporal arguments in (4.63) are taken with respect to dimensionless t_0. Equivalently, one may simply take $\eta_0 = 1$.

4.3.2   Preliminary dimensional analysis

Before we proceed with numerical implementation of the dimensionless fixed-point equations, it is suggestive to make a preliminary dimensional analysis in order to estimate possible scaling exponents, thus providing us a starting point for a region in which we are going to look for scaling solutions.

Scaling with k

The dimensionless fixed-point equations (4.63) still involve some residual k-dependence. At the same time, δZ should have no explicit dependence on the cutoff scale k. We therefore demand $\mu_F = \tilde{\mu}_F = 0$, which yields

$$\Delta_F - 4\Delta_\rho + \Delta_3 + \tilde{\Delta}_3 + d - 2/\beta = 0, \tag{4.65a}$$

$$-\Delta_F - 2\Delta_\rho + 2\Delta_3 + d - 2/\beta = 0, \tag{4.65b}$$

In particular, this implies that the scaling dimensions of the quantum and classical three-point vertices are related to each other

$$\Delta_3 - \tilde{\Delta}_3 = 2\left(\Delta_F - \Delta_\rho\right). \tag{4.66}$$

In our truncation scheme, Δ_3 and $\tilde{\Delta}_3$ are given by (4.62), for which $\Delta_3 - \tilde{\Delta}_3 = [g_{\text{cl}}] - [g_{\text{q}}]$, so that (4.66) yields

$$\frac{[g_{\text{cl}}] - [g_{\text{q}}]}{2} = \Delta_F - \Delta_\rho, \tag{4.67}$$

as one would expect.

Similarly, the condition of no explicit k-dependence for δZ_ρ requires $\mu_\rho = \tilde{\mu}_\rho = 0$. Since $\mu_F = \mu_\rho$, it only leads to a single further constraint: $-\Delta_F - \Delta_\rho + \Delta_4 + d - 1/\beta = 0$.

Spatio-temporal scaling

Under the approximation (4.48) we find $k\partial_k\Gamma^{(2)}_{k,\mathbf{ab}} \simeq k\partial_k\Sigma_{k,\mathbf{ab}}$. To estimate scaling properties of the full propagator in the present truncation scheme, we may therefore investigate how

does $\Gamma_{\mathbf{ab}}^{(2)} \sim \Sigma_{k\to 0, \mathbf{ab}}$ behave with respect to scaling transformations. Contracting, as usual, with $G^{R/A}$ we end up with the equations that can be schematically written as

$$F\left(t, t', \mathbf{p}\right) \sim \int_{t_0}^{t} \mathrm{d}t_1 \int_{t_0}^{t'} \mathrm{d}t_2 \int_{\mathbf{q}} \rho(\ldots) S_{\mathrm{clqcl}}^{(3)}(\ldots) F(\ldots) S_{\mathrm{clqcl}}^{(3)}(\ldots) F(\ldots) \rho(\ldots)$$

$$+ \int_{t_0}^{t} \mathrm{d}t_1 \int_{t_0}^{t'} \mathrm{d}t_2 \int_{\mathbf{q}} \rho(\ldots) S_{\mathrm{clqcl}}^{(3)}(\ldots) \rho(\ldots) S_{\mathrm{qqq}}^{(3)}(\ldots) \rho(\ldots) \rho(\ldots), \qquad (4.68a)$$

$$\rho\left(t, t', \mathbf{p}\right) \sim \int_{t}^{t_2} \mathrm{d}t_1 \int_{t}^{t'} \mathrm{d}t_2 \int_{\mathbf{q}} \rho(\ldots) S_{\mathrm{clclq}}(\ldots) \rho(\ldots) S_{\mathrm{clqcl}}(\ldots) F(\ldots) \rho(\ldots)$$

$$+ \int_{t}^{t'} \mathrm{d}t_1 \int_{\mathbf{q}} \rho(\ldots) S_{\mathrm{clclqcl}}^{(4)}(\ldots) F(\ldots) \rho(\ldots). \qquad (4.68b)$$

Employing the definitions introduced in Sec. 4.2.5 and performing a full spatio-temporal scaling transformation of both sides we obtain

$$\text{classical}: \quad -\Delta_F = -2/\beta - 2\Delta_\rho - 2\Delta_F + d + 4 + 2/\beta, \qquad (4.69a)$$

$$\text{quantum}: \quad -\Delta_F = -2/\beta - 4\Delta_\rho + d + 4 + 2/\beta, \qquad (4.69b)$$

from the first and the second terms of (4.68a), respectively. Recalling (4.31) the first equation yields

$$\text{classical}: \quad \frac{\Delta_F - d}{2} = 2 - 1/\beta, \qquad (4.70)$$

Upon invoking the particle-number conservation constraint $\Delta_F = d$ we conclude that the left-hand side shall vanish. Therefore, based on a simple power counting we expect $\beta \simeq 1/2$. The second equation, on the other hand, gives

$$\text{quantum}: \quad \beta = \frac{4}{\Delta_F + d + 4} \simeq \frac{1}{1 + d/2}. \qquad (4.71)$$

Note that the results (4.70) and (4.71) coincide in $d = 2$ spatial dimensions. We thus conclude that $d_c = 2$ is a special dimension, which sets a border between the cases when the 'classical' loop dominates over the 'quantum' one, and vice-versa.[3] One may therefore expect that for $d > d_c$ neglecting the quantum contribution $\Sigma_F^{(\mathrm{q})}$ is a reliable approximation, cf. the discussion in Sec. 4.2.9. In the nonequilibrium quantum dynamics literature, this is often referred to as the *classical statistical approximation* [41, 148, 149]. In the following, we are going to adopt this approximation in order to further simplify the equations.

A pure-spatial scaling transformation at some fixed time τ_* is more involved. Note that time derivatives in the bare vertices will generally result in factors of the form $\omega_{\mathbf{p}}^2 + \omega_{\mathbf{p}}/\tau_* + 1/\tau_*^2$. Suppose the region $\omega_{\mathbf{p}} \gg 1/\tau_*$ has the biggest support in the loop integral. In that

---

[3]Coincidentally, $d_c = 2$ is also the upper critical dimension of a quantum phase transition in a single component Bose gas [140].

case, one would obtain

$$\text{classical}: \quad \kappa = d + 4, \tag{4.72a}$$

$$\text{quantum}: \quad \kappa = 4 - 2z_0 - d, \tag{4.72b}$$

which does not look too promising, cf. (2.19).[4] If we instead suppose that the contribution $\omega_{\mathbf{p}} \ll 1/\tau_*$ dominates, then

$$\text{classical}: \quad \kappa = d + 4 - 2z_0, \tag{4.73a}$$

$$\text{quantum}: \quad \kappa = 4 - 4z_0 - d. \tag{4.73b}$$

Recall that we assumed the excitations to be linear ($z_0 = 1$). From the first equation, we therefore expect $\kappa \simeq d + 2$, which is comparable to the usual $\kappa \simeq d + 1$ result, see (2.25c) and [57, 64, 150]. Finally, combining (4.31) with the assumption $\Delta_F = d$ we obtain

$$\gamma = \beta \left(\kappa - \Delta_F \right) \simeq \begin{cases} 1, & \kappa \simeq d + 2, \\ 2, & \kappa \simeq d + 4, \end{cases} . \tag{4.74}$$

for $\beta \simeq 1/2$. The equation for ρ provides no new information: the scaling properties of the first term in (4.68b) are identical to those of the first term of (4.68a), while the second term gives $-\Delta_\rho = -1/\beta - 2\Delta_\rho - \Delta_F + d + 4$, which under the same assumptions as above yields (4.70).

4.4 Numerical solution of the fixed-point equations

In this section, we finally show how the equations derived in the previous sections can be solved numerically and discuss how the resulting solutions may be analyzed in order to extract scaling exponents associated with nonthermal fixed points.

The code for this work has been written using Julia language [151]. All symbolic computations were carried out by the *Symbolics.jl* package [152]. Numerical integrations over n-dimensional rectangular domains were done using an adaptive integrator [153] implemented in the *HCubature.jl* library. The integration over triangular temporal domain, cf. Fig. 4.2, was performed using the Grundmann–Möller quadrature [154] from the *GrundmannMoeller.jl* package. When performing integration, all the relative errors were taken to be 10^{-2}, which is not visible in any of the following plots.

For the regulator, we used the exponential shape function (4.40) with $a = b = 1$ and $c \in [0; \kappa/4]$. We found no significant difference when varying c, so in the following all the plots are using data obtained with $c = \kappa/4$. Finally, in all the cases below, we consider $d = 3$ spatial dimensions.

---

[4]It should be noted, however, that the constraint (2.19) was based on the bi-directional cascade picture. Here, on the other hand, we consider a single IR cascade only.

4.4.1   General structure of the equations and residual temporal scaling

Taking all the approximations discussed in the previous sections into account we may rewrite the equations for δZ in the form more suitable for numerical purposes:

$$\delta Z_F \left(\eta, \eta', x\right) - \delta Z_F \left(\varepsilon^{1/\beta}\eta, \varepsilon^{1/\beta}\eta', x/\varepsilon^2\right) \simeq \lambda_d f_\varepsilon \left(\eta, \eta', x; \boldsymbol{\kappa}\right), \tag{4.75a}$$

$$\delta Z_\rho \left(\eta, \eta', x\right) - \delta Z_\rho \left(\varepsilon^{1/\beta}\eta, \varepsilon^{1/\beta}\eta', x/\varepsilon^2\right) \simeq \lambda_d \left[g_\varepsilon \left(\eta, \eta', x; \boldsymbol{\kappa}\right) + l_\varepsilon \left(\eta, \eta', x; \boldsymbol{\kappa}\right)\right]. \tag{4.75b}$$

Here, $\lambda_d \equiv C_d \hat{g}_{\text{cl}}^2$ plays the role of a dimensionless coupling, where C_d is given by (4.D.3) and stems from the angular integration, see App. 4.D. The functions f_ε, g_ε, and l_ε can be written as

$$f_\varepsilon \left(\eta, \eta', x\right) = \frac{\int\limits_0^\infty \mathrm{d}y \int\limits_{-1}^1 \mathrm{d}\zeta \int\limits_1^\eta \mathrm{d}\eta_1 \int\limits_1^{\eta'} \mathrm{d}\eta_2 \, D_F \left(x, y, \zeta, \varepsilon\right) L_F \left(\eta, \eta', x, \zeta, \eta_1, \eta_2, y\right)}{\hat{F} \left(\eta, \eta', x\right)}, \tag{4.76a}$$

$$g_\varepsilon \left(\eta, \eta', x\right) = \frac{\int\limits_0^\infty \mathrm{d}y \int\limits_{-1}^1 \mathrm{d}\zeta \int\limits_\eta^{\eta_2} \mathrm{d}\eta_1 \int\limits_\eta^{\eta'} \mathrm{d}\eta_2 \, D_\rho^{(\text{nt})} \left(x, y, \zeta, \varepsilon\right) L_\rho^{(\text{nt})} \left(\eta, \eta', x, \zeta, \eta_1, \eta_2, y\right)}{\hat{\rho} \left(\eta, \eta', x\right)}, \tag{4.76b}$$

$$l_\varepsilon \left(\eta, \eta', x\right) = \frac{\int\limits_0^\infty \mathrm{d}y \int\limits_{-1}^1 \mathrm{d}\zeta \int\limits_\eta^{\eta'} \mathrm{d}\eta_1 \, D_\rho^{(\text{t})} \left(y, \zeta, \varepsilon\right) L_\rho^{(\text{t})} \left(\eta, \eta', x, \zeta, \eta_1, \eta_2, y\right)}{\hat{\rho} \left(\eta, \eta', x\right)}. \tag{4.76c}$$

where D_X and L_X can be found in (4.E.6) and (4.E.7 – 4.E.9), respectively (see App. 4.E for more details). The integration over $[0, \infty)$ can be mapped to a finite region $[0, 1]$ by performing a change of variable, e.g., $y = \text{atanh}(w)$ or $y = w/(1 - w)$. In this work, we use the former map.

Finally, we have also introduced the notation $\boldsymbol{\kappa} = (\kappa, \gamma)$ for the collection of scaling exponents. Together with the coupling λ_d, there are therefore three unknowns and only two equations. The missing equation will be discussed in Sec. 4.4.3.

In Sec. 4.2.6, we have already hinted that since time variables are not affected by the regulator, temporal scaling should persist even in the $k \to \infty$ limit. On the other hand, due to a quasiparticle nature of the taken Ansatz, one still expects a suppression in the frequency domain. Recalling that δZ_F and δZ_ρ are even functions and thus performing the cosine Wigner transform, we expect from (4.23) the following ω-dependence of the δZ functions in the regulator-dominated regime:

$$\delta Z_{F/\rho}^W \left(\tau, \omega \to 0, x \to 0\right) = -\frac{\sin \left(2\omega\tau\right)}{\omega} + \dots, \tag{4.77}$$

where, for brevity, we dropped the hats from the dimensionless variables $\hat{\tau}$ and $\hat{\omega}$. As can be observed in Fig. 4.3, the sinc function indeed describes the low-frequency part of the numerical data quite accurately.
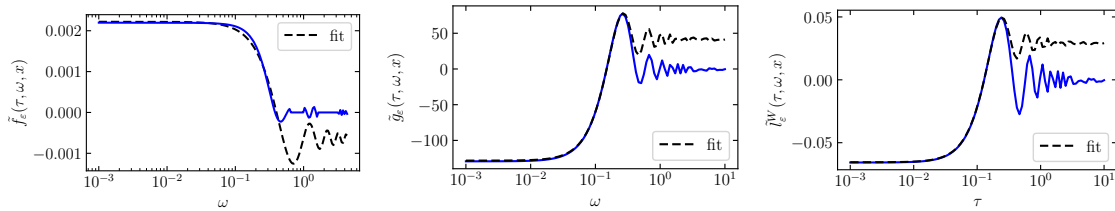
Figure 4.3. The dependence of $\tilde{f}_\varepsilon^W$ (left), $\tilde{g}_\varepsilon^W$ (middle), and $\tilde{l}_\varepsilon^W$ (right) on ω at $\tau = 8$, $x = 10^{-4}$ for fixed $\kappa = 4.2$, $\gamma = 0.5$, and $\varepsilon = 10^{-4}$ in $d = 3$ spatial dimensions plotted in a semi-log scale. The fitting function is given by $m(\omega) = -a\omega^{-1}\sin(\omega/\omega_0) + c$. The parameters used for the fits are $(a, \omega_0, c) = (-4.51 \cdot 10^{-4}, 15.8 \cdot 10^{-2}, -6.35 \cdot 10^{-4})$, $(10.2, 6 \cdot 10^{-2}, 41.2)$, and $(5.2 \cdot 10^{-3}, 5.5 \cdot 10^{-2}, 2.9 \cdot 10^{-2})$ for $\tilde{f}_\varepsilon^W$, $\tilde{g}_\varepsilon^W$, and $\tilde{l}_\varepsilon^W$, respectively. Note that the extracted values of ω_0 are consistent with the expectation $1/2\tau = 6.25 \cdot 10^{-2}$ for all the functions, with the exception of $\tilde{f}_\varepsilon^W$. Even for that case, however, by simply looking at the plot one can clearly see that the fitting routine overestimates ω_0 by a factor of ~ 2, which can be attributed to a poor quality of data for $\tilde{f}_\epsilon^W$ in the region $\omega \gtrsim \omega_0$, where the numerical scheme becomes less stable. Analogous computations for $\tau = 16$ (not shown here) yield ω_0 consistent with $1/2\tau = 3.125 \cdot 10^{-2}$

4.4.2   Removing divergences

In fact, however, the functions plotted in Fig. 4.3 are not exactly the ones defined in (4.76). Recall that ε was introduced as a ratio between the lower k_1 and the upper k_2 cutoff scale values. By construction, $\delta Z_{k \to 0}$ has to vanish, so it is suggestive to take $k_1 = 0$ or, equivalently, $\varepsilon \to 0$. However, as mentioned in Sec. 2.2.2, in order for a system's quasiparticle density to be finite, an IR cutoff is required if the system demonstrates a strong power-law behavior in the $p \to 0$ limit. For scaling forms with an infrared plateau, this regularization appeared naturally, through the scale p_Λ. In our case, there is no such natural IR cutoff scale,[5] so we ought to keep $\varepsilon > 0$.

Nevertheless, for ε such that $\omega/\varepsilon^z \gg 1$, $x/\varepsilon^2 \gg 1$, we expect the second terms on the left-hand side of (4.75) to give either a vanishing or a purely singular contribution. We may therefore generally write

$$X_{\varepsilon \to 0}^W(\tau, \omega \to 0, x \to 0) = a_X + b_X \varepsilon^{-p_X} + c_X \varepsilon^{-p_X + 1} + \ldots, \tag{4.78}$$

with $X \in \{f, g, l\}$, with $p_X > 0$ corresponding to the ε-diverging case. The desired '-1 term' is given by the regular part a_X, so we should develop an efficient method of extracting it.

---

[5] Also, even in the case of scaling forms with a natural regularization, one may restrict oneself to studying the power-law region only. This way, one may trade having a less complicated scaling form to working with a simpler fixed point equation.
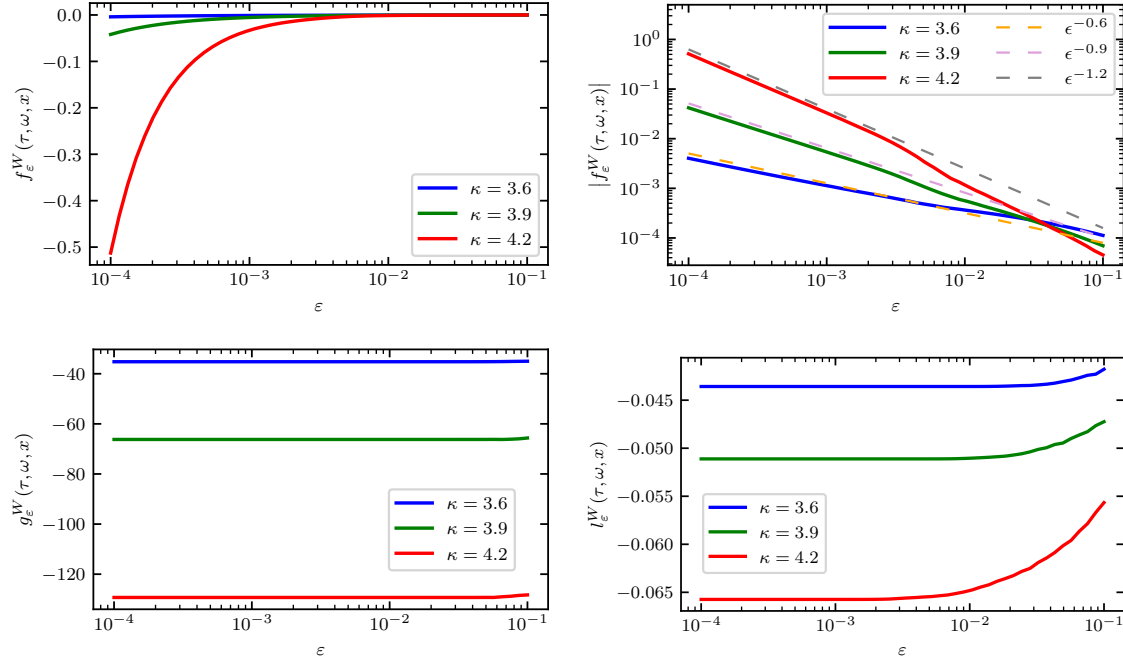
Figure 4.4. The dependence of f_ε^W (top left), g_ε^W (bottom left), and l_ε^W (bottom right) on ε for different values κ plotted in a semi-logarithmic scale. Top right: the only divergent function (f_ε^W) plotted in a double-logarithmic scale. All the plots correspond to fixed $\tau = 8$, $\omega = 0$, $x = 10^{-4}$, and $\gamma = 0.5$ in $d = 3$ spatial dimensions.

Now, since the cutoff scale k does not concern the temporal part of the loop, it is natural to expect that p_X shall come from the momentum divergence only. Examining in each case the most divergent contribution and making use of a simple power counting, one readily finds $p_f = \kappa - d$, $p_g = -d$, and $p_l = \kappa - d - 2$. Following the arguments in Sec. 4.3.2 we are going to restrict ourselves to $d \leq \kappa \leq d + 2$. We thus expect only f_ϵ^W to diverge, with the degree of divergence $p_X \leq 2$. This estimate is indeed corroborated by the numerical computations, see Figs. 4.4 and 4.5.

To remove the divergent contribution and get access to the constant part a_X, it is thus sufficient to take[6]

$$\tilde{X}_\varepsilon^W := X_\varepsilon^W + \frac{2\varepsilon \partial_\varepsilon X_\varepsilon^W}{p_X - 1} + \frac{\varepsilon^2 \partial_\varepsilon^2 X_\varepsilon^W}{p_X (p_X - 1)}. \tag{4.79}$$

As one can see in Fig. 4.6, the procedure described in (4.79) indeed removes the ε-divergence leaving only the regular part. Furthermore, as illustrated by Fig. 4.5, even for quantities that do not suffer from ε-divergences it might be beneficial to consider $\tilde{X}_\varepsilon^W$ instead of X_ε^W since it gives an access to the regular part already at relatively large values of ε, for which numerical integration is more stable. On the other hand, as computations involving ε-derivatives

---

[6]As a remark, we note that the derivatives in (4.79) can be again performed symbolically using the *Symbolics.jl* library, so no approximate methods are needed.
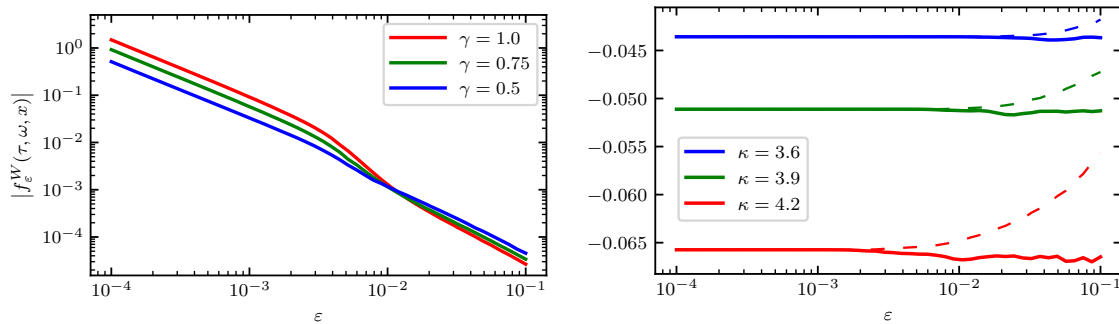
Figure 4.5. Left: The dependence of f_ε^W on ε for different values of γ and fixed $\kappa = 4.2$ in a double-logarithmic scale. Right: The dependence of $\tilde{l}_\varepsilon^W$ (solid line) and l_ε^W (dashed line) on ε for different values of γ and fixed $\kappa = 4.2$ plotted in a semi-logarithmic scale. Both plots correspond to $\tau = 8$, $\omega = 0$, and $x = 10^{-4}$.
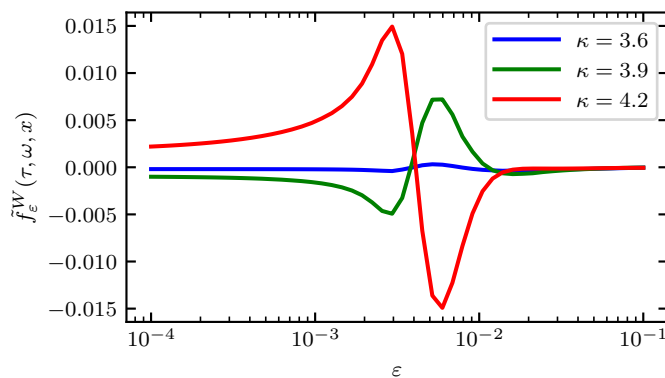

Figure 4.6. The dependence of $\tilde{f}_\varepsilon^W$ on ε after removing the ε-divergence plotted in a semi-logarithmic scale. The plots are done at fixed $\gamma = 0.5$, $\tau = 8$, $\omega = 0$, and $x = 10^{-4}$ and different values of κ.

are more time consuming, in practice it is also advantageous to reduce the number of derivatives taken. Because of that, in the following, we are going to employ the simplified version of (4.79) for l_ε^W: $\tilde{l}_\varepsilon^W = l_\varepsilon^W + \varepsilon \partial_\varepsilon l_\varepsilon^W / (p_l - 1)$, and make no modifications at all for g_ε^W: $\tilde{g}_\varepsilon^W = g_\varepsilon^W$.

4.4.3 Time dependence and the missing equation

Recall that our goal is to find such κ (and λ_d) that the asymptotics of δZ_F and δZ_ρ in the suppressed region give -1. According to the discussion in Sec. 4.2.4, such values of the exponents correspond to proper scaling solutions. However, as we have just argued, in our case, the cutoff-dominated regime remains τ-dependent, cf. (4.2.4). This implies that the value κ^* for which the desired limits -1 are achieved may depend on τ.

Indeed, taking the limit $\omega\tau \ll 1$ we can extract the coupling constant using (4.75b)

together with (4.77):

$$\lambda_d^*(\tau) = - \left. \frac{2\tau}{\tilde{g}_{\varepsilon\to0}^W(\tau,\omega,x;\boldsymbol{\kappa}^*) + \tilde{l}_{\varepsilon\to0}^W(\tau,\omega,x;\boldsymbol{\kappa}^*)} \right|_{\omega\to0,x\to0}. \tag{4.80}$$

Now, plugging this into (4.75a) and defining

$$Q_\varepsilon(\tau;\boldsymbol{\kappa}) \equiv \left. \frac{\tilde{f}_\varepsilon^W(\tau,\omega,x;\boldsymbol{\kappa})}{\tilde{g}_\varepsilon^W(\tau,\omega,x;\boldsymbol{\kappa}) + \tilde{l}_\varepsilon^W(\tau,\omega,x;\boldsymbol{\kappa})} \right|_{\omega\to0,x\to0} \tag{4.81}$$

the condition that both δZ_F and δZ_ρ reach -1 can be rewritten as $Q_{\varepsilon\to0}(\tau;\boldsymbol{\kappa}^*) = 1$ for any τ. As expected, this might require time-dependent scaling exponents $\boldsymbol{\kappa}^*(\tau)$ such that

$$Q_{\varepsilon\to0}(\tau;\boldsymbol{\kappa}^*) = 1, \quad \left(\partial_\tau + \frac{\partial\kappa_i^*}{\partial\tau}\frac{\partial}{\partial\kappa_i^*}\right) Q_{\varepsilon\to0}(\tau;\boldsymbol{\kappa}^*) = 0. \tag{4.82}$$

Therefore, upon fixing γ^*, the solutions κ^* and λ_d^* will generally depend on both γ^* and τ. The remaining missing equation then follows from the self-consistency condition that the input temporal scaling (characterized by γ^*) is also the same for the regularized propagator in the presence of δZ, computed with $\boldsymbol{\kappa}^*$ and λ_d^*.

Recall, however, that by assumption $\partial_\tau\gamma^* = \partial_\tau\kappa^* = 0$, so in practice, even before checking for the aforementioned self-consistency condition, one can use time-independence of the scaling exponents as a guiding principle when looking for potential solutions. In Fig. 4.7, one can see the dependence of $\tilde{f}_\varepsilon^W$, $\tilde{g}_\varepsilon^W$, and $\tilde{l}_\varepsilon^W$ on τ for different fixed values of the scaling exponents. Notably, the scaling with τ shows no strong dependence on κ, but for the most part only on the exponent γ. This dependence is further explored in Fig. 4.8, where we find that the scaling with τ is given by $\tau^{3+\gamma}$, $\tau^{3-2\gamma}$, and $\tau^{3-\gamma}$ for $\tilde{f}_\epsilon^W$, $\tilde{g}_\epsilon^W$, and $\tilde{l}_\epsilon^W$, respectively, at least for not too large values of τ.
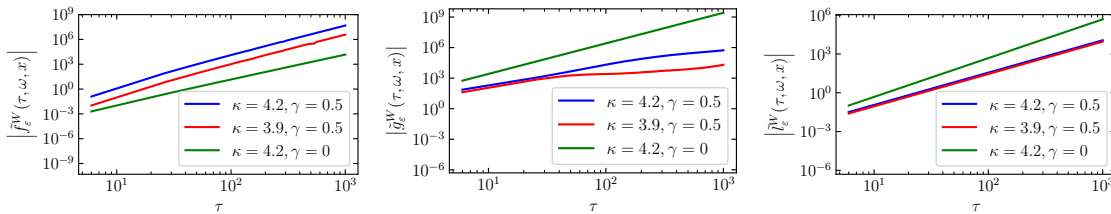
Figure 4.7. The dependence of $\tilde{f}_\varepsilon^W$ (left), $\tilde{g}_\varepsilon^W$ (middle), and $\tilde{l}_\varepsilon^W$ (right) on τ at $x = 10^{-4}$, $\omega = 0$ for fixed $\varepsilon = 10^{-4}$ and different values of κ and γ in $d = 3$ spatial dimensions plotted in a log-log scale.

4.4.4 Searching for solutions and residual x-dependence

At this point, we have completely covered the dependence of X_ε on both of the temporal arguments (τ and ω) as well as on the regularization parameter ε. The only variable that has
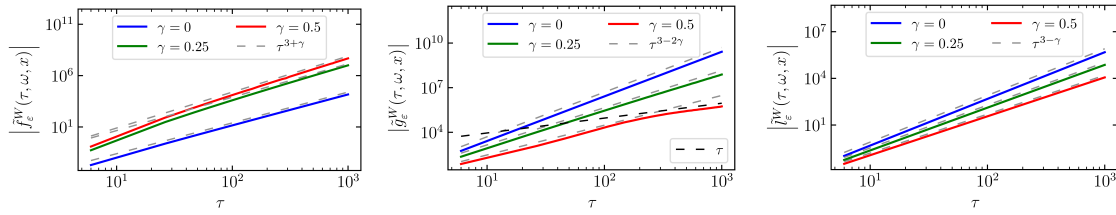
Figure 4.8. The dependence of $\tilde{f}_\varepsilon^W$ (left), $\tilde{g}_\varepsilon^W$ (middle), and $\tilde{l}_\varepsilon^W$ (right) on τ in $d = 3$ spatial dimensions at $x = 10^{-4}$, $\omega = 0$ for fixed $\varepsilon = 10^{-4}$ and $\kappa = 4.2$ and different values of γ plotted in a log-log scale.
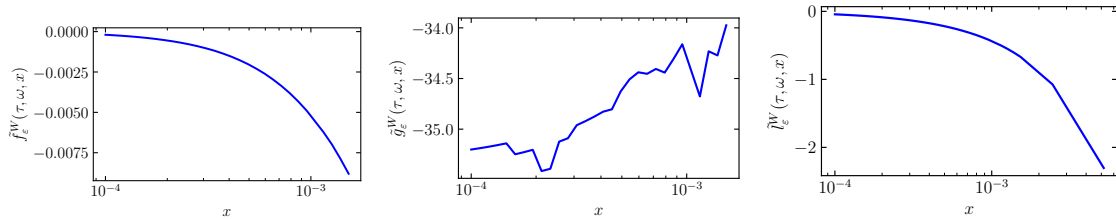

Figure 4.9. The dependence of $\tilde{f}_\varepsilon^W$ (left), $\tilde{g}_\varepsilon^W$ (middle), and $\tilde{l}_\varepsilon^W$ (right) on x in $d = 3$ spatial dimensions at $\tau = 8$, $\omega = 0$ for fixed $\kappa = 3.6$, $\gamma = 1/2$, and $\varepsilon = 10^{-4}$ plotted in a semi-logarithmic scale.

not yet been properly addressed is x. For the method to work, we need a finite $x \to 0$ limit after all the ε-divergences are subtracted. As can be seen in Fig. 4.9, however, only $\tilde{g}_\varepsilon^W$ has a finite $x \to 0$ limit, whereas the other two functions vanish as they approach $x = 0$. In principle, since the functions $\tilde{f}_\varepsilon^W$, $\tilde{g}_\varepsilon^W$, and $\tilde{l}_\varepsilon^W$ do not enter the definitions (4.80) and (4.81) independently, it is possible that their dependencies on x cancel each other in the $x \to 0$ limit. However, as shown in App. 4.F, that's not the case.

Recall that, at least for the case of f_ε^W, we had to remove the ε-divergence by performing the operation described in (4.79). It is therefore suggestive to associate the absence of a finite $x \to 0$ limit with the procedure (4.79). However, as one can see in Fig. 4.10, even without removing the ε-divergences, f_ε^W still tends to vanish as $x \to 0$, albeit with a different power law. Interestingly, however, as shown in Figs. 4.11 and 4.12, the asymptotic $x \to 0$ behavior shows a very mild dependnce on both κ and γ. For $\tilde{f}_\varepsilon^W$, we always find an approximate $x^{3/2}$ behavior, whereas $\tilde{g}_\varepsilon^W$ decreases linearly as $x \to 0$.

This suggests a possible explanation for the observed absence of a nontrivial $x \to 0$ limit. From Sec. 4.2.3, it is clear that a non-vanishing limit $\delta Z_{k \to \infty}$ is only required if the flow alters the propagators at finite cutoff scale k. If, however, the flow has a form that is proportional to the propagator itself, the deviation δZ_k from the full scaling can vanish even in the $k \to \infty$ limit since the propagator keeps its full form throughout the flow. In the chosen approximation scheme, this scenario then implies $k \partial_k \Sigma_{k,\mathbf{ab}} \propto \Gamma_{\mathbf{ab}}^{(2)} - \Gamma_{k,\mathbf{ab}}^{(2)}$.
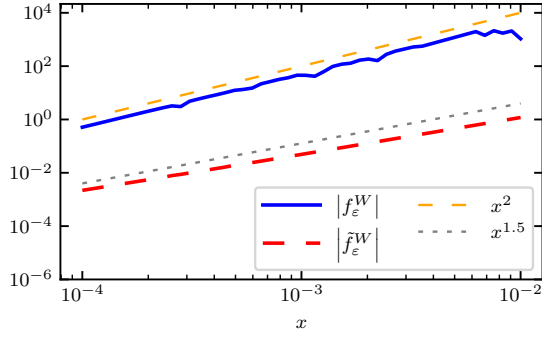
Figure 4.10. The dependence of f_ε^W (solid blue) and $\tilde{f}_\varepsilon^W$ (dashed red) on x in $d = 3$ spatial dimensions at $\tau = 8$, $\omega = 0$ for fixed $\kappa = 4.2$, $\gamma = 1/2$, and $\varepsilon = 10^{-4}$ plotted in a log-log scale.
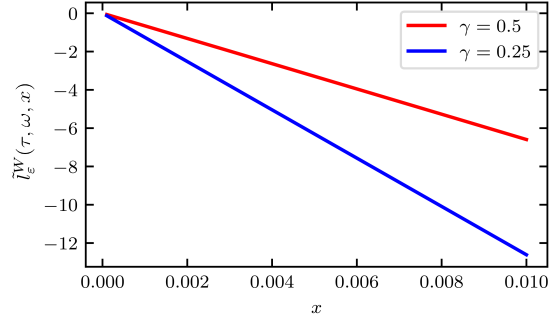
Figure 4.11. The dependence of $\tilde{l}_\varepsilon^W$ on x in $d = 3$ spatial dimensions at $\tau = 8$, $\omega = 0$ for fixed $\kappa = 4.2$, $\varepsilon = 10^{-4}$ and different values of γ plotted in a linear scale.

A second option is that the ε-divergence removal procedure is performed in such a manner that it spoils the x-dependence. This is hinted at by the fact that the observed asymptotic behavior of f_ε^W before the regularization differs from that of $\tilde{f}_\varepsilon^W$ after removing the ε-divergence. Curiously, for l_ε^W, the effect of the divergence-removing procedure on the x-dependence depends on whether the case is divergent or not, i.e., if $p_l > 0$ or $p_l < 0$. When $p_l < 0$, the procedure (4.79) seems to have no effect on the x-dependence of l_ε^W at all. On the other hand, for $p_l > 0$, while not altering the linear behavior, the operation (4.79) dramatically changes the slope (and even the sign). See Fig. 4.13 for both cases. We thus conclude that the procedure (4.79) requires a careful reexamination.

Finally, the problem might be on the numerical side. The integrals (4.76) are characterized by a strongly singular structure of their integrands. In particular, they have a limited support in the momentum domain. When mapped to the finite $w \in [0, 1]$ integration region, the integrands typically have a very narrow peak around either $w \approx 0$, $w \approx 1$, or both, depending on values of the input scaling exponents. Because of that, especially in the limiting cases, numerical integration can often become unstable, even for adaptive schemes, which is especially evident in Fig. 4.12. A clever coordinate transformation, similar to, e.g., the one described in [155], which would help to smooth out such singular structures depending on the input scaling exponents, is therefore highly desirable.

4.5 Conclusions

In this work, we have proposed a new approach to searching for nonthermal fixed point solutions based on the renormalization group framework. To that end, we derived the fixed-point
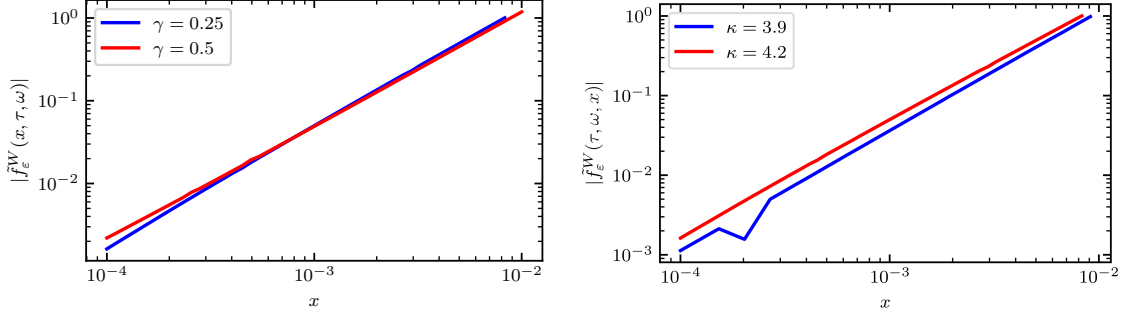
Figure 4.12. The dependence of $\tilde{f}_\varepsilon^W$ on x in $d = 3$ spatial dimensions at $\tau = 8$, $\omega = 0$ for fixed $\varepsilon = 10^{-4}$ and $\kappa = 3.9$ (left) or $\gamma = 1/4$ (right) and different values of γ (left) or κ (right) plotted a log-log scale. In both cases, the power-law behavior is given by $x^{1.5}$.
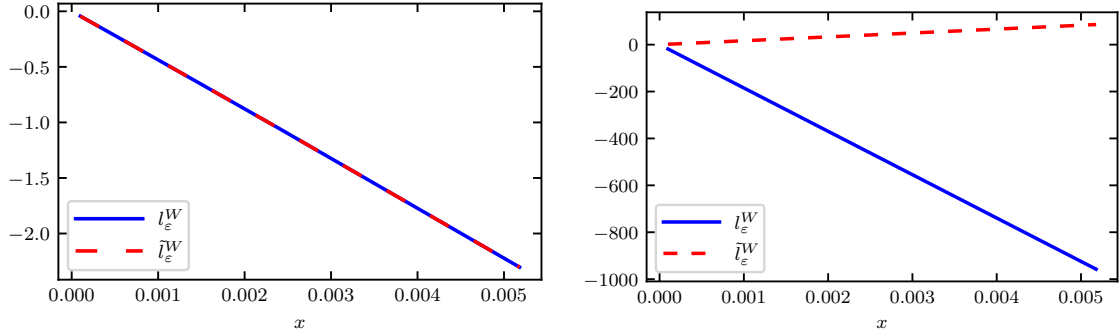

Figure 4.13. The dependence of $\tilde{l}_\varepsilon^W$ (solid blue) and l_ε^W (dashed red) on x in $d = 3$ spatial dimensions at $\tau = 8$, $\omega = 0$, $\varepsilon = 10^{-4}$, and fixed $\gamma = 0.5$ for $\kappa = 3.6$ (left) and $\kappa = 5.6$ (right) plotted in a linear scale.

equations that control universal scaling properties of the statistical and spectral functions at a nonthermal fixed point. We then argued that in the limit of interest the equations can be significantly simplified, becoming accessible for numerical methods. Due to the presence of strong IR divergence (characteristic of NTFP solutions), however, a divergence-removing procedure had to be introduced in order to extract the relevant regular part of a solution. We then demonstrated how one can work around the residual temporal scaling stemming from the absence of regularization in the time domain. Apart from the momentum-dependence in the regulator-dominated regime, the numerical data shows the expected behavior, indicating that the proposed method can be used to search for and classify possible universal scaling solutions in far-from-equilibrium many-body systems once the momentum-dependence problem is fixed. For the latter, we have proposed three possible sources of origin. The most probable explanation is that the divergence-removing procedure affects the small-momentum behavior, thus spoiling the asymptotic limit of interest. A careful reexamination is therefore required and is currently work in progress. After the issue is fixed, we expect the

proposed approach to play a central role in a complete categorization of possible nonthermal fixed points into different universality classes. In addition, it can be seen as complementary to other numerical methods such as, e.g., classical-statistical simulations.

APPENDIX

4.A   Galilean invariance of the nonrelativistic Bose gas

4.A.1   Covariant derivative

The action (4.3) enjoys the symmetry under Galilean transformations,

$$
t \to t' = t, \qquad\qquad \mathbf{x} \to \mathbf{x}' = R\mathbf{x} + \mathbf{v}t,
$$
$$
\psi(x) \to \psi'(x') = \mathrm{e}^{\mathrm{i}\gamma(x)}\psi(x)\,, \quad \psi^*(x) \to \psi^{*\prime}(x') = \mathrm{e}^{-\mathrm{i}\gamma(x)}\psi^*(x)\,, \tag{4.A.1}
$$

with

$$
\gamma(x) = m\left(R^{-1}\mathbf{v}\cdot\mathbf{x} + \frac{\mathbf{v}^2 t}{2} \right). \tag{4.A.2}
$$

In the density-phase representation the same transformation reads

$$
n(x) \to n'(x') = n(x)\,, \quad \theta(x) \to \theta'(x') = \theta(x) + \gamma(x)\,. \tag{4.A.3}
$$

Using

$$
\partial_{t'} = \partial_t - R^{-1}\mathbf{v}\cdot\nabla, \quad \nabla' = R\nabla \tag{4.A.4}
$$

we therefore find

$$
\partial_t\theta(x) \to \partial_{t'}\theta'(x') = \partial_t\theta(x) - R^{-1}\mathbf{v}\cdot\nabla\theta(x) - \frac{1}{2}m\mathbf{v}^2\,,
$$
$$
\nabla\theta(x) \to \nabla'\theta'(x') = R\nabla\theta(x) + m\mathbf{v}\,. \tag{4.A.5}
$$

Thus, the combination

$$
D_t\theta = \partial_t\theta - \frac{1}{2m}\left(\nabla\theta\right)^2 \tag{4.A.6}
$$

is Galilei-invariant.

4.A.2   Slavnov–Taylor identities for vertices

Let us also discuss how Galilei symmetry restricts the form of interaction terms of our EFT. For simplicity, let's consider the case $R = I$. Then, an infinitesimal Galilean boost acts on the classical component of the field as

$$
\varphi'_{\mathrm{cl}}(t,\mathbf{x}) = \varphi_{\mathrm{cl}}(t, \mathbf{x}-\mathbf{v}t) + m\mathbf{v}\cdot\mathbf{x} - \frac{m\mathbf{v}^2 t}{2} = \varphi_{\mathrm{cl}}(t,\mathbf{x}) + m\mathbf{v}\cdot\mathbf{x} - t\mathbf{v}\cdot\nabla\varphi(t,\mathbf{x}) + O(v^2), \tag{4.A.7}
$$

so that the generator of the boost is given by

$$
\mathcal{F}_{\mathrm{cl}}[x;\varphi] = m\mathbf{v}\cdot\mathbf{x} - t\mathbf{v}\cdot\nabla\varphi_{\mathrm{cl}}(t,\mathbf{x}). \tag{4.A.8}
$$

Likewise, for the quantum/response field,

$$\mathcal{F}_q[x;\varphi] = -t\mathbf{v} \cdot \nabla\varphi_q(t,\mathbf{x}). \tag{4.A.9}$$

The Slavnov–Taylor identity (3.104) associated with the Galilean symmetry therefore reads

$$\int_x \left\{ [m\mathbf{v} \cdot \mathbf{x} - t\mathbf{v} \cdot \nabla\phi_{cl}(x)] \, \Gamma_{cl}^{(1)}(x) - t\mathbf{v} \cdot \nabla\phi_q(x) \, \Gamma_q^{(1)}(x) \right\} = 0, \tag{4.A.10}$$

Taking one derivative with respect to ϕ_{cl} and then one with respect to ϕ_q then yields

$$\int_x \left\{ [m\mathbf{v} \cdot \mathbf{x} - t\mathbf{v} \cdot \nabla\phi_{cl}(x)] \, \Gamma_{clclq}^{(3)}(x,y,z) - t\mathbf{v} \cdot \nabla\delta(x-y) \, \Gamma_{clq}^{(2)}(x,z) \right.$$
$$\left. - t\mathbf{v} \cdot \nabla\delta(x-z) \, \Gamma_{qcl}^{(2)}(x,y) - t\mathbf{v} \cdot \nabla\phi_q(x) \, \Gamma_{qclq}^{(3)}(x,y,z) \right\} = 0. \tag{4.A.11}$$

Evaluating at $\phi_{cl} = \text{const}$, $\phi_q = 0$ we end up with

$$\int_x m\mathbf{v} \cdot \mathbf{x} \, \Gamma_{clclq}^{(3)}(x,y,z) = -y^0 \mathbf{v} \cdot \nabla_y \Gamma_{clq}^{(2)}(y,z) - z^0 \mathbf{v} \cdot \nabla_z \Gamma_{qcl}^{(2)}(z,y). \tag{4.A.12}$$

Taking time-locality into account and with a slight abuse of notation we then obtain

$$\int_{\mathbf{x}} m\mathbf{v} \cdot \mathbf{x} \, \Gamma_{clclq}^{(3)}(t;\mathbf{x},\mathbf{y},\mathbf{z}) = -t\mathbf{v} \cdot \left[\nabla_{\mathbf{y}}\Gamma_{clq}^{(2)}(t;\mathbf{y},\mathbf{z}) + \nabla_{\mathbf{z}}\Gamma_{qcl}^{(2)}(t;\mathbf{z},\mathbf{y}) \right]. \tag{4.A.13}$$

Going to Fourier space and using that $\mathbf{v}$ is arbitrary we finally find

$$\partial_{\mathbf{p}}\Gamma_{clclq}^{(3)}(t;\mathbf{p},\mathbf{q},\mathbf{r})\big|_{\mathbf{p}=0} = m^{-1}t \left[\mathbf{q}\,\Gamma_{clq}^{(2)}(t;\mathbf{q},\mathbf{r}) + \mathbf{r}\,\Gamma_{qcl}^{(2)}(t;\mathbf{q},\mathbf{r}) \right]. \tag{4.A.14}$$

Likewise, by taking one more ϕ_{cl} one may obtain

$$\partial_{\mathbf{p}}\Gamma_{clclclq}^{(4)}(t;\mathbf{p},\mathbf{q},\mathbf{r},\mathbf{l})\big|_{\mathbf{p}=0} = m^{-1}t \left[\mathbf{q}\,\Gamma_{clclq}^{(3)}(t;\mathbf{q},\mathbf{r},\mathbf{l}) + \mathbf{r}\,\Gamma_{clclq}^{(3)}(t;\mathbf{r},\mathbf{q},\mathbf{l}) + \mathbf{l}\,\Gamma_{qclcl}^{(3)}(t;\mathbf{l},\mathbf{q},\mathbf{r}) \right].$$
$$\tag{4.A.15}$$

The t-factors here should be understood as anti-derivatives.

4.B Choice of units and fields redefinition

Consider the action (4.32). Rescaling the fields and choosing the units such that

$$t' = t, \quad \mathbf{x}' = \sqrt{a_0/b_0}\,\mathbf{x} \equiv c_0^{-1}\mathbf{x}, \quad \phi_{cl}' = \frac{(c_0^d a_0/f_0)^{1/2}}{m}\phi_{cl}, \quad \phi_q' = \frac{(c_0^d a_0 f_0)^{1/2}}{m}\phi_q \tag{4.B.1}$$

and omitting the primes one obtains

$$\Gamma[\phi_{cl},\phi_q] = \int_{x,t_0} \left\{ \frac{1}{2}\left[\partial_t\phi_{cl}\partial_t\phi_q - t^{\beta-1}\nabla\phi_{cl}\nabla\phi_q\right] - \frac{g_{cl}}{4}\partial_t\phi_q\left(\nabla\phi_{cl}\right)^2 - \frac{g_{cl}}{2}\partial_t\phi_{cl}\nabla\phi_{cl}\nabla\phi_q \right.$$
$$\left. + \frac{g_{cl}^2}{4}\left(\nabla\phi_{cl}\right)^3\nabla\phi_q - \frac{g_q}{16}\partial_t\phi_q\left(\nabla\phi_q\right)^2 + \frac{g_{cl}g_q}{16}\nabla\phi_{cl}\left(\nabla\phi_q\right)^3 + (\text{qq} - \text{term}) \right\}, \tag{4.B.2}$$

with the effective coupling constants $g_{\mathrm{cl}} = a_0 f_0^{1/2}/(b_0 c_0^{d/2})$, $g_{\mathrm{q}} = g_{\mathrm{cl}}/f_0^2$. To close the discussion, let us show that (4.B.1) leaves the $\mathrm{q} - \mathrm{q}$-component parameter-free. Indeed, upon rescaling $\mathbf{x}' = c_0^{-1}\mathbf{x}$ one readily obtains

$$\frac{1}{2} \int_{t,t',\mathbf{x}} \phi_{\mathrm{q}}(t,\mathbf{x})\, \Gamma_{\mathrm{qq}}^{(2)}(t,t',\mathbf{x})\, \phi_{\mathrm{q}}(t',\mathbf{x}) = \frac{c_0^d}{2} \int_{t,t',\mathbf{x}'} \phi_{\mathrm{q}}(t, c_0\mathbf{x}')\, \Gamma_{\mathrm{qq}}^{(2)}(t, t', c_0\mathbf{x}')\, \phi_{\mathrm{q}}(t', c_0\mathbf{x}').$$

(4.B.3)

Using eqs. (4.32) to (4.34) we find

$$\begin{aligned}
\Gamma_{\mathrm{qq}}^{(2)}(t,t',c_0\mathbf{x}) &= \int_{t_1} \left[f(t,t_1)\, \Gamma_{\mathrm{clq}}^{(2)}(t_1, t', c_0\mathbf{x}) - \Gamma_{\mathrm{qcl}}^{(2)}(t, t_1, c_0\mathbf{x})\, f(t_1, t') \right] \\
&= \frac{a_0 f_0}{m^2}\, \bar{\Gamma}_{\mathrm{qq}}^{(2)}(t, t', \mathbf{x}),
\end{aligned}$$

(4.B.4)

where $\bar{\Gamma}_{\mathrm{qq}}^{(2)}$ is a parameter-free function. Therefore,

$$\frac{1}{2} \int_{t,t',\mathbf{x}} \phi_{\mathrm{q}}(t,\mathbf{x})\, \Gamma_{\mathrm{qq}}^{(2)}(t,t',\mathbf{x})\, \phi_{\mathrm{q}}(t',\mathbf{x}) = \frac{a_0 f_0 c_0^d}{2m^2} \int_{t,t',\mathbf{x}'} \phi_{\mathrm{q}}(t, c_0\mathbf{x}')\, \bar{\Gamma}_{\mathrm{qq}}^{(2)}(t, t', \mathbf{x}')\, \phi_{\mathrm{q}}(t', c_0\mathbf{x}').$$

(4.B.5)

Finally, defining $\phi_{\mathrm{q}}'(t,\mathbf{x}) = m^{-1}(c_0^d a_0 f_0)^{1/2}\, \phi_{\mathrm{q}}(t, c_0\mathbf{x})$, as we did in (4.B.1), we end up with a parameter-free $\mathrm{q} - \mathrm{q}$-term.

4.C   Diagrammatics

To better visualize contributions entering the kernels $I_{k,\mathbf{ab}}$, it is convenient to come up with a diagrammatic representation of $\tilde{G}_k$, $k\partial_k\tilde{G}_k$, and $\Gamma_k^{(n \geq 3)}$. In this work, we are going to adopt the following notation for the (deformed) propagators and derivatives thereof,

$$t_1 \overset{\mathbf{p}}{\underset{\bullet}{\rule{2cm}{0.4pt}}} t_2 = \tilde{F}_k(t_1, t_2, \mathbf{p}), \qquad t_1 \overset{\mathbf{p}}{\rule{2cm}{0.4pt}} t_2 = k\partial_k\tilde{F}_k(t_1, t_2, \mathbf{p}), \quad \text{(4.C.1a)}$$

$$t_1 \overset{\mathbf{p}}{\underset{\bullet}{\text{- - -}}} t_2 = \tilde{G}_k^A(t_1, t_2, \mathbf{p}), \qquad t_1 \overset{\mathbf{p}}{\text{- - -}} t_2 = k\partial_k\tilde{G}_k^A(t_1, t_2, \mathbf{p}), \quad \text{(4.C.1b)}$$

$$t_1 \overset{\mathbf{p}}{\underset{\bullet}{\text{- - -}}} t_2 = \tilde{G}_k^R(t_1, t_2, \mathbf{p}), \qquad t_1 \overset{\mathbf{p}}{\text{- - -}} t_2 = k\partial_k\tilde{G}_k^R(t_1, t_2, \mathbf{p}), \quad \text{(4.C.1c)}$$

as well as vertices,

$$= \Gamma^{(3)}_{k,\mathrm{clclq}}\left(t_1, \mathbf{p}_1, \ldots, t_3, \mathbf{p}_3\right), \qquad (4.\mathrm{C}.2\mathrm{a})$$

$$= \Gamma^{(3)}_{k,\mathrm{qqq}}\left(t_1, \mathbf{p}_1, \ldots, t_3, \mathbf{p}_3\right), \qquad (4.\mathrm{C}.2\mathrm{b})$$

$$= \Gamma^{(4)}_{k,\mathrm{qclclcl}}\left(t_1, \mathbf{p}_1, \ldots, t_4, \mathbf{p}_4\right), \qquad (4.\mathrm{C}.2\mathrm{c})$$

$$= \Gamma^{(4)}_{k,\mathrm{clqqq}}\left(t_1, \mathbf{p}_1, \ldots, t_4, \mathbf{p}_4\right). \qquad (4.\mathrm{C}.2\mathrm{d})$$

With this notation in mind, contributions to kernels I_{qq} and I_{clq} can be depicted as shown in Fig. 4.14. Diagrams entering $I_{k,\mathrm{qcl}}$ can be obtained by mirroring those contributing to $I_{k,\mathrm{clq}}$.
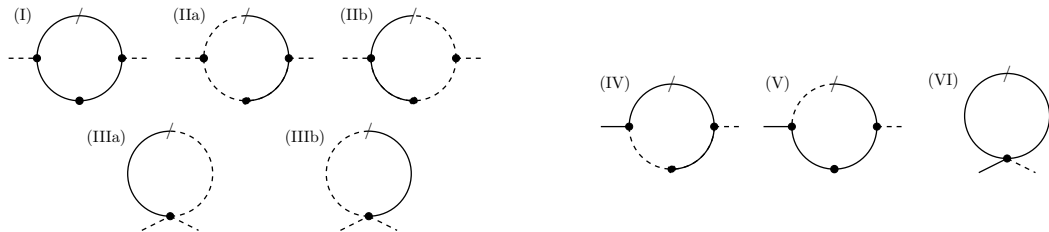

Figure 4.14. Diagrams contributing to $I_{k,\mathrm{qq}}$ (left) and $I_{k,\mathrm{clq}}$ (right). As argued in the main text, the tadpole diagrams (IIIa) and (IIIb) vanish due to causal reasons.

4.D   Volume element

The volume element $\mathrm{d}^d\mathbf{q}\,/(2\pi)^d$ in spherical coordinates,

$$
\begin{aligned}
q_1 &= q\cos(\chi_1),\\
q_2 &= q\sin(\chi_1)\cos(\chi_2),\\
q_3 &= q\sin(\chi_1)\sin(\chi_2)\cos(\chi_3),\\
&\;\;\vdots\\
q_{d-1} &= q\sin(\chi_1)\cdots\sin(\chi_{d-2})\cos(\chi_{d-1}),\\
q_d &= q\sin(\chi_1)\cdots\sin(\chi_{d-2})\sin(\chi_{d-1}),
\end{aligned}
\tag{4.D.1}
$$

reads

$$
\frac{\mathrm{d}^d\mathbf{q}}{(2\pi)^d} = q^{d-1}\,\mathrm{d}q\,\frac{\sin^{d-2}\chi_1\,\sin^{d-3}\chi_2\cdots\sin\chi_{d-2}\,\mathrm{d}\chi_1\cdots\mathrm{d}\chi_{d-1}}{(2\pi)^d},
\tag{4.D.2}
$$

with $\chi_1,\ldots,\chi_{d-2}\in[0,\pi]$ and $\chi_{d-1}\in[0,2\pi)$. A generic integrand will be a function of $\mathbf{p}$, $\mathbf{q}$, and $\mathbf{p}\cdot\mathbf{q}$. Due to rotational symmetry we can always choose $\mathbf{p}=(p,0,0,\ldots,0)$ such that the integrand only depends on χ_1. The remaining angular integration can be readily performed resulting in a d-depending prefactor:

$$
\begin{aligned}
C_d &\equiv \frac{1}{(2\pi)^d}\int_0^{2\pi}\mathrm{d}\chi_{d-1}\int_0^\pi\mathrm{d}\chi_{d-2}\sin\chi_{d-2}\ldots\int_0^\pi\mathrm{d}\chi_2\sin^{d-3}\chi_2 = \frac{2\pi}{(2\pi)^d}\prod_{n=1}^{d-3}\frac{\sqrt{\pi}\,\Gamma\!\left(\frac{n+1}{2}\right)}{\Gamma\!\left(\frac{n+2}{2}\right)}\\
&= \frac{\pi^{(d-3)/2}}{(2\pi)^{d-1}}\frac{1}{\Gamma\!\left(\frac{d-1}{2}\right)} = \frac{1}{2^{d-1}\pi^{(d+1)/2}}\frac{1}{\Gamma\!\left(\frac{d-1}{2}\right)} = \frac{\Omega_{d-1}}{(2\pi)^d},
\end{aligned}
\tag{4.D.3}
$$

which is nothing but the total $(d-1)$-dimensional solid angle Ω_{d-1} divided by $(2\pi)^d$. We thus conclude

$$
\int_{\mathbf{q}}\ldots \to C_d\int_0^\infty\mathrm{d}q\,q^{d-1}\int_0^\pi\mathrm{d}\chi_1\sin^{d-2}\chi_1\ldots = C_d\int_0^\infty\mathrm{d}q\,q^{d-1}\int_{-1}^1\mathrm{d}\zeta\left(1-\zeta^2\right)^{(d-3)/2}\ldots
\tag{4.D.4}
$$

Note that this result does not hold for $d=1$ where the integration should be replaced by the summation $\zeta=\pm1$. On the other hand, (4.D.4) is compatible with $d=2$. Indeed, in that case,

$$
\begin{aligned}
\int\frac{\mathrm{d}^2\mathbf{q}}{(2\pi)^2}f(q,\mathbf{q}\cdot\mathbf{e_p}) &= \frac{1}{(2\pi)^2}\int_0^\infty\mathrm{d}q\,q\int_{-\pi}^\pi\mathrm{d}\chi\,f(q,\cos\chi)\\
&= \frac{1}{(2\pi)^2}\int_0^\infty\mathrm{d}q\,q\int_0^\pi\mathrm{d}\chi\,f(q,\cos\chi) + \frac{1}{(2\pi)^2}\int_0^\infty\mathrm{d}q\,q\int_{-\pi}^0\mathrm{d}\chi\,f(q,\cos\chi)\\
&= \frac{1}{(2\pi)^2}\int_0^\infty\mathrm{d}q\,q\int_0^\pi\mathrm{d}\chi\,f(q,\cos\chi) - \frac{1}{(2\pi)^2}\int_0^\infty\mathrm{d}q\,q\int_\pi^0\mathrm{d}\chi\,f(q,\cos(-\chi))\\
&= \frac{2}{(2\pi)^2}\int_0^\infty\mathrm{d}q\,q\int_0^\pi\mathrm{d}\chi\,f(q,\cos\chi) = -\frac{2}{(2\pi)^2}\int_0^\infty\mathrm{d}q\,q\int_0^\pi\frac{\mathrm{d}\cos\chi}{\sin\chi}f(q,\cos\chi)\\
&= \frac{2}{(2\pi)^2}\int_0^\infty\mathrm{d}q\,q\int_{-1}^1\frac{\mathrm{d}\zeta}{\sqrt{1-\zeta^2}}f(q,\zeta).
\end{aligned}
\tag{4.D.5}
$$

4.E   Numerical integrals

The ε-dependent parts in the dimensionless equations (4.63) come solely from the regularization functions introduced in (4.46). Together with the momentum-volume prefactor $D(y, \zeta) = (1 - \zeta^2)^{(d-3)/2} \, y^{d/2-1}$, cf. (4.D.4), their combined effect can be written as

$$D_F\left(x, y, \zeta, \varepsilon\right) = -\frac{1}{2} D(y, \zeta) \left[P_F\left(y\right) P_F\left(u\right) - P_F\left(y/\varepsilon^2\right) P_F\left(u/\varepsilon^2\right)\right],$$

$$D_\rho^{(\text{nt})}\left(x, y, \zeta, \varepsilon\right) = D(y, \zeta) \left[P_F\left(y\right) P_\rho\left(u\right) - P_F\left(y/\varepsilon^2\right) P_\rho\left(u/\varepsilon^2\right)\right], \qquad (4.\text{E}.6)$$

$$D_\rho^{(\text{t})}\left(y, \zeta, \varepsilon\right) = D(y, \zeta) \left[P_F\left(y\right) - P_F\left(y/\varepsilon^2\right)\right],$$

where $u = x + y + 2\zeta\sqrt{xy}$, see (4.61). Introducing the functions

$$
\begin{aligned}
L_\rho^{(\text{nt})}\left(\ldots\right) = &\left[\partial_{\eta_1}\hat{\rho}\left(\eta, \eta_1, x\right) \hat{\rho}\left(\eta_1, \eta_2, u\right) \hat{F}\left(\eta_1, \eta_2, y\right) \partial_{\eta_2}\hat{\rho}\left(\eta_2, \eta', x\right) y \left(\zeta\sqrt{x} + \sqrt{y}\right)^2 \right. \\
&+ \partial_{\eta_1}\hat{\rho}\left(\eta, \eta_1, x\right) \hat{\rho}\left(\eta_1, \eta_2, u\right) \partial_{\eta_2}\hat{F}\left(\eta_1, \eta_2, y\right) \hat{\rho}\left(\eta_2, \eta', x\right) \zeta\sqrt{xy} \left(x + y + 2\zeta\sqrt{xy}\right) \\
&+ \partial_{\eta_1}\hat{\rho}\left(\eta, \eta_1, x\right) \partial_{\eta_2}\hat{\rho}\left(\eta_1, \eta_2, u\right) \hat{F}\left(\eta_1, \eta_2, y\right) \hat{\rho}\left(\eta_2, \eta', x\right) \zeta y\sqrt{x} \left(\zeta\sqrt{x} + \sqrt{y}\right) \\
&+ \hat{\rho}\left(\eta, \eta_1, x\right) \partial_{\eta_1}\hat{\rho}\left(\eta_1, \eta_2, u\right) \hat{F}\left(\eta_1, \eta_2, y\right) \partial_{\eta_2}\hat{\rho}\left(\eta_2, \eta', x\right) \zeta y\sqrt{x} \left(\zeta\sqrt{x} + \sqrt{y}\right) \\
&+ \hat{\rho}\left(\eta, \eta_1, x\right) \partial_{\eta_1}\hat{\rho}\left(\eta_1, \eta_2, u\right) \partial_{\eta_2}\hat{F}\left(\eta_1, \eta_2, y\right) \hat{\rho}\left(\eta_2, \eta', x\right) x\sqrt{y} \left(\sqrt{x} + \zeta\sqrt{y}\right) \\
&+ \hat{\rho}\left(\eta, \eta_1, x\right) \partial_{\eta_1}\partial_{\eta_2}\hat{\rho}\left(\eta_1, \eta_2, u\right) \hat{F}\left(\eta_1, \eta_2, y\right) \hat{\rho}\left(\eta_2, \eta', x\right) \zeta^2 xy \\
&+ \hat{\rho}\left(\eta, \eta_1, x\right) \hat{\rho}\left(\eta_1, \eta_2, u\right) \partial_{\eta_1}\hat{F}\left(\eta_1, \eta_2, y\right) \partial_{\eta_2}\hat{\rho}\left(\eta_2, \eta', x\right) \sqrt{xy} \left(\zeta\sqrt{x} + \sqrt{y}\right) \left(\sqrt{x} + \zeta\sqrt{y}\right) \\
&+ \hat{\rho}\left(\eta, \eta_1, x\right) \hat{\rho}\left(\eta_1, \eta_2, u\right) \partial_{\eta_1}\partial_{\eta_2}\hat{F}\left(\eta_1, \eta_2, y\right) \hat{\rho}\left(\eta_2, \eta', x\right) x \left(\sqrt{x} + \zeta\sqrt{y}\right)^2 \\
&\left.+ \hat{\rho}\left(\eta, \eta_1, x\right) \partial_{\eta_2}\hat{\rho}\left(\eta_1, \eta_2, u\right) \partial_{\eta_1}\hat{F}\left(\eta_1, \eta_2, y\right) \hat{\rho}\left(\eta_2, \eta', x\right) \zeta x\sqrt{y} \left(\sqrt{x} + \zeta\sqrt{y}\right)\right], \quad (4.\text{E}.7)
\end{aligned}
$$

$$L_\rho^{(\text{t})}\left(\ldots\right) = \hat{\rho}\left(\eta, \eta_1, x\right) \hat{F}\left(\eta_1, \eta_1, y\right) \hat{\rho}\left(\eta_1, \eta', x\right) xy \left(1 + 2\zeta\right), \qquad (4.\text{E}.8)$$

$$
\begin{aligned}
L_F\left(\ldots\right) = &\left[\partial_{\eta_1}\hat{\rho}\left(\eta, \eta_1, x\right) \hat{F}\left(\eta_1, \eta_2, u\right) \hat{F}\left(\eta_1, \eta_2, y\right) \partial_{\eta_2}\hat{\rho}\left(\eta_2, \eta', x\right) y \left(\zeta\sqrt{x} + \sqrt{y}\right)^2 \right. \\
&+ \partial_{\eta_1}\hat{\rho}\left(\eta, \eta_1, x\right) \hat{F}\left(\eta_1, \eta_2, u\right) \partial_{\eta_2}\hat{F}\left(\eta_1, \eta_2, y\right) \hat{\rho}\left(\eta_2, \eta', x\right) \sqrt{xy} \left(\zeta\sqrt{x} + \sqrt{y}\right) \left(\sqrt{x} + \zeta\sqrt{y}\right) \\
&+ \partial_{\eta_1}\hat{\rho}\left(\eta, \eta_1, x\right) \partial_{\eta_2}\hat{F}\left(\eta_1, \eta_2, u\right) \hat{F}\left(\eta_1, \eta_2, y\right) \hat{\rho}\left(\eta_2, \eta', x\right) \zeta y\sqrt{x} \left(\zeta\sqrt{x} + \sqrt{y}\right) \\
&+ \hat{\rho}\left(\eta, \eta_1, x\right) \partial_{\eta_1}\hat{F}\left(\eta_1, \eta_2, u\right) \hat{F}\left(\eta_1, \eta_2, y\right) \partial_{\eta_2}\hat{\rho}\left(\eta_2, \eta', x\right) \zeta y\sqrt{x} \left(\zeta\sqrt{x} + \sqrt{y}\right) \\
&+ \hat{\rho}\left(\eta, \eta_1, x\right) \partial_{\eta_1}\hat{F}\left(\eta_1, \eta_2, u\right) \partial_{\eta_2}\hat{F}\left(\eta_1, \eta_2, y\right) \hat{\rho}\left(\eta_2, \eta', x\right) x\sqrt{y} \left(\sqrt{x} + \zeta\sqrt{y}\right) \\
&+ \hat{\rho}\left(\eta, \eta_1, x\right) \partial_{\eta_1}\partial_{\eta_2}\hat{F}\left(\eta_1, \eta_2, u\right) \hat{F}\left(\eta_1, \eta_2, y\right) \hat{\rho}\left(\eta_2, \eta', x\right) \zeta^2 xy \\
&+ \hat{\rho}\left(\eta, \eta_1, x\right) \hat{F}\left(\eta_1, \eta_2, u\right) \partial_{\eta_1}\hat{F}\left(\eta_1, \eta_2, y\right) \partial_{\eta_2}\hat{\rho}\left(\eta_2, \eta', x\right) \sqrt{xy} \left(\zeta\sqrt{x} + \sqrt{y}\right) \left(\sqrt{x} + \zeta\sqrt{y}\right) \\
&+ \hat{\rho}\left(\eta, \eta_1, x\right) \hat{F}\left(\eta_1, \eta_2, u\right) \partial_{\eta_1}\partial_{\eta_2}\hat{F}\left(\eta_1, \eta_2, y\right) \hat{\rho}\left(\eta_2, \eta', x\right) x \left(\sqrt{x} + \zeta\sqrt{y}\right)^2 \\
&\left.+ \hat{\rho}\left(\eta, \eta_1, x\right) \partial_{\eta_2}\hat{F}\left(\eta_1, \eta_2, u\right) \partial_{\eta_1}\hat{F}\left(\eta_1, \eta_2, y\right) \hat{\rho}\left(\eta_2, \eta', x\right) \zeta x\sqrt{y} \left(\sqrt{x} + \zeta\sqrt{y}\right)\right], \quad (4.\text{E}.9)
\end{aligned}
$$

with the dimensionless propagators

$$\hat{\rho}\left(\eta, \eta', x\right) = \frac{\sin\left[\omega(\eta + \eta', x)\left(\eta - \eta'\right)\right]}{\omega(\eta + \eta', x)},$$

$$\hat{F}\left(\eta, \eta', x\right) = \frac{(\eta + \eta')^{-\gamma}}{x^{\kappa/2}} \cos\left[\omega(\eta + \eta', x)\left(\eta - \eta'\right)\right], \qquad (4.\text{E}.10)$$

where $\omega(\eta + \eta', x) = (\eta + \eta')^{\beta-1} x^{1/2}$, the dimensionless equations (4.63) take the form (4.75) and (4.76). All the derivatives in (4.E.7 – 4.E.9) are taken analytically by virtue of the *Symbolics.jl* library.

4.F Combined (x, τ)-dependence of the Q-ratio and the dimensionless coupling constant λ

As discussed in the beginning of Sec. 4.4.4, despite having a problem with the residual x-dependence, one could still try to extract the coupling (4.80) and the 'Q-ratio' (4.81), at least for a fixed value of x. Indeed, while $\tilde{f}_\varepsilon$, $\tilde{g}_\varepsilon^W$, and $\tilde{l}_\varepsilon^W$ depend on x, their dependencies may cancel each other resulting in x-independent quantities in the $x \to 0$ limit.

In Fig. 4.15, one can see the dependence of Q and λ_d on time τ for different values of x (note the extended time window). From this plot it may seem as if the coupling constant[7] does not depend on x. This, however, can be readily explained by the fact that, for chosen values of scaling exponents, the x-independent contribution $\tilde{g}_\varepsilon$ dominates over the x-dependent $\tilde{l}_\varepsilon$, cf. Fig. 4.9.

One could also imagine the existence of a constant region in the combined (τ, x)-plane. If such region existed, it could give a hint on how to approach the desired suppressed limit. In Figs. 4.16 and 4.17, we depict the full (τ, x)-dependence of $\tilde{f}_\varepsilon^W$, $\tilde{g}_\varepsilon^W$, and $\tilde{l}_\varepsilon^W$ as well as of the of the coupling and the Q-ratio. Unfortunately, no constant region is found.

Finally, let us address the observed coupling's time-dependence. In [64], it was proposed that the nonthermal fixed point associated with the late-time dynamics of a multicomponent Bose gas is Gaussian. The large-τ asymptotic behavior of the coupling λ is therefore of great interest. Curiously, for a given choice of scaling exponents ($\kappa = 3.9$, $\gamma = 0.5$), the coupling constant does not show a monotonic dependence on time, see Fig. 4.17. When averaged over different values of x, the coupling rather first drops dramatically until slowly rising again at later times, all the while remaining small ($\lambda \ll 1$) in the given time window, see Fig. 4.18. At the moment, it is unclear whether the observed behavior is physical or not and, if so, whether this behavior is expected to be shared by a proper scaling solution κ_*.

---

[7]Strictly speaking, for $\kappa \neq \kappa^*$, the expression (4.80) cannot be identified with the effective dimensionless coupling constant.

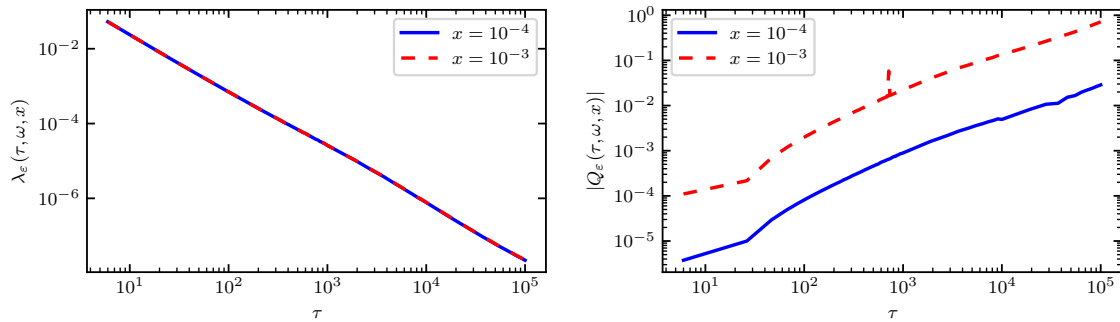**Figure 4.15.** The dimensionless scaling coupling (4.80) (left) and the ratio (4.81) (right) at late times τ for fixed $\omega = 0$, $\varepsilon = 10^{-4}$, $\kappa = 4.2$, $\gamma = 0.5$ and different values of x in $d = 3$ spatial dimensions plotted in a log-log scale.
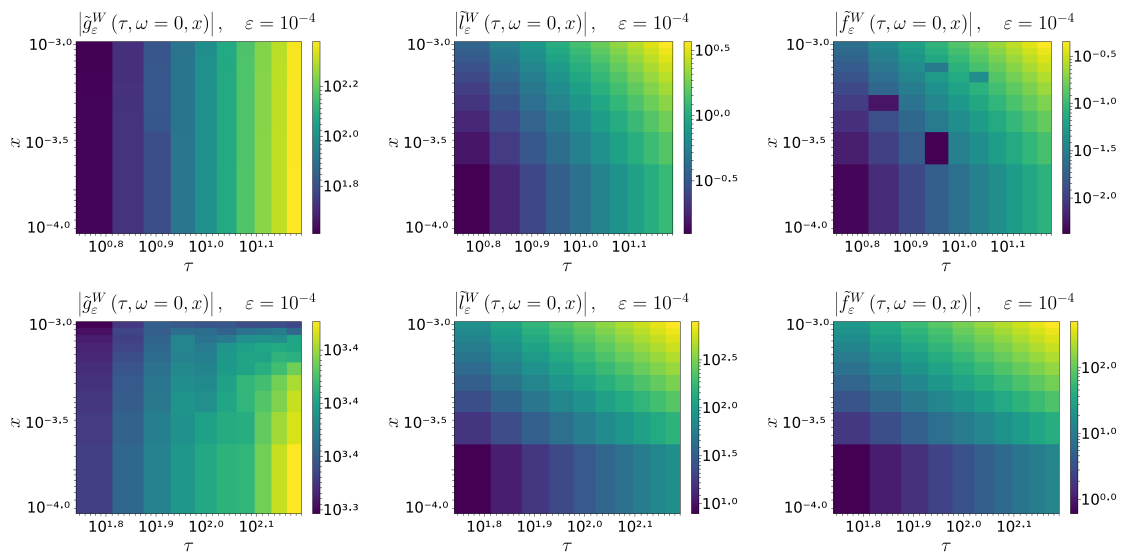

Figure 4.16. The dependence of $\tilde{g}_\varepsilon^W$ (left), $\tilde{l}_\varepsilon^W$ (middle), and $\tilde{f}_\varepsilon^W$ (right) on (τ, x) in $d = 3$ spatial dimensions at fixed $\omega = 0$, $\varepsilon = 10^{-4}$, $\kappa = 3.9$, and $\gamma = 0.5$ plotted in a log-log scale. Top row: $\tau \in [6, 15]$; bottom row: $\tau \in [60, 150]$. In each case, $x \in [10^{-4}, 10^{-3}]$. The dark spots on the $\tilde{f}_\varepsilon^W$ heatmap are due to numerical instabilities.
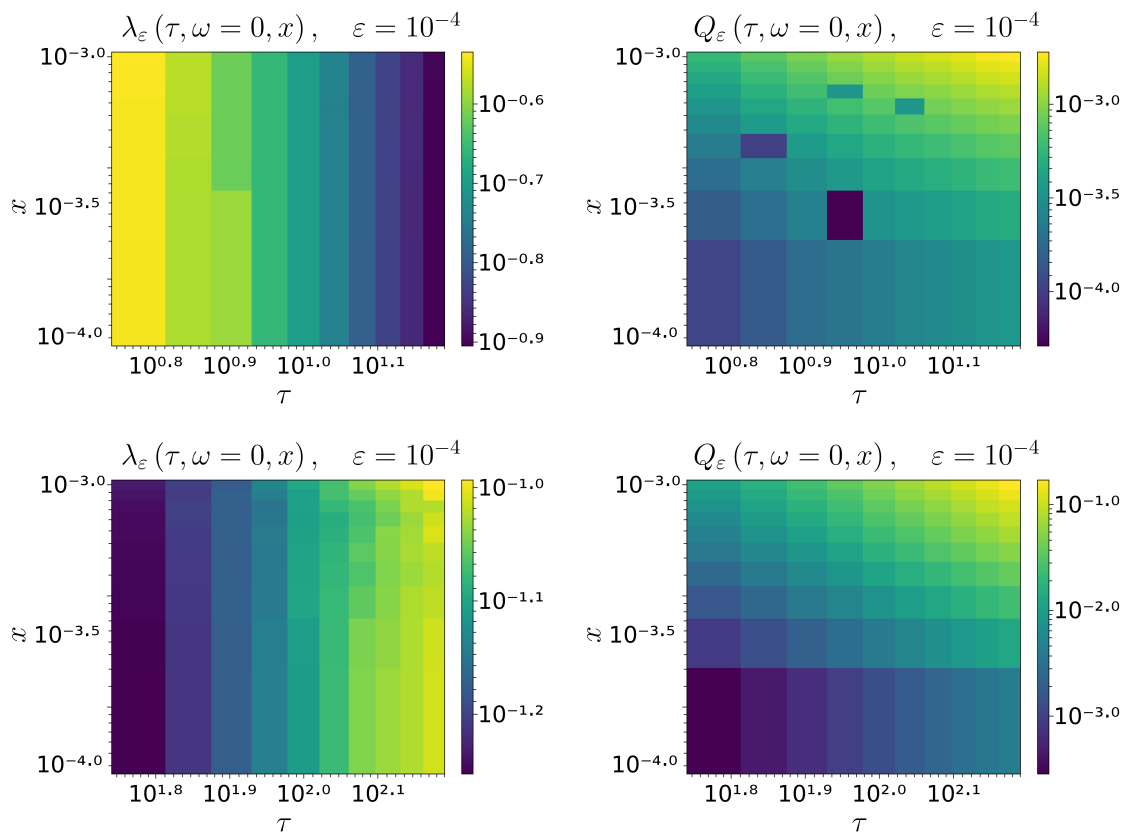
Figure 4.17. The dependence of λ (left) and Q_ε (right) on (τ, x) in $d = 3$ spatial dimensions at fixed $\omega = 0$, $\varepsilon = 10^{-4}$, $\kappa = 3.9$, and $\gamma = 0.5$ plotted in a log-log scale. Top row: $\tau \in [6, 15]$; bottom row: $\tau \in [60, 150]$. In each case, $x \in [10^{-4}, 10^{-3}]$.
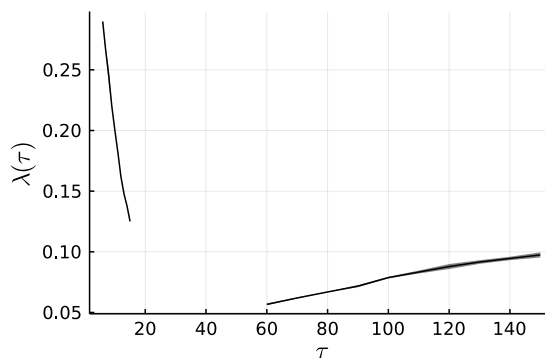

Figure 4.18. The dimensionless coupling λ as a function of τ in $d = 3$ spatial dimensions at fixed $\omega = 0$, $\varepsilon = 10^{-4}$, $\kappa = 3.9$, $\gamma = 0.5$ plotted in a linear scale. The coupling was averaged over different values of x, cf. Fig. 4.17, resulting in a statistical error depicted by the confidence ribbon.

Chapter 5

Far-from-equilibrium states in ultrarelativistic hadron-hadron collisions

Another relevant example of a quantum many-body system far from equilibrium can be found on the opposite side of the energy spectrum: in ultrarelativistic heavy-ion collisions. A complete understanding of thermalization process of such systems is still lacking and thus remains an open problem. A significant progress has been made in two opposing limits. The first one is the strong-coupling limit, which can be studied by means of dual descriptions in supersymmetric Yang–Mills theories [156–160]. In this work, we instead focus on the opposite (weak-coupling) limit, in particular on the aspects of universal scaling dynamics observed for small couplings [82].

To set the scene, we first provide a basic introduction to hadron structure in the context of high energy physics. We will then argue that at sufficiently high energies colliding nuclei can be described by a (semi)classical effective field theory, known as the *color glass condensate (CGC)*. Finally, we will discuss how a collision of two CGC Lorentz-contracted sheets eventually leads to a formation of a far-from-equilibrium boost-invariant non-Abelian plasma, whose dynamics can be described by means of perturbative kinetic theory, which will be the subject of Ch. 6.

5.1   Parton model and the perturbative picture of hadron structure

Our goal is to understand what kind of a nonequilibrium state is formed upon colliding two hadrons at extremely high energies. Obviously, to that end, one first has to understand the structure of a single ultrarelativistic hadron. In high energy physics, the way one probes the internal structure of a hadron is by scattering some other particle off it. Consider, for
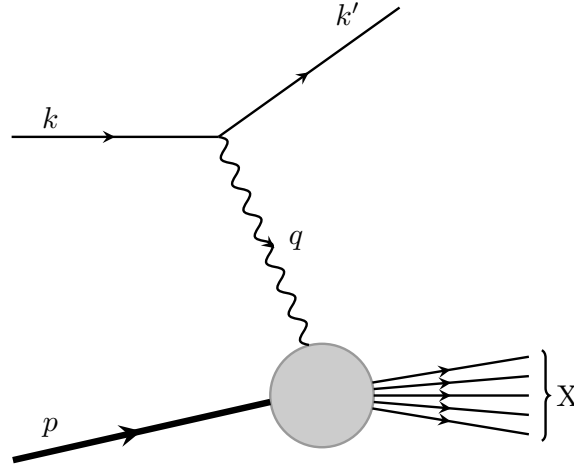
Figure 5.1. Kinematics of deep inelastic scattering.

instance, a scattering $lh \to lX$ of some lepton (say, an electron) with momentum k on a hadron (for example, a proton) with momentum p, as depicted in Fig. 5.1. After interacting by exchanging a virtual photon (or a Z boson) of transfer momentum q, the outgoing lepton will have an altered momentum k', while the target hadron may, in general, 'shatter' into many new particles. The kinematics of this process, known as the *deep inelastic scattering (DIS)*, can be described using the standard Lorentz invariants:

$$Q^2 = -q^2 > 0, \quad \nu = p \cdot q = M(E' - E),$$
$$x = \frac{Q^2}{2\nu} = \frac{Q^2}{2M(E - E')}, \quad 0 \le x \le 1, \tag{5.1}$$
$$y = \frac{p \cdot q}{p \cdot k} = 1 - E'/E, \quad 0 \le y \le 1.$$

Here, M is the hadron mass and the energy variables E and E' refer to the target rest frame. For an elastic scattering process, $(p + q)^2 = M^2$ and $E' = E$ such that $x = 1$ and $y = 0$.

The structure of a target (hadron) as 'seen' by the virtual photon is parameterized by *structure functions* $F_i(x, Q^2)$, which are defined via the lepton scattering cross sections as [161]

$$\frac{\mathrm{d}^2\sigma}{\mathrm{d}x\mathrm{d}y} = \frac{8\pi\alpha^2 ME}{Q^4} \left\{ \left[\frac{1 + (1 - y)^2}{2} \right] 2xF_1(x, Q^2) \right.$$
$$\left. + (1 - y) \left[F_2(x, Q^2) - 2xF_1(x, Q^2) \right] - \frac{M}{2E} xyF_2(x, Q^2) \right\}, \tag{5.2}$$

for a charged lepton scattering in the limit where the weak sector can be ignored, $Q^2 < M_Z^2$. In the *Bjorken limit*, the structure functions show an approximate scaling law [162]

$$F_i(x, Q^2) \to F_i(x), \quad Q^2, \nu \to \infty, x \text{ fixed.} \tag{5.3}$$

This implies that the virtual exchange boson scatters off pointlike constituents, referred collectively as *partons*. In the modern language of QCD, we can identify them with *quarks*.

The parton model of deep inelastic scattering is most easily formulated in the *infinite-momentum frame* (also known as the *Breit frame*), in which the hadron is moving very fast, $p^\mu \approx (P, 0, 0, P)$ with $P \gg M$. Suppose that, in this frame, the photon scatters off a quark constituent that moves parallel with the hadron and carries a fraction ξ of its momentum, i.e., $p_q^\mu = \xi p^\mu$. From the momentum conservation, $p'_q = p_q + q$ and thus

$$0 \approx m_q^2 = (p_q + q)^2 = \xi^2 p^2 + 2\xi p \cdot q + q^2 \approx 2\xi p \cdot q - Q^2, \qquad (5.4)$$

which implies $\xi \approx x$. Therefore, the variable x has a nice and simple interpretation in the Breit frame: it is a fraction of the hadron's total momentum carried by the parton in a scattering characterized by the Bjorken variable of value x. From QED, the leading-order spin-averaged differential cross section for $lq \to lq$ is given by

$$\frac{\mathrm{d}\hat{\sigma}}{\mathrm{d}Q^2} = \frac{2\pi\alpha^2 e_q^2}{Q^4} \left[1 + (1-y)^2 \right] \to \frac{\mathrm{d}^2\hat{\sigma}}{\mathrm{d}x\mathrm{d}Q^2} = \frac{4\pi\alpha^2}{Q^4} \left[1 + (1-y)^2 \right] \frac{1}{2} e_q^2 \delta(x - \xi). \quad (5.5)$$

At the same time, neglecting M in (5.2) and using $Q^2 = 2MxyE$ we have

$$\frac{\mathrm{d}^2\sigma}{\mathrm{d}x\mathrm{d}Q^2} \approx \frac{4\pi\alpha^2}{Q^4} \left\{ \left[\frac{1 + (1-y)^2}{2} \right] F_1(x, Q^2) + \frac{1-y}{x} \left[F_2(x, Q^2) - 2xF_1(x, Q^2) \right] \right\}. \tag{5.6}$$

By comparing (5.5) with (5.6) we conclude that the structure functions for scattering off a parton with momentum fraction ξ are given by

$$\hat{F}_2(x, Q^2) = xe_q^2 \delta(x - \xi) = 2x\hat{F}_1(x, Q^2). \qquad (5.7)$$

The actual structure functions, however, are not delta functions, but rather smooth distributions. This gives rise to a simple *parton model*:

- $q(\xi, Q^2) \, \mathrm{d}\xi$ represents the probability that a quark q carries momentum fraction $[\xi, \xi + \mathrm{d}\xi]$ of a total hadron;

- the virtual exchange boson scatters incoherently off the constituents.

The hadron structure functions are thus obtained by weighting the quark structure functions with the *parton distribution functions* (PDFs) q:

$$F_2(x, Q^2) = 2xF_1(x, Q^2) = \sum_q \int_0^1 \mathrm{d}\xi \, q(\xi, Q^2) xe_q^2 \delta(x - \xi) = \sum_q xe_q^2 q(x, Q^2), \quad (5.8)$$

where the summation goes over possible flavors of (anti-)quarks. It can be shown that the constraint $2xF_1 = F_2$, known as the *Callan–Cross relation* [163], actually reflects the spin-$1/2$ nature of quarks.
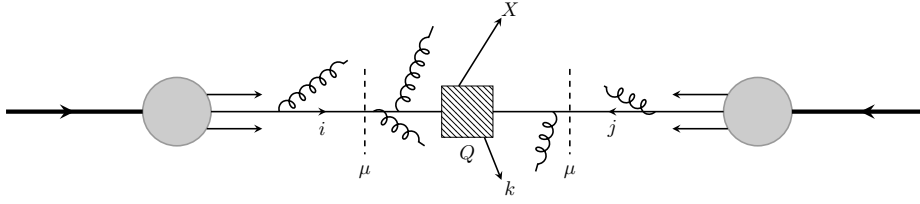
Figure 5.2. Schematic depiction of factorization in hadron-hadron collisions.

Assuming there are no other constituents the integral $\sum_q \int_0^1 dx\, xq(x)$ should be equal to 1. In actuality, however, it is observed $\sum_q \int_0^1 dx\, xq(x) < 1$. The remaining momentum then must be carried by some other, electroweak-neutral, constituents. From the modern perspective of QCD, we immediately recognize in these constituents *gluons*, vector bosons mediating the strong interaction, with their respective PDF usually denoted by $g(x, Q^2)$.

Though the above probabilistic picture of hadron internal structure has been formulated from the perspective of DIS, it can be applied to the case of hadron-hadron collisions thanks to the property of *factorization of hard processes in QCD* [164]. To sketch how it works, consider a hadronic process $h_1 h_2 \to kX$ schematically depicted in Fig. 5.2. Here, h_i are the initial hadrons, whereas k is some triggering particle or pair of particles specifying the relevant momentum-transfer scale Q, which is in general somewhat smaller than the center-of-mass energy $\sqrt{s}$. For instance, it could be a W or a Z boson, some other hadron, a jet of transverse momentum p_T, etc. Finally, by X we understand a totally inclusive collection of final states. Loosely speaking, factorization then states that one can write a total cross section as

$$\sigma = \sum_{i,j} \int dx_1\, f_i(x_1, \mu^2) \int dx_2\, f_j(x_2, \mu^2)\, \hat{\sigma}_{ij}\left(x_1 x_2 s, \alpha_s(Q^2), Q^2/\mu^2\right), \qquad (5.9)$$

where μ is a *factorization scale* and $\hat{\sigma}_{ij}$ is the partonic cross-section that can be computed in perturbation theory, provided Q^2 is large enough. Crucially, the PDFs entering (5.9) are the same PDFs that we have just discussed in the context of deep inelastic scatterings. In other words, parton densities are *universal* between different reactions. On a practical side, this allows one to extract PDFs from, for example, DIS experiments, such as the ZEUS experiment at HERA, and then use them as inputs in other setups. On a more conceptual level, it tells us that we may adopt the same probabilistic picture of hadrons' internal structure when studying physics of, e.g., ultrarelativistic heavy-ion collisions.

The typical x-values relevant for latter processes are $x_{1,2} \propto Q/\sqrt{s}$ for central rapidities [165]. Importantly, note that for colliders with high center-of-mass energies $\sqrt{s}$, such as RHIC or LHC, contributing partons correspond to small values of Bjorken x. For that reason, one may often find in the literature identification of high-energy physics with the so-called 'small-x physics'. Therefore, in order to understand the initial state in, e.g., rel-
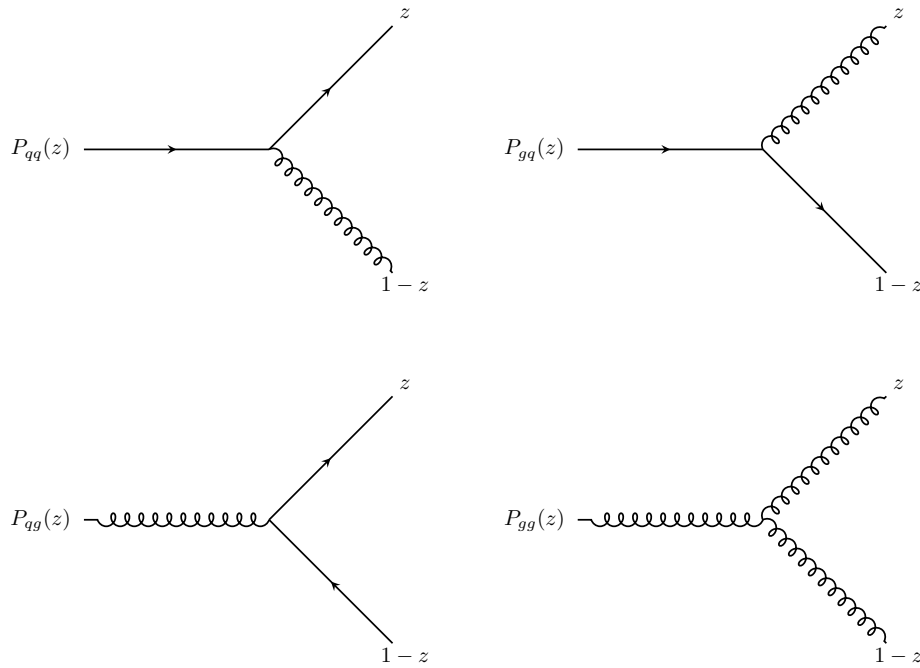
Figure 5.3. Pictorial representation of the splitting functions P_{ij} entering the DGLAP equations.

ativistic heavy-ion collisions, one has to understand how parton distributions functions behave as $x \to 0$. This regime, in which Q is finite (and fixed), while $x \to 0$, is often referred to as the *Regge–Gribov limit*.

Within the perturbative paradigm, the dependence of parton distribution functions f_i on their arguments x and Q^2 is governed by two sets of integro-differential equations. The dependence on Q^2 (at fixed x) is given by the celebrated *Dokshitzer–Gribov–Lipatov–Altarelli–Parisi (DGLAP) equations* [166–168]:

$$\frac{\partial f_i(x, \mu^2)}{\partial \ln Q^2} = \frac{\alpha_s(Q^2)}{2\pi} \sum_j \int_x^1 \frac{\mathrm{d}\xi}{\xi} P_{ij}\left(x/\xi; \alpha_s(Q^2)\right) f_j(\xi, Q^2), \qquad (5.10)$$

where the *splitting functions* P_{ij} admit expansion in the coupling constant, $P_{ij}(z; \alpha_s) = P_{ij}^{(0)}(z) + (\alpha_s/2\pi) P^{(1)}(z) + O(\alpha_s^2)$. Physically, (to leading order) $P_{ij}(z)$ can be understood as a probability density of a parton j branching into a parton i with momentum fraction z and another parton with momentum fraction $1 - z$, see Fig. 5.3. The exact form of these kernels is not important for the following discussion, so let us only mention that P_{qg} and P_{gg} experience a singularity as $z \to 0$ reflecting the fact that the low-x region is dominated by gluons.

However, the DGLAP equations themselves do not allow us to study this regime. Firstly, because they rather describe the evolution in Q^2 direction. And secondly, because some of the assumptions entering their derivation break down as $x \to 0$. To see that, we recall that, effectively, the DGLAP equations sum over leading powers of $[\alpha_s \ln Q^2]^n$ emerging

from a multiparton emission in a region of phase space where the partons have strongly-ordered transverse momenta, $Q^2 \gg k_{nT}^2 \gg \ldots k_{1T}^2$ [161]. Such a resummation scheme is appropriate when $\ln Q^2 \ll \ln(1/x)$. As mentioned above, however, for collisions with high center-of-mass energies, typical x-values are so small that the opposite limit $\ln Q^2 \ll \ln(1/x)$ is usually more relevant. In this regime, one instead has to resum terms proportional to $\alpha_s \ln(1/x)$. Such a resummation to all orders is accomplished by the *Balitsky–Fadin–Kuraev–Lipatov (BFKL) equation* [169, 170],

$$\frac{\partial \varphi(x, \mathbf{q}^2)}{\partial \ln(1/x)} = \frac{\alpha_s(\mathbf{q}^2) N_c}{\pi^2} \int \mathrm{d}^2 \mathbf{k} \, K(\mathbf{q}, \mathbf{k}) \varphi(x, \mathbf{k}^2), \qquad (5.11)$$

which is usually written in terms of the unintegrated gluon distribution defined as

$$x g(x, Q^2) = \int^{Q^2} \mathrm{d}^2 \mathbf{k} \, \varphi(x, \mathbf{k}^2). \qquad (5.12)$$

Similarly to the DGLAP case, the kernel $K(\mathbf{q}, \mathbf{k})$ can be computed order by order using perturbation theory, given Q^2 is still sufficiently large. To leading order,[1] it is given by [172]

$$K(\mathbf{q}, \mathbf{k}) = \frac{1}{(\mathbf{q} - \mathbf{k})^2} - \frac{1}{2} \int \mathrm{d}^2 \mathbf{p} \, \frac{\mathbf{k}^2}{\mathbf{p}^2 (\mathbf{k} - \mathbf{p})^2} \delta(\mathbf{k} - \mathbf{q}) . \qquad (5.13)$$

Neglecting scale-dependence of the running coupling, $\alpha_s(\mathbf{q}^2) \to \alpha_0$, the leading-order BFKL equation can be solved analytically yielding

$$\varphi(x, Q^2) \sim x^{-\lambda}, \quad \lambda = \frac{4\alpha_0 N_c}{\pi} \ln 2, \qquad (5.14)$$

which suggests that the gluon distribution experiences a power-law growth at small x and can grow arbitrarily as $x \to 0$.

5.2 Saturation and color glass condensate

In the previous section, we have outlined the perturbative picture of hadron internal structure. In particular, we have seen how perturbative QCD predicts a rapid increase of the parton distributions at small values of Bjorken x, cf. Fig. 5.4. Such an increase, however, cannot go indefinitely. For example, on the basis of very general principles such as unitarity, analyticity and crossing, it has been shown that the total cross-section for the strong interactions cannot grow faster than $\ln^2 s$ [173], whereas the BFKL solution implies a power-law growth. It has been therefore realized since long time ago that at some point this rapid growth has to be tamed [174]. Physically, the rapid growth at $x \to 0$ is due to the radiation of small-x partons (mostly gluons and, to a lesser extent, $q\bar{q}$-pairs emitted from gluons). In

---

[1] A nice pedagogical discussion of the next-to-leading results can be found in [171].
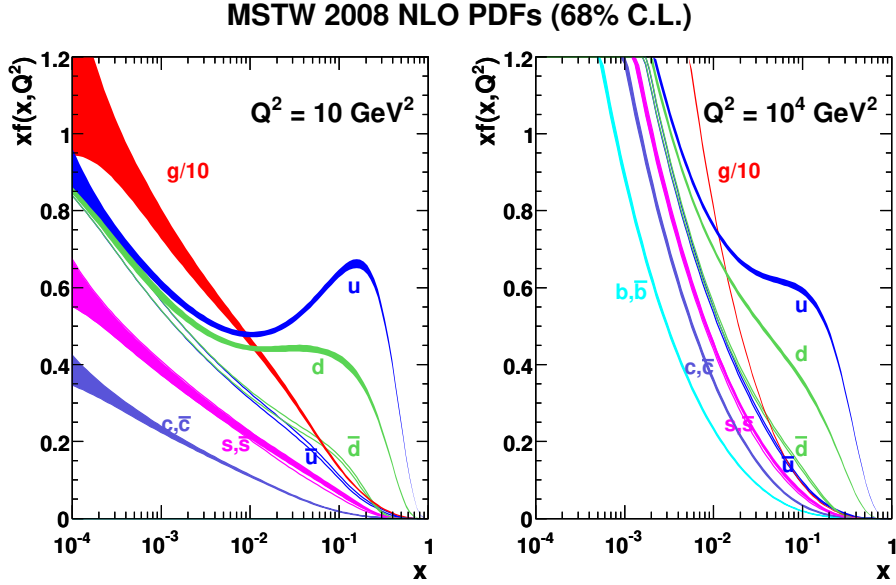
Figure 5.4. Parton distribution functions of a proton at $Q^2 = 10\,\text{GeV}^2$ (left) and $Q^2 = 10^4\,\text{GeV}^2$ (right) computed to next-to-leading order in the strong coupling α_s. Figure taken from [183].

the BFKL formalism, the latter are assumed to be non-interacting, which is reflected by the fact that the equation is linear. When the density of partons becomes too large, however, this assumption no longer holds and one has to take into account *gluon recombination* effects. At some point, this effect will balance the emission marking the *saturation* of gluons. On an algebraic level, the interaction effects can be incorporated by adding appropriate nonlinear terms to the BFKL equation emerging from resumming a certain class of diagrams. Among such modified equations the most well-known are the *Gribov–Levin–Ryskin–Mueller–Qiu* (GLR-MQ) [174, 175], the *Balitsky–Kovchegov* (BK) [176–178], and the *Jalilian-Marian– Iancu–McLerran–Weigert–Leonidov–Kovner* (JIMWLK) [172, 179–182] *equations*. Behind these complicated nonlinear integro-differential equations, however, lies an appealing (semi)classical effective field theory that we will discuss shortly.

We begin with a simple geometric argument that will give an estimate of where in the (x, Q^2)-space one might expect the saturation. The number of gluons (per unit of longitudinal phase space) with transverse momenta $\leq Q^2$ is given by $xg(x, Q^2)$. Upon dividing it by πR^2, where R is the hadron radius, we obtain the respective density in the transverse plane. Multiplying it by the typical gluon-gluon cross section $\sigma_{gg}(Q^2) \sim \alpha_s(Q^2)/Q^2$ we get the probability for gluons to interact with other gluons (geometrically, one can think of "overlapping"). This probability becomes of order one for Q^2 lower than the critical value

$$Q_s^2(x) \sim \alpha_s(Q_s^2)\frac{xg(x, Q_s^2)}{R^2}, \tag{5.15}$$

known as the *saturation scale*. For nuclei with the atomic number A, we have $g(x, Q^2) \propto A$ and $R \propto A^{1/3}$ such that $Q_s^2 \sim A^{1/3}$. To estimate the x-dependence, we can make use of the leading-order BFKL solution (5.14) to obtain

$$Q_s^2(x, A) \sim A^\delta x^{-\lambda}, \quad \delta \approx 1/3. \tag{5.16}$$

Hence, for sufficiently large nuclei and/or high enough energies this dynamically generated scale is hard, $Q_s^2 \gg \Lambda_{\text{QCD}}^2$. For LHC, for instance, estimates give $Q_s \sim 2 - 3\,\text{GeV}$ for nuclei [184, 185]. The saturation physics therefore operates well in the weak-coupling region, $\alpha_s(Q_s^2) \ll 1$. Nevertheless, this regime cannot be described by naive perturbation theory. Indeed, at saturation, $g(x, Q_s^2) \sim 1/\alpha_s$, so propagators in the loops are amplified by $1/\alpha_s$ hindering the expansion in α_s. These large occupation numbers (corresponding to strong classical fields $A \sim 1/g$), however, suggest the use of (semi)classical methods.

As for any other effective theory, the next ingredient for a classical effective field theory is the idea of separation of scales. To see this separation more clearly, let us again consider a hadron in the Breit frame moving in the z direction. Due to the kinematics of the problem it is suggestive to work using *light-cone coordinates*, $x^\pm = (x^0 \pm x^3)/\sqrt{2}$. As has been established, the majority of partons have a very small fraction x of the total momentum. There are, however, still a few constituents (mostly valence quarks) with a large fraction of momentum $x = O(1)$. Because of the time dilation, their dynamics is considerably slowed down and they therefore appear static to the observer. The only relevant information about these 'fast' partons is the color current they carry. This current is longitudinal[2] and, since the constituents are static, it does not depend on x^+, which plays the role of time:

$$J_a^\mu(x) = \delta^{\mu+}\rho_a(x^-, \mathbf{x}_T), \tag{5.17}$$

with ρ being the spatial distribution of color charge, and for brevity we absorbed the $\sqrt{2}$ prefactor. By virtue of the uncertainty relation, $\Delta x^\mp \sim 1/p^\pm$, we deduce that, since p^+ is large, the support of the color charge density ρ is concentrated around $x^- = 0$,[3] an in the literature one often considers the limiting case $\rho_a(x^-, \mathbf{x}_T) = \delta(x^-)\rho_a(\mathbf{x}_T)$. At the same time, the dependence on $\mathbf{x}_T$ is more complicated and reflects the distribution of the fast partons on the sheet transverse to the propagation axis. As the peculiar arrangement of the color charges is not known, the function $\rho(x^-, \mathbf{x}_T)$ may be considered as a random variable with a probability distribution $W[\rho]$. For observables that involve averaging over many hadronic configurations (e.g., over many hadrons in a beam), the expectation value is obtained by

---

[2]Indeed, recall that for quarks $J = (\rho, \rho\mathbf{v})$. But in our case $v^3 \approx 1$, whereas $v^{1,2} \approx 0$, so that the only nonzero component is $J^+ \approx \sqrt{2}\rho$.

[3]A similar argument may also be used to more carefully justify the slow dependence on x^+ by using that p^- is small.

taking the average:

$$\langle O \rangle = \int \mathcal{D}\rho \, W[\rho] O[\rho] \,, \tag{5.18}$$

where $O[\rho]$ is the value of this observable computed for a given color density ρ_a.

The constituents with small Bjorken x ('wee' partons, as called by Feynman), on the other hand, have a time evolution that cannot be neglected. Their dynamics has to be described by the first-principle Yang-Mills action. The coupling between the 'fast' and the 'slow' modes can be approximated by a current term $J_\mu A^\mu$, known as *eikonal approximation*. The resulting effective action thus reads

$$S_{\text{eff}} = \int \mathrm{d}^4 x \left(-\frac{1}{4} F_{\mu\nu}^a F^{a\mu\nu} + J_{a\mu} A_a^\mu \right), \tag{5.19}$$

which goes by the name of the color glass condensate (CGC) model [186–188].

Note that in order for the produced small-x field configurations to be parametrically large $A \sim 1/g$, so should be the sources J [94]. With that in mind, let us make some simple power counting. To that end, we first note that schematically the CGC Lagrangian has a form

$$\mathcal{L}_{\text{eff}} \supset A^2 + gA^3 + g^2 A^4 + JA. \tag{5.20}$$

Consider now a simply connected diagram D with n_{E} external legs (emitted wee partons), n_{I} internal lines[4], n_{L} loops, n_{J} sources, and n_3 and n_4 cubic and quartic vertices, respectively. Using

$$n_{\text{E}} + 2n_{\text{I}} = n_{\text{J}} + 3n_3 + 4n_4 \tag{5.21}$$

together with

$$n_{\text{L}} = n_{\text{I}} - n_3 - n_4 - n_{\text{J}} + 1, \tag{5.22}$$

we find

$$D \sim g^{n_3 + 2n_4} J^{n_{\text{J}}} = g^{n_{\text{E}} + 2(n_{\text{L}}-1)} \left(gJ\right)^{n_{\text{J}}}. \tag{5.23}$$

We observe that in the saturation regime, where $J \sim 1/g$, the magnitude of the diagram does not depend on the number of inserted currents. Therefore, computation of an observable at a given order in α_s requires resummation of all the diagrams obtained by inserting extra sources to the relevant diagram.

The leading order (LO) in α_s is, expectedly, achieved when $n_{\text{L}} = 0$, i.e., at a tree-level, which corresponds to solving the classical Yang-Mills equation,

$$\left(D_\mu F^{\mu\nu}\right)_a = J_a^\nu, \tag{5.24}$$

---

[4]Note that the internal lines here correspond to bare Yang-Mills propagators and are thus not amplified by α_s^{-1}.

that has to be accompanied by a retarded boundary condition $\lim_{x^0 \to -\infty} A^\mu = 0$. A convenient choice of gauge for solving this equation turns out to be the covariant gauge $\partial_\mu A^\mu = 0$, in which it boils down to a simple Poisson equation [189]

$$\nabla_T^2 A_{\text{cov}}^+ = -J^+, \quad A_{\text{cov}}^- = A_{\text{cov}}^i = 0. \tag{5.25}$$

On the other hand, we are eventually interested in the gluon distribution function, which is related to the two-point function of gluon fields. However, the latter is not a gauge-invariant object and one can show that the partonic interpretation of the propagator only holds in the *light-cone gauge* $A^+ = 0$ [190–192]. Therefore, to find the distribution, one has to transform the solution of (5.25) to the light-cone gauge. This can be achieved by the transformation

$$A_{\text{LC}}^+(x^-, \mathbf{x}_T) = V^\dagger(x^-, \mathbf{x}_T) A_{\text{cov}}^+(x^-, \mathbf{x}_T) V(x^-, \mathbf{x}_T) - \frac{\mathrm{i}}{g} V^\dagger(x^-, \mathbf{x}_T) \partial_- V(x^-, \mathbf{x}_T) = 0\,,$$

$$A_{\text{LC}}^-(x^-, \mathbf{x}_T) = -\frac{\mathrm{i}}{g} V^\dagger(x^-, \mathbf{x}_T) \partial_+ V(x^-, \mathbf{x}_T) = 0\,, \tag{5.26}$$

$$A_{\text{LC}}^i(x^-, \mathbf{x}_T) = \frac{\mathrm{i}}{g} V^\dagger(x^-, \mathbf{x}_T) \partial_i V(x^-, \mathbf{x}_T)\,,$$

where we have used $\partial^\pm = \partial_\mp \equiv \partial/\partial x^\mp$ and $\partial^i = -\partial_i$. We note that, thanks to the high-energy kinematics, the gauge transformation did not generate an A^--component, so the only non-vanishing part of the field in this gauge is its transverse components A^i, which take a pure gauge form. Solving (5.26) we find

$$V(x^-, \mathbf{x}_T) = \mathcal{P} \exp\left[-\mathrm{i}g \int_{-\infty}^{x^-} \mathrm{d}y^-\, A_{\text{cov}}^+(y^-, \mathbf{x}_T)\right], \tag{5.27}$$

in which one immediately recognizes a *Wilson line*. Since $A^+(y^-, \mathbf{x}_T)$ is very localized around $y^- = 0$, the Wilson line's exponential has a $\Theta(x^-)$-like discontinuity in the vicinity of $x^- = 0$. As the transverse component A^i is essentially a logarithmic derivative of V with respect to x_i, we conclude that

$$A_{\text{LC}}^i(x^-, \mathbf{x}_T) \approx \Theta(x^-) A_{\text{LC}}^i(x^- = +\infty, \mathbf{x}_T) \equiv \Theta(x^-) \alpha^i(\mathbf{x}_T). \tag{5.28}$$

One can further show that the two-point correlation function of the transverse components in the light-cone gauge

$$\varphi^{\text{WW}}(x, \mathbf{q}^2) = \frac{1}{2\pi^2} \int \mathrm{d}^2\mathbf{x}_T\, \mathrm{d}^2\mathbf{y}_T\, e^{\mathrm{i}\mathbf{q}\cdot(\mathbf{x}_T - \mathbf{y}_T)} \left\langle \text{Tr}\left[\alpha^i(\mathbf{x}_T)\alpha^i(\mathbf{y}_T)\right]\right\rangle, \tag{5.29}$$

known as the *Weizsäcker-Williams gluon distribution*, corresponds to the unintegrated distribution (5.12) introduced above [189].[5] Here, the trace goes over color indices and the averaging is understood in the (5.18) sense.

---

[5]As will be explained at the end of this section, the x-dependence of φ^{WW} enters via the weight functional $W[\rho]$.

The only ingredient left to be specified in order to compute (5.29) is the probability density $W[\rho]$. Note first that in general the division of modes into dynamical fields and those that form static sources is arbitrary. The weight functional $W[\rho]$ is therefore expected to depend on a cutoff in rapidity $y_{\text{cut}} \equiv \log(1/x_{\text{cut}})$ that separates the two types of degrees of freedom. In the simplest approximation, one takes into account color charge of the valence quarks only, corresponding to a relatively large value of the cutoff scale y_0. As anything but valence quarks is disregarded, quantum loop corrections are completely neglected in this model. To still have a strong color source and operate with statistically large number of constituents forming it, one then considers hadrons with large atomic number $A \gg 1$. The small-x wee gluons, having a large longitudinal coherence length, probe the whole nucleus coherently in the longitudinal direction. On the other hand, in the transverse direction, a typical probe area $S_T \sim 1/Q^2$ is much smaller than the nucleon size since $Q^2 \gg \Lambda_{\text{QCD}}^2$. A wee gluon therefore interacts with a color contained in a tube of cross size S_T passing through a parametrically large number $n \sim A^{1/3}$ of nucleons in the longitudinal direction. At each point in the transverse plane, the resulting charge comes from summation over color charges of the individual partons, and thus differs from point to point and is random. On average, this charge is zero since the nucleus is color-free as a whole and its charge is distributed evenly in the transverse direction. Furthermore, since the valence quarks come from separate nucleons, they are expected to be uncorrelated with one another in the longitudinal direction. As there are parametrically large number of them, the sum of their uncorrelated charges is expected to be normally distributed due the central limit theorem. We therefore conclude that the weight functional takes a simple Gaussian form:

$$W_{y_0}[\rho] = \mathcal{N} \exp \left\{ -\frac{1}{2} \int \mathrm{d}^2\mathbf{x}_T \int_{-\infty}^{+\infty} \mathrm{d}x^- \frac{\rho_a(x^-, \mathbf{x}_T)\rho_a(x^-, \mathbf{x}_T)}{\mu^2(x^-)} \right\}. \qquad (5.30)$$

Here, $\mu(x^-)$ is some function characterizing color-charge fluctuations. Parametrically, it is naturally closely related to the saturation scale: $Q_s^2 \sim \alpha_s \int_{-\infty}^{+\infty} \mathrm{d}x^- \, \mu^2(x^-)$.

Thanks to its simple Gaussian form, the approximation (5.30), known as the *McLerran–Venugopalan (MV) model* [186–188], enables one to compute the gluon distribution even without fully resorting to numerical methods, which was first done in [193]. In particular, the limiting case of large and small $q_T = |\mathbf{q}_T|$ can be done analytically. For $q_T \gg Q_s$, one recovers the perturbative Bremsstrahlung α_s/q_T^2 spectrum. For $q_T \ll Q_s$, this rapid power-law growth gets tamed and is replaced by a much milder logarithmic growth $\alpha_s^{-1} \log(Q_s/q_T)$, marking the saturation:

$$\varphi^{\text{WW}}(x, q_T^2) \sim \begin{cases} \alpha_s^{-1} \log(Q_s/q_T), & q_T \ll Q_s, \\ \alpha_s q_T^{-2}, & q_T \gg Q_s. \end{cases} \qquad (5.31)$$

In Fig. 5.5, we schematically sketch the MV gluon distribution φ multiplied by the two-
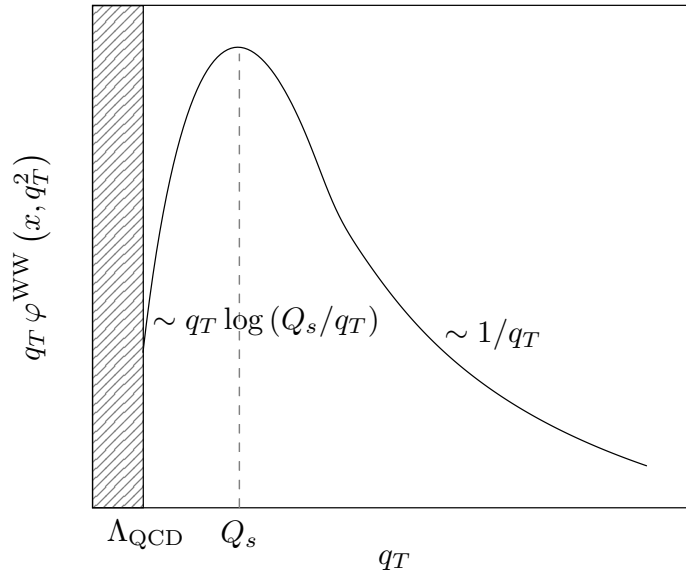
Figure 5.5. Schematic depiction of the phase-space distribution of gluons within the McLerran–Venugopalan model.

dimensional phase-space factor q_T. Note that the majority of gluons have a transverse momentum $\sim Q_s$.

As a final remark, let us briefly discuss the cutoff-dependence mentioned earlier. Going beyond tree-level, it will explicitly enter in loop corrections as an upper limit in the integrals over longitudinal momenta (modes with $y > y_{\text{cut}}$ are included via the source J_a^μ). Suppose we change this cutoff $y_{\text{cut}} \to y_{\text{cut}} + \delta y$ (equivalently, $x_{\text{cut}} \to x_{\text{cut}} - \delta x$). It turns out that at one loop, for a large class of observables, this leads to a linear dependence on δy:

$$\delta O[\rho] = \delta y\, \mathcal{H} O[\rho] + y_{\text{cut}} - \text{independent terms}, \tag{5.32}$$

where $\mathcal{H}$ is a universal (i.e., observable-independent) operator known as the JIMWLK Hamiltonian [172, 179–182], which is self-adjoint:

$$\int \mathcal{D}\rho\, (\mathcal{H}\mathcal{O}_1[\rho])\, \mathcal{O}_2[\rho] = \int \mathcal{D}\rho\, \mathcal{O}_1[\rho]\, (\mathcal{H}\mathcal{O}_2[\rho]). \tag{5.33}$$

Furthermore, since the sources now include modes with rapidities in $[y_{\text{cut}}, y_{\text{cut}} + \delta y]$, the weight functional has to change as well: $W_{y_{\text{cut}}} \to W_{y_{\text{cut}}+\delta y} = W_{y_{\text{cut}}} + \delta W_{y_{\text{cut}}}$. On the other hand, expectation values of observables should not depend on our choice of the cutoff. Therefore,

$$\langle O \rangle = \int \mathcal{D}\rho\, (W_y[\rho] + \delta W_y[\rho])\, (O[\rho] + \delta y\, \mathcal{H} O[\rho])$$
$$= \langle O \rangle + \int \mathcal{D}\rho\, O[\rho]\, (\delta y\, \mathcal{H} W_y[\rho] + \delta W_y) + O\left(\delta y^2\right). \tag{5.34}$$

where we have used (5.33) and dropped the 'cut' subscript for brevity. As have been already mentioned, this result is universal for a large class of test operators, which implies that the

bracket in the last line should vanish. Taking the $\delta y \to 0$ limit we then obtain

$$\partial_y W_y[\rho] = -\mathcal{H} W_y[\rho] \,, \tag{5.35}$$

which is the aforementioned JIMWLK equation. Note that it is of Wilsonian-RG nature as it describes how the effective theory changes upon iteratively integrating out high-energy modes (gradually incorporating produced dynamical fields as sources for modes of smaller Bjorken x), cf. Sec. 3.4.

The explicit form and a derivation of $\mathcal{H}$ can be found in, e.g., [194]. Schematically, it can be written as

$$\mathcal{H} W_y = \frac{1}{2} \frac{\delta}{\delta \rho} \cdot \left(\chi \cdot \frac{\delta}{\delta \rho} W_y \right) , \tag{5.36}$$

where the kernel $\chi[\rho]$ is positive definite and can contain arbitrary powers of ρ. In other words, the JIMWLK evolution is described by a *functional Fokker–Planck equation*. Though it is extremely complicated, one can still make some simple observations. Recall that the MV probability density (5.30) was Gaussian, with its variance directly related to the saturation scale. Being of the Fokker-Planck type, the JIMWLK equation will change this variance as $y = \log(1/x)$ increases. Hence, at next-to-leading order (NLO), the saturation scale Q_s, which at tree-level was constant, generates some x-dependence, cf. (5.16). Looking at (5.31), we see then that in the saturation region the NLO solution experiences only a logarithmic growth in x, as desired.

5.3   Glasma, instabilities, and overoccupied plasma

Let us finally move to collisions of two high-energy hadrons. Within the framework introduced in the previous section, the projectiles can be considered as two CGC sheets propagating along the $x^+ = 0$ and $x^- = 0$ worldlines, respectively, until colliding at $x^+ = x^- = 0$. Formulated in the algebraic language, to leading order in α_s, one now has to solve the classical Yang-Mills equation in the presence of the current

$$J_a^\mu(x) = \delta^{\mu+} \rho_{1,a}(x^-, \mathbf{x}_T) + \delta^{\mu-} \rho_{2,a}(x^+, \mathbf{x}_T) \,. \tag{5.37}$$

Because of the causal structure of the problem, the (t, z)-plane can be separated into four regions as depicted in Fig. 5.6. For each of the currents separately, we already know the solution in the light-cone gauge $A^\pm = 0$ of the respective projectile. As has been mentioned when discussing the transformation (5.26), due to the high-energy kinematics properties of the problem, solutions to the equation associated with one of the nuclei will automatically satisfy the light-cone gauge condition of the other one. Therefore, solutions in the regions (I), (II), and (III), which are causally connected only to one of the nuclei, are already known.
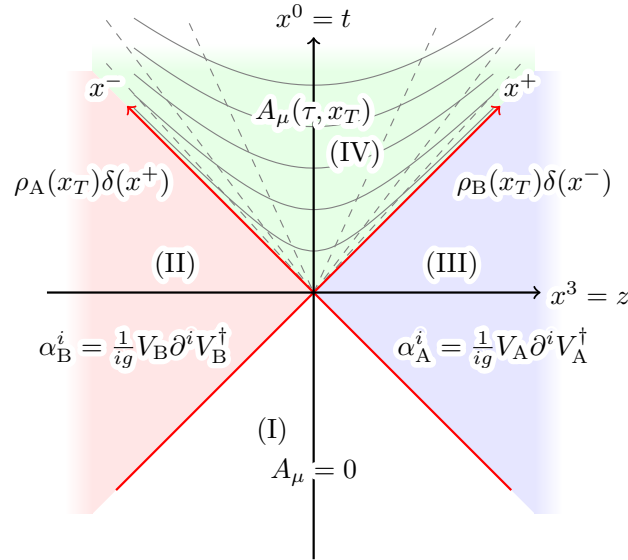
Figure 5.6. Spacetime structure of an ultrarelativistic hadron-hadron collision. The gray hyperbolas in region (IV) are contour lines of constant proper time τ, whereas the straight dashed lines are isolines of spacetime rapidity η, see (5.38) for the definitions. Figure taken from [195].

The region (IV), however, is causally connected to both of the nuclei. Recall that in the case of a single nucleus we were able to set both A^+ and A^- to zero by appealing to two arguments. The first one ($A^+ = 0$) was simply a gauge choice, while the other one was a result of the current being independent of the light-cone time x^+. This does no longer hold in the case of two nuclei, where there is a dependence on both x^+ and x^-. Consequently, inside the forward light cone, we may only set one of the components to zero. A common choice is the *Fock–Schwinger gauge* $A^\tau \equiv (x^- A^+ + x^+ A^-)/\tau = 0$, where we have introduced the *proper time* $\tau \equiv \sqrt{t^2 - z^2} = \sqrt{2x^+ x^-}$. This gauge has a nice property of coinciding with the two light-cone gauges $A^\pm = 0$ on the $x^\pm = 0$ surfaces, respectively. The third (in addition to the transverse ones) nonvanishing component in this gauge is A^η, which will be properly introduced shortly.

At extremely high collision energies, the solution is expected to be (longitudinally) boost-invariant in the *mid-rapidity region*.[6] Because of that, a convenient choice of co-

---

[6]The mid-rapidity (or central rapidity) region is the region of phase-space where $y \approx \eta \approx 0$ in the center-of-mass frame. Usually, it is the region of most interest since particles there are either created during the collision process or are already present in the beams but underwent several rescattering events. Generally, it is also accompanied by two regions corresponding to the initial projectiles' rapidities ($y \approx \pm y_P$, for the symmetric case), called the *fragmentation regions*. In the phase-space distribution plot, they typically lead to having two peaks around $y \approx \pm y_P$. Under longitudinal boosts, these peaks shift and are thus clearly not boost-invariant. However, since they correspond mostly to particles that were not involved in any collisions, one usually ignores them and concentrates on the mid-rapidity part.

ordinates in the forward light cone is given by the aforementioned proper time τ and the spacetime rapidity η:

$$\tau \equiv \sqrt{t^2 - z^2} = \sqrt{2x^+x^-}, \quad \eta \equiv \frac{1}{2}\ln\left(\frac{t+z}{t-z}\right) = \frac{1}{2}\ln\left(x^+/x^-\right). \tag{5.38}$$

Being a four-vector, the gauge field A'^μ after coordinate transformation can be expressed as

$$A'^\mu(x') = \frac{\partial x'^\mu}{\partial x^\nu}A^\nu(x), \tag{5.39}$$

so that

$$\begin{aligned} A^\tau &= \frac{\partial\tau}{\partial x^+}A^+ + \frac{\partial\tau}{\partial x^-}A^- = \frac{1}{\tau}\left(x^-A^+ + x^+A^-\right), \\ A^\eta &= \frac{\partial\eta}{\partial x^+}A^+ + \frac{\partial\eta}{\partial x^-}A^- = \frac{1}{\tau^2}\left(x^-A^+ - x^+A^-\right), \end{aligned} \tag{5.40}$$

while the covariant components A_τ and A_η can be obtained using the metric tensor $g_{\mu\nu} = \mathrm{diag}(1, -1, -1, -\tau^2)$.

To complete formulating the problem of describing the evolution inside the forward light cone, one still has to specify the initial condition. Since we know the solution outside the region (IV), the classical field configurations A^i and A^η immediately after the collision $(\tau = 0^+)$ can be determined by simply matching the solution in the regions (II) and (III) to that in the forward light cone (IV). To achieve this, one employs the Ansatz [196],

$$\begin{aligned} A^i(\tau, \mathbf{x}_T) &= \Theta(-x^+)\,\Theta(x^-)\,\alpha_1^i(\mathbf{x}_T) + \Theta(x^+)\,\Theta(-x^-)\,\alpha_2^i(\mathbf{x}_T) \\ &\quad + \Theta(x^+)\,\Theta(x^-)\,\alpha_3^i(\tau, \mathbf{x}_T), \\ A^\eta(\tau, \mathbf{x}_T) &= \Theta(x^+)\,\Theta(x^-)\beta(\tau, \mathbf{x}_T), \end{aligned} \tag{5.41}$$

which reflects the afore-outlined causal structure of the solution. Here, α_1 and α_2 are the solutions associated each with their respective current $\rho_{1,2}$. Upon inserting (5.41) into the equations of motion a number of terms with δ-functions will rise from differentiating the Heaviside functions. The matching condition is then achieved by requiring the coefficients of such terms to vanish. The result reads

$$\begin{aligned} A^i(\tau = 0^+, \mathbf{x}_T) &= \alpha_3^i(\tau = 0^+, \mathbf{x}) = \alpha_1^i(\mathbf{x}_T) + \alpha_2^i(\mathbf{x}_T), \\ A^\eta(\tau = 0^+, \mathbf{x}_T) &= \beta(\tau = 0^+, \mathbf{x}_T) = \frac{ig}{2}\left[\alpha_1^i(\mathbf{x}_T), \alpha_2^i(\mathbf{x}_T)\right], \end{aligned} \tag{5.42}$$

together with $\partial_\tau\alpha_3^i(\tau = 0^+, \mathbf{x}_T) = \partial_\tau\beta(\tau = 0^+, \mathbf{x}_T) = 0$. Here, $[\cdot, \cdot]$ denotes the usual commutator, which, despite $\alpha_{1,2}$ being classical objects, needs not to vanish due to the matrix nature of the latter. Physically, such a field configuration results in nonzero longitudinal chromo-electric and chromo-magentic fields in the laboratory frame [197]:

$$E^z(\tau = 0^+, \mathbf{x}_T) = -ig\left[\alpha_1^i(\mathbf{x}_T), \alpha_2^i(\mathbf{x}_T)\right], \quad B^z(\tau = 0^+, \mathbf{x}_T) = ig\epsilon_{ij}\left[\alpha_1^i(\mathbf{x}_T), \alpha_2^i(\mathbf{x}_T)\right], \tag{5.43}$$
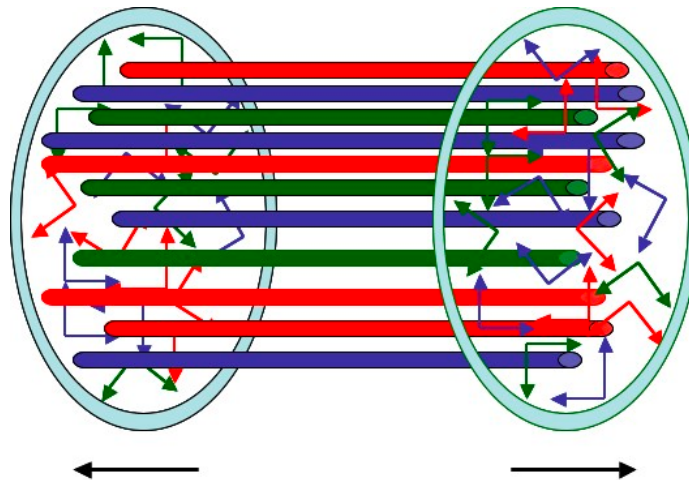
Figure 5.7. Schematic depiction of the longitudinal chromo-electric and chromo-magnetic fields forming the glasma. Figure taken from [198].

where ϵ_{ij} is the Levi–Civita symbol. Following their formation, these boost-invariant fields will be contained within color flux tubes of transverse size $\sim Q_s^{-1}$ (which is the only relevant transverse scale) between the two separating nuclei, see Fig. 5.7 for a schematic depiction.

For $\tau > 0$, the field equations describing the evolution of such *glasma* flux tubes can only be solved numerically (by means of real-time lattice methods). In the remainder of this section, we will briefly outline some key aspects of the early-time dynamics, which will set the scene for the next chapter. For details, see [195, 199, 200] and references therein.

Initially, the fully longitudinal glasma fields (5.43) give rise to a very peculiar form of the energy-momentum tensor, $T^{\mu\nu} = \mathrm{diag}(\epsilon, \epsilon, \epsilon, -\epsilon)$, with $\epsilon = (E_x^2 + E_y^2 + E_z^2 + B_x^2 + B_y^2 + B_z^2)/2$. Importantly, the longitudinal pressure P_L is negative. This leads to a period of rapid relaxation, after which P_L vanishes on a time scale $\tau \sim Q_s^{-1}$, whereupon a description in terms of on-shell gluons becomes applicable and the system settles into free-streaming expansion characterized by $P_L \approx 0$, $P_T \approx \epsilon/2$, and $\epsilon(\tau) \sim \tau^{-1}$. At the leading (fully classical) order, the system remains stuck in such a highly anisotropic state, which is clearly in contrast to the experimentally observed (fast) isotropization.

One thus has to go beyond the LO approximation and introduce quantum fluctuations (generated by the NLO corrections) to the initial state. These (boost non-invariant) fluctuations have been observed to be unstable, experiencing a rapid exponential growth $\sim \exp(\sqrt{Q_s\tau})$ and thus becoming of order of the leading-order classical field on times scales $\tau_0 \sim Q_s^{-1} \ln^2(\alpha_s^{-1})$, after which the growth saturates. Since the initial seed for these fluctuations is statistically distributed, they contribute to the classical field with an arbitrary phase and, by the time τ_0, a comparable amplitude. At this time scale, one thus expects a decay of the classical field due to phase decoherence, $\langle A \rangle \sim 0$, in favor of large fluctuations, $\langle AA \rangle \sim 1/g^2$.

The corresponding picture is that of an overoccupied non-Abelian plasma. In accordance with the above discussion, gluons constituting the plasma come from radiation of the flux tubes. As the latter have a typical transverse size Q_s^{-1}, it is reasonable to expect that most of the radiated gluons will have $p_T \sim Q_s$. Furthermore, due to the initial field's boost-invariance, the distribution at $\tau \sim \tau_0$ is still expected to be extremely anisotropic. The degree of initial anisotropy as well as the magnitude of the initial overoccupancy are sensitive to the value of the coupling constant and uncertainties associated with higher-order corrections. To capture a wide range of different initial conditions, the phase-space distribution characterizing the initial state of the strongly correlated non-Abelian plasma is often modeled as [82, 201, 202]

$$f(\tau_0, p_T, p_z) = \frac{n_0}{2g^2} \Theta \left(Q_s - \sqrt{\mathbf{p}_T^2 + (\xi_0 p_z)^2} \right), \tag{5.44}$$

with $\tau_0 \sim Q_s^{-1} \ln^2(\alpha_s^{-1})$, the initial anisotropy parameter $\xi_0 > 1$, and the initial overoccupancy parameter typically $n_0 < 1$, cf. also (3.17). Here, the distribution is assumed to be averaged over spin and color degrees of freedom. Note that due to the momentum volume factor, most gluons indeed sit at $p_T \sim Q_s$. For practical purposes (e.g., numerical simulations), one often adopts a smoother, Gaussian-like family of initial conditions [14, 203].

This initial condition serves as a starting point for the ensuing dynamics at times $\tau > \tau_0$. Interestingly, the early-time evolution admits a dual description. On the one hand, due to large occupancies, the system's dynamics can be described within the classical statistical approximation [204], which provides a powerful tool for first-principle numerical investigations. For more analytically oriented purposes, however, a more convenient choice is the kinetic-theory framework, which we will be the subject of the next chapter.

Chapter 6

Stability analysis of nonthermal fixed points in longitudinally expanding kinetic theory

We have seen in the previous chapter how collisions of ultrarelativistic hadrons lead to the formation of an approximately boost-invariant overoccupied non-Abelian plasma. As discussed in Ch. 2, such extreme initial conditions are perfect candidates for a universal self-similar dynamics. In the following, we will argue that a scaling dynamics characterized by a nonthermal fixed point is indeed expected in such systems. Using the Hamiltonian formulation of kinetic theory we will then perform a stability analysis and find the relaxation rate to this nonthermal fixed point.

6.1   Boost-invariant kinetic theory

We begin by considering the structure of a kinetic equation in longitudinally boost-invariant systems [205, 206]. In the absence of external forces, the Boltzmann equation reads

$$\left(\frac{\partial}{\partial t} + \mathbf{v} \cdot \frac{\partial}{\partial \mathbf{x}}\right) f = -C[f] \,, \tag{6.1}$$

where $f(t, \mathbf{x}, \mathbf{p})$ is the distribution function in phase space, $\mathbf{v}$ is the velocity associated with a quasiparticle of momentum $\mathbf{p}$, and $C[f]$ is the collision integral. For boost-invariant systems, a convenient choice of coordinates [207] involves spacetime and momentum rapidities

$$\eta = \frac{1}{2} \ln\left(\frac{t+z}{t-z}\right) \quad \text{and} \quad y = \frac{1}{2} \ln\left(\frac{E+p_z}{E-p_z}\right) = \operatorname{artanh}(v_z) \,, \tag{6.2}$$

respectively, as well as the longitudinal proper time $\tau = \sqrt{t^2 - z^2}$, cf. (5.38). The latter is invariant under boosts in z direction, whereas both y and η transform additively. Therefore, a

boost-invariant distribution function can only depend on its longitudinal arguments through τ and $y - \eta$:

$$f(t, \mathbf{x}, \mathbf{p}) \to f(\tau, \mathbf{x}_\perp, y - \eta, \mathbf{p}_T). \tag{6.3}$$

The derivatives entering the Boltzmann equation then take a form

$$\frac{\partial f}{\partial t} = \left(\frac{t}{\tau} \frac{\partial}{\partial \tau} + \frac{z}{\tau^2} \frac{\partial}{\partial \eta} \right) f, \quad \frac{\partial f}{\partial z} = \left(-\frac{z}{\tau} \frac{\partial}{\partial \tau} - \frac{t}{\tau^2} \frac{\partial}{\partial \eta} \right) f, \tag{6.4}$$

from which one readily obtains

$$\left(\frac{\partial}{\partial t} + v_z \frac{\partial}{\partial z} \right) f = \frac{\cosh(y - \eta)}{\cosh y} \left(\frac{\partial}{\partial \tau} - \frac{\tanh(y - \eta)}{\tau} \frac{\partial}{\partial y} \right) f, \tag{6.5}$$

where we have used $\partial_\eta f = -\partial_y f$. Assuming transverse homogeneity and isotropy this is precisely the left-hand side of the Boltzmann equation.

Furthermore, thanks to boost-invariance, it suffices to consider the system's spacetime evolution in the plane $z = \eta = 0$ only.[1] The distribution at any $z \neq 0$ can then be obtained by applying the appropriate Lorentz boost. It is left to simplify the $\tanh(y)\partial_y f$ part. To that end, we note that the derivative here is taken at fixed p_T and that $p_z = \sqrt{m^2 + p_T^2} \sinh y$. Hence, $\tanh(y)\partial_y f = p_z \partial_{p_z} f$ and we end up with

$$\left(\frac{\partial}{\partial \tau} - \frac{p_z}{\tau} \frac{\partial}{\partial p_z} \right) f = -C[f], \tag{6.6}$$

where for the following convenience f is now understood as a function of τ, p_T, and p_z. Note that the second term on the left-hand side is absent in the standard Boltzmann equation and is due to the longitudinal expansion (hence the name 'longitudinally expanding kinetic theory').

6.2   Collision kernel and the Fokker-Planck approximation

To complete a formulation of the kinetic-theory problem, it is left to specify the collision kernel $C[f]$. At leading order in α_s, this generally requires including $2 \leftrightarrow 2$ elastic scatterings and effective $1 \leftrightarrow 2$ collinear[2] radiation processes [65]:

$$C[f] = C^{2 \leftrightarrow 2}[f] + C^{1 \leftrightarrow 2}[f]. \tag{6.7}$$

---

[1]Note that, for $z = 0$, one has $\tau = t$. Nevertheless, we will keep the notation τ for aesthetic reasons.

[2]For strictly massless quasiparticles, $1 \leftrightarrow 2$ process are kinematically forbidden unless particles are exactly collinear. In the case of small (effective) masses, the inelastic part is therefore dominated by nearly collinear splittings/mergings. Depending on the formation time, additional soft collisions may appear during the splitting process disrupting the coherence between nearly collinear excitations (the *Landau–Pomeranchuk–Migdal (LPM) effect*). In such cases, one has to resum $1 + n \to 2 + n$ processes in order to get the correct $1 \leftrightarrow 2$ splitting/merging rate. See [65, 208] for a more detailed discussion.

Before we proceed, it is useful to first consider the stage that occurs before any scattering/splitting events take place. Known as the *free-streaming* regime, it can described by the vanishing collision integrals: $C^{2\leftrightarrow2}[f] = C^{1\leftrightarrow2}[f] = 0$. Now, the initial spectrum is dominated by hard gluons with $p_T \sim Q_s$ and $p_z \sim Q_s/\xi_0 \ll Q_s$. In the absence of any interactions, the longitudinal momenta would be simply redshifted due to the expansion $\sqrt{\langle p_z^2 \rangle} \sim \tau^{-1}$ (making the distribution even narrower), while the typical occupancy and transverse momentum $\langle p_T \rangle$ would remain unchanged. However, once elastic collisions start taking place, they begin to redistribute momenta, leading to broadening of the distribution and dropping of the typical occupancy of hard gluons. The initial stage can therefore be understood as a competition between the two processes, suggesting to investigate the elastic part $C^{2\leftrightarrow2}$ more closely.

The scattering integral that describes $2 \leftrightarrow 2$ elastic collisions can be schematically written as

$$C_{\rm el}[f] = \frac{1}{2} \int_{\mathbf{q,k,l}} \frac{|M(p,q,k,l)|^2}{2\omega_{\mathbf{p}}2\omega_{\mathbf{q}}2\omega_{\mathbf{k}}2\omega_{\mathbf{l}}} (2\pi)^4 \, \delta\left(\omega_{\mathbf{p}} + \omega_{\mathbf{q}} - \omega_{\mathbf{k}} - \omega_{\mathbf{l}}\right) \delta\left(\mathbf{p} + \mathbf{q} - \mathbf{k} - \mathbf{l}\right)$$
$$\times \left[(1 + f_{\mathbf{p}})(1 + f_{\mathbf{q}}) f_{\mathbf{k}} f_{\mathbf{l}} - f_{\mathbf{p}} f_{\mathbf{q}} (1 + f_{\mathbf{k}})(1 + f_{\mathbf{l}})\right]. \tag{6.8}$$

In vacuum, the scattering matrix of a gluon-on-gluon process is given by [161]

$$|M(p,q,k,l)|^2 = 128\pi^2 \alpha_s^2 N_c^2 \left(3 - \frac{tu}{s^2} - \frac{su}{t^2} - \frac{ts}{u^2}\right), \tag{6.9}$$

where s, t, and u are the usual Mandelstam variables. For small momentum transfers, however, the matrix element (6.9) is in fact infrared divergent. One therefore has to take into account medium effects, which regulate the divergence by generating an effective *Debye screening mass*

$$m_D^2(\tau) \sim \alpha_s N_c \int \frac{\mathrm{d}^3\mathbf{p}}{(2\pi)^3} \frac{f\left(\tau, p_T, p_z\right)}{\sqrt{p_T^2 + p_z^2}}, \tag{6.10}$$

Using (5.44) it is easy to see that the initial value of m_D^2 is suppressed by the factor f_0/ξ_0 as compared to the hard scale Q_s. In addition, as a result of the longitudinal expansion, it decreases during the free-streaming regime $m_D^2(\tau) \sim \tau^{-1}$ (as we will argue, this result is not affected by elastic collisions). Consequently, the screening mass is a much softer scale as compared to Q_s and, as will be verified *a posteriori*, even to the typical size of p_z.

In other words, the elastic part of the collision integral is dominated by scatterings that involve small momenta transfers of order m_D. From the perspective of single quasiparticle, this translates to a Brownian motion in momentum space. Therefore, as has been first demonstrated in the classical work by Landau [209], in this limit the Boltzmann equation takes a simplified Fokker–Planck form. For gluons, standard computations, which can be found in, e.g., [210], then give

$$C^{2\leftrightarrow2}[f] \approx -4\pi \alpha_s^2 N_c^2 \mathcal{L} \nabla_{\mathbf{p}} \left[I_a \nabla_{\mathbf{p}} f + I_b \frac{\mathbf{p}}{|\mathbf{p}|} f(1 + f)\right], \tag{6.11}$$

where

$$I_a[f] = \int \frac{\mathrm{d}^3\mathbf{p}}{(2\pi)^3} f(\tau, p_T, p_z) \left[1 + f(\tau, p_T, p_z) \right], \quad I_b[f] = 2 \int \frac{\mathrm{d}^3\mathbf{p}}{(2\pi)^3} \frac{f(\tau, p_T, p_z)}{\sqrt{p_T^2 + p_z^2}}, \quad (6.12)$$

and

$$\mathcal{L} = \log p_{\max}/p_{\min} \qquad (6.13)$$

is the *Coulomb logarithm.* Here, $p_{\max}$ and $p_{\min}$ can be understood as the maximum and minimum allowed momentum transfers, respectively. Note that the UV cutoff was not required in the original scattering integral, but was provided naturally by a limited support of the distributions. A natural choice is thus $p_{\min}^2 \sim m_D^2$ and $p_{\max}^2 \sim \langle p_T^2 \rangle$.

Finally, in the highly anisotropic limit, the leading-order contribution is given by the term with the highest derivative in p_z:

$$C^{2\leftrightarrow 2}[f] \approx -\hat{q}\partial_{p_z}^2 f, \qquad (6.14)$$

where the momentum diffusion parameter $\hat{q}$ reads

$$\hat{q}(\tau) \approx 4\pi\alpha_s^2 N_c^2 \mathcal{L} \int \frac{\mathrm{d}^3\mathbf{p}}{(2\pi)^d} f^2(\tau, p_z, p_T), \qquad (6.15)$$

in the overoccupied limit $f \gg 1$.

The physical picture behind (6.15) is simple: the longitudinal momentum diffuses as $\langle p_z^2 \rangle \sim \hat{q}\tau$, while $\langle p_T \rangle$ remains essentially unaffected since the size of a typical 'kick' m_D is too small as compared to the characteristic transverse scale Q_s. The diffusion coefficient can be estimated as $\hat{q} \sim \alpha_s^2 n_h^2/(Q_s^2\sqrt{\langle p_z^2 \rangle})$, where n_h is the hard-gluon number density. Due to the number-conserving nature of the Fokker–Planck kernel, the latter would be constant in time if there was no expansion. The longitudinal expansion, however, implies that $n_h \sim Q_s^2/(\alpha_s\tau)$. Putting everything together we thus conclude

$$\langle p_T \rangle \sim Q_s \sim \text{const.}, \quad \langle p_z^2 \rangle \sim Q_s^2/(Q_s\tau)^{2/3}. \qquad (6.16)$$

Furthermore, using $Q_s^2/(\alpha_s\tau) \sim n_h \sim f_h Q_s^2 \sqrt{\langle p_z^2 \rangle}$ and $m_D^2 \sim \alpha_s n_h/Q_s$ one readily obtains

$$f_h \sim \alpha_s^{-1}/(Q_s\tau)^{2/3}, \quad m_D^2 \sim Q_s/\tau. \qquad (6.17)$$

Note that $m_D \ll p_z$ since $Q_s\tau \gg 1$, justifying the adopted Fokker-Planck picture.

In the above discussion, we have completely neglected soft collinear splittings, without providing any justification. In reality, one can show that, due to the collinear enhancement, inelastic processes are of the same order as the elastic scatterings. However, their primary impact is a production of soft gluons. On the other hand, initially, both the screening mass, the particle number, and the energy are dominated by hard gluons, so their behavior at this stage, which we have just considered, is not affected by soft partons.

This picture starts breaking down once the typical hard-gluon occupancy becomes of order one, which happens at $Q_s\tau \sim \alpha_s^{-3/2}$. At this point, soft gluons' contribution start overcoming the screening mass m_D and one can no longer ignore their role in thermalization. We close with a remark that the above considerations outline, in fact, only the first phase of a more general '*bottom-up*' thermalization scenario, which was proposed by Baier, Mueller, Schiff, and Son *(BMSS)* as a possible description for the equilibration of an overoccupied non-Abelian plasma in the limit of extremely weak couplings. In this work, however, we will concentrate on the first stage only.

6.3   Scaling and prescaling

In the language of scaling dynamics, the behavior (6.16) and (6.17) during the first stage of bottom-up can be understood as a nonthermal fixed point solution,

$$f\left(\tau, p_T, p_z\right) \stackrel{\text{sclaing}}{=} \tau^\alpha f_S\left(\tau^\beta p_T, \tau^\gamma p_z\right), \tag{6.18}$$

with the scaling exponents $\alpha_{\text{BMSS}} = -2/3$, $\beta_{\text{BMSS}} = 0$, $\gamma_{\text{BMSS}} = 1/3$. In a variant of bottom-up including the effects of plasma instabilities [211], the exponents are slightly different and expected to be $\alpha_{\text{BD}} = -3/4$, $\beta_{\text{BD}} = 0$, $\gamma_{\text{BD}} = 1/4$. While exact values of the scaling exponents are not completely settled[3], the existence of such a universal scaling attractor is well established and has been observed also numerically using classical-statistical lattice simulations [81, 82] as well as effective kinetic theory [14].

On the other hand, not much is known about how the system evolves to such a self-similar regime. In [13] (in the context of ultracold atomic systems) and [14], it was proposed that already before achieving fully developed scaling the system may exhibit a dramatic reduction in complexity such that its dynamics can be described by a few slowly evolving quantities. In particular, numerically solving the leading-order QCD kinetic theory [65] it was observed that much before the scaling with universal exponents is established, the evolution is already governed by the fixed-point scaling function with time-dependent scaling exponents [14]. Such a regime, coined *prescaling*, is characterized by a distribution function evolving according to

$$f\left(\tau, p_T, p_z\right) \stackrel{\text{presclaing}}{=} \tau^{\alpha(\tau)} f_S\left(\tau^{\beta(\tau)} p_T, \tau^{\gamma(\tau)} p_z\right), \tag{6.19}$$

with non-universal time-dependent exponents $\alpha(\tau)$, $\beta(\tau)$, and $\gamma(\tau)$. One can therefore regard prescaling as a partial fixed point at which the scaling function f_S has already reached

---

[3]In particular, it is still unclear which of the scenarios [212] and [211] is realized. Whereas lattice classical-statistical simulations seem to favor the original bottom-up prediction [82], kinetic results were found to be equally close to both of the predictions [14]. In each case, neither scenario can be excluded as both lie within the confidence interval.

its fixed-point form, whereas the scaling exponents α, β, and γ still deviate from their asymptotic values. In the original work, such a description in terms of a small number of slowly evolving degrees of freedom was compared to the conventional hydrodynamics [14], with the key difference that in this case, instead of a local equilibrium with slowly varying temperature, density, etc., one has a scaling solution with slowly varying exponents.

In the remainder of this chapter, we are going to derive approximate equations that describe the dynamics of scaling exponents in longitudinally expanding kinetic theory with a Fokker-Planck collision kernel discussed in the previous section. We will also derive the stability equations for scaling exponents, which can be interpreted as relaxation equations to a nonthermal fixed point and demonstrate for the first time that the nonthermal fixed point is stable under small perturbations.

6.4 Hamiltonian formulation of kinetic theory

In order to derive equations governing the prescaling dynamics, we are going to employ the Hamiltonian formulation of kinetic theory [202, 213, 214], the key points of which we will briefly summarize in this section.

6.4.1 Moment equations

Our goal is to recast the problem into an (infinite) set of ordinary differential equations for quantities that characterize the distribution f. While this choice is not unique, inspired by the original work [14], we pick moments of the occupation number f,

$$n_{n,m}(\tau) \equiv \int \frac{\mathrm{d}^d \mathbf{p}}{(2\pi)^d} p_z^{2n} p_T^m f\left(\tau, p_z, p_T\right), \tag{6.20}$$

for this purpose. Although for a general collision integral the expression

$$\int \frac{\mathrm{d}^d \mathbf{p}}{(2\pi)^d} p_z^{2n} p_T^m \mathcal{C}[f]\left(\tau, p_z, p_T\right) \tag{6.21}$$

does not have a simple form in terms of the moments $n_{n,m}$, in this work, we are going to focus on the kernel (6.15), for which a nonlinearity in f enters only through the parameter $\hat{q}$, which allows to reformulate the problem in the form

$$\partial_{\log \tau} n_{n,m} = -\mathcal{H}_{n,m;n',m'} n_{n',m'}, \tag{6.22}$$

with the 'Hamiltonian' $\mathcal{H}$ given by

$$\mathcal{H}_{n,n;n',m'} = \left[(2n+1)\delta_{n,n'} - q2n(2n-1)\delta_{n-1,n'}\right]\delta_{m,m'}. \tag{6.23}$$

Here, for further convenience we have also introduced $q \equiv \tau \hat{q}$. Note that the Hamiltonian (6.23) has a simple block diagonal structure.

Adopting Dirac notation we rewrite the equation (6.22) in a more convenient manner:

$$\partial_y |\psi(y)\rangle = -\hat{H}(q(y)) |\psi(y)\rangle, \quad y \equiv \log \tau/\tau_0, \tag{6.24}$$

with

$$n_{n,m} \equiv \langle n, m|\psi\rangle, \quad \mathcal{H}_{n,m;n'm'} \equiv \left\langle n, m \left| \hat{H} \right| n', m' \right\rangle, \tag{6.25}$$

where the inner product is given by $l^2 (\mathbb{Z}_{\geq 0} \times \mathbb{Z}_{\geq 0})$ and $\{|n, m\rangle \equiv |n\rangle \otimes |m\rangle\}$ span the respective natural basis,

$$|0,0\rangle = \begin{pmatrix} 1 \\ 0 \\ 0 \\ \vdots \end{pmatrix} \otimes \begin{pmatrix} 1 \\ 0 \\ 0 \\ \vdots \end{pmatrix}, \quad |1,0\rangle = \begin{pmatrix} 0 \\ 1 \\ 0 \\ \vdots \end{pmatrix} \otimes \begin{pmatrix} 1 \\ 0 \\ 0 \\ \vdots \end{pmatrix}, \quad \dots \tag{6.26}$$

Equation (6.24) with the Hamiltonian (6.23) will be the subject of discussion in the remaining text.

6.4.2 Adiabatic approximation

One notes that $\hat{H}$ depends on y only through the parameter $q(y)$. This immediately suggests applying the well-known adiabatic approximation from quantum mechanics. In contrast to quantum mechanics (of closed systems), however, the operator $\hat{H}$ is not necessarily (anti-)Hermitian and hence the method requires some modifications. A particularly convenient generalization to the case of non-Hermitian yet diagonalizable Hamiltonians, which we summarize below, was developed in [215].

The key idea is instead of the original 'wave function' $|\psi(y)\rangle$ to consider the 'equivalent solution'

$$|\chi(y)\rangle \equiv U(q(y))^{-1} |\psi(y)\rangle \tag{6.27}$$

where U is a transformation that diagonalizes $\hat{H}$ at each instance y,

$$U(q)^{-1} \hat{H}(q) U(q) = \text{diag}(\lambda_1(q), \lambda_2(q), \dots) \equiv \hat{H}_{\text{d}}(q). \tag{6.28}$$

For example, in the standard basis $\{|k\rangle\}$ this transformation reads

$$U(q) = \sum_k |v_k(q)\rangle \langle k|, \quad \hat{H}(q) |v_k(q)\rangle = \lambda_k(q) |v_k(q)\rangle. \tag{6.29}$$

Now, one may easily check that $|\chi(y)\rangle$ satisfies the equation that is similar to (6.24),

$$\partial_y |\chi(y)\rangle = -\hat{H}_{\text{e}}(q(y)) |\chi(y)\rangle, \tag{6.30}$$

but with the modified Hamiltonian

$$\hat{H}_{\mathrm{e}}(q) = \hat{H}_{\mathrm{d}}(q) + U(q)^{-1}\partial_y U(q). \tag{6.31}$$

At this point, we split the second term into diagonal and off-diagonal parts and introduce

$$\hat{H}_0(q) = \hat{H}_{\mathrm{d}}(q) + \text{diagonal part of } \left[U(q)^{-1}\partial_y U(q)\right] \tag{6.32}$$

and

$$\hat{V}(q) = \text{off-diagonal part of } \left[U(q)^{-1}\partial_y U(q)\right], \tag{6.33}$$

so that

$$\hat{H}_{\mathrm{e}}(q) = \hat{H}_0(q) + \hat{V}(q). \tag{6.34}$$

One can already guess that the diagonal part $\hat{H}_0(q)$ governs adiabatic element of the evolution, whereas the off-diagonal piece $\hat{V}(q)$ gives rise to non-adiabatic transitions between the quasi-energy levels. Furthermore, since $\hat{V}(q)$ vanishes when there is no time-dependence, we anticipate that one can treat $\hat{V}(q)$ as a perturbation if $q(y)$ depends on y slowly enough. We will therefore look for solutions in the form

$$|\chi(y)\rangle = \sum_{l=0}^{\infty} \left|\chi^{(l)}(y)\right\rangle. \tag{6.35}$$

Here, the functions $\chi^{(l)}$ can be found iteratively order by order as

$$\partial_y \left|\chi^{(0)}(y)\right\rangle = -\hat{H}_0(q(y))\left|\chi^{(0)}(y)\right\rangle, \tag{6.36a}$$

$$\partial_y \left|\chi^{(l)}(y)\right\rangle = -\hat{H}_0(q(y))\left|\chi^{(l)}(y)\right\rangle - \hat{V}(q)\left|\chi^{(l-1)}(y)\right\rangle, \tag{6.36b}$$

where $l \geq 1$. The procedure is initiated with the zeroth order solution, which is given by

$$\left|\chi^{(0)}(y)\right\rangle = \exp\left[-\int_0^y \mathrm{d}z\,\hat{H}_0(q(z))\right]|\chi(0)\rangle, \tag{6.37}$$

with $|\chi(0)\rangle \equiv U(q(0))^{-1}|\psi(0)\rangle$. Since the expression for $\left|\chi^{(0)}\right\rangle$ involves the evolution operator of a diagonal part of the Hamiltonian $\hat{H}_0$, it is convenient to work in the basis of its eigenvectors. We can choose them to be

$$|0\rangle = \begin{pmatrix} 1 \\ 0 \\ 0 \\ \vdots \end{pmatrix}, \quad |1\rangle = \begin{pmatrix} 0 \\ 1 \\ 0 \\ \vdots \end{pmatrix}, \quad \dots \quad . \tag{6.38}$$

The corresponding eigenvalues read $\epsilon_n = \lambda_n + \partial_y \gamma_n$, with γ_n being the non-Hermitian generalization of the *Berry phase*,

$$\gamma_n(y) = \int_0^y \mathrm{d}z\,\langle n| U(q(z))^{-1}\partial_z U(q(z))|n\rangle. \tag{6.39}$$

Expanding the l-th order solution in this basis as

$$\left|\chi^{(l)}(y)\right\rangle = \sum_n C_n^{(l)}(y) \exp\left[-\int_0^y dz\, \epsilon_n(q(z))\right] |n\rangle \tag{6.40}$$

and substituting it into (6.36) we obtain, for $l \geq 1$,

$$\sum_m \partial_y C_m^{(l)}(y) \exp\left[-\int_0^y dz\, \epsilon_m(q(z))\right] |m\rangle$$

$$-\sum_m C_m^{(l)}(y)\,\epsilon_m(y) \exp\left[-\int_0^y dz\, \epsilon_m(q(z))\right] |m\rangle$$

$$= -\sum_m C_m^{(l)}(y)\,\epsilon_m(q(y)) \exp\left[-\int_0^y dz\, \epsilon_m(q(z))\right] |m\rangle$$

$$-\sum_m C_m^{(l-1)}(y) \exp\left[-\int_0^y dz\, \epsilon_m(q(z))\right] \hat{V}(q(y)) |m\rangle\,, \tag{6.41}$$

where we have used $\hat{H}_0 |m\rangle = \epsilon_m |m\rangle$. First, we notice that the last term on the left-hand side cancels the first term on the right-hand side. Multiplying both sides by $\langle n|$ and using the orthogonality condition $\langle n|m\rangle = \delta_{mn}$ we then readily get

$$\partial_y C_n^{(l)}(y) = -\sum_m V_{nm}(y) \exp\left[-\int_0^y ds\, \omega_{nm}(s)\right] C_m^{(l-1)}(y), \tag{6.42}$$

with

$$\omega_{nm}(y) \equiv \epsilon_m(q(y)) - \epsilon_n(q(y)) \tag{6.43}$$

and

$$V_{nm}(y) \equiv \langle n| \hat{V}(q(y)) |m\rangle\,. \tag{6.44}$$

We thus conclude

$$C_n^{(l)}(y) = -\sum_m \int_0^y dz\, V_{nm}(z) \exp\left[-\int_0^z ds\, \omega_{nm}(s)\right] C_m^{(l-1)}(z)\,, \tag{6.45a}$$

$$C_n^{(0)}(y) = C_n^{(0)} = \langle n|\chi(0)\rangle = \left\langle n\left| U\left(q(0)\right)^{-1}\right| \psi(0)\right\rangle\,, \tag{6.45b}$$

which closes the construction. As a closing side remark, one can prove that there is also no ambiguity regarding the choice of the instantaneous eigenfunctions $|v_k(q)\rangle$. In other words, $\left|\psi^{(l)}\right\rangle$ are invariant under reparameterizations

$$|v_k(y)\rangle \to e^{\phi_k(y)} |v_k(y)\rangle \tag{6.46}$$

at each order of perturbation theory.

Now that we have outlined the general framework, let us go back to the specific case of the Fokker-Planck collision kernel (6.23), for which one has to double the number of

indices: $|n\rangle \to |n, m\rangle$, cf. (6.26). Simple computations yield (see App. 6.A)

$$
U_{nm,kl}(q) = \begin{cases} \binom{n}{k} \dfrac{(2n-1)!!}{(2k-1)!!} q^{n-k} \delta_{ml}, & n \geq k, \\[2ex] 0, & \text{otherwise}, \end{cases}
\tag{6.47}
$$

with

$$
U(q)^{-1} = U(-q),
\tag{6.48}
$$

and

$$
\epsilon_{nm}(q) = 2n+1, \quad V_{nm,kl}(q) = \partial_y q\, n\, (2n-1)\, \delta_{n,k+1} \delta_{ml}.
\tag{6.49}
$$

Knowing U^{-1} one may also express zeroth-order coefficients $C_{nm}^{(0)}$ in terms of initial moments of the distribution:

$$
C_{nm}^{(0)} = \langle n, m | U(q(0))^{-1} | \psi(0) \rangle = \sum_{k,l} \langle n, m | U(q(0))^{-1} | k, l \rangle \langle k, l | \psi(0) \rangle
$$
$$
= \sum_{k=0}^{n} \binom{n}{k} \frac{(2n-1)!!}{(2k-1)!!} (-q(\tau_0))^{n-k} n_{k,m}(\tau_0).
\tag{6.50}
$$

6.5   Prescaling regime

We are now ready to study the time-dependent scaling exponents (prescaling) in the adiabatic approximation of the Hamiltonian formalism. To make analytical progress, we will define a small expansion parameter and will investigate the scaling exponents' behavior at leading and next-to-leading orders.

First, consider the l-th order contribution to the (n, m)-th moment of the distribution function:

$$
\langle n, m | \psi^{(l)}(y) \rangle = \sum_{kp} C_{kp}^{(l)}(y)\, e^{-(2k+1)y} \langle n, m | U(q) | k, p \rangle
$$
$$
= \sum_{k=0}^{n} \binom{n}{k} \frac{(2n-1)!!}{(2k-1)!!} C_{km}^{(l)}(y)\, e^{(n-3k-1)y} \hat{q}^{n-k}.
\tag{6.51}
$$

Here, we have used (6.47) to get the second line. For the perturbation (6.49) the iterative relation (6.45) takes a very simple form:

$$
C_{km}^{(l)}(y) = -\sum_{pr} \int_0^y dz\, V_{km,pr}(z) \exp\left[-\int_0^z ds\, \omega_{km,pr}(s) \right] C_{pr}^{(l-1)}(z)
$$
$$
= -k(2k-1) \int_0^y dz\, \partial_z q(z)\, e^{2z} C_{k-1m}^{(l-1)}(z).
\tag{6.52}
$$

Upon repeating the procedure (6.52) l times one readily obtains

$$C_{km}^{(l)}(y) = C_{k-lm}^{(0)}(-1)^l \frac{k!}{(k-l)!} \frac{(2k-1)!!}{(2k-2l-1)!!}$$

$$\times \int_0^y dz_1 \int_0^{z_1} dz_2 \dots \int_0^{z_{l-1}} dz_l\, \mathcal{V}(z_1)\mathcal{V}(z_2)\dots\mathcal{V}(z_l)\,, \qquad (6.53)$$

with $C_{km}^{(l>k)} \equiv 0$ and $\mathcal{V}(z) \equiv \exp(2z)\, \partial_z q(z)$. We now recall that

$$\int_0^y dz_1 \int_0^{z_1} dz_2 \dots \int_0^{z_{l-1}} dz_l\, \mathcal{V}(z_1)\mathcal{V}(z_2)\dots\mathcal{V}(z_l)$$

$$= \int_0^y dz_1 \int_0^{z_1} dz_2 \dots \int_0^{z_{l-1}} dz_l\, \mathcal{T}\{\mathcal{V}(z_1)\mathcal{V}(z_2)\dots\mathcal{V}(z_l)\}$$

$$= \frac{1}{l!}\int_0^y dz_1 \int_0^y dz_2 \dots \int_0^y dz_l\, \mathcal{T}\{\mathcal{V}(z_1)\mathcal{V}(z_2)\dots\mathcal{V}(z_l)\}\,, \qquad (6.54)$$

where $\mathcal{T}$ is a time-ordering operator. Since $\mathcal{V}(z_i)$ are ordinary numbers, the time-ordering operator drops out and we are left with

$$C_{km}^{(l)}(\tau) = (-1)^l C_{k-lm}^{(0)} \binom{k}{l} \frac{(2k-1)!!}{(2k-2l-1)!!} \left[\frac{v(\tau)}{\Delta(\tau)}\right]^l\,, \qquad (6.55)$$

where we went back to $\tau = \tau_0 \exp(y)$ (setting also $\tau_0 = 1$ for brevity). Here, we have also introduced the functions

$$v(\tau) = \frac{1}{\tau^3 \hat{q}(\tau)} \int_1^\tau d\tau'\, (\tau')^2 \frac{\partial q(\tau')}{\partial \tau'} = \frac{1}{\tau^3 \hat{q}(\tau)} \int_1^\tau d\tau'\, (\tau')^2 \hat{q}(\tau') \left[1 + \frac{\partial \log \hat{q}(\tau')}{\partial \log \tau'}\right] \qquad (6.56)$$

and

$$\Delta(\tau) = \frac{1}{\tau^3 \hat{q}(\tau)}, \qquad (6.57)$$

which will later serve as an expansion parameter. Putting everything together we end up with

$$\langle n, m | \psi^{(l)}(\tau) \rangle = (2n-1)!! n! \tau^{n-1} [\hat{q}(\tau)]^n [-v(\tau)]^l$$

$$\times \sum_{k=l}^n \frac{C_{k-lm}^{(0)}}{l!(k-l)!(n-k)!(2k-2l-1)!!} [\Delta(\tau)]^{k-l}\,. \qquad (6.58)$$

6.5.1 Perturbative expansion

To go further, we need to truncate the series (6.58). To do so, let us first estimate the large-time behavior of the quantities entering the expansion (6.58). Near the fixed point, $\hat{q} \sim \tau^{2\alpha_* - 2\beta_* - \gamma_*}$ implying the large-time behavior

$$\Delta(\tau \gg 1) \sim \tau^{-2\alpha_* + 2\beta_* + \gamma_* - 3}. \qquad (6.59)$$

Hence, if $2\alpha_* - 2\beta_* - \gamma_* + 3 > 0$, we expect $\Delta(\tau)$ to decay at large times τ and therefore may use it as a small parameter, at least when the scaling exponents are not too far off their asymptotic values. Note that this condition holds both for the bottom-up [212] and for the modified [211] scaling solutions. On contrary, for v the same analysis results in

$$v(\tau \gg 1) \sim \text{const.} \qquad (6.60)$$

One may even easily estimate the asymptotic value as

$$v(\tau \to \infty) = \frac{1 + 2\alpha_* - 2\beta_* - \gamma*}{3 + 2\alpha_* - 2\beta_* - \gamma_*}. \qquad (6.61)$$

We thus conclude that the k-th term in $\langle n, m | \psi^{(l)}(\tau) \rangle$ at large times scales as

$$\langle n, m | \psi^{(l)}(\tau \gg 1) \rangle_{k\text{-th term}} \sim \tau^{n-1} \hat{q}^n \Delta^{k-l}, \quad n \geq k \geq l, \qquad (6.62)$$

with $\Delta(\tau)$ playing a role of the small parameter. The leading order (LO) contribution to $\langle n, m | \psi^{(l)}(y) \rangle$ is then given by the l-th term in (6.58),

$$\langle n, m | \psi^{(l)}(\tau) \rangle_{\text{LO}} \sim \tau^{n-1} \hat{q}^n, \quad n \geq l, \qquad (6.63)$$

the next-to-leading (NLO) contribution is given by the $(l+1)$-st term,

$$\langle n, m | \psi^{(l)}(\tau) \rangle_{\text{NLO}} \sim \tau^{n-1} \hat{q}^n \Delta, \quad n \geq l+1, \qquad (6.64)$$

and so forth. Importantly, this behavior is independent of l, which alludes to a possible need of resummation of all the terms of the same kind:

$$\langle n, m | \psi(\tau) \rangle = \underbrace{\sum_{l=0}^{n} \langle n, m | \psi^{(l)}(\tau) \rangle_{l\text{-th term}}}_{\text{LO} \iff O(\Delta^0)} + \underbrace{\sum_{l=0}^{n-1} \langle n, m | \psi^{(l)}(\tau) \rangle_{(l+1)\text{-st term}}}_{\text{NLO} \iff O(\Delta^1)} + \dots, \qquad (6.65)$$

see Fig. 6.1 for visualization and more details.

At this point, we are finally in a position to derive equations that govern the prescaling dynamics at next-to-leading order. According to the above discussion, at this level of approximation, the (n, m)-th moment of the distribution takes the form

$$\langle n, m | \psi(\tau) \rangle_{\text{NLO}} = (2n-1)!! \tau^{n-1} \hat{q}(\tau)^n \left\{ C_{0m}^{(0)} \sum_{l=0}^{n} \binom{n}{l} [-v(\tau)]^l \right.$$
$$\left. + C_{1m}^{(0)} n \Delta(\tau) \sum_{l=0}^{n-1} \binom{n-1}{l} [-v(\tau)]^l \right\}. \qquad (6.66)$$

Recognizing the binomial expansion we readily obtain

$$\langle n, m | \psi(\tau) \rangle_{\text{NLO}} = a_{nm} \tau^{n-1} \hat{q}(\tau)^n [1 - v(\tau)]^n \left\{ 1 + b_m \frac{n \Delta(\tau)}{1 - v(\tau)} \right\}, \qquad (6.67)$$

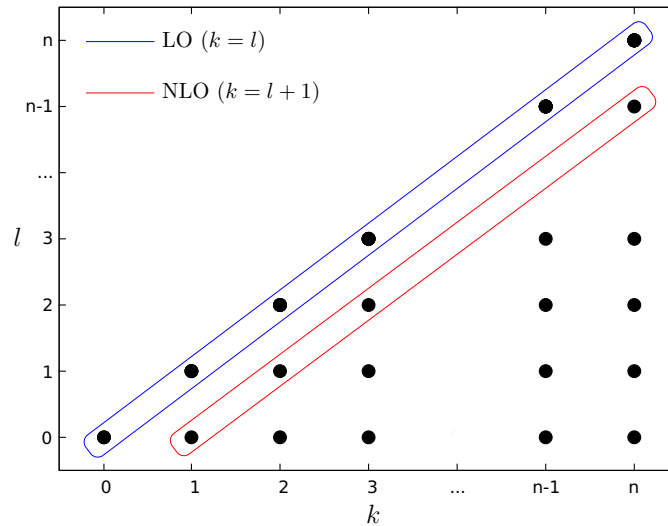with $a_{nm} = C_{0m}^{(0)}(2n-1)!!$ and $b_m = C_{1m}^{(0)}/C_{0m}^{(0)}$.

Figure 6.1. Schematic depiction of the resummation scheme. At any order l of perturbation theory the leading-order (blue) and the next-to-leading-order (red) contributions to $\langle n, m | \psi \rangle$ are given by the l-th and $(l+1)$-st term in the expansion (6.58), respectively. In both cases the resulting behavior does not depend on the order l, cf. (6.63) and (6.64), so that one has to take all the orders of perturbation theory into account. Figure taken from [216].

6.5.2 Fixed-point equations

Up until this point, we have not assumed any particular ansatz for the time evolution of moments $n_{n,m}$ of the distribution function. If the prescaling assumption (6.19) holds, however, we can recast the equations for the moments in terms of time-dependent scaling exponents. Following the original work [14], in order to reflect instantaneous scaling properties we redefine the exponents in (6.19) as

$$\tau^{\alpha(\tau)} \to \exp\left[\int_1^\tau \frac{\mathrm{d}\tau'}{\tau'} \alpha\left(\tau'\right) \right], \tag{6.68}$$

which for constant α reduces to the power law τ^α. The rate of change of a particular moment $n_{n,m}$, as well as of the momentum diffusion parameter $\hat{q}$, is given by a linear combination of scaling exponents:[4]

$$\frac{\partial \log n_{n,m}(\tau)}{\partial \log \tau} = \alpha(\tau) - (m+2)\,\beta(\tau) - (2n+1)\,\gamma(\tau)\,, \tag{6.69a}$$

$$\frac{\partial \log \hat{q}(\tau)}{\partial \log \tau} = 2\alpha(\tau) - 2\beta(\tau) - \gamma(\tau)\,. \tag{6.69b}$$

---

[4]Note that in general the Coulomb logarithm (6.13) also depends on time as $\mathcal{L} \sim \log\left(\langle p_T^2 \rangle / m_D^2\right)$, which would lead to corrections to (6.69b). However, this time-dependence is expected to be only logarithmic during the (pre)scaling regime. For that reason, in the following, we will assume $\mathcal{L}$ to be constant. In a similar recent study [217], the authors took this time-dependence into account and demonstrated that it leads to a small shift in the resulting scaling exponents.

This also implies

$$\frac{\partial v(\tau)}{\partial \log \tau} = [1 + 2\alpha(\tau) - 2\beta(\tau) - \gamma(\tau)] [1 - v(\tau)] - 2v(\tau) \,, \tag{6.70a}$$

$$\frac{\partial \log \Delta(\tau)}{\partial \log \tau} = -3 - 2\alpha(\tau) + 2\beta(\tau) + \gamma(\tau) \,. \tag{6.70b}$$

Taking then the log of both sides of (6.67) and after that the derivative with respect to $\log \tau$ we end up with

$$\alpha - (m+2)\,\beta - (2n+1)\,\gamma = n - 1 + n\,(2\alpha - 2\beta - \gamma) + n\frac{2v}{1-v}$$
$$- n\,(1 + 2\alpha - 2\beta - \gamma) + \frac{\partial}{\partial \log \tau} \log\left(1 + b_m \frac{n\Delta}{1-v}\right). \tag{6.71}$$

Since the NLO approximation is $O(\Delta)$, we have to expand also the log term on the right-hand side to first order in Δ to be consistent. After some simple algebra, one then eventually arrives at

$$\alpha - 2\beta - \gamma + 1 - m\beta - 2n\left[\gamma + \frac{v}{1-v} - \frac{b_m \Delta}{(1-v)^2}\right] = 0 \,. \tag{6.72}$$

First, we observe that in order for this equation to hold for any n and m (as it should during prescaling), one has to impose

$$\alpha(\tau) - 2\beta(\tau) - \gamma(\tau) + 1 = 0 \,. \tag{6.73}$$

One recognizes in (6.73) the scaling relation that follows from conservation of the total particle number [82]. This reflects the particle-number-conserving nature of the elastic collision kernel. It is then suggestive to also demand that the term containing m and the term containing n should individually vanish identically, too. This would result in another constraint

$$\beta(\tau) = 0 \,, \tag{6.74}$$

which together with (6.73) indicates energy conservation [82]. The remaining equation then reads

$$\gamma + \frac{v}{1-v} = \frac{b_m \Delta}{(1-v)^2} \,. \tag{6.75}$$

For this condition to hold b_m has to be m-independent. Since

$$b_m = \frac{C_{1m}^{(0)}}{C_{0m}^{(0)}} = 1 - q(\tau_0)\frac{n_{1m}(\tau_0)}{n_{0m}(\tau_0)} \,, \tag{6.76}$$

see (6.50), the latter holds as long as $n_{1m}(\tau_0)/n_{0m}(\tau_0)$ does not depend on m. An important class of distributions for which this condition is always satisfied is given by separable distributions, i.e., $f(\tau_0, p_T, p_z) = f_1(\tau_0, p_T)\,f_2(\tau_0, p_z)$. Let us note that initial conditions of
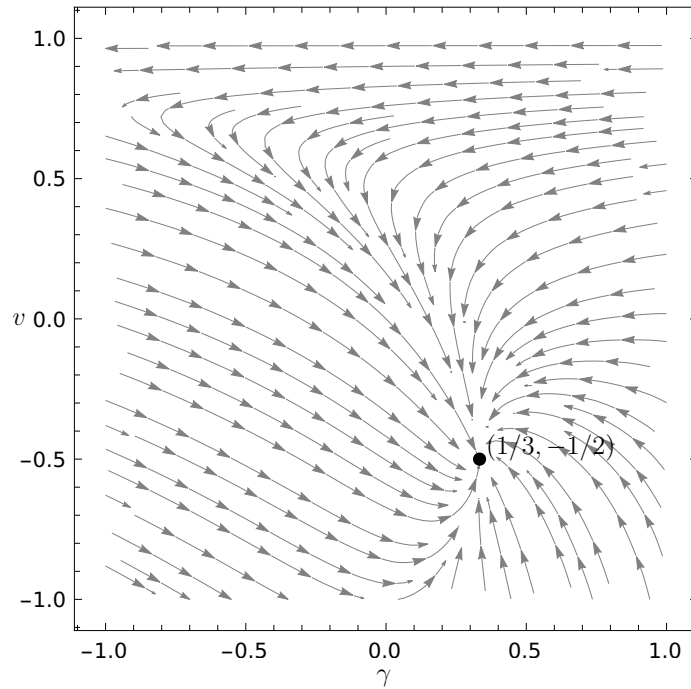
Figure 6.2. The flow diagram of (6.79). A single fixed point $(1/3, -1/2)$ corresponds to the 'bottom-up' scaling [212]. Figure taken from [216].

this kind were employed in the work [14], in which prescaling with time-dependent scaling exponents was originally observed.

We have already derived the equation (6.70a) governing the dynamics of v during prescaling. To obtain a similar equation for the remaining scaling exponent γ, we first take one more logarithmic derivative of both sides of (6.75):

$$\frac{\dot{\gamma} + \dot{v}/(1 - v)^2}{\gamma + v/(1 - v)} = \frac{\partial \log \Delta}{\partial \log \tau} + \frac{2\dot{v}}{1 - v}, \tag{6.77}$$

where $\dot{\mathcal{O}} \equiv \partial_{\log \tau} \mathcal{O}$. Finally, using (6.70a) and (6.70b) and imposing the constraints (6.73) and (6.74) one ends up with the system of differential equations:

$$\dot{\boldsymbol{\kappa}} = \boldsymbol{\mathcal{B}}(\boldsymbol{\kappa}), \tag{6.78}$$

where we have introduced $\boldsymbol{\kappa} = (\gamma, v)$ and

$$\mathcal{B}_\gamma(\boldsymbol{\kappa}) = -\frac{v^2 + 2v - 1 - (1 - v)^2 \gamma^2 + 4(1 - v)\gamma}{(1 - v)^2}, \tag{6.79a}$$

$$\mathcal{B}_v(\boldsymbol{\kappa}) = \gamma - 1 - (\gamma + 1)v. \tag{6.79b}$$

The above equations resemble flow equations describing a running of couplings in the context of renormalization group flow, cf. (3.128). The flow diagram of (6.79) is depicted in Fig. 6.2.

Scaling is achieved when the flow reaches a fixed point

$$\mathcal{B}\left(\boldsymbol{\kappa}_*\right) \stackrel{\text{scaling}}{=} 0. \tag{6.80}$$

Using (6.79) one recognizes the standard bottom-up scaling exponents, $\alpha_* = -2/3, \quad \beta_* = 0, \quad \gamma_* = 1/3, v_* = -1/2$, cf. (6.61), as a stable fixed point of the flow equations (6.78). Indeed, using the standard notation $\delta\boldsymbol{\kappa} \equiv \boldsymbol{\kappa} - \boldsymbol{\kappa}_*$ one has

$$\delta\dot{\boldsymbol{\kappa}} \stackrel{\text{bottom-up}}{=} \begin{pmatrix} -2 & 0 \\ 3/2 & -4/3 \end{pmatrix} \delta\boldsymbol{\kappa} + O\left(\delta\kappa_i^2\right). \tag{6.81}$$

The corresponding characteristic polynomial reads $(\lambda + 2)(\lambda + 4/3)$ resulting in two (simple) eigenvalues $\lambda_1 = -2, \quad \lambda_2 = -4/3$, with the respective eigenvectors $\mathbf{h}_1 = (-4/9, 1)^T$, $\mathbf{h}_2 = (0, 1)^T$.

The general solution near the fixed point is therefore given by

$$\delta\boldsymbol{\kappa} = K_1 \tau^{\lambda_1} \mathbf{h}_1 + K_2 \tau^{\lambda_2} \mathbf{h}_2, \tag{6.82}$$

or explicitly,

$$\delta\gamma(\tau) = -\frac{4}{9}K_1\tau^{-2}, \quad \delta v(\tau) = K_1\tau^{-2} + K_2\tau^{-4/3}, \tag{6.83}$$

which describes evolution in the vicinity of the bottom-up attractor.

6.6   Conclusions

In this work, we studied the self-similar evolution phenomena in Fokker-Planck type kinetic theory. Using the Hamiltonian formalism of kinetic theory and adiabatic approximation we were able to derive the flow equations of the time-dependent scaling exponents. The fixed point of scaling exponents for the Fokker-Planck kinetic theory coincides with the scaling exponents characterizing the early stage of the bottom-up thermalization scenario [212].

Working at next-to-leading order in the small expansion parameter, we found the relaxation rate for scaling exponents to the fixed point and demonstrated its stability. This analysis lays ground for the study of scaling phenomena in more complex systems, such as full QCD kinetic theory.

APPENDIX

6.A   Computation of U, $\hat{H}_0$, and $\hat{V}$

6.A.1   Solving the eigenproblem

To find a transformation U that diagonalizes the matrix (6.23), one shall solve the corresponding eigenproblem.

$$\hat{H}(q)\,|v_{k,l}\rangle = \lambda_{k,l}\,|v_{k,l}\rangle. \tag{6.A.1}$$

Here, the subscript enumerates eigenvalues and eigenvectors. Since $\hat{H}$ has a block diagonal structure, it obviously suffices to study only one block as generalization to the full case is straightforward. In Dirac notation,

$$\sum_{n'}\left\langle n\left|\hat{H}(q)\right|n'\right\rangle \langle n'|v_k\rangle = \lambda_k\,\langle n|v_k\rangle, \tag{6.A.2}$$

with

$$\langle n|\,\hat{H}(q)\,|n'\rangle = (2n+1)\,\delta_{n,n'} - q\,2n\,(2n-1)\,\delta_{n-1,n'}. \tag{6.A.3}$$

Since $\hat{H} - \lambda\hat{I}$ is bidiagonal and determinant of a bidiagonal matrix is equal to product of its diagonal elements, the characteristic equation simply reads

$$\prod_{n\geq 0}(2k+1-\lambda) = 0, \tag{6.A.4}$$

from which we easily deduce

$$\lambda_k = 2k+1. \tag{6.A.5}$$

Plugging this into (6.A.2) yields the recursion relation

$$\langle n-1|v_k\rangle = \frac{n-k}{qn(2n-1)}\,\langle n|v_k\rangle, \quad n \geq 1. \tag{6.A.6}$$

One can verify that $\langle n < k|v_k\rangle = 0$. It is then suggestive to set $\langle k|v_k\rangle = 1$ and compute the remaining components of each eigenvector ascending with

$$\langle n|v_k\rangle = q\,\frac{n(2n-1)}{n-k}\,\langle n-1|v_k\rangle, \quad n > k. \tag{6.A.7}$$

Hence,

$$\langle n|v_k\rangle = \prod_{p>k}^{n}\frac{p}{p-k}(2p-1)\,q = \binom{n}{k}\frac{(2n-1)!!}{(2k-1)!!}\,q^{n-k}, \quad n > k. \tag{6.A.8}$$

Here, we have used

$$\prod_{p>k}^{n}\frac{p}{p-k} = \frac{(k+1)\cdot(k+2)\cdot\ldots\cdot n}{1\cdot 2\cdot\ldots\cdot(n-k)} = \frac{n!}{k!(n-k)!} = \binom{n}{k} \tag{6.A.9}$$

and

$$\prod_{\substack{p=1 \\ p>k}}^{n}(2p-1) = \frac{\prod_{p=1}^{n}(2p-1)}{\prod_{p=1}^{k}(2p-1)} = \frac{(2n-1)!!}{(2k-1)!!}, \tag{6.A.10}$$

with the standard convention $(-1)!! = 1$. We therefore conclude

$$U_{nm}(q) = \begin{cases} \binom{n}{m} \dfrac{(2n-1)!!}{(2m-1)!!} q^{n-m}, & n \geq m, \\ 0, & \text{otherwise.} \end{cases} \tag{6.A.11}$$

6.A.2 Finding $U(q)^{-1}$

For brevity, we are going to temporarily denote the entries of $U(q)$ and $U(q)^{-1}$ by a_{nm} and b_{nm}, respectively. Let us prove that

$$U(q)^{-1} = U(-q) \iff b_{nm} = (-1)^{n-m} a_{nm}. \tag{6.A.12}$$

We are going to do so by induction. First, we note that since $U(q)$ is lower triangular, $U(q)^{-1}$ is also lower triangular. The diagonal elements of a product are then just a product of diagonal elements, which implies $1 = a_{nn}b_{nn} = b_{nn}$. The second row yields, on top of that, one nontrivial condition:

$$0 = a_{10}b_{00} + a_{11}b_{10} = a_{10} + b_{10} \implies b_{10} = -a_{10}. \tag{6.A.13}$$

Now that we have already showed the base case, it is only left to show that if $b_{kn} = (-1)^{n-k}a_{kn}$ for $k < m$, then $b_{mn} = (-1)^{n-m}a_{mn}$. In general, the m-th row results in $m-1$ nontrivial conditions of the form

$$\sum_{k=m-l}^{m} a_{mk}b_{km-l} = 0, \quad l = 1, \ldots, m, \tag{6.A.14}$$

from which it follows

$$b_{mm-l} = -\sum_{k=m-l}^{m-1} a_{mk}b_{km-l} = -\sum_{k=m-l}^{m-1} (-1)^{k-m+l}a_{mk}a_{km-l}, \tag{6.A.15}$$

where we have used that, by assumption, $b_{kn} = (-1)^{n-k}a_{kn}$ for $k < m$. Now we plug in the expression for a_{mn} to get

$$\begin{aligned} b_{mm-l} = -&\sum_{k=m-l}^{m-1} (-1)^{k-m+l} \frac{m!}{k!(m-k)!} \frac{k!}{(m-l)!(k-m+l)!} \\ \times &\frac{(2m-1)!!}{(2k-1)!!} \frac{(2k-1)!!}{(2m-2l-1)!!} q^{m-k}q^{k-m+l} \\ \overset{r=k-m+l}{=} &\, q^l \frac{(2m-1)!!}{(2m-2l-1)!!} \frac{m!}{(m-l)!} \sum_{r=0}^{l-1} \frac{(-1)^{r+1}}{(l-r)!r!}. \end{aligned} \tag{6.A.16}$$

It remains to show that the last sum is equal to $(-1)^l/l!$. Indeed,

$$\sum_{r=0}^{l-1} \frac{(-1)^{r+1}}{(l-r)!r!} = -\frac{1}{l!} \sum_{r=0}^{l-1} (-1)^r \binom{l}{r} = \frac{(-1)^l}{l!}, \tag{6.A.17}$$

where we have used the identity

$$\sum_{r=0}^{k} (-1)^r \binom{n}{r} = (-1)^k \binom{n-1}{k}. \tag{6.A.18}$$

Plugging this into (6.A.16) we finally get

$$b_{mm-l} = \binom{m}{l} \frac{(2m-1)!!}{(2m-2l-1)!!} (-q)^l = (U(-q))_{mm-l}, \tag{6.A.19}$$

which closes the proof.

6.A.3   Computing $\hat{H}_0$ and $\hat{V}$

Finally, let us compute $\hat{H}_0$ and $\hat{V}$. To that end, we first take the derivative of $U(q)$ using (6.A.11):

$$\dot{U}_{nm}(q) = \begin{cases} \binom{n}{m} \dfrac{(2n-1)!!}{(2m-1)!!} (n-m) q^{n-m-1}\dot{q}, & n > m, \\[2ex] 0, & \text{otherwise.} \end{cases} \tag{6.A.20}$$

Since $\dot{U}(q)$ is again lower triangular and in addition its diagonal elements are all zero and $U(q)^{-1}$ is lower triangular, too, the product of two, $U(q)^{-1}\dot{U}(q)$, will be lower triangular with zero diagonal elements as well. Hence, $\left[U(q)^{-1}\dot{U}(q)\right]_{nm} = 0$ for $n \leq m$. To get the remaining entries, we simply multiply the two matrices:

$$\begin{aligned} \left[U(q)^{-1}\dot{U}(q)\right]_{nm} &= \dot{q} \sum_{k=m+1}^{n} \binom{n}{k}\binom{k}{m} \frac{(2n-1)!!}{(2k-1)!!} \frac{(2k-1)!!}{(2m-1)!!} (k-m)(-1)^{n-k} q^{n-m-1} \\ &= \dot{q}(-q)^{n-m-1}(m+1)\frac{(2n-1)!!}{(2m-1)!!} \sum_{k=m+1}^{n} (-1)^{k-m-1} \binom{n}{k}\binom{k}{m+1} \\ &= \dot{q}(-q)^{n-m-1}(m+1)\frac{(2n-1)!!}{(2m-1)!!} \delta_{n,m+1} \\ &= \dot{q}(m+1)\frac{(2m+1)!!}{(2m-1)!!} \delta_{n,m+1} = \dot{q}n(2n-1)\delta_{n,m+1}, \end{aligned} \tag{6.A.21}$$

where we have used the identity

$$\sum_{k=m}^{n} (-1)^{k-m} \binom{k}{m}\binom{n}{k} = \delta_{mn}. \tag{6.A.22}$$

Chapter 7

General conclusion

In this work, we investigated universal far-from-equilibrium scaling dynamics in two different systems, using two different methods, concentrating on two different aspects.

The first part of this thesis was dedicated to universal dynamics happening exactly at a nonthermal fixed point, taking an ultracold atomic system as an example. Based on general concepts of the renormalization group framework, in which scaling solutions can be understood as fixed points of the RG flow, we developed an alternative approach to systematically obtain scaling solutions associated with nonthermal fixed points. To achieve that, we first employed a convenient parameterization for correlation functions near a fixed point as a sum of a full (scaling) part and a deviation δZ from it. Following the analogy to the usual RG approach to critical phenomena, in which information about the universal scaling properties is encoded in the behavior of such deviations, we subsequently derived fixed-point equations for δZ. We then demonstrated that the asymptotics of δZ provide a set of equations for scaling exponents characterizing a given nonthermal fixed point. We have further shown how the fixed-point equations can be greatly simplified in this asymptotic limit of interest. Using physical considerations we were then able to narrow down the number of unknowns in order to close the system of equations, which we thereafter solved numerically. Apart from the momentum-dependence in the regulator-dominated regime, the numerical data shows the expected behavior, indicating that the proposed method can be used to search for and classify possible universal scaling solutions in far-from-equilibrium many-body systems once the momentum-dependence issue, which we discussed in detail in Sec. 4.4.4, is fixed. We expect that the latter can be related to the divergence-removing procedure developed in Sec. 4.4.2. A careful reexamination is therefore required and is work in progress. After the problem is resolved, this approach is expected to pave the way for a complete categorization of possible far-from-equilibrium scaling solutions into different universality classes based on scale-invariance principles.

In the second half, the center of our attention shifted toward high-energy systems and

phenomena preceding the final scaling limit. According to the famous bottom-up thermalization scenario, one expects emergence of the universal self-similar dynamics during early stages of the evolution in a longitudinally expanding overoccupied non-Abelian plasma. Using the Hamiltonian formulation of kinetic theory we were able to shed some light on how the system approaches such an attractor and, importantly, its stability properties under small perturbations. We showed that the bottom-up nonthermal fixed point is stable (within the Fokker–Planck approximation) and computed the associated relaxation rates.

There are many directions in which one can go within each of the problems separately. For example, for the RG part, an accessible scheme for numerically solving the fixed-point equations beyond the first iteration would be very welcome. In addition, one could improve the truncation scheme (e.g., by going past classical vertices), study more involved scaling forms, or perhaps work directly with the 'fundamental' bosonic degrees of freedom instead of the effective ones. Likewise, a straightforward improvement in the prescaling project would be to go beyond the simple Fokker–Planck description of a non-Abelian plasma. Particularly appealing sounds the idea of including inelastic collisions in some approximate form, to see whether an additional fixed point (corresponding to the second stage of bottom-up thermalization) emerges and if the two fixed points could be connected by a (modified) prescaling regime. On a more fundamental level, the question of universality of the relaxation exponents is of great interest.

Perhaps, an even more intriguing prospect is the idea of combining the projects. For instance, an immediate question is whether the scaling dynamics during the first stage of bottom-up thermalization could be obtained using the functional renormalization group approach developed for an ultracold Bose gas. Conversely, one could try applying the Hamiltonian kinetic formalism to study stability properties of nonthermal fixed points in ultracold atomic systems. In [13], a different type of prescaling regime was observed, in which certain 'moments of the distribution' had already behaved as if they were at a nonthermal fixed point, whereas others still deviated from the fixed-point scaling. One may naturally ask if the Hamiltonian approach to kinetic theory can be applied to study partial fixed points of such kind as well. This question is directly related to the possibility of recasting a kinetic equation into a set of moment equations. While the general case looks hopeless, one can still try to consider a class of relatively simple collision integrals and assume a simplified scaling form. For example, in [217], the authors demonstrated that the scaling function of a nonthermal fixed point characterized by the Fokker–Planck collision kernel is Gaussian. While such a particularly simple structure has to be attributed to the diffusive nature of the collision integral, it suggests that, perhaps, a relatively small number of independent moments characterizing the distribution could suffice to observe (approximate) partial fixed points.

Notations and conventions

Units

Throughout the whole thesis, unless fundamental physical constants are written explicitly, we assume natural (Planck) units implying $\hbar = c = k_B = 1$.

Spacetime conventions

In this work, spatial variables are denoted by bold letters $\mathbf{x}$ and their co- and contravariant components by Latin indices, x_i or x^i. Regular letters are reserved to indicate a collection of both the spatial and the corresponding temporal coordinates: $x = (x^0, \mathbf{x})$. We adopt the $(-, \ldots, -, +)$ metric convention such that the product of two $(d+1)$-vectors, $x = (x^0, x^1, \ldots, x^d) \equiv (x^0, \mathbf{x})$ and $y = (y^0, y^1, \ldots, y^d) \equiv (y^0, \mathbf{y})$, is given by $x \cdot y = x^0 y^0 - \mathbf{x} \cdot \mathbf{y}$.

Fourier transform

We define the Fourier transform as

$$\mathcal{F}[f](p) \equiv \tilde{f}(p) = \int \frac{\mathrm{d}^{d+1}}{(2\pi)^{d+1}} \mathrm{e}^{-\mathrm{i}p \cdot x} f(x) \,, \quad \mathcal{F}^{-1}[\tilde{f}](x) \equiv f(x) = \int \mathrm{d}^{d+1}x \, \mathrm{e}^{\mathrm{i}p \cdot x} \tilde{f}(p) \,.$$

(7.1)

Whenever there is no risk of confusion, the tilde on the Fourier transform may be omitted.

Integrals

The following short-hand notation for integrals in real and Fourier spaces is often employed:

$$\int_x = \int \mathrm{d}^{d+1}x \,, \quad \int_q = \int \frac{\mathrm{d}^{d+1}q}{(2\pi)^{d+1}} \,,$$

(7.2)

and likewise for an integration over spatial variables ($\mathbf{x}$ or $\mathbf{p}$) only. The notation for integrals over Schwinger-Keldysh contour is shortened as

$$\int_{\mathcal{C}} \mathrm{d}x^0 \int \mathrm{d}^d\mathbf{x} = \int_{x,\mathcal{C}} \,.$$

(7.3)

For the case of Keldysh-rotated variables, where the integration goes from t_0 to $+\infty$, we adopt

$$\int_{t_0}^{+\infty} \mathrm{d}x^0 \int \mathrm{d}^d\mathbf{x} = \int_{x,t_0} . \tag{7.4}$$

Convolution

We use the symbol $\circ$ to denote the convolution operation of two functions:

$$(A \circ B)(x_1, x_2) = \int_y A(x_1, y) B(y, x_2) . \tag{7.5}$$

Depending on the context, the integration may go either over all the spacetime arguments or over the temporal coordinate only.

DeWitt notation

Throughout this thesis, we occasionally employ the short-hand DeWitt notation, in which spacetime arguments and internal indices are merged into a single multi-index covering both: $\varphi^a(x) = \varphi^{\mathbf{a}}$. The combined integration/summation over spacetime coordinates/internal field indices can then be written as a scalar product:

$$\sum_a \int \mathrm{d}^{d+1}x \, \varphi^a(x) \, \chi_a(x) = \sum_{\mathbf{a}} \varphi^{\mathbf{a}} \chi_{\mathbf{a}} = \varphi \cdot \chi . \tag{7.6}$$

Bibliography

[1] M. Gring, M. Kuhnert, T. Langen, T. Kitagawa, B. Rauer, M. Schreitl, I. Mazets, D. A. Smith, E. Demler, and J. Schmiedmayer, "Relaxation and Prethermalization in an Isolated Quantum System", Science **337**, 1318 (2012).

[2] J. Berges, S. Borsányi, and C. Wetterich, "Prethermalization", Phys. Rev. Lett. **93**, 142002 (2004).

[3] T. Langen, S. Erne, R. Geiger, B. Rauer, T. Schweigler, M. Kuhnert, W. Rohringer, I. E. Mazets, T. Gasenzer, and J. Schmiedmayer, "Experimental observation of a generalized Gibbs ensemble", Science **348**, 207 (2015).

[4] E. T. Jaynes, "Information Theory and Statistical Mechanics", Phys. Rev. **106**, 620 (1957).

[5] E. T. Jaynes, "Information Theory and Statistical Mechanics. II", Phys. Rev. **108**, 171 (1957).

[6] S. Braun, M. Friesdorf, S. S. Hodgman, M. Schreiber, J. P. Ronzheimer, A. Riera, M. del Rey, I. Bloch, J. Eisert, and U. Schneider, "Emergence of coherence and the dynamics of quantum phase transitions", PNAS **112**, 3641 (2015).

[7] E. Nicklas, M. Karl, M. Höfer, A. Johnson, W. Muessel, H. Strobel, J. Tomkovic, T. Gasenzer, and M. K. Oberthaler, "Observation of scaling in the dynamics of a strongly quenched quantum gas", Phys. Rev. Lett. **115**, 245301 (2015).

[8] N. Navon, A. L. Gaunt, R. P. Smith, and Z. Hadzibabic, "Critical dynamics of spontaneous symmetry breaking in a homogeneous Bose gas", Science **347**, 167 (2015).

[9] C. Eigen, J. A. P. Glidden, R. Lopes, E. A. Cornell, R. P. Smith, and Z. Hadzibabic, "Universal prethermal dynamics of Bose gases quenched to unitarity", Nature **563**, 221 (2018).

[10] M. Schreiber, S. S. Hodgman, P. Bordia, H. P. Lüschen, M. H. Fischer, R. Vosk, E. Altman, U. Schneider, and I. Bloch, "Observation of many-body localization of interacting fermions in a quasirandom optical lattice", Science **349**, 842 (2015).

[11] N. Navon, A. L. Gaunt, R. P. Smith, and Z. Hadzibabic, "Emergence of a turbulent cascade in a quantum gas", Nature **539**, 72 (2016).

[12]B. Rauer, S. Erne, T. Schweigler, F. Cataldini, M. Tajik, and J. Schmiedmayer, "Recurrences in an isolated quantum many-body system", Science **360**, 307 (2018).

[13]C.-M. Schmied, A. N. Mikheev, and T. Gasenzer, "Prescaling in a far-from-equilibrium Bose gas", Phys. Rev. Lett. **122**, 170404 (2019).

[14]A. Mazeliauskas and J. Berges, "Prescaling and far-from-equilibrium hydrodynamics in the quark-gluon plasma", Phys. Rev. Lett. **122**, 122301 (2019).

[15]M. Prüfer, P. Kunkel, H. Strobel, S. Lannig, D. Linnemann, C.-M. Schmied, J. Berges, T. Gasenzer, and M. K. Oberthaler, "Observation of universal dynamics in a spinor Bose gas far from equilibrium", Nature **563**, 217 (2018).

[16]S. Erne, R. Bücker, T. Gasenzer, J. Berges, and J. Schmiedmayer, "Universal dynamics in an isolated one-dimensional Bose gas far from equilibrium", Nature **563**, 225 (2018).

[17]J. A. P. Glidden, C. Eigen, L. H. Dogra, T. A. Hilker, R. P. Smith, and Z. Hadzibabic, "Bidirectional dynamic scaling in an isolated Bose gas far from equilibrium", Nature Phys. **17**, 457 (2021).

[18]B. Widom, "Equation of State in the Neighborhood of the Critical Point", J. Chem. Phys. **43**, 3898 (1965).

[19]L. P. Kadanoff, "Scaling laws for Ising models near T_c", Physics Physique Fizika **2**, 263 (1966).

[20]K. G. Wilson, "Renormalization Group and Critical Phenomena. I. Renormalization Group and the Kadanoff Scaling Picture", Phys. Rev. B **4**, 3174 (1971).

[21]K. G. Wilson, "Renormalization Group and Critical Phenomena. II. Phase-Space Cell Analysis of Critical Behavior", Phys. Rev. B **4**, 3184 (1971).

[22]P. C. Hohenberg and B. I. Halperin, "Theory of Dynamic Critical Phenomena", Rev. Mod. Phys. **49**, 435 (1977).

[23]H. Janssen, "Field-theoretic methods applied to critical dynamics", in Dynamical critical phenomena and related topics, edited by C. Enz, Lecture Notes in Physics, Vol. 104 (1979).

[24]A. J. Bray, "Theory of phase-ordering kinetics", Adv. Phys. **43**, 357 (1994).

[25]P. Calabrese and A. Gambassi, "Ageing properties of critical systems", J. Phys. A: Math. Gen. **38**, R133 (2005).

[26]U. Frisch, *Turbulence: The Legacy of A. N. Kolmogorov* (Cambridge University Press, 2004).

[27]V. E. Zakharov, V. S. L'vov, and G. Falkovich, *Kolmogorov Spectra of Turbulence I: Wave Turbulence* (Springer, Berlin, 1992).

[28] S. Nazarenko, *Wave turbulence*, Lecture Notes in Physics, Vol. 825 (Springer Berlin, Heidelberg, 2011).

[29] M. Tsubota, "Quantum Turbulence", J. Phys. Soc. Jpn. **77**, 111006 (2008).

[30] W. Vinen, "An Introduction to Quantum Turbulence", J. Low Temp. Phys. **145**, 7 (2006).

[31] A. Maraga, A. Chiocchetta, A. Mitra, and A. Gambassi, "Aging and coarsening in isolated quantum systems after a quench: Exact results for the quantum O(N) model with $N \to \infty$", Phys. Rev. E **92**, 042151 (2015).

[32] A. Maraga, P. Smacchia, and A. Silva, "Linear ramps of the mass in the $O(N)$ model: Dynamical transition and quantum noise of excitations", Phys. Rev. B **94**, 245122 (2016).

[33] A. Chiocchetta, M. Tavora, A. Gambassi, and A. Mitra, "Short-time universal scaling in an isolated quantum system after a quench", Phys. Rev. B **91**, 220302 (2015).

[34] A. Chiocchetta, M. Tavora, A. Gambassi, and A. Mitra, "Short-time universal scaling and light-cone dynamics after a quench in an isolated quantum system in d spatial dimensions", Phys. Rev. B **94**, 134311 (2016).

[35] A. Chiocchetta, A. Gambassi, S. Diehl, and J. Marino, "Universal short-time dynamics: boundary functional renormalization group for a temperature quench", Phys. Rev. B **94**, 174301 (2016).

[36] A. Chiocchetta, A. Gambassi, S. Diehl, and J. Marino, "Dynamical Crossovers in Prethermal Critical States", Phys. Rev. Lett. **118**, 135701 (2017).

[37] J. Marino and S. Diehl, "Driven markovian quantum criticality", Phys. Rev. Lett. **116**, 070407 (2016).

[38] J. Marino and S. Diehl, "Quantum dynamical field theory for nonequilibrium phase transitions in driven open systems", Phys. Rev. B **94**, 085150 (2016).

[39] K. Damle, S. N. Majumdar, and S. Sachdev, "Phase ordering kinetics of the Bose gas", Phys. Rev. A **54**, 5037 (1996).

[40] S. Mukerjee, C. Xu, and J. E. Moore, "Dynamical models and the phase ordering kinetics of the $s = 1$ spinor condensate", Phys. Rev. B **76**, 104519 (2007).

[41] G. Aarts, G. F. Bonini, and C. Wetterich, "Exact and truncated dynamics in nonequilibrium field theory", Phys. Rev. D **63**, 025012 (2000).

[42] L. A. Williamson and P. B. Blakie, "Universal Coarsening Dynamics of a Quenched Ferromagnetic Spin-1 Condensate", Phys. Rev. Lett. **116**, 025301 (2016).

[43] J. Hofmann, S. S. Natu, and S. Das Sarma, "Coarsening Dynamics of Binary Bose Condensates", Phys. Rev. Lett. **113**, 095702 (2014).

[44] L. A. Williamson and P. B. Blakie, "Coarsening and thermalization properties of a quenched ferromagnetic spin-1 condensate", Phys. Rev. A **94**, 023608 (2016).

[45] A. Bourges and P. B. Blakie, "Different growth rates for spin and superfluid order in a quenched spinor condensate", Phys. Rev. A **95**, 023616 (2017).

[46] A. Lamacraft, "Quantum Quenches in a Spinor Condensate", Phys. Rev. Lett. **98**, 160404 (2007).

[47] D. Rossini, A. Silva, G. Mussardo, and G. E. Santoro, "Effective Thermal Dynamics Following a Quantum Quench in a Spin Chain", Phys. Rev. Lett. **102**, 127204 (2009).

[48] E. G. Dalla Torre, E. Demler, and A. Polkovnikov, "Universal Rephasing Dynamics after a Quantum Quench via Sudden Coupling of Two Initially Independent Condensates", Phys. Rev. Lett. **110**, 090404 (2013).

[49] A. Gambassi and P. Calabrese, "Quantum quenches as classical critical films", Europhys. Lett. **95**, 66007 (2011).

[50] B. Sciolla and G. Biroli, "Quantum quenches, dynamical transitions, and off-equilibrium quantum criticality", Phys. Rev. B **88**, 201110 (2013).

[51] P. Smacchia, M. Knap, E. Demler, and A. Silva, "Exploring dynamical phase transitions and prethermalization with quantum noise of excitations", Phys. Rev. B **91**, 205136 (2015).

[52] J. Berges, A. Rothkopf, and J. Schmidt, "Non-thermal fixed points: Effective weak-coupling for strongly correlated systems far from equilibrium", Phys. Rev. Lett. **101**, 041603 (2008).

[53] C. Scheppach, J. Berges, and T. Gasenzer, "Matter-wave turbulence: Beyond kinetic scaling", Phys. Rev. A **81**, 033611 (2010).

[54] J. Berges and D. Sexty, "Strong versus weak wave-turbulence in relativistic field theory", Phys. Rev. D **83**, 085004 (2011).

[55] A. Piñeiro Orioli, K. Boguslavski, and J. Berges, "Universal self-similar dynamics of relativistic and nonrelativistic field theories near nonthermal fixed points", Phys. Rev. D **92**, 025041 (2015).

[56] J. Berges, "Nonequilibrium Quantum Fields: From Cold Atoms to Cosmology", Lecture notes of the Les Houches Summer School on 'Strongly interacting quantum systems out of equilibrium' (2015).

[57] I. Chantesana, A. Piñeiro Orioli, and T. Gasenzer, "Kinetic theory of nonthermal fixed points in a Bose gas", Phys. Rev. A **99**, 043620 (2019).

[58] J. F. Rodriguez-Nieva, A. Piñeiro Orioli, and J. Marino, "Far-from-equilibrium universality in the two-dimensional Heisenberg model", Proceedings of the National Academy of Sciences **119**, e2122599119 (2022).

[59] B. Nowak, D. Sexty, and T. Gasenzer, "Superfluid turbulence: Nonthermal fixed point in an ultracold Bose gas", Phys. Rev. B **84**, 020506(R) (2011).

[60] B. Nowak, J. Schole, D. Sexty, and T. Gasenzer, "Nonthermal fixed points, vortex statistics, and superfluid turbulence in an ultracold Bose gas", Phys. Rev. A **85**, 043627 (2012).

[61] J. Schole, B. Nowak, and T. Gasenzer, "Critical dynamics of a two-dimensional superfluid near a non-thermal fixed point", Phys. Rev. A **86**, 013624 (2012).

[62] M. Karl and T. Gasenzer, "Strongly anomalous non-thermal fixed point in a quenched two-dimensional bose gas", New J. Phys. **19**, 093014 (2017).

[63] J. Berges, "Controlled nonperturbative dynamics of quantum fields out of equilibrium", Nucl. Phys. **A699**, 847 (2002).

[64] A. N. Mikheev, C.-M. Schmied, and T. Gasenzer, "Low-energy effective theory of nonthermal fixed points in a multicomponent Bose gas", Phys. Rev. A **99**, 063622 (2019).

[65] P. B. Arnold, G. D. Moore, and L. G. Yaffe, "Effective kinetic theory for high temperature gauge theories", JHEP **01**, 030 (2003).

[66] A. Piñeiro Orioli and J. Berges, "Breaking the fluctuation-dissipation relation by universal transport processes", Phys. Rev. Lett. **122**, 150401 (2019).

[67] B. Nowak, J. Schole, and T. Gasenzer, "Universal dynamics on the way to thermalisation", New J. Phys. **16**, 093052 (2014).

[68] J. Berges and D. Sexty, "Bose condensation far from equilibrium", Phys. Rev. Lett. **108**, 161601 (2012).

[69] M. J. Davis, T. M. Wright, T. Gasenzer, S. A. Gardiner, and N. P. Proukakis, "Formation of Bose-Einstein Condensates", in *Universal Themes of Bose-Einstein Condensation*, edited by N. P. Proukakis, D. W. Snoke, and P. B. Littlewood (Cambridge University Press, 2017).

[70] B. Svistunov, "Highly nonequilibrium Bose condensation in a weakly interacting gas", J. Mosc. Phys. Soc. **1**, 373 (1991).

[71] J. Berges and G. Hoffmeister, "Nonthermal fixed points and the functional renormalization group", Nucl. Phys. **B813**, 383 (2009).

[72] M. Schmidt, S. Erne, B. Nowak, D. Sexty, and T. Gasenzer, "Nonthermal fixed points and solitons in a one-dimensional Bose gas", New J. Phys. **14**, 075005 (2012).

[73] B. Nowak, S. Erne, M. Karl, J. Schole, D. Sexty, and T. Gasenzer, "Non-thermal fixed points: universality, topology, & turbulence in Bose gases", in Proc. Int. School on Strongly Interacting Quantum Systems Out of Equilibrium, Les Houches, edited by T. G. et al. (2016).

[74] M. Karl, B. Nowak, and T. Gasenzer, "Tuning universality far from equilibrium", Sci. Rep. **3**, 2394 (2013).

[75] M. Karl, B. Nowak, and T. Gasenzer, "Universal scaling at non-thermal fixed points of a two-component Bose gas", Phys. Rev. A **88**, 063615 (2013).

[76] C. Ewerz, T. Gasenzer, M. Karl, and A. Samberg, "Non-thermal fixed point in a holographic superfluid", JHEP **05**, 070 (2015).

[77] J. Berges, K. Boguslavski, A. Chatrchyan, and J. Jaeckel, "Attractive versus repulsive interactions in the Bose-Einstein condensation dynamics of relativistic field theories", Phys. Rev. D **96**, 076020 (2017).

[78] J. Deng, S. Schlichting, R. Venugopalan, and Q. Wang, "Off-equilibrium infrared structure of self-interacting scalar fields: Universal scaling, Vortex-antivortex superfluid dynamics and Bose-Einstein condensation", Phys. Rev. **A97**, 053606 (2018).

[79] J. Berges and J. Jaeckel, "Far from equilibrium dynamics of Bose-Einstein condensation for Axion Dark Matter", Phys. Rev. D **91**, 025020 (2015).

[80] G. D. Moore, "Condensates in Relativistic Scalar Theories", Phys. Rev. D **93**, 065043 (2016).

[81] J. Berges, K. Boguslavski, S. Schlichting, and R. Venugopalan, "Turbulent thermalization process in heavy-ion collisions at ultrarelativistic energies", Phys. Rev. D **89**, 074011 (2014).

[82] J. Berges, K. Boguslavski, S. Schlichting, and R. Venugopalan, "Universal attractor in a highly occupied non-Abelian plasma", Phys. Rev. D **89**, 114007 (2014).

[83] J. Berges, K. Boguslavski, S. Schlichting, and R. Venugopalan, "Universality far from equilibrium: From superfluid Bose gases to heavy-ion collisions", Phys. Rev. Lett. **114**, 061601 (2015).

[84] J. Berges, K. Boguslavski, S. Schlichting, and R. Venugopalan, "Nonequilibrium fixed points in longitudinally expanding scalar theories: infrared cascade, Bose condensation and a challenge for kinetic theory", Phys. Rev. D **92**, 096006 (2015).

[85] J. Berges, "Introduction to nonequilibrium quantum field theory", AIP Conf. Proc. **739**, 3 (2004).

[86] T. Gasenzer, "Ultracold gases far from equilibrium", Eur. Phys. J. ST **168**, 89 (2009).

[87] L. P. Kadanoff and G. Baym, *Quantum Statistical Mechanics* (Benjamin, 1962).

[88] M. Lindner and M. M. Müller, "Comparison of Boltzmann equations with quantum dynamics for scalar fields", Phys. Rev. D **73**, 125002 (2006).

[89] A. Schachner, A. Piñeiro Orioli, and J. Berges, "Universal scaling of unequal-time correlation functions in ultracold Bose gases far from equilibrium", Phys. Rev. A **95**, 053605 (2017).

[90] R. Walz, K. Boguslavski, and J. Berges, "Large-N kinetic theory for highly occupied systems", Phys. Rev. D **97**, 116011 (2018).

[91] A. A. Petrov and A. E. Blechman, *Effective Field Theories* (World Scientific, 2016).

[92] C. P. Burgess, *Introduction to Effective Field Theory: Thinking Effectively about Hierarchies of Scale* (Cambridge University Press, 2020).

[93] J. Zinn-Justin, *Quantum Field Theory and Critical Phenomena*, 4th ed., International Series of Monographs on Physics, Vol. 113 (Clarendon Press, Oxford, 2002).

[94] F. Gelis, *Quantum Field Theory* (Cambridge University Press, 2019).

[95] J. M. Luttinger and J. C. Ward, "Ground-State Energy of a Many-Fermion System. II", Phys. Rev. **118**, 1417 (1960).

[96] J. M. Cornwall, R. Jackiw, and E. Tomboulis, "Effective action for composite operators", Phys. Rev. D **10**, 2428 (1974).

[97] E. A. Calzetta and B.-L. B. Hu, *Nonequilibrium Quantum Field Theory*, Cambridge Monographs on Mathematical Physics (Cambridge University Press, 2008).

[98] R. Baier and R. Kobes, "On the damping rate of a fast fermion in hot QED", Phys. Rev. D **50**, 5944 (1994).

[99] C. Banerjee, I. V. Fialkovsky, M. Lewkowicz, C. X. Zhang, and M. A. Zubkov, "Wigner-Weyl calculus in Keldysh technique", J. Comput. Electron. **20**, 2255 (2021).

[100] J. Berges and J. Cox, "Thermalization of quantum fields from time reversal invariant evolution equations", Phys. Lett. B **517**, 369 (2001).

[101] S. Juchem, W. Cassing, and C. Greiner, "Quantum dynamics and thermalization for out-of-equilibrium φ^4 theory", Phys. Rev. D **69**, 025006 (2004).

[102] J. Berges and S. Borsanyi, "Range of validity of transport equations", Phys. Rev. D **74**, 045022 (2006).

[103] A. Arrizabalaga, J. Smit, and A. Tranberg, "Equilibration in φ^4 theory in $3 + 1$ dimensions", Phys. Rev. D **72**, 025014 (2005).

[104] C. Wetterich, "Time evolution of nonequilibrium effective action", Phys. Rev. Lett. **78**, 3598 (1997).

[105] T. L. Curtright, D. B. Fairlie, and C. K. Zachos, *A Concise Treatise on Quantum Mechanics in Phase Space* (World Scientific, 2014).

[106] T. Curtright and C. K. Zachos, "Wigner trajectory characteristics in phase space and field theory", J. Phys. A **32**, 771 (1999).

[107] S. Barnett and P. Radmore, *Methods in Theoretical Quantum Optics* (Oxford University Press, 2002).

[108] R. Ott, T. V. Zache, and J. Berges, *Equal-time approach to real-time dynamics of quantum fields*, arXiv:2204.06463 [cond-mat.quant-gas].

[109] M. Prüfer, T. V. Zache, P. Kunkel, S. Lannig, A. Bonnin, H. Strobel, J. Berges, and M. K. Oberthaler, "Experimental extraction of the quantum effective action for a non-equilibrium many-body system", Nature Phys. **16**, 1012 (2020).

[110] T. V. Zache, T. Schweigler, S. Erne, J. Schmiedmayer, and J. Berges, "Extracting the field theory description of a quantum many-body system from experimental data", Phys. Rev. X **10**, 011020 (2020).

[111] A. Kamenev, *Field Theory of Non-Equilibrium Systems* (Cambridge University Press, 2011).

[112] P. Di Francesco, P. Mathieu, and D. Senechal, *Conformal Field Theory*, Graduate Texts in Contemporary Physics (Springer-Verlag, New York, 1997).

[113] A. Altland and B. D. Simons, *Condensed Matter Field Theory*, 2nd ed. (Cambridge University Press, 2010).

[114] G.-z. Zhou, Z.-b. Su, B.-l. Hao, and L. Yu, "Closed time path Green's functions and critical dynamics", Phys. Rev. B **22**, 3385 (1980).

[115] S. Weinberg, *The quantum theory of fields. Vol. 2: Modern applications* (Cambridge University Press, 2013).

[116] H. Nielsen and S. Chadha, "On how to count Goldstone bosons", Nucl. Phys. B **105**, 445 (1976).

[117] H. Watanabe and T. Brauner, "On the number of Nambu-Goldstone bosons and its relation to charge densities", Phys. Rev. D **84**, 125013 (2011).

[118] Y. Hidaka and Y. Minami, "Spontaneous symmetry breaking and Nambu–Goldstone modes in open classical and quantum systems", PTEP **2020**, 033A01 (2020).

[119] P. Heinen, "Phase Correlators in Gross–Pitaevskii Systems Far from Equilibrium", Master's thesis (Heidelberg University, 2020).

[120] I. Herbut, *A Modern Approach to Critical Phenomena* (Cambridge University Press, 2007).

[121] J. Cardy, *Scaling and Renormalization in Statistical Physics*, Cambridge Lecture Notes in Physics (Cambridge University Press, 1996).

[122] F. J. Wegner and A. Houghton, "Renormalization group equation for critical phenomena", Phys. Rev. A **8**, 401 (1973).

[123] K. G. Wilson and J. Kogut, "The renormalization group and the ϵ expansion", Phys. Rep. **12**, 75 (1974).

[124] J. Polchinski, "Renormalization and effective lagrangians", Nucl. Phys. B **231**, 269 (1984).

[125] C. Wetterich, "Exact evolution equation for the effective potential", Phys. Lett. B **301**, 90 (1993).

[126] T. R. Morris, "The exact renormalization group and approximate solutions", Int. J. Mod. Phys. A **9**, 2411 (1994).

[127] J. M. Pawlowski, "Aspects of the functional renormalisation group", Annals Phys. **322**, 2831 (2007).

[128] M. Salmhofer, *Renormalization: An Introduction*, Theoretical and Mathematical Physics (Springer Berlin, Heidelberg, 2007).

[129] J. Berges, N. Tetradis, and C. Wetterich, "Nonperturbative renormalization flow in quantum field theory and statistical physics", Phys. Rept. **363**, 223 (2002).

[130] H. Gies, "Introduction to the Functional RG and Applications to Gauge Theories", in *Renormalization Group and Effective Field Theory Approaches to Many-Body Systems*, edited by A. Schwenk and J. Polonyi, Lecture Notes in Physics, Vol. 852 (Springer Berlin, Heidelberg, 2012).

[131] B. Delamotte, "An Introduction to the Nonperturbative Renormalization Group", in *Renormalization Group and Effective Field Theory Approaches to Many-Body Systems*, edited by A. Schwenk and J. Polonyi, Lecture Notes in Physics, Vol. 852 (Springer Berlin Heidelberg, 2012).

[132] P. Kopietz, L. Bartosch, and F. Schütz, *Introduction to the Functional Renormalization Group*, Lecture Notes in Physics, Vol. 798 (Springer Berlin, Heidelberg, 2010).

[133] N. Dupuis, L. Canet, A. Eichhorn, W. Metzner, J. M. Pawlowski, M. Tissier, and N. Wschebor, "The nonperturbative functional renormalization group and its applications", Phys. Rept. **910**, 1 (2021).

[134] J. Berges and D. Mesterhazy, "Introduction to the nonequilibrium functional renormalization group", Nucl. Phys. Proc. Suppl. **228**, 37 (2012).

[135] S. Mathey, T. Gasenzer, and J. M. Pawlowski, "Anomalous scaling at nonthermal fixed points of Burgers' and Gross-Pitaevskii turbulence", Phys. Rev. A **92**, 023635 (2015).

[136] T. Gasenzer and J. M. Pawlowski, "Towards far-from-equilibrium quantum field dynamics: A functional renormalisation-group approach", Phys. Lett. B **670**, 135 (2008).

[137] T. Gasenzer, S. Kessler, and J. M. Pawlowski, "Far-from-equilibrium quantum many-body dynamics", Eur. Phys. J. C **70**, 423 (2010).

[138] L. Corell, A. K. Cyrol, M. Heller, and J. M. Pawlowski, "Flowing with the temporal renormalization group", Phys. Rev. D **104**, 025005 (2021).

[139] J. M. Pawlowski, D. F. Litim, S. Nedelko, and L. von Smekal, "Infrared behavior and fixed points in Landau gauge QCD", Phys. Rev. Lett. **93**, 152002 (2004).

[140] X. G. Wen, *Quantum field theory of many-body systems: From the origin of sound to an origin of light and electrons* (Oxford University Press, 2007).

[141] Y. Takahashi, "Towards the Many-Body Theory with the Galilei Invariance as a Guide: Part I", Fortschr. Phys. **36**, 63 (1988).

[142] Y. Takahashi, "Towards the Many-Body Theory with the Galilei invariance as a Gluide Part II", Fortschr. Phys. **36**, 83 (1988).

[143] M. Greiter, F. Wilczek, and E. Witten, "Hydrodynamic Relations in Superconductivity", Mod. Phys. Lett. B **03**, 903 (1989).

[144] D. T. Son and M. Wingate, "General coordinate invariance and conformal invariance in nonrelativistic physics: Unitary Fermi gas", Annals Phys. **321**, 197 (2006).

[145] J. O. Andersen, *Effective field theory for Goldstone bosons in nonrelativistic superfluids*, arXiv:cond-mat/0209243.

[146] K. Boguslavski and A. Piñeiro Orioli, "Unraveling the nature of universal dynamics in $O(N)$ theories", Phys. Rev. D **101**, 091902 (2020).

[147] T. Kloss and P. Kopietz, "Non-equilibrium time evolution of bosons from the functional renormalization group", Phys. Rev. B **83**, 205118 (2011).

[148] J. Berges and T. Gasenzer, "Quantum versus classical statistical dynamics of an ultracold Bose gas", Phys. Rev. A **76**, 033604 (2007).

[149] G. Aarts and J. Berges, "Classical aspects of quantum fields far from equilibrium", Phys. Rev. Lett. **88**, 041603 (2002).

[150] R. Walz, K. Boguslavski, and J. Berges, "Large-N kinetic theory for highly occupied systems", Phys. Rev. D **97**, 116011 (2018).

[151] J. Bezanson, A. Edelman, S. Karpinski, and V. B. Shah, "Julia: a fresh approach to numerical computing", SIAM Rev. **59**, 65 (2017).

[152] S. Gowda, Y. Ma, A. Cheli, M. Gwózdz, V. B. Shah, A. Edelman, and C. Rackauckas, "High-performance symbolic-numerics via multiple dispatch", ACM Commun. Comput. Algebra **55**, 92 (2021).

[153] A. Genz and A. Malik, "Remarks on algorithm 006: An adaptive algorithm for numerical integration over an N-dimensional rectangular region", J. Comput. Appl. Math. **6**, 295 (1980).

[154] A. Grundmann and H. M. Möller, "Invariant integration formulas for the n-simplex by combinatorial methods", SIAM J. Numer. Anal. **15**, 282 (1978).

[155] H. H. Homeier and E. Steinborn, "Numerical integration of functions with a sharp peak at or near one boundary using Möbius transformations", J. Comput. Phys. **87**, 61 (1990).

[156] P. M. Chesler and L. G. Yaffe, "Horizon formation and far-from-equilibrium isotropization in supersymmetric Yang-Mills plasma", Phys. Rev. Lett. **102**, 211601 (2009).

[157] P. M. Chesler and L. G. Yaffe, "Boost invariant flow, black hole formation, and far-from-equilibrium dynamics in $\mathcal{N} = 4$ supersymmetric Yang-Mills theory", Phys. Rev. D **82**, 026006 (2010).

[158] M. P. Heller, R. A. Janik, and P. Witaszczyk, "The characteristics of thermalization of boost-invariant plasma from holography", Phys. Rev. Lett. **108**, 201602 (2012).

[159] M. P. Heller, R. A. Janik, and P. Witaszczyk, "A numerical relativity approach to the initial value problem in asymptotically Anti-de Sitter spacetime for plasma thermalization - an ADM formulation", Phys. Rev. D **85**, 126002 (2012).

[160] I. Y. Aref'eva, "Holographic approach to quark–gluon plasma in heavy ion collisions", Physics-Uspekhi **57**, 527 (2014).

[161] R. K. Ellis, W. J. Stirling, and B. R. Webber, *QCD and collider physics* (Cambridge University Press, 2011).

[162] J. D. Bjorken, "Asymptotic Sum Rules at Infinite Momentum", Phys. Rev. **179**, 1547 (1969).

[163] C. G. Callan Jr. and D. J. Gross, "High-energy electroproduction and the constitution of the electric current", Phys. Rev. Lett. **22**, 156 (1969).

[164] J. C. Collins, D. E. Soper, and G. F. Sterman, "Factorization of Hard Processes in QCD", Adv. Ser. Direct. High Energy Phys. **5**, 1 (1989).

[165] L. Frankfurt, M. Strikman, and C. Weiss, "Small-x physics: From HERA to LHC and beyond", Ann. Rev. Nucl. Part. Sci. **55**, 403 (2005).

[166] V. N. Gribov and L. N. Lipatov, "Deep inelastic ep scattering in perturbation theory", Sov. J. Nucl. Phys. **15**, 438 (1972).

[167] G. Altarelli and G. Parisi, "Asymptotic Freedom in Parton Language", Nucl. Phys. B **126**, 298 (1977).

[168] Y. L. Dokshitzer, "Calculation of the Structure Functions for Deep Inelastic Scattering and e+ e- Annihilation by Perturbation Theory in Quantum Chromodynamics.", Sov. Phys. JETP **46**, 641 (1977).

[169] E. A. Kuraev, L. N. Lipatov, and V. S. Fadin, "The Pomeranchuk Singularity in Non-abelian Gauge Theories", Sov. Phys. JETP **45**, 199 (1977).

[170] I. I. Balitsky and L. N. Lipatov, "The Pomeranchuk Singularity in Quantum Chromodynamics", Sov. J. Nucl. Phys. **28**, 822 (1978).

[171] G. P. Salam, "An Introduction to leading and next-to-leading BFKL", Acta Phys. Polon. B **30**, 3679 (1999).

[172] J. Jalilian-Marian, A. Kovner, A. Leonidov, and H. Weigert, "The BFKL equation from the Wilson renormalization group", Nucl. Phys. B **504**, 415 (1997).

[173] M. Froissart, "Asymptotic behavior and subtractions in the Mandelstam representation", Phys. Rev. **123**, 1053 (1961).

[174] L. V. Gribov, E. M. Levin, and M. G. Ryskin, "Semihard Processes in QCD", Phys. Rept. **100**, 1 (1983).

[175] A. H. Mueller and J.-w. Qiu, "Gluon recombination and shadowing at small values of x", Nucl. Phys. B **268**, 427 (1986).

[176] I. Balitsky, "High-energy QCD and Wilson lines", in *At the frontier of particle physics*, edited by M. Shifman (World Scientific, 2001).

[177] Y. V. Kovchegov, "Small-x F_2 structure function of a nucleus including multiple pomeron exchanges", Phys. Rev. D **60**, 034008 (1999).

[178] Y. V. Kovchegov, "Unitarization of the BFKL pomeron on a nucleus", Phys. Rev. D **61**, 074018 (2000).

[179] J. Jalilian-Marian, A. Kovner, A. Leonidov, and H. Weigert, "The Wilson renormalization group for low x physics: Towards the high density regime", Phys. Rev. D **59**, 014014 (1998).

[180] H. Weigert, "Unitarity at small Bjorken x", Nucl. Phys. A **703**, 823–860 (2002).

[181] E. Iancu, A. Leonidov, and L. D. McLerran, "Nonlinear gluon evolution in the color glass condensate: I", Nucl. Phys. A **692**, 583 (2001).

[182] E. Iancu, A. Leonidov, and L. D. McLerran, "The renormalization group equation for the color glass condensate", Phys. Lett. B **510**, 133 (2001).

[183] A. D. Martin, W. J. Stirling, R. S. Thorne, and G. Watt, "Parton distributions for the LHC", Eur. Phys. J. C **63**, 189 (2009).

[184] E. Iancu and R. Venugopalan, "The color glass condensate and high-energy scattering in QCD", in *Quark-Gluon Plasma 3*, edited by R. C. Hwa and X.-N. Wang (World Scientific, 2003).

[185] F. Gelis, E. Iancu, J. Jalilian-Marian, and R. Venugopalan, "The Color Glass Condensate", Ann. Rev. Nucl. Part. Sci. **60**, 463 (2010).

[186] L. D. McLerran and R. Venugopalan, "Computing quark and gluon distribution functions for very large nuclei", Phys. Rev. D **49**, 2233 (1994).

[187] L. D. McLerran and R. Venugopalan, "Gluon distribution functions for very large nuclei at small transverse momentum", Phys. Rev. D **49**, 3352 (1994).

[188] L. D. McLerran and R. Venugopalan, "Green's functions in the color field of a large nucleus", Phys. Rev. D **50**, 2225 (1994).

[189] Y. V. Kovchegov and E. Levin, *Quantum chromodynamics at high energy* (Cambridge University Press, Aug. 2012).

[190] A. Bassetto, G. Nardelli, and R. Soldati, *Yang-Mills Theories in Algebraic Non-Covariant Gauges* (World Scientific, 1991).

[191] G. Leibbrandt, *Noncovariant Gauges* (World Scientific, 1994).

[192] A. V. Belitsky, X. Ji, and F. Yuan, "Final state interactions and gauge invariant parton distributions", Nucl. Phys. B **656**, 165 (2003).

[193] J. Jalilian-Marian, A. Kovner, L. D. McLerran, and H. Weigert, "Intrinsic glue distribution at very small x", Phys. Rev. D **55**, 5414 (1997).

[194] J.-P. Blaizot, E. Iancu, and H. Weigert, "Nonlinear gluon evolution in path integral form", Nucl. Phys. A **713**, 441 (2003).

[195] A. Ipp and D. I. Müller, "Progress on 3+1D Glasma simulations", Eur. Phys. J. A **56**, 243 (2020).

[196] A. Kovner, L. D. McLerran, and H. Weigert, "Gluon production from non-Abelian Weizsäcker-Williams fields in nucleus-nucleus collisions", Phys. Rev. D **52**, 6231 (1995).

[197] H. Fujii and K. Itakura, "Expanding color flux tubes and instabilities", Nucl. Phys. A **809**, 88 (2008).

[198] L. McLerran, "The CGC and the Glasma: Two Lectures at the Yukawa Institute", Prog. Theor. Phys. Suppl. **187**, 17 (2011).

[199] F. Gelis, "Color Glass Condensate and Glasma", Int. J. Mod. Phys. A **28**, 1330001 (2013).

[200] J. Berges, M. P. Heller, A. Mazeliauskas, and R. Venugopalan, "QCD thermalization: Ab initio approaches and interdisciplinary connections", Rev. Mod. Phys. **93**, 035003 (2021).

[201] J.-P. Blaizot and L. Yan, "Onset of hydrodynamics for a quark-gluon plasma from the evolution of moments of distribution functions", JHEP **11**, 161 (2017).

[202] J.-P. Blaizot and N. Tanji, "Angular mode expansion of the Boltzmann equation in the small-angle approximation", Nucl. Phys. A **992**, 121618 (2019).

[203] A. Kurkela and Y. Zhu, "Isotropization and hydrodynamization in weakly coupled heavy-ion collisions", Phys. Rev. Lett. **115**, 182301 (2015).

[204] A. H. Mueller and D. T. Son, "On the equivalence between the Boltzmann equation and classical field theory at large occupation numbers", Phys. Lett. B **582**, 279 (2004).

[205] G. Baym, "Thermal equilibration in ultra-relativistic heavy-ion collisions", Phys. Lett. B **138**, 18 (1984).

[206] A. H. Mueller, "The Boltzmann equation for gluons at early times after a heavy ion collision", Phys. Lett. B **475**, 220 (2000).

[207] J. D. Bjorken, "Highly relativistic nucleus-nucleus Collisions: The central rapidity region", Phys. Rev. D **27**, 140 (1983).

[208] P. B. Arnold, G. D. Moore, and L. G. Yaffe, "Photon and gluon emission in relativistic plasmas", JHEP **06**, 030 (2002).

[209] L. D. Landau, "Die kinetische Gleichung für den Fall Coulombscher Wechselwirkung", Phys. Z. Sowjetunion **10**, 154 (1936).

[210] J.-P. Blaizot, B. Wu, and L. Yan, "Quark production, Bose–Einstein condensates and thermalization of the quark–gluon plasma", Nucl. Phys. A **930**, 139 (2014).

[211] D. Bödeker, "The Impact of QCD plasma instabilities on bottom-up thermalization", JHEP **10**, 092 (2005).

[212] R. Baier, A. H. Mueller, D. Schiff, and D. T. Son, "'Bottom up' thermalization in heavy ion collisions", Phys. Lett. B **502**, 51 (2001).

[213] J.-P. Blaizot and L. Yan, "Fluid dynamics of out of equilibrium boost invariant plasmas", Phys. Lett. B **780**, 283 (2018).

[214] J. Brewer, L. Yan, and Y. Yin, "Adiabatic hydrodynamization in rapidly-expanding quark–gluon plasma", Phys. Lett. B **816**, 136189 (2021).

[215]C.-P. Sun, "High order adiabatic approximation for non-Hermitian quantum system and complexization of Berry's phase", Phys. Scripta **48**, 393 (1993).

[216]A. N. Mikheev, A. Mazeliauskas, and J. Berges, "Stability analysis of nonthermal fixed points in longitudinally expanding kinetic theory", Phys. Rev. D **105**, 116025 (2022).

[217]J. Brewer, B. Scheihing-Hitschfeld, and Y. Yin, "Scaling and adiabaticity in a rapidly expanding gluon plasma", JHEP **05**, 145 (2022).

Acknowledgements

First and foremost, I would like to thank my supervisor, Professor Thomas Gasenzer. He was very supportive during the whole time of my graduate studies and, not less importantly, gave me a lot of freedom in realizing my own ideas, always welcoming independent thinking.

Secondly, I am very beholden to Professor Jan Pawlowski. His guidance and advice were crucial for making progress in Ch. 4. I am also very grateful to Dr. Aleksas Mazeliauskas and Professor Jürgen Berges for giving me an opportunity to dip my toes in the waters of high-energy physics. I immensely enjoyed our collaboration. Furthermore, especially during the early days, I also greatly benefited from many discussions with Dr. Malo Tarpin.

Next, I would also like to thank all of my group colleagues, both current and previous: Philipp Heinen, Ido Siovitz, Niklas Rasch, Paul Große-Bley, Dr. Christian-Marcel Schmied, Dr. Stefanie Czischek, and many others. I also thank the SynQS collaboration and Professor Markus Oberthaler in particular for creating a very friendly atmosphere and an incredible research environment.

In addition, I would also like to mention and thank Professor Carlo Ewerz for kindly agreeing to be the second referee.

At this point, I want to express my appreciation for the Heidelberg Graduate School of Fundamental Physics (HGSFP) for accepting me to the $4 + 4$ programme and for the International Max Planck Research School for Quantum Dynamics (IMPRS-QD) for accepting and providing me with financial support during my doctoral studies.

Last but not least, I want to thank my family. It was only because of their unconditional and unlimited support that my journey to Heidelberg became possible. And, of course, my special thanks go to Dasha who kept reminding me that there are things in life beyond physics and who helped keeping me sane during the last weeks of writing this dissertation.